Unraveling the molecular mechanism underlying ALS-linked astrocyte toxicity for motor neurons

Burcin Ikiz

Submitted in partial fulfillment of the

requirements for the degree of

Doctor of Philosophy

under the Executive Committee

of the Graduate School of Arts and Sciences

COLUMBIA UNIVERSITY

2013

Abstract

Unraveling the molecular mechanism underlying ALS-linked astrocyte toxicity for motor neurons

Burcin Ikiz

Mutations in superoxide dismutase-1 (SOD1) cause a familial form of amyotrophic lateral sclerosis (ALS), a fatal paralytic disorder. Transgenic mutant SOD1 rodents capture the hallmarks of this disease, which is characterized by a progressive loss of motor neurons. Studies in chimeric and conditional transgenic mutant SOD1 mice indicate that non-neuronal cells, such as astrocytes, play an important role in motor neuron degeneration. Consistent with this non-cell autonomous scenario are the demonstrations that wild-type primary and embryonic stem cell-derived motor neurons selectively degenerate when cultured in the presence of either mutant SOD1-expressing astrocytes or medium conditioned with such mutant astrocytes. The work in this thesis rests on the use of an unbiased genomic strategy that combines RNA-Seq and "reverse gene engineering" algorithms in an attempt to decipher the molecular underpinnings of motor neuron degeneration caused by mutant astrocytes. To allow such analyses, first, mutant SOD1-induced toxicity on purified embryonic stem cell-derived motor neurons was validated and characterized. This was followed by the validation of signaling pathways identified by bioinformatics in purified embryonic stem cell-derived motor neurons, using both pharmacological and genetic techniques, leading to the discovery that nuclear factor kappa B (NF-κB) is instrumental in the demise of motor neurons exposed to mutant astrocytes *in vitro*. These findings demonstrate the usefulness of this novel genomic approach to study neurodegeneration and to point to NF-κB as a potential valuable therapeutic target for ALS.

Table of Contents

List of Figures and Tables

Acknowledgements

Over the past five years, I have had the privilege of collaborating with a number of talented individuals, all of whom provided significant contributions to the work described in this thesis.

First and foremost, I would like to thank Serge Przedborski for giving me the opportunity to do my doctoral training in his laboratory and for being an exceptional mentor over the years. His strong passion for science, adherence to excellence, and continual guidance in every aspect of my training had significant influence on me as a scientist, a professional, and an individual. I am forever grateful to him for all of the time, care, and effort that he has put into my training.

I would like to also thank Diane B. Re for all of her guidance over the years. She has been an amazing source of inspiration on how to be a scientist.

There are a number of individuals whom I would like to thank for the generous gift of their time, resources and collaborations. Gist Croft and Marine Prissette shared their CD2-expressing embryonic stem cells. Marine Prissette also taught me all of the details of embryonic stem cell experiments. Mariano Alvarez performed all of the RNA-Seq data analyses and patiently explained to me, over and over, the computational aspects of all of the analyses. David Park generously shared the adeno-associated viral vectors expressing green fluorescent protein and super repressive IκB.

The completion of this thesis would not have been possible without the contributions of both past and present members of the Przedborski Lab. I would like to especially thank Virginia Le Verche, Sudarshan Phani, Bobby Yu, Arnaud Jacquier, Tetsuya Nagata, and Dimitra Papadimitriou for their help and support as part of the ALS/SMA team; James Caicedo, Vernice Jackson-Lewis and Norma Romero for not only being the backbone of the lab, but also giving

me the basic tools and supplies that I needed to keep this project afloat; Christina Guardia, Rosa de Vries, Maja Tocilescu, Javier Blesa, and Yuhui Liu for their thoughtful advice and encouragement; Monika Jackowski and Mariela Flambury for administrative assistance.

I also would like to thank members of the Project ALS, Henderson, Wichterle, Monani, Pellizzoni, Jessell, and Shneider labs for their technical assistance and input on my project. I am grateful for the continuous support from the directors of the Doctoral Program in Neurobiology and Behavior: Carol Mason, Ken Miller, and Darcy Kelley; and the administrators: Cecil Oberbeck, Alla Kerzhner, and Elizabeth Ryan. I am also greatly thankful for the friendships of Nalini Colaco, Gulsen Surmeli, Wanying Zhang, Mattia Rigotti and Joseph Schumacher, who provided me with so much support and love over the years.

Finally, I am thankful for the time and thoughtful contributions of Christopher Henderson, Hynek Wichterle and Andrea Califano who have served as members of my thesis committee over the last four years. I am grateful to Pico Caroni for his willingness to read my thesis and join my committee as an outside examiner.

Lastly, I would like to acknowledge my parents, Belma and Osman, my sister, Deniz, my grandmother, Ayhan, and my husband, Chaitu, for their unconditional love and support. Without them, none of this would have been possible.

Dedication

I dedicate this thesis to my family in Turkey, the U.S., and Spain.

Chapter 1: Introduction

1.1. Amyotrophic Lateral Sclerosis

1.1.1. General definition

Amyotrophic lateral sclerosis (ALS), also known as "Lou Gehrig's disease" in the USA, is the most frequent adult-onset paralytic disorder. As reviewed by Rowland and collaborators (2010), the disease is found worldwide, with a prevalence of roughly 3-5 per 100,000 individuals. Onset of symptoms is usually in the fourth or fifth decade of life with about 10% of the cases beginning before the age of 40 and less than 5% before the age of 30. Common clinical features of ALS include muscle weakness and wasting followed by paralysis. The disease progresses rapidly with a mean survival of three years after diagnosis. Respiratory failure, due to respiratory muscle paralysis, is the primary cause of patient death (Mizutani et al., 1992). As discussed in more detail below, pathologically, ALS is characterized mainly by a loss of both upper and lower motor neurons (Hirano, 1996). To date, only a few approved treatments, such as mechanical ventilation and the drug riluzole, prolong survival to some extent in ALS patients. Therefore, not only is it absolutely necessary to develop more effective neuroprotective therapies, but it is also important that we find the mechanism by which motor neurons die in ALS and how the disease propagates and progresses.

1.1.2. Clinical presentation of the disease

1.1.2.1. Sporadic versus familial

ALS is essentially a sporadic disease, in that it occurs in absence of any apparent genetic linkage (Pasinelli and Brown, 2006). However, in roughly 10% of the cases, ALS is inherited, and in these rare cases, the phenotype can be transmitted either as an autosomal dominant or recessive

trait (Pasinelli and Brown, 2006). Of note, patients with familial ALS (fALS) are almost indistinguishable from sporadic ALS (sALS) patients, albeit typically, the former presents with a younger onset, a faster course of the disease, and a shorter survival after diagnosis (Rowland, 2010). Additionally, similar superoxide dismutase-1 (SOD1)- and TAR DNA binding protein-43 (TDP-43)-positive inclusions have been found in tissues from sALS and fALS patients (Arai et al., 2006; Bosco et al., 2010; Forsberg et al., 2010; Kato et al., 2000; Shibata et al., 1994). A multi-targeted drug named riluzole has been shown to have similar neuroprotective effects in sALS and fALS patients (Sojka et al., 1997). Moreover, cerebrospinal fluid samples from sALS and fALS cases have been shown to have comparable toxic effects on rat spinal cord neurons *in vitro* (Tikka et al., 2002). Collectively, these observations emphasize the striking similarities between sALS and fALS, and suggest that, while classification of sALS versus fALS might be important for genetic counseling, the mechanisms of neurodegeneration in both fALS and sALS may intersect. Thus, unraveling the molecular basis by which mutant gene products of fALS cause motor neuron degeneration may provide important insights into the pathogenesis of sALS.

1.1.2.2. Clinical forms of ALS

As mentioned above, in ALS, both the upper motor neurons [Figure 1.1; red] and the lower motor neurons [Figure 1.1; green] may be affected. However, the clinical presentation of ALS may differ depending on the extent of involvement of each type of motor neuron. The classical form of ALS involves primarily the upper motor neurons and the lower motor neurons that innervate the limbs. ALS is characterized by muscle weakness, muscle wasting, and fasciculation (which often predominate in the lower limbs), as well as by hyperactive tendon reflexes, spasticity, and Hoffman and Babinski signs (which often predominate in the upper limbs) (Przedborski et al., 2003; Rowland, 1998). In addition, as the disease advances, patients often

Figure 1.1: Schematic representation of upper (red) and lower motor neurons (green) that are affected in ALS

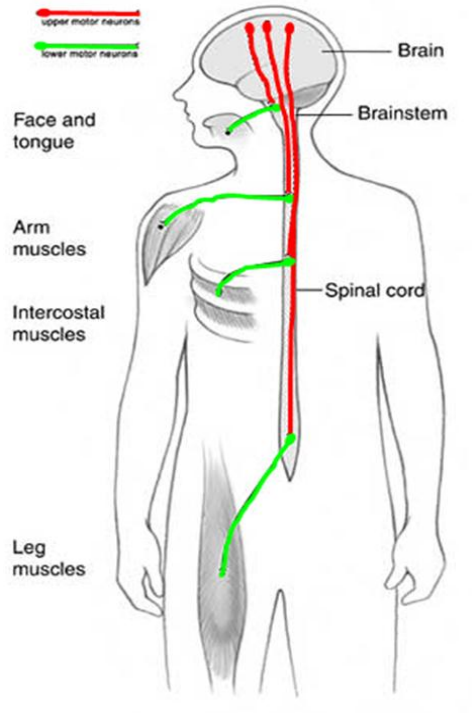

develop signs of bulbar involvement (i.e. involvement of the IX-XII cranial nerves leading to problems with speech, swallowing, tongue atrophy and twitching). Other cranial nerves are much less affected, especially those innervating the extrinsic muscles of the eyes (i.e. cranial nerves III, IV, and VI, which are typically spared in most patients, unless they are maintained alive for a long time by mechanical ventilation).

In addition to the classical form of ALS, there are three clinical variants that are labeled according to the major muscle regions affected during the disease process. These are:

- The bulbar form of ALS: where bulbar manifestations arise before the legs and arms are affected;
- Progressive muscle atrophy: patients with overt signs of lower motor neuron involvement, but no clear sign of upper motor neuron involvement;
- Primary lateral sclerosis: patients with marked upper motor neuron signs, but with very few or no signs of lower motor neuron involvement nor atrophy.

1.1.3. Neuropathology of ALS

The major pathological feature of ALS is the degeneration of upper and lower motor neurons. However, the neuropathology of ALS also includes degeneration of at least 30% of the small interneurons in the motor cortex and spinal cord, in addition to reactive gliosis (Ekblom et al., 1994; Kawamata et al., 1992; Murayama et al., 1991; Schiffer et al., 1996).

An established hallmark of ALS is the presence of various inclusion bodies in degenerating neurons and surrounding reactive astrocytes [Figure 1.2a] (Barbeito et al., 2004). Ubiquitinated inclusions [Figure 1.2b] are the most specific and the most common type of inclusions in ALS and are found in lower motor neurons of the brainstem and the spinal cord (Matsumoto et al., 1993) and in corticospinal upper motor neurons (Sasaki and Maruyama, 1994). These inclusions are classified as 'Lewy body-like' [Figure 1.2c] and 'Skein-like' [Figure 1.2d] (He and Hays, 2004; Kawashima et al., 1998).

Figure 1.2: Neuropathology of ALS

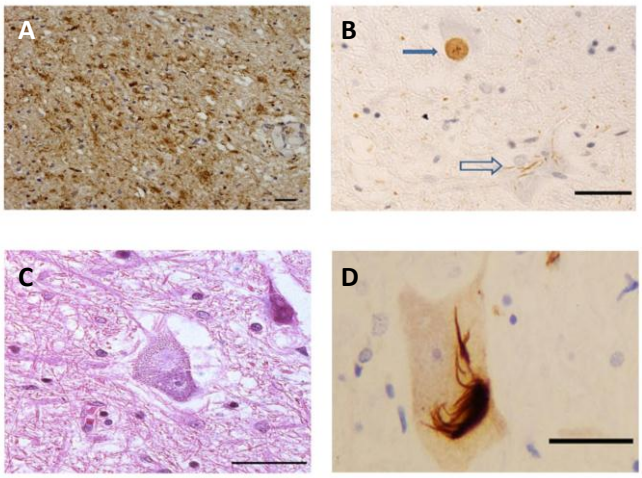

(A) Gliosis demonstrated in the spinal ventral horn using glial fibrillary acid protein (GFAP) antibody; (B) Lower motor neurons in ALS showing both compact (filled arrow) and skein-type (arrow) neuronal cytoplasmic inclusions stained for ubiquitin; (C) "Lewy-like hyaline inclusion" body in a spinal motor neuron; (D) p62 staining of a skein type inclusion (bar 50 μm). (Ince et al., 2011)

While the exact composition of these inclusions is not known, proteins identified so far include ubiquitin (Leigh et al., 1991) and SOD1 (Shibata et al., 1994). Moreover, accumulations of intermediate filament proteins are found in hyaline conglomerate inclusions and in axonal 'spheroids' in spinal cord motor neurons

(Corbo and Hays, 1992) as well as in pyramidal cells of the motor cortex (Troost et al., 1992) in ALS postmortem tissue.

Additionally, Bunina bodies, which are cystatin C-containing inclusions, are found in the cell bodies of motor neurons in ALS (Okamoto et al., 1993; Sasaki and Maruyama, 1994). These are now thought to be less specific for ALS than the ubiquitinated and neurofilamentous inclusions, as they are similar to structures found in neurons of aged rats and humans (Kusaka, 1999). Other neuropathological features of ALS include fragmentation of the Golgi apparatus (Gonatas et al., 1998), mitochondrial vacuolization (Okamoto et al., 1990) and ultrastructural abnormalities at synaptic terminals (Sasaki and Iwata, 1996).

1.2. Familial ALS and SOD1 mutations

1.2.1. Heterogeneity of fALS

As indicated above, fALS, which makes up about 10% of all ALS cases, is often inherited in an autosomal dominant manner, though rarer cases of autosomal recessive and X-linked disease do exist (Ince et al., 2011). fALS is genetically heterogeneous including 15 mapped loci and more than 10 identified causative genes. These genes are represented in Table 1.1 and include SOD1, TAR DNA binding protein (TARDBP) and 'fused in sarcoma' (FUS).

Table 1.1: ALS-associated genes

Gene Locus	Chromosomal locus	Gene	Onset/Inheritance	References
ALS1	21q22.1	SOD1	Adult/AD	(Rosen et al.,

				1993)
ALS2	2q33.2	Alsin	Juvenile/AR	(Hadano et al., 2001)
ALS3	18q21	Not identified	Adult/AD	(Hand and Rouleau, 2002)
ALS4	9q34	SETX	Juvenile/AD	(Chen et al., 2004)
ALS5	15q21.1	SPG11	Juvenile/AR	(Orlacchio et al., 2010)
ALS6	16p11.2	FUS	Adult/AD	(Kwiatkowski et al., 2009; Vance et al., 2009)
ALS7	20p13	Not identified	Adult/AD	(Sapp et al., 2003)
ALS8	20q13.3	VAPB	Adult/AD	(Nishimura et al., 2004)
ALS9	14q11.2	ANG	Adult/AD	(Greenway et al., 2006)
ALS10	1p36.2	TARDBP	Adult/AD	(Sreedharan et al., 2008)
ALS11	6q21	FIG4	Adult/AD	(Chow et al., 2009)
ALS12	10p15-p14	OPTN	Adult/AD & AR	(Maruyama et al., 2010)
ALS13	12q24	ATXN2	Adult/AD	(Elden et al., 2010)
ALSX	Xp11-q12	UBQLN2	Adult/X-linked	(Deng et al., 2011)
ALS-FTD	9q21-q22	Not identified	Adult/AD	(Hosler et al., 2000)

ALS + FTD	9p13.2-p21.3	C9ORF72	Adult/AD	(DeJesus-Hernandez et al., 2011; Renton et al., 2011; Vance et al., 2009)
FTD + FTD	9p13	SIGMAR1	Adult/AD	(Luty et al., 2010)
ALS + Dementia + PD	17q21	MAPT	Adult/AD	(Hutton et al., 1998)

All of the ALS and ALS-FTD associated genes identified to date, which account for, at most, 25-30% of all fALS cases (Andersen and Al-Chalabi, 2011; Ince et al., 2011). Please see the text for the extension of the gene names, as well as their function and types of mutations. AD, autosomal dominant; AR, autosomal recessive; FTD, frontotemporal dementia; PD, Parkinson's disease.

However, all of these ALS-associated genes identified to date can account for, at most, 25-30% of all cases of fALS keeping the doors open for a lot more discoveries in the genetics of the disease (Andersen and Al-Chalabi, 2011). Below is a selection of the most important genes followed by a review of mutations in SOD1.

1.2.1.1. Alsin (ALS2)

Alsin is a GTPase regulator, whose recessive mutations cause a slowly progressive, juvenile-onset, upper motor neuron-phenotype disease (Hadano et al., 2001).

1.2.1.2. Senataxin (SETX)

SETX is presumed to be involved in RNA processing. While the dominantly inherited missense mutations cause a young onset, very slow evolving form of ALS (Chen et al., 2004), recessive

mutations of SETX can result in ataxia, oculomotor apraxia type 2, axonal sensorimotor neuropathy, or a hereditary motor neuropathy (Moreira et al., 2004).

1.2.1.3. TAR DNA binding protein (TARDBP)

The discovery of neuronal cytoplasmic inclusions containing TDP-43 in patients with ALS or frontotemporal dementia prompted the analysis of TARDBP, the gene that encodes the TDP-43 protein, in fALS families. TARDBP mutations have been reported in 4-6% of fALS cases without SOD1 mutations and in 0-2% of diagnosed sALS cases (Andersen and Al-Chalabi, 2011).

Under normal circumstances, TDP-43 is involved in RNA processing, gene splicing, transcription regulation, and mRNA modulation (Van Deerlin et al., 2008). The mutations in TARDBP are found to result in redistribution of TDP-43 from the nucleus to the cytoplasm in neurons and glia in the spinal cord. Masu *et al.* (2009) and Nishimura *et al.* (2010) argue that the mislocalization of TDP-43 and impaired TDP-43 trafficking, due to mutations in TARDBP, might be the cause of the motor neuron toxicity. To test this hypothesis, Wegorzewska *et al.* (2011) created transgenic mice expressing a mutated human TDP-43 that causes fALS. These mutant mice develop a clinical syndrome similar to human ALS, including ubiquitinated aggregate pathology with selective vulnerability of cortical upper motor neurons and spinal motor neurons, increase in astrocyte and microglia activation in cortical layer 5, and loss of spinal motor neurons, axons and muscle fibers at end-stage (Wegorzewska et al., 2009). However, this animal model does not mimic the disease as well as the SOD1 models do. The differences between these models include the lack of cytoplasmic aggregates of TDP-43, the loss of approximately 20% versus 50% spinal motor neurons at end-stage, and the appearance of

cortical and descending corticospinal tract pathology before developing lower motor neuron degeneration in mutant TDP-43 mice versus mutant SOD1 mice (Wegorzewska et al., 2009). Due to these differences, the TDP-43 model is not as well studied as the SOD1 model, which will be discussed in more detail later in the chapter.

1.2.1.4. 'Fused in Sarcoma' (FUS)

The FUS protein resembles TDP-43 with functions involved in alternative splicing, genomic maintenance, and transcription factor regulation. FUS mutations are found in 4-6% of fALS and 0.7-1.8 of sALS cases (Kwiatkowski et al., 2009; Vance et al., 2009). Pathological findings of neuronal cytoplasmic accumulation of FUS protein, in the absence of TDP-43 staining, have been found in patients with FUS mutations. However, it is unclear whether the toxicity in mutant FUS cases is mediated through abnormal RNA modulation and metabolism, or by mislocalization of protein in the cell. Together, the discovery of mutations in TDP-43 and FUS has directed the focus of ALS research towards the roles played by RNA metabolism and processing in this disease.

1.2.1.5. VAMP-associated protein type B (VAPB)

VAPB is involved in intracellular membrane transportation and is primarily located in the endoplasmic reticulum (ER). A mutation of this gene induces the formation of insoluble cytoplasmic aggregates containing the mutant protein (Nishimura et al., 2004).

1.2.1.6. Angiogenin (ANG)

ANG shares a metabolic pathway with vascular endothelial growth factor (VEGF), which is implicated in ALS (Greenway et al., 2006). So far, 17 ANG missense mutations have been found as rare causes of ALS.

1.2.1.7. Optineurin (OPTN)

While mutations in OPTN were initially reported in primary open angle glaucoma and ataxia patients, Maruyama *et al.* (2010) identified three mutations in patients with fALS or sALS, including both autosomal dominant and autosomal recessive mutations. One of these mutations was associated with OPTN cytoplasmic inclusions, where the authors found that TDP-43 and SOD1 inclusions of sALS and SOD1-associated ALS were also immunolabeled by OPTN antibodies. This implied the possibility of a shared pathogenesis between sALS and fALS. Additionally, the authors demonstrated that the nonsense and missense mutations of OPTN eliminated the inhibitory role of nuclear factor kappa B (NF-κB), which is an oxidative stress transcription factor involved in regulating neuronal cell death and inflammation. These results suggested that NF-κB might be a therapeutic target for ALS. This will be discussed further in the later stages of this thesis.

1.2.1.8. Ataxin-2 (ATXN2)

While CAG-trinucleotide repeat expansion in the ATXN2 gene to 34 or more repeats is associated with spinocerebellar ataxia type 2, intermediate-length polyQ expansion (27-33 repeats) on one allele of ATXN2 has been found to be a significant risk factor for ALS in North American patients (Elden et al., 2010).

1.2.1.9. The 9p21 locus (C9ORF72)

Most recently, $(GGGGCC)_n$, a massive hexanucleotide-repeat expansion in the intron between noncoding exons 1a and 1b of the uncharacterized gene C9ORF72, has been found to be an ALS causative gene (DeJesus-Hernandez et al., 2011; Renton et al., 2011). While normal individuals have, at most, 23 repeats, individuals with ALS or frontotemporal dementia can have up to 1,600 repeats. Moreover, this expansion seems to account for a significant portion of fALS and sALS cases, about 40% of fALS and 7-10% of sALS cases (Morris et al., 2012), and thus far, is more represented than any of the other identified genes, which makes this gene a very promising one for further study.

1.2.2. SOD1 mutations

SOD1 is a 153-amino acid, abundant, ubiquitously expressed homodimeric cytosolic enzyme whose only known activity is to dismutate superoxide to hydrogen peroxide (Longo et al., 1996). Catalysis by SOD1 is mediated in two asymmetric steps by an essential copper atom, which is alternately reduced and oxidized by superoxide. Two other types of superoxide, mitochondrial SOD2 and extracellular SOD3, exist, but thus far, no mutations in these isoforms have been described (Cleveland and Rothstein, 2001).

Mutations in SOD1 are the most common in fALS, accounting for about 20% of the cases (Rosen et al., 1993). So far, more than 150 mutations have been found in SOD1 along the peptide sequence causing the mutant protein to misfold and accumulate [Figure 1.3] (http://alsod.iop.kcl.ac.uk/). All of these mutations give rise to a very similar disease phenotype in humans, even though the disease duration and age at onset may vary among patients with

Figure 1.3: ALS-causing mutations lie throughout the SOD1 polypeptide

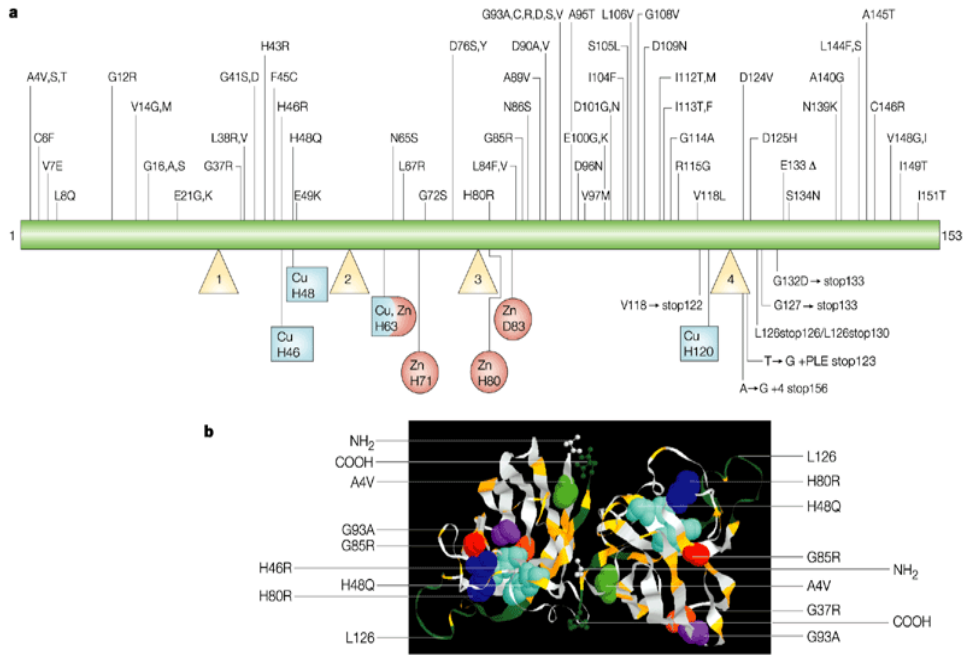

(A) Well-known mutations in the 153-amino-acid SOD1 polypeptide that cause ALS; and (B) their positions in the three-dimensional structure of crystallized human SOD1. (Cleveland and Rothstein, 2001)

different SOD1 mutations (Cudkowicz et al., 1997). Moreover, these SOD1 mutations, which are present at birth and are ubiquitously expressed in all tissues, produce a rapidly progressive adult-onset degenerative disease in which motor neurons are the primary cell types affected.

1.2.2.1. Causative hypotheses

Several hypotheses have been proposed to provide an explanation of how a multitude of mutations in SOD1 can give rise to the same ALS-like phenotype. Some of these hypotheses are discussed below.

1.2.2.1.1. Conformational changes

The first hypothesis is that most, if not all, of the known SOD1 mutations lead to a relaxed conformation of the protein. These less-tightly folded enzymes thus catalyze aberrant copper-mediated chemistry either by allowing oxidation of aberrant substrates (i.e. substrates that normally will never gain access to the catalytic site) or by handling the copper clumsily and frequently releasing it. The latter might allow free copper to catalyze unwanted oxidative reactions, which might result in oxidative stress-linked toxicity. Although *in vitro* findings supporting the oxidative stress hypothesis exist in the literature (Goto et al., 2000), three lines of evidence continue to offer strong evidence against the primary toxicity of SOD1 mutants arising from aberrant oxidative chemistry: (a) the insensitivity of toxicity to the level of SOD1 activity (Bruijn et al., 1998); (b) the undiminished toxicity despite lower copper loading *in vivo* in mice (Subramaniam et al., 2002); and (c) the paucity of evidence for increased markers of oxidative damage in SOD1-mediated human disease (Bowling et al., 1993; Ferrante et al., 1997) and in mutant SOD1 mouse models (Williamson et al., 2000).

1.2.2.1.1. Loose zinc binding

A second hypothesis is that mutant SOD1 binds to structural zinc less effectively than wild-type SOD1. Mutant SOD1 depletion of zinc in primary motor neurons was found to provoke rapid neuronal death in a manner that is dependent on neuronal nitric oxide synthase, accompanied by elevated levels of protein-bound nitrotyrosine (Estevez et al., 1999). However, this view remains controversial as it is unclear how all of the 150 different mutations can affect the binding of zinc. Moreover, *in vivo* studies have shown that limiting nitric oxide production either by ablating or inhibiting neuronal nitric oxide synthase provides marginal benefit to transgenic mice expressing

mutant SOD1 (Facchinetti et al., 1999), suggesting that the disease pathology observed in these mice is not caused by the mutant SOD1 depletion of zinc in motor neurons. Additionally, tyrosine nitration of proteins was not detected in $SOD1^{G37R}$ and $SOD1^{G85R}$ mutant mice (Bruijn et al., 1997; Williamson et al., 2000).

1.2.2.1.3. Propensity to aggregate

Mutant SOD1 misfolding results in cytoplasmic ubiquitin-positive protein aggregates that are potentially toxic for motor neurons. This pathological characteristic is also visible in sALS cases. One study has shown that forced expression of SOD1 mutants by microinjection provokes mutant-dependent aggregates selectively in motor neurons, but not in sensory or hippocampal neurons, followed by cell death (Bruening et al., 1999; Durham et al., 1997). Moreover, aggregates as well as acute toxicity can be ameliorated by elevating the level of the protein-folding chaperone HSP70 (Bruening et al., 1999). These *in vitro* findings highly support the hypothesis of toxicity arising from mutant-mediated protein misfolding.

Regardless of which of the above hypotheses may be correct, it seems certain that the changes that occur in SOD1 caused by mutations provoke the demise of motor neurons, not through a loss-of-function, but rather through a gain-of-function effect. The most salient arguments in favor of this assertion are the following. Although SOD1 is thought to be essential for living organisms (Halliwell and Gutteridge, 1991), mutant mice deficient in this enzyme thrive and do not develop an ALS phenotype (Reaume et al., 1996). In contrast, transgenic rodents expressing either catalytically active SOD1 mutations (Gurney et al., 1994; Wong et al., 1995) or catalytically inactive SOD1 mutations (Bruijn et al., 1997; Wang et al., 2003) mimic the

clinical and neuropathological hallmarks of ALS. Furthermore, transgenic mice expressing high levels of wild-type human SOD1 are healthy (Gurney et al., 1994) and co-overexpression of mutant SOD1 with wild-type human SOD1 does not lead to the rescue of the paralytic phenotype (Bruijn et al., 1998).

1.2.3. Mode of action of mutant SOD1 and current *in vitro* models of ALS:

To date, it has been proposed that mutant SOD1 cytotoxity involves a number of different mechanisms, such as oxidative stress (Wiedau-Pazos et al., 1996; Yim et al., 1996), protein aggregation (Durham et al., 1997), aberrant protein-protein interactions (Kunst et al., 1997), decreased binding affinity of zinc (Estevez et al., 1999), mitochondrial dysfunction (Liu et al., 2004), excitotoxicity (Plaitakis and Caroscio, 1987), glutamate transporter failure (Rothstein et al., 1992), endoplasmic reticulum stress (Kikuchi et al., 2006; Saxena et al., 2009), and apoptosis (Kostic et al., 1997) none of which are mutually exclusive. Some of these proposed mechanisms are described, in more detail, below:

1.2.3.1. Oxidative stress

The proposed mechanism on how mutant SOD1 can result in oxidative stress is already explained in the section above. Moreover, it has been found that extracellular mutant SOD1 causes injury to and death of motor neurons in the presence of microglia (Zhao et al., 2010). In tbe light of the existing data collected so far, it can be concluded that while oxidative stress is one of the major characteristics of ALS pathogenesis, it may not be the primary cause of mutant SOD1 toxicity on motor neurons.

1.2.3.2. Mitochondrial dysfunction

Another proposed mechanism is that misfolded SOD1 damages mitochondria by being deposited onto the cytoplasmic face of the outer membrane of the mitochondria in spinal cord (Israelson et al., 2010; Liu et al., 2004). ATP levels have also been reported to be decreased in spinal cords of presymptomatic and symptomatic transgenic mutant SOD1 mice (Browne et al., 2006; Mattiazzi et al., 2002). It has also been shown that ALS mitochondria are degenerated with an altered ultrastructure and impaired dynamics (Magrane et al., 2009). More recently, Magrane *et al.* (2012) followed mitochondria in mutant SOD1-expressing motor neurons using a mitochondria-targeted fluorescent probe and found that mitochondrial dynamics alterations and bioenergetics dysfunctions work together in triggering synaptic alterations in mutant SOD1-expressing motor neurons. Moreover, mitochondrial dysfunction seems not to be limited to neurons as this has also been observed in mutant SOD1 astrocytes (Cassina et al., 2008). These findings suggest that not only mitochondrial dysfunction is a key feature of mutant SOD1 disease pathogenesis, but might also have a contributory role in motor neuron degeneration during the disease process.

1.2.3.3. Glutamate Excitotoxicity

Glutamate excitotoxicity, the excessive firing of motor neurons due to failure to remove synaptic glutamate, is observed both in transgenic mutant SOD1 mouse models, and in fALS and sALS patient samples (Ilieva et al., 2009). The first evidence of abnormalities in glutamate handling in ALS came from the discovery of large increases in the levels of glutamate in the cerebrospinal fluid of ALS patients (Rothstein et al., 1990; Shaw et al., 1995), which is now reported in about

40% of sALS patients (Spreux-Varoquaux et al., 2002). These findings were followed by a significant elevation of extracellular central nervous system glutamate levels in transgenic ALS mice (Alexander et al., 2000).

Furthermore, mutant SOD1 expression correlates well with disturbances in glutamate transmission in transgenic ALS mice, where loss of excitatory amino acid transporter 2 (EAAT2) protein expression, the main glutamate transporter in astrocytes responsible for 90% of the total glutamate uptake, was found in spinal cords from $SOD1^{G85R}$ mice (Bruijn et al., 1997). This study led to the proposal that impaired glutamate uptake in transgenic ALS mice might cause excitotoxic killing of motor neurons. However, it was not clear in the study whether the loss of expression of EAAT2 was due to the loss of the protein or to the lack of recognition by its antibodies. In favor of the loss of EAAT2 protein expression hypothesis, aberrant editing of mRNA was observed, which was suggested to lead to aberrant EAAT2 synthesis. Moreover, the astrocytic overexpression of EAAT2 was found to rescue motor defects and neurodegeneration, but not lifespan in transgenic mutant SOD1 mice (Guo et al., 2003). In contrast, the Shaw group found that the two splice forms of EAAT2 RNA that have been reported to account for the EAAT2 protein loss are not expressed significantly more in ALS patients than in controls, indicating that the involvement of EAAT2 transcripts in ALS is not primary (Meyer et al., 1999). Finally, it was found that the partial disruption of endogenous EAAT2 in transgenic mutant SOD1 mice potentiated neuronal loss and slightly worsened mortality (Pardo et al., 2006). All of these outcomes support a secondary and modifying role for EAAT2 in motor neuron degeneration through its loss in mutant SOD1-expressing astrocytes.

Another hypothesis about the role of glutamate transporters in the ALS disease process comes from the Trotti group, where the group argues that glutamate transporters might be

present, but hypofunctional due to post-translational damage (Trotti et al., 2001). While different studies point to a defect in EAAT2 in ALS, it remains unclear whether this alteration is a cause or a consequence of the disease, and whether the EAAT2 defect may have any pathogenic significance. This is because other glutamate transporters that are presumably not affected in ALS are also expressed by both astrocytes and neurons.

1.2.3.4. Endoplasmic reticulum stress

It is also believed that some misfolded proteins, such as mutant SOD1, are sent to the endoplasmic reticulum (ER), even though they lack the proper signal peptide for the translocation. The excess of misfolded proteins in the ER may cause an ER-associated protein degradation response, which leads to ER-stress. This stress, in turn, may activate ER stress-related cell death signaling pathways, including apoptosis (Kikuchi et al., 2006). Consistent with these findings, the Caroni group (this study will be discussed, in more detail, in "Selective degeneration of motor neurons in ALS" section of this chapter) has found an up-regulation of ER stress-related genes in vulnerable motor neurons of presymptomatic transgenic mutant SOD1 mice (Saxena et al., 2009).

1.2.3.5. Apoptosis

Despite considerable efforts, the initial noxious signal linking mutant SOD1 to known downstream death-related molecular pathways, such as apoptosis, remains mysterious. Over the years, various attempts have been made to unravel such initial signals using *in vitro* models of motor neuron degeneration for SOD1-linked ALS. However, under basal culture conditions, the expression of mutant SOD1 did not induce, by itself, any detectable cell death in primary motor

neurons isolated from transgenic mutant SOD1 animals (Kuo et al., 2004; Raoul et al., 2002). It only triggered some morphological and electrophysiological abnormalities and minimal cell death in models of stably transfected motor neuron cell lines (Maxwell et al., 2004; Pasinelli et al., 1998; Sathasivam and Shaw, 2005). To circumvent this problem, different strategies have been tried to challenge motor neuron survival with stressors that presumably mimic aspects of the disease. For instance, mutant SOD1-expressing cell lines were challenged by serum starvation (Sathasivam and Shaw, 2005), enzymatically-induced oxidative stress (Pasinelli et al., 1998), or toxins, such as cyclosporin A (Maxwell et al., 2004). Similarly, mutant SOD1-expressing primary motor neurons were challenged by Fas, nitric oxide (Raoul et al., 2002) or excitotoxins like kainate (Spalloni et al., 2004). In all of these studies, the challenged mutant cells showed an increased vulnerability compared to the cells expressing human wild-type or endogenous forms of SOD1. In addition to these interventions, there has been a significant amount of interest in the field to find models that are pathogenically and pathologically similar to ALS and specific to motor neurons.

1.2.4. Transgenic mutant SOD1 animal models

So far, the majority of ALS research has focused on transgenic rodents expressing mutant SOD1, since sALS and fALS are clinically and pathologically almost indistinguishable from each other. At present, there are 12 different human SOD1 mutations expressed in mice [Table 1.2] (Turner and Talbot, 2008). These include 9 missense and 3 C-terminal truncated variants. Among these, transgenic $SOD1^{G93A}$ mice are the most commonly used mouse model in ALS research, followed by $SOD1^{G37R}$, $SOD1^{G85R}$, and $SOD1^{G86R}$ rodents. These mutants either are abundantly expressed,

stable, and active (such as in $SOD1^{G93A}$ and $SOD1^{G37R}$) or marginally expressed, and unstable with negligible activity (such as in $SOD1^{G85R}$) in the central nervous system.

Table 1.2: Transgenic mutant SOD1 mouse models

SOD1 mutant	SOD1 activity (fold)	Disease onset (months)	Disease duration (months)	References
$SOD1^{A4Va}$	nd	8	3	(Deng et al., 2006)
$SOD1^{G37R}$	14.5	4-6	nd	(Wong et al., 1995)
$SOD1^{H46R}$	nd	5	1	(Chang-Hong et al., 2005)
$SOD1^{H46R/H48Q}$	0	4-6	nd	(Wang et al., 2002)
SOD1 H46R/H48Q/H63G/H120G	0	8-12	nd	(Wang et al., 2003)
$SOD1^{L84V}$	nd	5-6	1	(Tobisawa et al., 2003)
$SOD1^{G85R}$	0	8-14	0.5	(Bruijn et al., 1997)
$SOD1^{G86R}$	0	3-4	1	(Ripps et al., 1995)
$SOD1^{D90A}$	6-8	12	2	(Jonsson et al., 2006)
$SOD1^{G93A}$	11	3-4	1-2	(Gurney et al., 1994)
$SOD1^{I113T}$	nd	12	2	(Kukigawa,

				2000)
SOD1^{L126X}	nd	7-9	nd	(Wang et al., 2005a)
	nd	11	0.75	(Deng et al., 2006)
SOD1^{L126delTT}	0	15	1	(Watanabe et al., 2005)
SOD1^{G127X}	0	8	0.25	(Jonsson et al., 2004)

The information about all of the existing transgenic mutant SOD1 mouse models; taken from the review of Turner and Talbot (2008). Please see text for more information on the clinical and neuropathological characteristics of these mice. nd, not described.

The time course of clinical and neuropathological features of transgenic SOD1^{G93A} mice is summarized in Figure 1.4. These mice develop hindlimb tremors and muscle weakness around 90 days detected by locomotor deficits, progressing to paralysis and premature death at around 120-140 days (Gurney et al., 1994). Pathologically, neuromuscular junctions degenerate at around 47 days of age, in a manner that is selective for fast-fatigable motor units (Fischer et al., 2004; Pun et al., 2006). Moreover, proximal axonal loss is prominent after 80 days of age, coinciding with motor impairment. This is followed by about 50% loss of lower motor neurons after 100 days of age (Fischer et al., 2004). Pathological features of spinal motor neurons include mitochondrial vacuolization (Dal Canto and Gurney, 1995), Golgi apparatus fragmentation (Mourelatos et al., 1996), neurofilament-positive inclusions (Tu et al., 1996), and cytoplasmic SOD-immunoreactive aggregates (Johnston et al., 2000). Spinal cords are also characterized by astrocytosis and microgliosis around symptom onset (Hall et al., 1998). Similar features are observed in transgenic SOD1^{G37R} mice and in transgenic SOD1^{G85R} mice, but with a much later

disease onset and much shorter disease duration for SOD1^{G85R} mice. [Table 1.2] (Bruijn et al., 1997).

Figure 1.4: Time course of clinical and neuropathological events in transgenic mutant SOD1^{G93A} mice

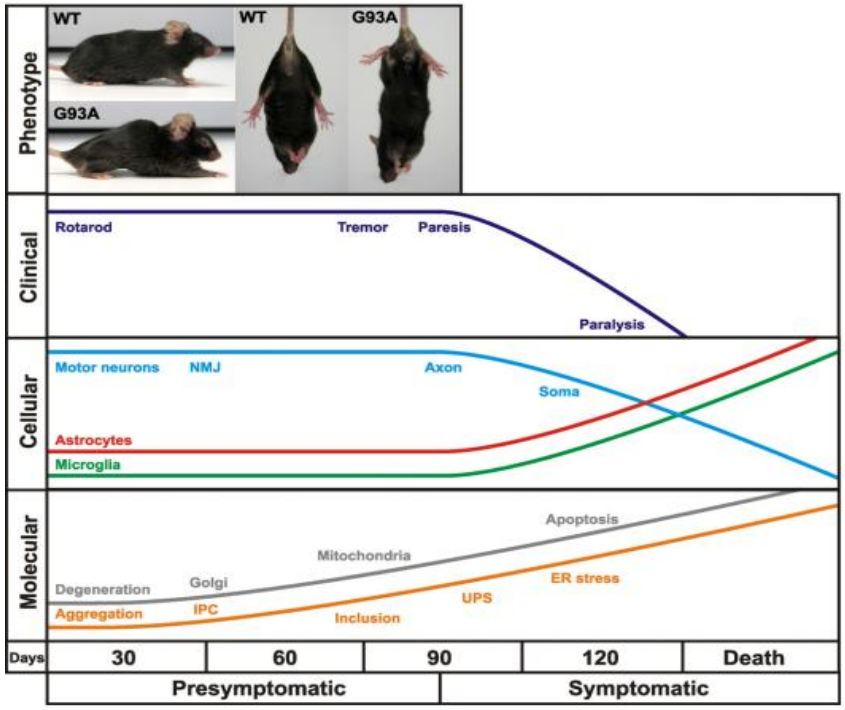

Mice develop hindlimb tremor, weakness, and locomotor deficits at about 90 days, which is preceded by distal synaptic and axonal degeneration. These symptoms are followed by fatal paralysis about 1 month later concomitant with spinal motor neuron loss and reactive gliosis. *IPC: insoluble protein complexes; NMJ: neuromuscular junction; UPS: ubiquitin-proteasome system.* (Guégan et al., 2001; Turner and Talbot, 2008)

Despite the close similarities between the phenotype of transgenic mice expressing mutant SOD1 and human ALS patients, including the early and specific neurodegeneration of corticospinal motor neurons and related subcerebral projection neurons (Ozdinler et al., 2011), the animal model differs from the human disease in few ways: First, vacuolar degeneration, which is seen in transgenic mice, has not been a well-established pathology of motor neurons from ALS patients. And second, neurofilamentous accumulation in cell bodies and proximal axons is infrequent in transgenic rodents, but is more prominent in ALS patients. Regardless of

these limitations, however, transgenic mutant SOD1 rodents are excellent experimental models of ALS, which have been used in most of the ALS research so far in understanding the biology and pathogenesis of the disease.

1.3. Motor neuron death in ALS

1.3.1. Death mechanism in transgenic mutant SOD1 animals

One of the main features of ALS that have been studied in transgenic mutant SOD1 mouse models has been the mechanism by which motor neurons die. Whether motor neurons die by apoptosis, which is a form of programmed cell death – whose morphological hallmarks include cytoplasmic and nuclear condensation, compaction of nuclear chromatin into circumscribed masses along the inside of the nuclear membrane, and structural preservation of organelles (Guégan and Przedborski, 2003) – has been an important question in the field. In transgenic mutant SOD1 animals, dying neurons were found to be atrophic with large vacuoles in the cytoplasm due to dilated rough ER, Golgi apparatus, and mitochondria (Dal Canto and Gurney, 1995).

Ultrastructural studies from our laboratory have shown that sick neurons in transgenic mutant SOD1 mice have diffusely condensed cytoplasm and nuclei with irregular shapes (Guégan and Przedborski, 2003). While apoptotic cells are observed in the anterior horn of end-stage transgenic $SOD1^{G93A}$ mice [Figure 1.5a], they are rare in number. These results suggest that neuronal cells die by apoptosis in transgenic mutant SOD1 animals. However, apoptosis, since it is observed as being rare in number, may not be the only form of cell death observed in motor neurons. Also, apoptotic markers are known to be short-lived, and thus, might not be sufficient to tell which form of death motor neurons go through.

Figure 1.5: Illustration of apoptosis in spinal cord of transgenic mutant SOD1^{G93A} mice

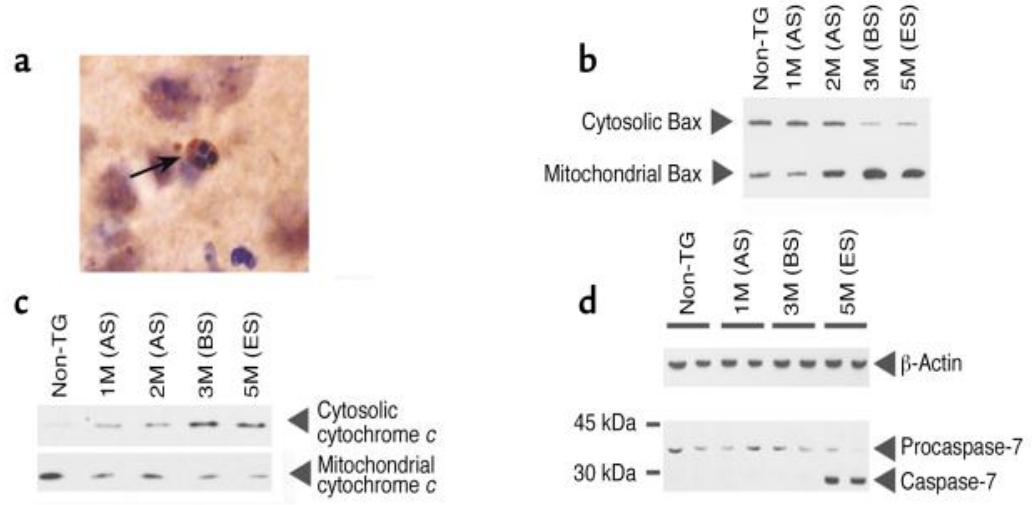

(A) Apoptotic cells found in the anterior horn of an end-stage transgenic mutant SOD1^{G93A} mouse; (B) Western blot analysis of spinal cord extracts shows the relocation of Bax from the cytosol to the mitochondria over the course of the disease, suggesting an increase in the active form of pro-apoptotic Bax; (C) Coincidental changes of cytochrome *c* in the opposite direction; (D) Effector caspases, such as caspase-7, are activated later in the disease process. *1M (AS): 1 month, asymptomatic stage; 2M (AS): 2 months, asymptomatic stage; 3M (BS): 3 months, beginning of symptoms; 5M (ES): 5 months, end stage; Non-TG: non-transgenic littermates.* Taken from Guegan *et al.* (2003)

Besides exhibiting certain morphological features, apoptotic cells also activate various molecular pathways, including the Bcl-2 family and the caspases. In human ALS cases and transgenic SOD1^{G93A} mice, anti-apoptotic Bcl-2 mRNA expression is significantly decreased and pro-apoptotic Bax mRNA is increased in the lumbar spinal cord compared to controls (Mu et al., 1996; Vukosavic et al., 1999). In addition, our group has observed an increase in the expression of the active form of Bax (i.e. translocation of Bax from cytosol to mitochondria) over the course of the disease process (Guégan and Przedborski, 2003) [Figure 1.5b]. Moreover, overexpression of Bcl-2 has been found to mitigate neurodegeneration and to prolong survival in transgenic SOD1^{G93A} mice (Kostic et al., 1997). Interestingly, a study crossing Bax-deficient mice with transgenic SOD1^{G93A} mice found that Bax deletion does not prevent neuromuscular denervation or mitochondrial vacuolization. However, it completely rescues motor neurons from death,

mildly extends lifespan (mean = 157 ± 9 days versus 137 ± 7 days) and delays motor dysfunction (136 ± 13 days versus 119 ± 11 days) in Bax-deficient/mutant SOD1 mice (Gould et al., 2006). This study suggested a complete dissociation between motor neuron death and motor dysfunction in ALS. In a subsequent study, Reyes *et al.* (2010) bred conditionally-deficient, in the central nervous system, *Bax* and *Bak* mice with transgenic $SOD1^{G93A}$ mice, and found that the neuronal deletion of *Bax* and *Bak* prevented motor neuronal loss and axonal degeneration, delayed onset of motor manifestations (167 ± 8 days versus 139 ± 4 days), and extended survival (136 ± 5 days versus 111 ± 4 days). Collectively, the above data support the idea that the apoptotic machinery contributes to the natural course of the ALS-like phenotype in transgenic mutant SOD1 mice.

Similarly, our group has found increased content of pro-apoptotic cytosolic cytochrome *c* and active caspase 7 in transgenic $SOD1^{G93A}$ mice over the course of the disease, but only after the onset of paralysis (Guégan and Przedborski, 2003) [Figure 1.5c-d respectively]. Consistent with these results has been the finding showing that the prevention of mitochondrial cytochrome *c* release lengthens the lifespan of transgenic $SOD1^{G93A}$ mice (Zhu et al., 2002).

1.3.2. Differential susceptibility of spinal motor neurons in ALS

While studying transgenic mutant SOD1 animal models as a whole provides clues about the death mechanism motor neurons go through in ALS, it was only when motor neuron subtypes and pools were studied separately that the field began to learn about the different levels of susceptibility/resistance of spinal motor neurons. Spinal motor neurons segregate into three subtypes: alpha, beta, and gamma. Of these, the most abundant subtype, alpha-motor neurons, innervate contractile skeletal fibers and are classified according to the function of the fiber type that they innervate: fast-twitch fatigable (FF), fast-twitch fatigue-resistant (FR), and slow-twitch

fatigue-resistant (S) (Burke et al., 1973). In ALS, axons of FF motor neurons followed by FR motor neurons are far more likely to show degeneration than those of S motor neurons, many of which survive until the later stages of the disease (Fischer et al., 2004; Frey et al., 2000; Hegedus et al., 2007; Pun et al., 2006).

Following the different susceptibilities of spinal motor neuron subtypes, the Caroni group performed an *in vivo* longitudinal gene array study on lumbar motor neurons that are selectively vulnerable (VUL, i.e. the FF motor neurons) or resistant (RES, i.e. the FR and S motor neurons) (Saxena et al., 2009). This study revealed that the subtype-selective ER stress responses influence disease manifestations (Saxena et al., 2009). Indeed, in this study, it was shown that VUL motor neurons are selectively prone to ER stress and, in the gene array analyses, these motor neurons gradually up-regulate ER stress markers in mouse models of fALS. Moreover, the group showed that ubiquitin signals increase in both VUL and RES motor neurons 25-30 days before the earliest denervations, while an unfolded protein response (UPR) coupled with early stress management pathways is initiated only in VUL motor neurons followed by an abrupt down-regulation at age P30 [Figure 1.6]. Saxena *et al.* showed that this transition is followed by selective axonal degeneration and spreading of stress.

Moreover, salubrinal, a known inhibitor of eIF2α phosphatase enzymes, provided clear protection against axon pathology and neuromuscular denervation and delayed disease progression. In contrast, when the ER stress was increased chronically, a hastening of disease manifestations was noted. These results suggested that cell-type-selective ER stress responses influence the clinical manifestations and progression of the disease in fALS mouse models. Thus, these results support the subtype-selective vulnerability of motor neurons in ALS and the consensus that ER stress plays a role in the ALS disease process.

Figure 1.6: Early increase in stress and UPR pathways in vulnerable motor neurons in transgenic mutant SOD1 mice

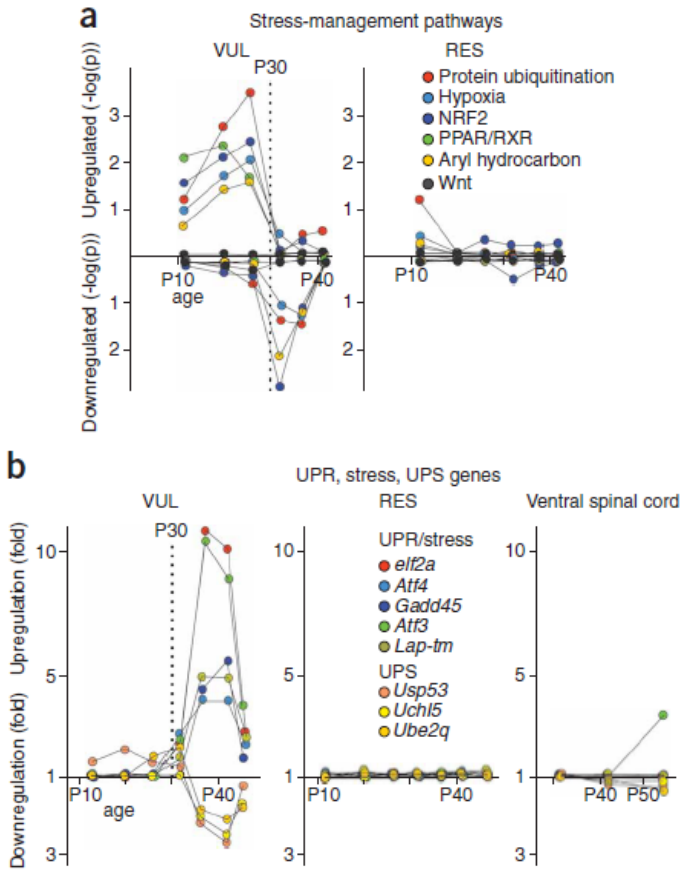

(A) Vulnerable (VUL) motor neurons exhibit an early up-regulation of stress management pathways, followed by their abrupt down-regulation at P30; (B) VUL motor neurons show an up-regulation of UPR- and stress-related genes and down-regulation of UPS-related genes from P32 on. Taken from Saxena *et al.* (2009)

Another example of degeneration occurring in a subset of motor neurons has been found by Raoul *et al.*, where the group demonstrated that about 50% death occurs in cultured primary spinal motor neurons through the activation of the Fas death receptor-mediated pathway involving two parallel death cascades [Figure 1.7a] (Raoul et al., 2002). This pathway includes the activation of the kinases ASK1 and p38, the transcription of neuronal nitric oxide synthase, and the up-regulation of Fas ligand [Figure 1.7b] (Raoul et al., 2006; Raoul et al., 2002). This group, along with others, suggested a role for this specific pathway in the cell-autonomous motor neuron degeneration in transgenic mutant SOD1 models due to the following findings: (1) Motor

neurons purified from mutant SOD1 embryos are 100-fold more sensitive to Fas activation than their control counterparts (Raoul et al., 2002); (2) Fas/nitric oxide pathway is up-regulated *in vivo* months before the onset of symptoms (Raoul et al., 2006; Veglianese et al., 2006; Wengenack et al., 2004); and (3) the administration of siRNA to Fas in transgenic mutant SOD1 mice extended lifespan in these mice (Locatelli et al., 2007).

Figure 1.7: Fas-mediated motor neuron death

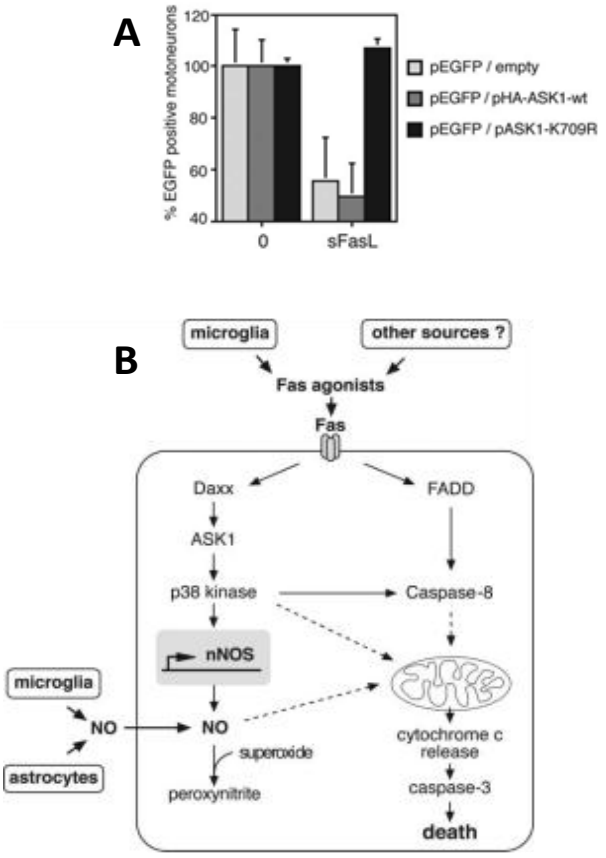

(A) When treated with Fas ligand (sFasL), EGFP positive motor neurons show about 50% loss after 48 hours in culture. Motor neurons are transfected with an expression vector coding for the EGFP (pEGFP) in combination with vectors coding for either an empty vector, wild-type HA-tagged ASK1 (pHA-ASK1), or the dominant-negative form of ASK1 (ASK1-K709R). Motor neurons that are treated with sFasL and transfected with dominant-negative vector showed a rescue of loss, suggesting that ASK1 is required for Fas-induced motor neuron death; (B) The schematic of the Fas-mediated death pathway that can be triggered by environmental stimuli. (Raoul et al., 2002)

1.3.3. Non-cell autonomous contribution to motor neuron death

Once the field discovered the selective susceptibility of motor neuron subtypes, one of the main questions became whether motor neurons die in a cell autonomous, i.e. damage within a selective population of cells alone is enough to produce disease (Ilieva et al., 2009), or non-cell autonomous manner. The Caroni group was the first to address this question. Here, this group utilized a Thy1 expression cassette to drive high constitutive expression of mutant SOD1 in postnatal motor neurons, including upper and lower motor neurons (Lino

et al., 2002). In this study, the group showed that restricted expression of mutant SOD1 in postnatal motor neurons did not cause motor neuron pathology or disease. Furthermore, the group produced double transgenic mice by crossing human SOD1 minigene G93A mice with Thy1-SOD1 G93A mice, which had about 2-fold higher SOD1 G93A expression in spinal cord than single transgenic mice. These double transgenic mice, however, did not exhibit any significant difference in the onset or progression of the disease (Lino et al., 2002). Assuming that the level of overexpression of mutant SOD1 was sufficient to bring about the ALS phenotype, this study suggests that the accumulation of mutant SOD1 primarily in postnatal motor neurons is necessary but not sufficient to induce motor neuron degeneration.

This study was followed a year later by that of a consortium of three laboratories, who generated different chimeric mice that were mixtures of normal and mutant SOD1-expressing cells (Clement et al., 2003). To assess whether mutant SOD1-expressing non-neuronal cells can influence neighboring wild-type neurons, these investigators analyzed spinal cord sections from the chimeric animals at end-stage and found ubiquitin-positive protein aggregates, which are an early sign of neuronal damage, in neuronal processes and, to a lesser extent, in cell bodies [Figure 1.8]. These ubiquitin-positive aggregates were not detected in neurons of wild-type mice. In the same study, the group also found that wild-type non-neuronal cells can mitigate the demise of mutant SOD1-expressing motor neurons compared to those in parental transgenic mutant SOD1 mice (Clement et al., 2003). This study was the first to show the non-cell autonomous contribution to motor neuron death in ALS. Subsequently, Yamanaka *et al.* (2008a) generated chimeric mice in which all motor neurons and oligodendrocytes expressed mutant SOD1 in a cellular environment containing variable numbers of wild-type non-motor neurons. In most of these chimeras, the presence of wild-type non-motor neurons significantly delayed the onset of

Figure 1.8: Non-cell autonomous damage caused by mutant SOD1 neighboring non-neuronal cells to motor neurons

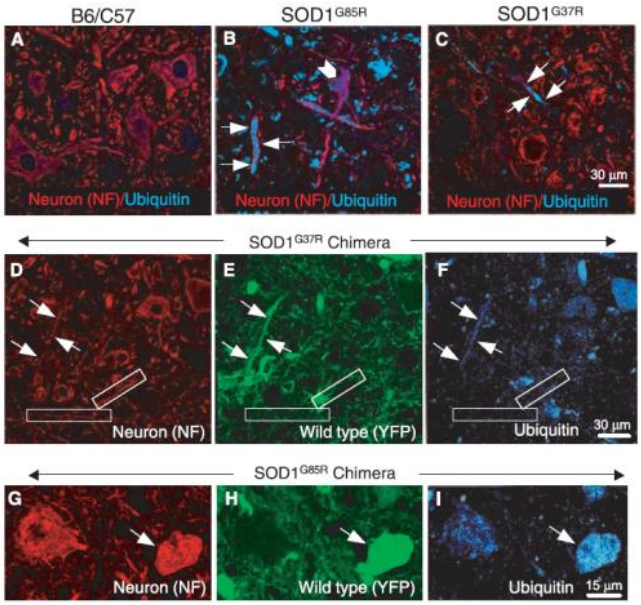

Confocal images of (A) wild-type; (B) $SOD1^{G85R}$; and (C) $SOD1^{G37R}$ mice spinal cord cross section lumbar regions are stained with neurofilament SMI32 (red), and ubiquitin (blue) antibodies. Ubiquitin-positive aggregates (arrows) are present in the cell bodies of mutant animals. (D-I) Arrows point to a wild-type axon or cell body (green) with elevated levels of ubiquitin compared with a mutant axon (boxed). Taken from Clement *et al.* (2003)

motor neuron degeneration, suggesting that symptom onset in ALS is a non-cell autonomous phenomenon.

1.3.4. ALS-linked astrocyte toxicity for motor neurons:

1.3.4.1. *In vitro:*

The studies discussed above were a breakthrough in the understanding of the ALS disease process because these investigators discovered the non-cell autonomous role of neighboring cells in ALS. However, none of these studies identified which of the neighboring cells are precisely responsible for the demise of motor neurons. The first group to address this question was the Barbeito group in 2005, who suggested that FGF-1, released by oxidative stress from motor neurons, might have a role in activating neighboring astrocytes, which could, in turn, initiate motor neuron apoptosis in ALS through a p75 low affinity neurotrophin receptor ($P75^{NTR}$)-dependent mechanism (Cassina et al., 2005). This study was the first one to suggest a non-cell autonomous role for astrocytes, the most abundant type of glia cells which, under healthy conditions, provide nutritional and structural support to motor neurons.

Expanding this study, the Przedborski group showed that mutant SOD1-expressing astrocytes release a factor that is selectively toxic to primary motor neurons using an *in vitro* co-culture model of motor neurons and glia (Nagai et al., 2007). Worth noting is the fact that, the group found that the expression of mutant SOD1 in primary mouse spinal motor neurons did not cause the demise of these cells up to 14 days in culture, but rather resulted in mild morphometric alterations [Figure 1.9a] (Nagai et al., 2007). Conversely, Di Giorgio *et al.* (2007), who used a very similar co-culture strategy as the Przedborski group, with the exception that their embryonic stem cell-derived motor neurons were kept *in vitro* for much longer period of time, found that the expression of mutant SOD1 in motor neurons was associated with a progressive loss of motor neurons [Figure 1.9b] (Di Giorgio et al., 2007). Regardless of the reasons for this apparent discrepancy, both studies agree on the fact that some non-cell autonomous mechanisms contribute to the demise of motor neurons in this *in vitro* model of ALS. Furthermore, the Przedborski group has shown that the toxicity of mutant astrocytes is specific for motor neurons [Figure 1.10a-b] and that not every type of cell expressing mutant SOD1, such as fibroblasts, can kill motor neurons [Figure1.10e]. Moreover, the group has found that medium conditioned

Figure 1.9: Mutant SOD1 astrocyte-derived toxicity for motor neurons

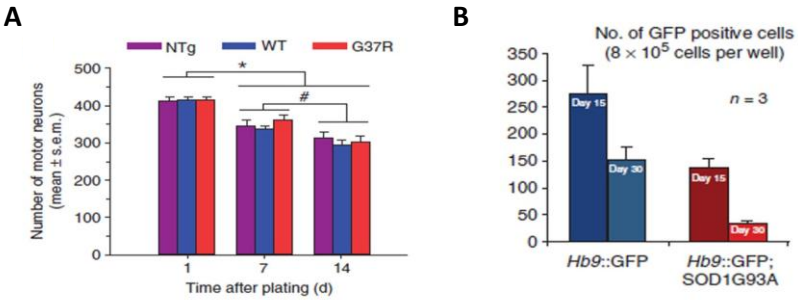

(A) The non-transgenic (NTg), transgenic wild-type SOD1 (WT), and transgenic mutant $SOD1^{G37R}$ (G37R) primary motor neurons (PMNs) show no difference in number after 1, 7, and 14 days *in vitro* (Nagai et al., 2007). (B) GFP^{+} motor neurons that derived from *Hb9::GFP:SOD1G93A* cells showed more loss over time than the neurons that derived from *Hb9::GFP* cells, suggesting a cell-autonomous contribution (Di Giorgio et al., 2007).

specifically with mutant SOD1-expressing astrocytes selectively kills motor neurons [Figure 1.10c-e].

Figure 1.10: Medium conditioned specifically with mutant SOD1-expressing astrocytes selectively kills motor neurons

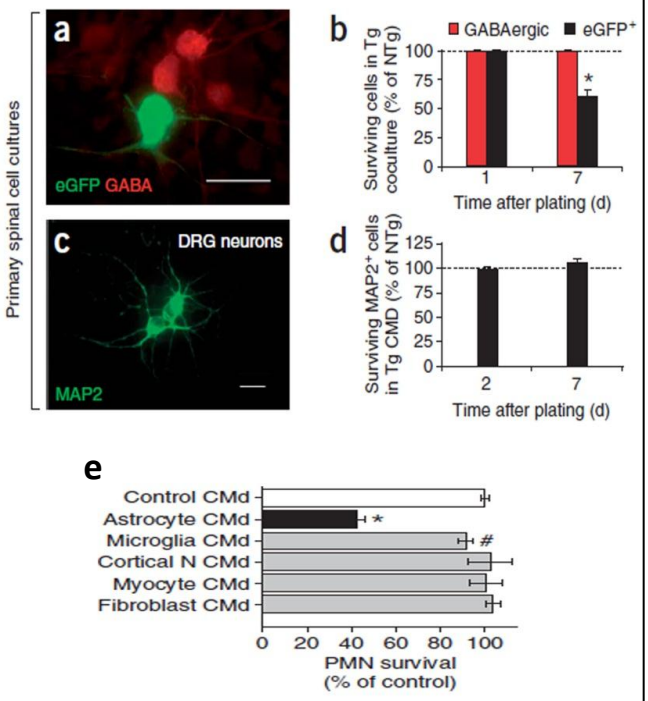

(A) Primary motor neurons (PMNs) on an astrocyte monolayers immunostained for eGFP and GABA at 7 days; (B) The percentage of surviving PMNs on mutant monolayers at 7 days is lower than that of GABAergic neurons; (C-D) The percentages of surviving Map2-positive DRG neurons exposed to conditioned medium (CMd) from mutant astrocytes at 2 versus 7 days are identical; (E) In comparison to CMd from mutant astrocytes, CMd from other mutant cells have no effect on PMN survival. (Nagai et al., 2007)

Following these studies, Xiao *et al.* (2007) tested the toxic effect of mutant SOD1-expressing microglia in co-culture with motor neurons. This group found that, following the activation with lipopolysaccharide, mutant microglia released more nitric oxide, more superoxide, and less insulin-like growth factor-1 than wild-type microglia. Moreover, the group showed that in co-culture, mutant microglia induced more motor neuron death, as well as decrease in neurite numbers and length, than do wild-type microglia. The group also observed, however, less than 20% motor neuron death, which was much less than the effect shown by our group with mutant SOD1-expressing astrocytes.

Advancing the investigation of the non-cell autonomous contribution of astrocytes in ALS, the Kaspar group generated astrocytes from postmortem tissue from both fALS and sALS patients. They showed, in co-culture and conditioned medium, that these astrocytes from both

patient groups were similarly toxic for motor neurons [Figure 1.11] (Haidet-Phillips et al., 2011). The group also demonstrated that the knock-down of SOD1 expression significantly attenuated astrocyte-derived motor neuron toxicity. This study was the first to indicate the role of astrocytes as a non-cell autonomous component in sALS.

Figure 1.11: Astrocytes derived from sALS and fALS patients cause motor neuron death *in vitro*

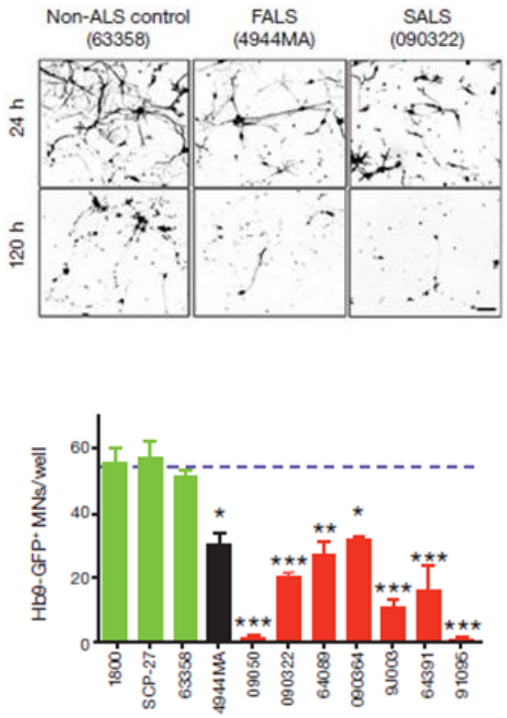

Motor neurons 24 or 120 hours after being exposed to medium conditioned with either non-ALS control, fALS or sALS astrocytes (Haidet-Phillips et al., 2011). Quantification of motor neurons shows that astrocytes derived from sALS or fALS patients are toxic for motor neurons. 1800, SCP-27 & 63358 are non-ALS control cell lines. (Scale bar, 100 µm)

1.3.4.2. *In vivo:*

The first study that investigated the non-cell autonomous contribution of mutant SOD1-expressing astrocytes *in vivo* came from Yamanaka *et al.*, where the group mated *loxSOD1*^{G37R} mice with mice carrying Cre recombinase driven by the GFAP promoter (Yamanaka et al., 2008b). The group found that the diminished mutant SOD1 expression in GFAP^{+} cells did not alter the age at onset of the motor manifestations, but did delay microglial activation and significantly slowed disease progression (Yamanaka et al., 2008b). While this study was a helpful first study to understand the effects of mutant astrocytes on the ALS disease process, it had one major pitfall: GFAP is a marker of reactive astrocytes that is known not to be robustly expressed *in vivo* before activation. In fact, in an *in vivo* gene array study performed by

the Barres group at Stanford University, GFAP has been found to be expressed rather weakly in the mouse brain (Cahoy et al., 2008). Aldh1l1, in the same study, on the other hand, was found to be the main marker for astrocytes. Thus, GFAP might not have been the best promoter to study the role of mutant SOD1 in astrocytes in this mouse model of ALS.

Figure 1.12: Focally-transplanted astrocytes are neuroprotective in mutant SOD1 rats

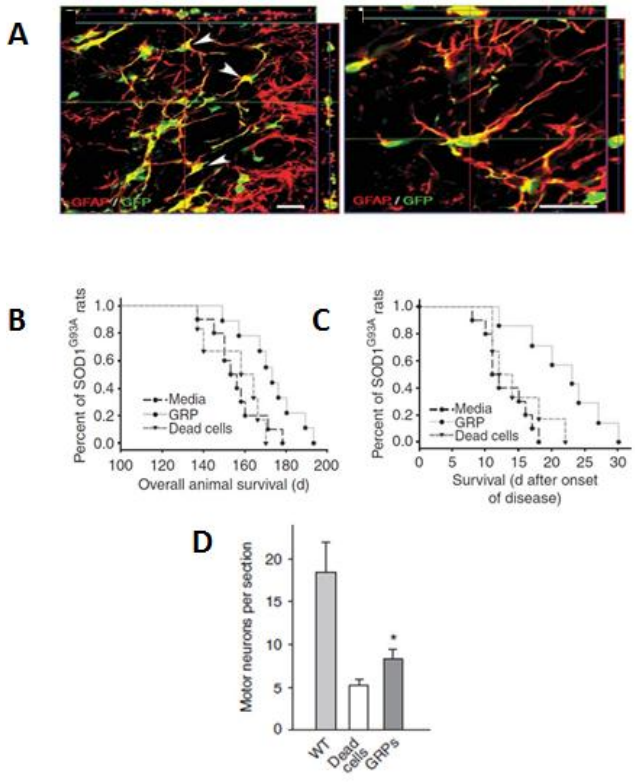

(A) GFP positive GRPs efficiently differentiated into $GFAP^+$ astrocytes following transplantation; (B) Transplanted GRPs significantly increased overall animal survival; (C) and prolonged disease duration. (D) Transgenic mutant SOD1 rats had significantly reduced numbers of cervical motor neurons. Taken from Lepore *et al.* (2008)

Additionally, in a focal transplantation-based astrocyte replacement study, Lepore *et al.* (2008) transplanted lineage-restricted astrocyte precursors, glial-restricted precursors (GRPs), around cervical spinal cord respiratory motor neurons in transgenic $SOD1^{G93A}$ rats. These transplanted GRPs survived in diseased tissue, differentiated efficiently into astrocytes [Figure 1.12a], and reduced microgliosis. They also extended survival [Figure 1.12b] and disease duration [Figure 1.12c], attenuated motor neuron loss [Figure 1.12d], and slowed declines in forelimb motor and respiratory physiological function (Lepore et al., 2008). Moreover, in a later study, the same group managed to transplant human GRPs into cervical spinal cord of

transgenic $SOD1^{G93A}$ mice. However, these transplants neither accelerated nor slowed progression of disease in mutant SOD1 mice, including the unchanged outcome measures for weight loss, survival, declines in hindlimb and forelimb grip strength, disease onset, and disease duration (Lepore et al., 2011).

1.3.5. Unraveling the molecular mechanism underlying the ALS-linked astrocyte toxicity for motor neurons

After the discovery of the mutant SOD1-expressing astrocyte toxicity for motor neurons *in vitro* and *in vivo*, we wanted to elucidate the molecular mechanism underlying this toxicity. To do this, we initially followed a candidate-based approach where we investigated the relevance of molecules, previously found by other groups, in our *in vitro* model system. Below is a review of some of these investigations.

First, Van Damme *et al.* (2007) found that, in co-culture, wild-type but not mutant SOD1-expressing astrocytes up-regulate the glutamate receptor subunit, GluR2, in motor neurons through an unidentified soluble factor. Under healthy conditions, GluR2 protects motor neurons from excitotoxicity by producing receptors impermeable to Ca^{2+}. The group showed that mutant SOD1-expressing astrocytes have reduced GluR2-regulating capacity rendering motor neurons vulnerable to excitotoxicity (Van Damme et al., 2007). Addressing this proposed mechanism, our group compared glutamate levels in medium conditioned with mutant versus wild-type astrocytes and found no significant difference between these two types of medium (data not shown). Furthermore, the Przedborski group also found that the application of CNQX, a potent AMPA/kainate receptor antagonist that was shown to prevent the phenotype observed by Van Damme *et al.*, did not mitigate the toxic actions of mutant astrocytes on motor neurons (Nagai et

al., 2007). Thus, we inferred that this mechanism is not relevant to what we are observing in our system.

Secondly, following the oxidative stress theory, Vargas *et al.* thought that the activation of redox-sensitive nuclear factor erythroid-2-related transcription factor 2 (Nrf2) is coordinated with the up-regulation of antioxidant defenses. The group found that the astrocyte-selective up-regulation of Nrf2 produced a significant delay in symptom onset in transgenic mutant SOD1 mice (Vargas et al., 2008a). Following this finding, we looked at the differential activity of Nrf2, using Western blot, and found Nrf2 to be localized more in the nuclei of motor neurons after 48 hours of exposure to medium conditioned with mutant astrocytes than in the nuclei of motor neurons exposed to medium conditioned with wild-type astrocytes (data not shown), suggesting an increase in Nrf2 activity. Moreover, in our model system, we found that the addition of tBHQ, shown to increase Nrf2 activity (Li et al., 2005), resulted in a moderate increase (15 ± 2%) in motor neuron survival (data not shown). While very preliminary, these data were consistent with those of Vargas *et al.*

Then, Di Giorgio and collaborators performed a gene array comparing mutant SOD1-expressing glia to wild-type glia and found *prostaglandin D2* (*PGD2*) *receptor* to be up-regulated by more than 14-fold in mutant glia, along with several cytokines, such as *Mcp2*, *Cxcl7*, and *Rantes* at smaller fold changes (Di Giorgio et al., 2008). While they showed a partial rescue of motor neuron loss with a specific antagonist to the PGD2 receptor, these researchers never validated their gene array results using qRT-PCR or Western blot. Furthermore, our group tested a series of PGD2 antagonists, including the one used by Di Giorgio *et al.*, but did not observe any neuroprotection (data not shown). Our group also failed to detect any increase in PGD2 receptor levels in mutant SOD1-expressing astrocytes compared to wild-type astrocytes

using Western blot (data not shown). Thus, while the study was interesting in showing relevance to non-cell autonomous contribution to human motor neurons, some of the molecular results reported in this work could not be reproduced by our group. This may be due to the variability and the differences between the purity of the astrocyte cultures of the groups.

A gene expression profiling study of spinal cord astrocytes from presymptomatic transgenic $SOD1^{G93A}$ mice, performed by the Shaw group, revealed impairment of the astrocyte lactate efflux transporter, which resulted in a significant decrease in spinal cord lactate levels (Ferraiuolo et al., 2011a). Similarly, the Rothstein group has shown that the most abundant lactate transporter in the central nervous system, monocarboxylate transporter 1, is reduced in patients and mouse models of ALS and might be contributory to how oligodendroglia produce neurotoxicity during the disease process (Lee et al., 2012). Additionally, the Shaw group's study also showed an increase in nerve growth factor (NGF) production, which resulted in the activation of the $p75^{NTR}$ receptor in neighboring motor neurons (Ferraiuolo et al., 2011a). The investigators have also found increased levels of pro-NGF in cerebrospinal fluid of ALS patients. Similarly, the Barbeito group found that $p75^{NTR}$, triggered by NGF, is implicated in the selective loss of motor neurons from transgenic mutant SOD1 mice (Cassina et al., 2005). Following these results, our group tested several blocking antibodies for the $p75^{NTR}$ receptor in our co-culture model system, but found no beneficial effect on motor neuron survival (data not shown). Therefore, it is unlikely that the $p75^{NTR}$ pathway is involved in the mechanism of mutant SOD1 astrocyte-derived motor neuron toxicity that we are studying.

Another mutant SOD1 astrocyte-derived motor neuron toxicity mechanism proposal came from the Raoul group, where the group showed that mutant SOD1-expressing astrocytes kill motor neurons through an interferon-gamma (IFN-γ)/LIGHT-mediated pathway [Figure

1.13] (Aebischer et al., 2011). The group further demonstrated that IFN-γ is up-regulated in spinal cords of mutant SOD1^{G93A} mice and that targeted deletion of *Light* in transgenic mice delays the progression but not the onset of symptoms (Aebischer et al., 2011).

In their next study, the group observed significantly increased levels of IFN-γ in human sALS spinal cords compared to control cases. They also observed that LIGHT and its receptor, LT-βR, are expressed mostly in motor neurons, but both in ALS and control cases. They also found that the LIGHT levels are increased in human ALS spinal cords (Aebischer et al., 2012). These results suggested that the IFN-γ-triggered LIGHT pathway might contribute to human ALS pathogenesis. Our group is currently examining the involvement of IFN-γ in our co-culture model using motor neurons from IFN-γ knockout animals and assessing the survival of these motor neurons. Our group has also tested a LT-βR antagonist (Alexis Biochemicals) and an IFN-γ neutralizing antibody (Sigma) in our co-culture model and did not observe any improvement on the survival of motor neurons. Both of these compounds were used by the Raoul group (Aebischer et al., 2011).

Figure 1.13: An alternative IFN-γ/LIGHT pathway-mediated mutant astroctye-derived motor neuron toxicity mechanism

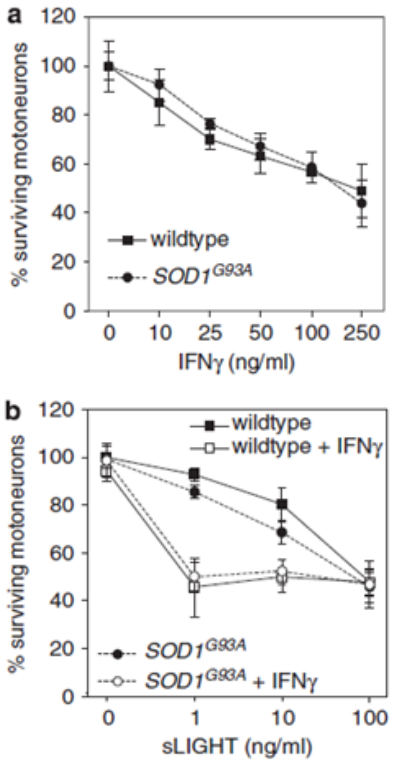

(A) IFN-γ was added to motor neuron cultures from wild-type or mutant embryos 24 hours after plating at indicated concentrations. Motor neuron survival was determined 48 hours later. (B) Mutant and wild-type motor neurons were treated 24 hours after being plated, with sLIGHT and with or without IFN-γ (10 ng/ml). Taken from Aebischer *et al.* (2011)

As one can deduce from all of the above, thus far, all of the candidate-based investigations we have performed have been unsuccessful. **That is why, for this thesis project, it was decided to use an unbiased RNA-Seq method to elucidate the molecular basis of the ALS-linked mutant astrocyte toxicity for motor neurons.** Moreover, most of the above-mentioned studies have focused on identifying the toxic factor released from mutant SOD1-expressing astrocytes and the receptors that are subsequently activated in motor neurons, but not on the death signaling pathways that are activated in motor neurons in response to mutant astrocytes.

While these are interesting questions to investigate and these studies have added substantial insights into answering some of the questions that were asked, the results from the above-mentioned studies have been hard to interpret when taken together, because the mechanisms, which have been suggested by the different cited groups, were looking from the astrocyte point-of-view and were all different. This difference can be overcome when the mechanism is studied from the motor neuron point of view, since the selective loss of motor neurons has been consistent across all of these non-cell autonomous disease models. As a result, for this thesis, it was decided to focus, not on astrocytes, but on wild-type motor neurons upon exposure to mutant SOD1-expressing astrocytes.

It was also decided to specifically focus on the molecular mechanism that occurs in these motor neurons before they become committed to die. Indeed, a significant number of studies seem to investigate motor neuron degeneration by looking at late-stage events, when many of the motor neurons are already committed to die. It was believed that searching for neuroprotective targets at such a stage may thus not be very fruitful. Consequently, this thesis

work was set on the premise that unraveling early molecular alterations in motor neurons may be more promising in terms of finding effective therapeutic avenues for ALS.

Accordingly, this thesis work first focused on characterizing a well-controlled *in vitro* model of non-cell autonomous motor neuron degeneration, where the timing of the toxicity and the point of no return for motor neurons were identified. Moreover, in this model system, cultured motor neurons needed to be purified and be in large enough quantities so that sufficient amounts of RNA could be extracted for genomic studies. Thus, the first goal was to address these prerequisites and the results of these first set of investigations are presented and discussed in Chapter 2 of this thesis.

In Chapter 2, an *in vitro* model of ALS composed of purified wild-type embryonic stem cell-derived motor neurons was characterized in which, following 7 days of exposure to mutant astrocyte-conditioned medium, about half of the motor neurons are lost. This finding is identical to what the Przedborski group has previously observed with primary spinal motor neurons and mutant astrocytes (Nagai et al., 2007). Capitalizing on this cell model system characterized in Chapter 2**,** an RNA-Seq assay was used to identify gene alterations germane to the toxicity of the mutant astrocytes by elucidating relevant molecular pathways that are dysregulated in motor neurons. To analyze the results of this assay, a reverse gene engineering algorithm generated by the Califano group (Carro et al., 2010) was utilized to infer transcription factors whose activities are altered in this model system. The findings from this analysis are presented and discussed in Chapter 3 of this thesis. Finally, as described in Chapter 4, NF-κB was discovered to be one of the most dysregulated transcription factors in the model system studied. Using Western blot and a specialized ELISA kit, an increase in the transcriptional activity of NF-κB was demonstrated in motor neurons exposed to mutant astrocyte-conditioned medium. In addition, both the

pharmacological and genetic inhibition of NF-κB in motor neurons was shown to result in the full rescue of these neurons *in vitro.*

The main conclusions of this thesis work are the following. This is the first time that the reverse gene engineering algorithm is used in a model of neurodegeneration and the results from this thesis work demonstrate that such new approaches may be quite powerful for identifying pathogenic mechanisms. Furthermore, NF-κB has been found to be instrumental in mediating the demise of motor neurons in response to mutant astrocytes in our *in vitro* model of ALS. If this finding faithfully reflects a key pathogenic event in ALS, then drug development projects aimed at identifying and testing (pre-clinically, first, and then clinically) NF-κB antagonists may have to be considered.

Chapter 2: Validation of a non-cell autonomous model of ALS using purified embryonic stem cell-derived motor neurons exposed to mutant astrocyte-conditioned medium

2.1. Introduction

2.1.1. Primary versus embryonic stem cell-derived motor neurons

Following the publication from our laboratory on the toxic effect of mutant SOD1-expressing astrocytes on the survival of motor neurons (Nagai et al., 2007), our aim was to elucidate the molecular mechanism underlying this non-cell autonomous neurodegenerative model. To achieve this stated goal, we initially performed a number of candidate-based investigations, which failed to provide us with enough insights into the molecular signaling driving the demise of motor neurons in this *in vitro* ALS model. Consequently, we thought to change the strategy and search for the molecular underpinning of this motor neuron death phenotype from a candidate-based to an unbiased genomic approach using an RNA-Seq assay; this assay is discussed in more detail in the next chapter.

As a prerequisite to performing the proposed genomic assay, it was necessary to obtain purified motor neurons in large quantities. In the initial studies by Nagai and collaborators (2007), which revealed the non-cell autonomous role of astrocytes in ALS, primary spinal motor neurons were mainly used. Several investigators have shown such neuronal preparations to be suitable for probing the molecular basis of selective motor neuron degeneration caused by mutant SOD1 (Raoul et al., 2002). However, for this thesis work, obtaining sufficient numbers of purified primary motor neurons from embryonic day 12.5 mouse spinal cords would be quite

challenging. Furthermore, using immortalized cell lines, such as neuroblastoma, was not desirable, since the goal of this work was to explore the molecular mechanism of neuronal death. Therefore, it was decided to use a readily-expandable source of motor neurons that is provided by embryonic stem cells subjected to the differentiation protocol published by Wichterle *et al.* (2002).

Indeed, based on the knowledge gained from developmental studies of motor neuron identity specifications [Figure 2.1a], Wichterle and collaborators (2002) developed a method to differentiate mouse embryonic stem cells into motor neurons with an efficacy of about 30% *in vitro*. Embryonic stem cells were obtained from a transgenic mouse line in which the gene for

Figure 2.1: Differentiation of embryonic stem cell-derived motor neurons

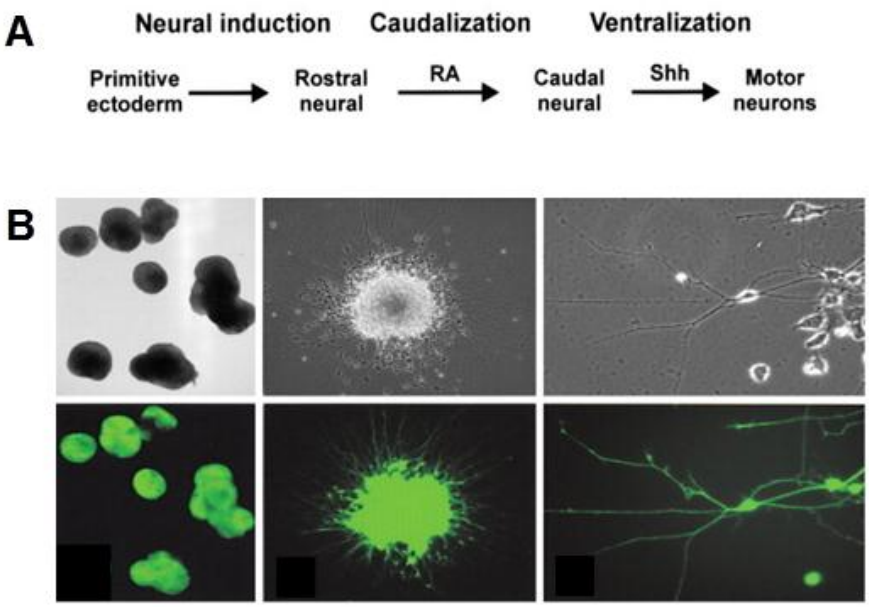

(A) This schematic shows the progressive steps in motor neuron specification, where neural inductive signals convert primitive ectodermal cells to a rostral neural fate, followed by a more caudal identity with the addition of retinoic acid (RA). Spinal progenitors, then, are converted to motor neurons by sonic hedgehog (Shh) signaling. (B) Bright-field and fluorescence images show eGFP expression in embryoid bodies grown for 5 days with retinoic acid and sonic hedgehog. These embryonic stem cell-derived motor neurons extend beautiful processes on matrigel 2 days after plating. Excerpted from Wichterle *et al.* (2002)

enhanced green fluorescent protein (eGFP) is expressed under the control of the motor neuron specific homeobox gene *Hb9* promoter. In this method, mouse embryonic stem cells are first grown in aggregate cultures for 2 days to form embryoid bodies. Then, embryoid bodies are grown for 2 to 3 days and treated with retinoic acid and sonic hedgehog for caudalization and ventralization, respectively. At this point, the embryoid bodies take the identity of motor neuron progenitor cells. Upon being plated for 2 days on matrigel, which is a gelatinous protein mixture that resembles the complex extracellular environment found in many tissues, these cells morphologically resemble to primary spinal motor neurons [Figure 2.1b] (Wichterle et al., 2002).

At the end of the differentiation process, these embryonic stem cell-derived motor neurons not only express specific motor neuron markers such as Hb9 and Islet1 (Wichterle et al., 2002) but also exhibit a special spinal motor neuron identity belonging to the brachial lateral motor column (Peljto et al., 2010). During development, *in vivo*, motor neurons acquire columnar identities: medial, hypaxial, or lateral, which determine their settling positions in the ventral spinal cord as well as the selection of the muscles that they innervate (Jessell, 2000).

In addition, embryonic stem cell-derived motor neurons display an interesting change in identity depending on the medium they are treated with during differentiation. Peljto et al. (2010) has shown that embryonic stem cell-derived motor neurons that are treated only with retinoic acid and sonic hedgehog show a rostral and cervical medial motor column-like identity. On the other hand, the neurons that are treated with a caudalizing/ventralizing (CV) medium that contains Advanced DMEM/F12/Neurobasal medium supplemented with 10% KnockOut Serum Replacement result in the generation of spinal motor neurons with brachial and lateral motor column characteristics [Figure 2.2a]. Motor neurons that are treated with CV medium also show a higher expression of FoxP1, a member of the winged-helix/forkhead transcription factors, than

LIM/homeobox protein Lhx3 (Peljto et al., 2010) [Figure 2.2b], suggesting that the generated

Figure 2.2: Brachial and lateral motor column identity of embryonic stem cell-derived motor neurons

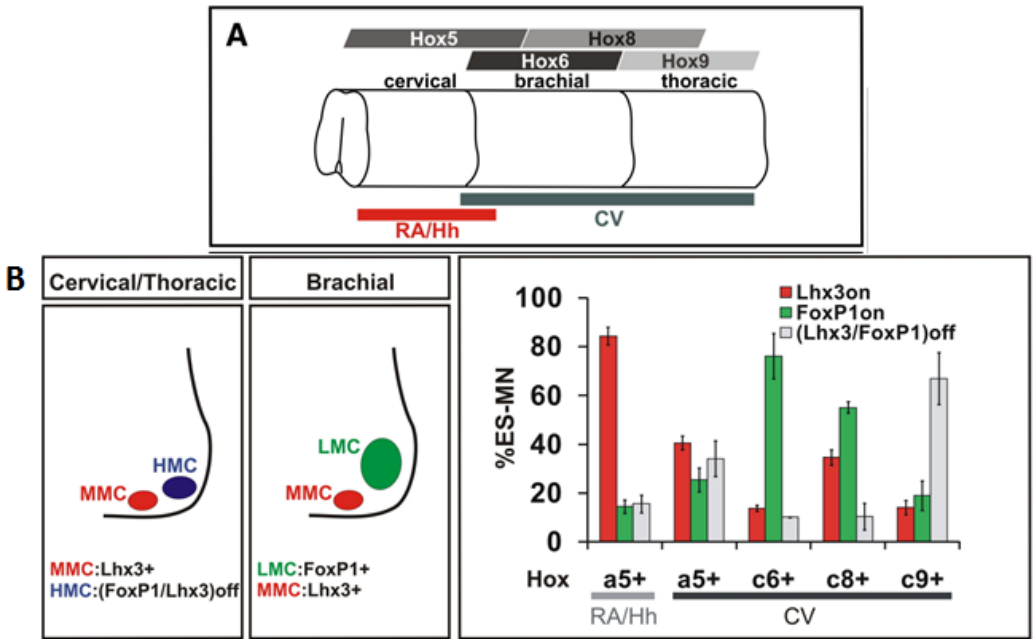

(A) Upon exposure to CV medium vs. retinoic acid and sonic hedgehog only (RA/Hh), embryonic stem cell derived motor neurons display a change in identity from rostral and cervical, expressing *Hox5* gene, to brachial and thoracic, expressing *Hox6*, *Hox8*, *Hox9* developmental genes. (B) Similarly, there is an increase in the expression of FoxP1 over Lhx3 in the embryonic stem cell-derived motor neurons that are treated with CV medium vs. RA/Hh, where Foxp1 is a marker of lateral motor column (LMC) and Lhx3 a marker of median motor column (MMC). HMC: hypaxial motor column; a5: Hoxa5; c6: Hoxc6; c8: Hoxc8; c9: Hoxc9 genes. Taken from Peljto *et al.* (2010)

motor neurons are lateral motor column neurons.

In addition to similarities on the basis of molecular markers and morphology, embryonic stem cell-derived motor neurons have also been shown to be functionally comparable to spinal motor neurons. For example, when grafted *in ovo*, embryonic stem cell-derived motor neurons also migrate to the ventral spinal cord and send out axons along motor nerve tracts (Wichterle et al., 2009). Furthermore, embryonic stem cell-derived motor neurons have been shown to innervate muscle fibers both *in vitro* and *in vivo* (Miles et al., 2004; Soundararajan et al., 2006;

Yohn et al., 2008). They also develop many functional properties, such as expressing receptors for excitatory and inhibitory transmitter systems, developing electrophysiological properties necessary to produce appropriate patterns of action potential firing, and forming cholinergic synapses with muscle cells in culture (Miles et al., 2004). All of these features of embryonic stem cell-derived motor neurons demonstrate how structurally and functionally similar these neurons are to primary motor neurons.

Figure 2.3: Visualization of primary and embryonic stem cell-derived motor neurons

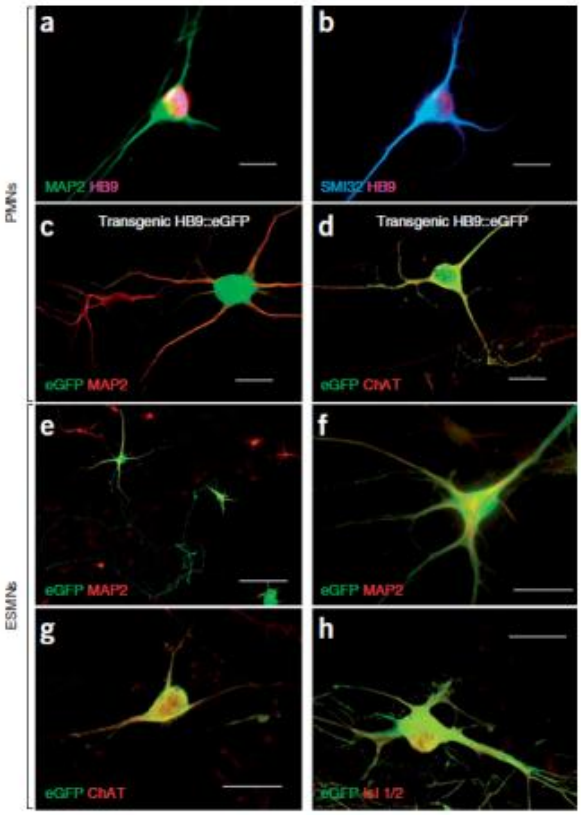

Immunostaining of primary neuronal cultures shows (A) $Map2^{+}Hb9^{+}$ and (B) $SMI32^{+}Hb9^{+}$ large primary motor neurons (PMNs) derived from non-transgenic mouse embryos. Double immunostaining of primary neuronal cultures shows (C) $Map2^{+}eGFP^{+}$ and (D) $ChAT^{+}eGFP^{+}$ PMNs derived from a transgenic Hlxb9-GFP1Tmj embryo. Embryonic stem cell-derived motor neurons (ESMNs) expressing eGFP under the Hb9 promoter are immunopositive for (E-F) Map2; (G) ChAT; and (H) Islet 1/ 2. (Scale bars, 50 μm [A-D, F-H], 100 μm [E]) Taken from Nagai *et al.* (2007)

Hence, using the method generated by Wichterle *et al.* (2002), our group produced embryonic stem cell-derived motor neurons. Some of these common features were immunopositivity for the pan-neuronal marker, microtubule-associated protein 2 (Map2), and for motor neuron markers, cholinergic transmitter synthetic enzyme choline acetyltransferase (ChAT) and Islet1/2 [Figure 2.3] (Nagai et al., 2007). In addition, embryonic stem cell-derived motor neurons co-cultured on mutant SOD1-expressing astrocyte monolayers showed the same

Figure 2.4: Sensitivity of embryonic stem cell-derived motor neurons to mutant astrocyte-released toxicity

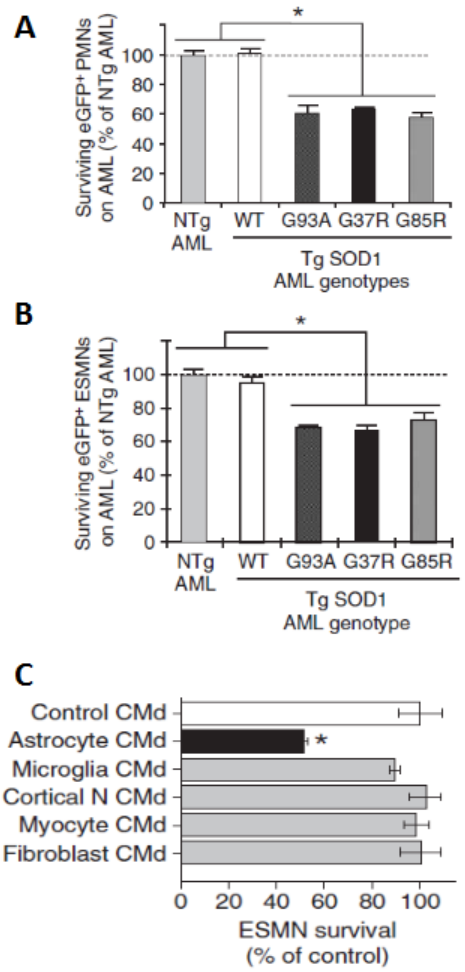

(A) 7 days after plating, there are about 40-50% less primary motor neurons (PMNs) in co-culture with mutant SOD1 G93A, G37R, and G85R, than with non-transgenic (NTg) or transgenic wild-type SOD1 (WT) astrocyte monolayers (AML). (B) Embryonic stem cell-derived motor neurons (ESMNs) plated on mutant AML behaved similarly to PMNs. (C) In contrast to medium conditioned (CMd) with mutant astrocytes, CMd with mutant cerebral cortical neurons, skeletal myotubes, microglia or skin fibroblasts had no effect on ESMN survival compared with controls. Values represent mean ± s.e.m from at least three independent experiments performed at least in triplicate, analyzed by two-way ANOVA followed by a Newman-Keuls *post hoc* test. (Nagai et al., 2007)

magnitude of loss as primary motor neurons co-cultured on mutant astrocyte monolayers [Figure 2.4a-b] (Nagai et al., 2007). Similarly, embryonic stem cell-derived motor neurons and primary motor neurons were found to be identically susceptible to medium conditioned with mutant SOD1-expressing astrocytes [Figure 2.4c] (Nagai et al., 2007). These results illustrate how similar the sensitivities of primary and embryonic stem cell-derived motor neurons are with respect to the toxicity mediated by mutant SOD1-expressing astrocytes and how suitable embryonic stem cell-derived motor neurons appear to be to study the molecular mechanism underlying this toxic phenotype.

2.1.2. Involvement of Bax

Nagai *et al.* first used wild-type

embryonic stem cell-derived motor neurons to understand whether the decline in the number of motor neurons after 7 days of exposure to the toxicity emanating from mutant SOD1-expressing astrocytes was actually due to neuronal death. To address this issue, the group compared the percentage of dying wild-type embryonic stem cell-derived motor neurons co-cultured with either mutant astrocytes or wild-type astrocytes using the DNA dye ethidium homodimer (EthD), which selectively permeates the damaged membranes of the dying cells. The level of EthD-labeled embryonic stem cell-derived motor neurons at 7 days was found to be 1.34 fold higher upon co-culture with mutant astrocyte monolayers than with wild-type astrocyte monolayers [Figure 2.5a] (Nagai et al., 2007). This suggested a decrease in the survival of motor neurons that are co-cultured on mutant astrocyte monolayers. Then, to determine whether this astrocyte-related non-cell autonomous mechanism kills motor neurons by apoptosis, the membrane-permeable DNA dye Hoechst 33342 [Figure 2.5b-c], as well as immunocytochemistry for fractin [Figure 2.5b], which is a caspase 3-activated β-actin fragment, were used (Nagai et al., 2007). Looking at the fractin-immunostained cells after 7 days, Nagai *et al.* observed that the percentage of fractin-positive cells with condensed nuclei was 1.51 fold higher in co-cultures with mutant astrocyte monolayers than in co-cultures with wild-type monolayers [Figure 2.5d] (Nagai et al., 2007). Furthermore, all cells that stained for Hoechst 33342 also stained for the apoptotic DNA fragmentation marker, terminal dUTP nick-end labeling (TUNEL) [Figure 2.5c] (Nagai et al., 2007). These results indicated an increase in apoptosis in cells co-cultured on mutant astrocyte monolayers.

Figure 2.5: Embryonic stem cell-derived motor neurons die through a Bax-dependent mechanism when co-cultured with mutant astrocyte monolayers

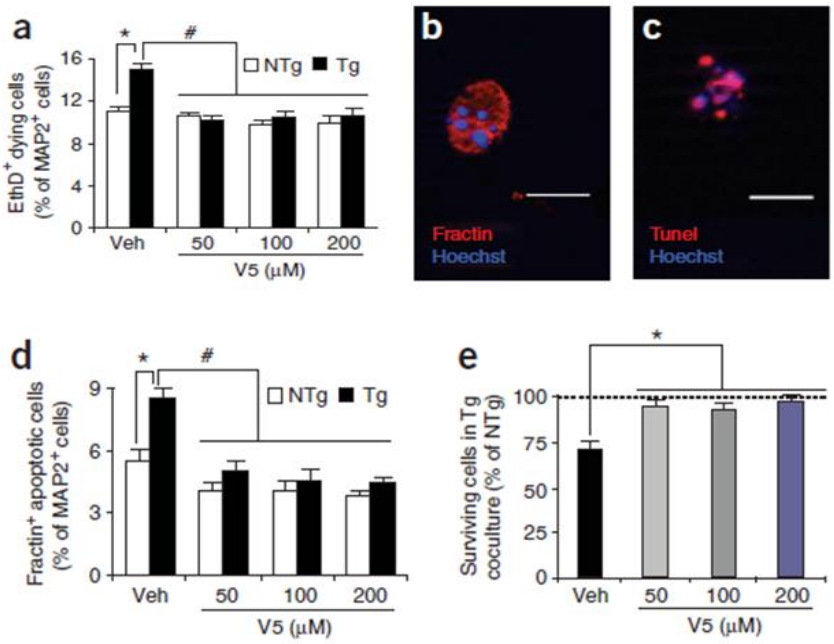

7 days after plating, the Bax inhibitor, V5, decreases the percentages of embryonic stem cell-derived motor neurons labeled with (A) EthD; (D) Map2 and fractin; and (E) increases the percentage of surviving embryonic stem cell-derived motor neurons. Furthermore, all embryonic stem cell-derived motor neurons immunopositive for fractin show (B) DNA condensations, as evidenced by Hoechst 33342; and (C) DNA fragmentation, as evidenced by TUNEL (Scale bar, 20 μm). Values represent mean ± s.e.m from at least three independent experiments performed at least in triplicate, analyzed by two-way ANOVA followed by a Newman-Keuls *post hoc* test. (Nagai et al., 2007)

Previously, it has been reported that the toxicity of mutant SOD1 involves the mitochondrial-dependent apoptotic machinery and, more specifically, the Bcl-2 family (Guégan and Przedborski, 2003; Pasinelli et al., 2004). Consistent with these observations, Nagai *et al.* have shown that the membrane-permeable pentapeptide VPMLK (V5), which inhibits the pro-apoptotic molecule Bax (Sawada et al., 2003), mitigates the death of motor neurons caused by mutant SOD1-expressing astrocytes [Figure 2.5e] (Nagai et al., 2007). Subsequently, the group has demonstrated that deletion of the *Bax* gene also prevents motor neuron death in this *in vitro* model (data not shown). Based on these results, the group has concluded that mutant astrocytes kill motor neurons via an exogenously-activated Bax-dependent death signaling pathway.

However, at this point, the nature of the transducing signaling pathways engaged in wild-type motor neurons by mutant astrocytes is still not known nor are the molecular pathways that lie either upstream or downstream to Bax. Therefore, the use of a combination of genomics and bioinformatics methodologies may represent a powerful alternative to unraveling the outstanding molecular questions to our hitherto marginally fruitful candidate-based approaches.

This new genomic approach, however, required substantial amounts of RNA from the cells of interest (i.e. wild-type motor neurons), as well as those transcripts being harvested at the optimal time for such investigations to generate meaningful information. Accordingly, the studies that have been carried out to address the above requirements, namely to produce and purify wild-type embryonic stem cell-derived motor neurons, to standardize the culture conditions, and to define the time-course of wild-type embryonic stem cell-derived motor neurons degeneration in response to mutant astrocyte-conditioned medium, are presented and discussed in this chapter.

2.2. Results

2.2.1. Embryonic stem cell-derived motor neurons are efficiently purified using magnetic-activated cell sorting

In order to validate the use of embryonic stem cell-derived motor neurons exposed to mutant astrocyte-conditioned medium as a non-cell autonomous model of ALS, it was first necessary to find an efficient method to purify these motor neurons. The aim was to obtain transcriptional information that pertained to motor neurons without affecting the susceptibility of the embryonic stem cell-derived motor neurons to mutant astrocytes. Using this rationale, the purification

efficiency of two well-established cell isolation methods, fluorescence-activated cell sorting (FACS) and magnetic-activated cell sorting (MACS), were compared.

After following the protocol established by Wichterle *et al.* (2002) to differentiate embryonic stem cells into motor neurons, FACS was first performed to isolate motor neurons that expressed high levels of eGFP under the control of the motor neuron specific promoter, *Hb9* [Figure 2.6a]. Consistent with the findings from Wichterle *et al* (2002), $eGFP^{+}$ neurons showed

Figure 2.6: Embryonic stem cell-derived motor neurons are efficiently purified using Magnetic-Activated Cell Sorting

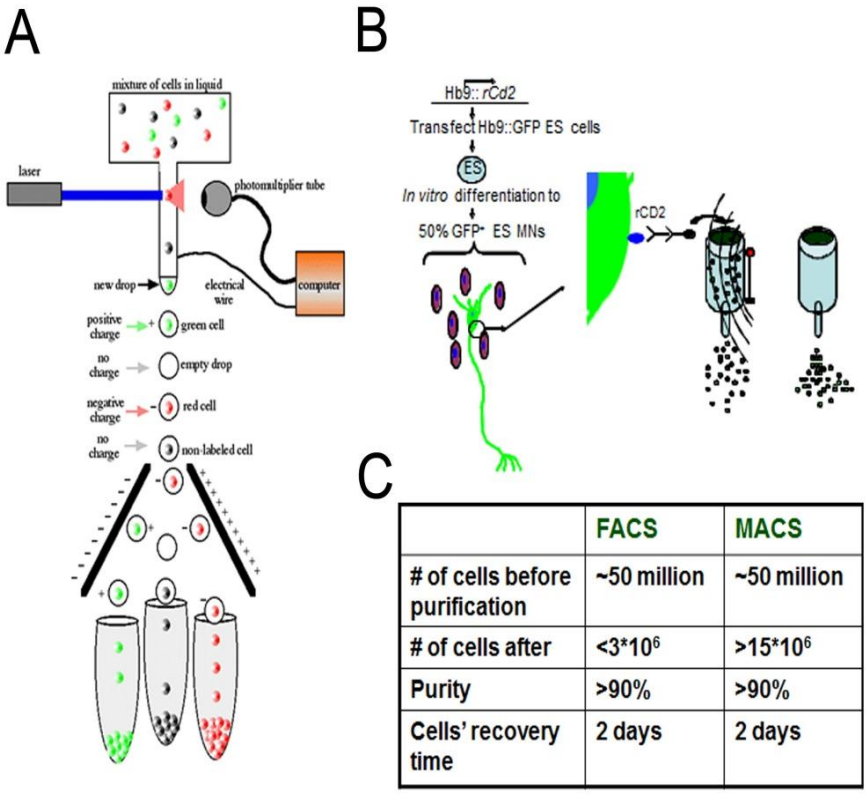

	FACS	MACS
# of cells before purification	~50 million	~50 million
# of cells after	$<3*10^6$	$>15*10^6$
Purity	>90%	>90%
Cells' recovery time	2 days	2 days

(A) Fluorescence-Activated Cell Sorting (FACS) and (B) Magnetic-Activated Cell Sorting (MACS) work using embryonic stem cell-derived motor neurons that express eGFP under the Hb9 promoter for FACS and an extra surface marker, CD2, for MACS. (C) The comparison of MACS with FACS proves MACS to be the preferred isolation method for embryonic stem cell-derived motor neurons.
(FACS image source: http://www.bio.davidson.edu/courses/genomics/method/facs.html)

more than 90% purity in culture [Figure 2.6c]. Furthermore, neurons that were treated with neurotrophic factors, such as ciliary neurotrophic factor (CNTF), glial cell line-derived neurotrophic factor (GDNF), and brain-derived neurotrophic factor (BDNF), extended long processes 2 days after purification. However, the total yield of $eGFP^+$ neurons obtained from this method was small having started with about 50 million differentiated but non-purified embryonic stem cell-derived motor neurons before the purification process and ending with less than 3 million embryonic stem cell-derived motor neurons after the process [Figure 2.6c]. This suggested that FACS puts a mechanical constraint on the motor neurons, which could potentially result in the selection of more resistant cells in the population. To avoid this potential problem, it was decided to utilize the mechanically gentler MACS technique to purify embryonic stem cell-derived motor neurons.

For MACS, initially, the $p75^{NTR}$ antibody, which is one of the earliest markers for motor neurons, was used to select motor neurons from the embryonic stem cell population. However, none of the commercially available antibodies that were tried managed to bind mouse motor neurons efficiently (data not shown). Therefore, motor neuron cultures derived from embryonic stem cells engineered to express cluster of differentiation-2 (CD2), a cell adhesion molecule found on the surface of T and natural killer cells (Peterson and Seed, 1987), were used. These modified embryonic stem cells expressed both eGFP and CD2 under the Hb9 promoter [Figure 2.6b]. To obtain this embryonic stem cell line, Gist Croft, from the Henderson group, had cloned the full-length rat *CD2* gene into a vector downstream to the 9kb mouse *Hb9* promoter. He followed the cloning with these subsequent steps: (1) insertion of a neomycin (Neo)-resistant gene under the control of the mouse phosphoglycerate kinase (PGK) promoter; (2) transfection of the HBG1 Hb9::GFP cell line, which was the same as the 9kb promoter used before; (3)

selection of stable neomycin-resistant clones; (4) differentiation of these clones into motor neurons; (5) screening for CD2 expression in Hb9::GFP motor neurons; and (6) screening for the ability of five of the best CD2-expressing lines to facilitate the MACS purification. He found clone-9 to be the best MACS purified line (data not shown), and consequently, this was the cell line used for the studies in this thesis.

Incidentally, among a host of surface markers, CD2 was selected to isolate embryonic stem cell-derived motor neurons by MACS for several reasons. First of all, CD2 is a well-described epitope that is immunologically tractable (i.e. a good number of working antibodies against this marker have been established). Secondly, it is not trypsin sensitive, which is important since trypsin is used during the differentiation of embryonic stem cell-derived motor neurons. Third, CD2 is not expressed in neural cells, which were the target cells to purify. And fourth, these cells expressing CD2 never showed any difference in survival or outgrowth when compared with their HBG1 parental lines (data not shown), suggesting that expression of CD2 does not cause any detectable phenotype. Thus, the comparison of purification methods for mouse embryonic stem cell-derived motor neurons could now be performed.

Similar to FACS, once embryonic stem cell-derived motor neurons were differentiated, the MACS protocol, which consisted of incubating the cells with anti-rat CD2 antibody (Invitrogen) followed by anti-mouse magnetic microbeads (Miltenyi Biotec) as a secondary antibody, was carried out. The cells were then passed through a magnetic column (Miltenyi Biotec) to separate Hb9::GFP-$CD2^{+}$ cells from other types of cells in culture [Figure 2.6b]. Post-sorting, the cells were then collected in embryonic stem cell-derived motor neuron medium and plated for culture (please see the Experimental Methods for more details). In comparison to FACS, MACS proved to be a more efficient purification method in that, the entire process for

MACS took about 4 hours, whereas for FACS, it took about 6 hours to achieve the same degree of purity of over 90%. Also important is the fact that the yield of motor neurons was about 5-fold greater with MACS than with FACS, since constantly, about 15 million motor neurons were obtained with MACS versus less than 3 million with FACS, starting from the same number of about 50 million before the purification process [Figure 2.6c]. Therefore, MACS, as opposed to FACS, was used for this project.

Once it was determined that MACS was the preferred method of purifying embryonic stem cell-derived motor neurons, the next step was to assess the changes in the percentage of cell types in the purified versus the non-purified cell cultures. Following the MACS purification, the number of $GFAP^+$ cells in culture dropped from approximately 25% to 3% and the number of non-motor neuronal neurons (i.e. $Map2^+/GFP^-$ cells) dropped from about 33% to 2%, resulting in a sharp increase in the percentage of motor neuron (i.e. $Map2^+/GFP^+$ cells) yield from about 32% to 92% ± 3% (mean ± s.e.m, n=5) [Figure 2.7]. Moreover, $Hb9::GFP^+$ embryonic stem cell-derived motor neurons showed almost 99% coherence with $Hb9^+$, and over 95% coherence with $Islet1^+$ and $ChAT^+$ neurons in

Figure 2.7: Purified embryonic stem cell cultures yield of over 90% motor neurons

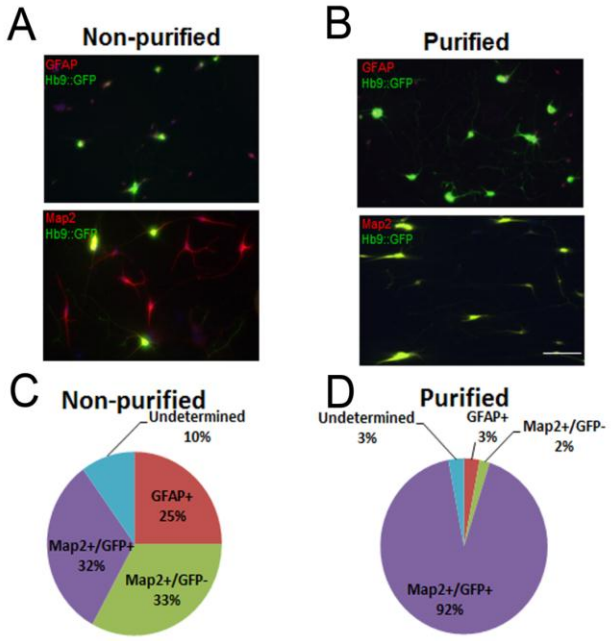

Immunostaining (A-B) and counting (C-D) show that while in the non-purified cultures, the percentage of $Map2^+/GFP^+$ motor neurons is about 32%, this percentage is about 92% in the purified cultures. Values represent mean ± s.e.m from five independent experiments performed at least in triplicate, analyzed by Student's t-test.

Figure 2.8: Purified embryonic stem cell-derived motor neurons strongly correlate with other motor neuronal markers

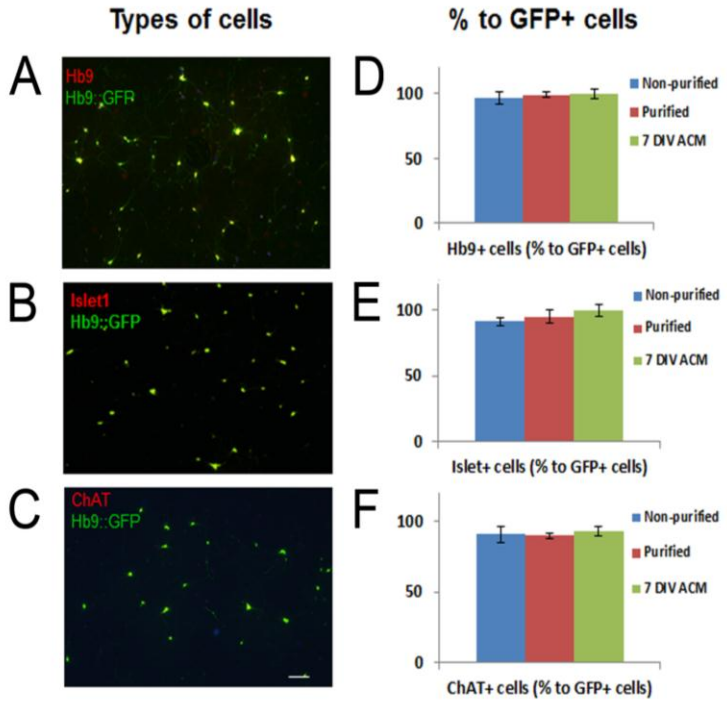

This figure, consisting of images formed by immunostaining (A-C) and graphs by counting (D-F), exhibits how strongly (over 95%) $eGFP^{+}$ purified embryonic stem cell-derived motor neurons are immunoreactive for other motor neuron markers, such as Hb9 (A, D); Islet1 (B, E); and ChAT (C, F). The stainings were either done on purified or non-purified embryonic stem cell-derived motor neurons that were put in fresh media for 2 days or on neurons exposed to astrocyte-conditioned media for 7 days. Values represent mean ± s.e.m from five independent experiments performed at least in triplicate, analyzed by Student's t-test.

purified, as well as in non-purified, cultures [Figure 2.8]. This indicates a strong correlation between purified motor neurons and the well-established motor neuron markers. Finally, all of these data strengthen the point that MACS is a very effective method for purifying embryonic stem cell-derived motor neurons for these studies.

2.2.2. Exposure to mutant astrocyte-conditioned medium kills purified embryonic stem cell-derived motor neurons in culture over a 7-day period

After establishing the purification method, next to be tested was whether motor neuron death similar to that previously observed under the same conditions using non-purified primary and embryonic stem cell-derived motor neurons (Nagai et al., 2007) could be observed in the purified embryonic stem cell-derived motor neurons. Using the new *in vitro* model discussed above, the number of surviving purified embryonic stem cell-derived motor neurons that were exposed to either mutant astrocyte-

Figure 2.9: Exposure to mutant astrocyte-conditioned medium kills purified embryonic stem cell-derived motor neurons in culture over a 7-day period

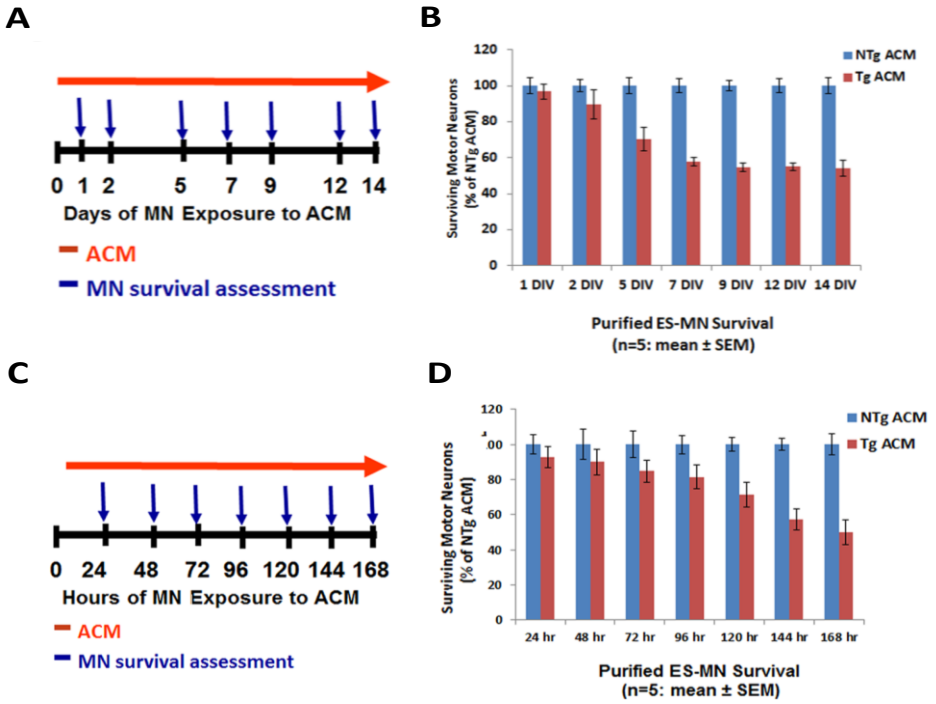

(A) Purified embryonic stem cell-derived motor neurons (ES-MNs) were exposed to astrocyte-conditioned medium (ACM) for 14 days and their survival was assessed on the 1st, 2nd, 5th, 7th, 9th, 12th and 14th days *in vitro* (DIV). (B) The time course revealed a progressive decay in number of surviving ES-MNs exposed to mutant (Tg) ACM until 7 days of exposure, after which cell number maintained a plateau until 14 days *in vitro*. (C) The schematic showing the hours of ES-MN exposure to ACM. The survival assessment was done every 24 hours during the 7-day period. (D) ES-MNs that were exposed to Tg vs. non-transgenic (NTg) ACM showed a progressive decay in number until it reached about a 50% loss after 168 hours of exposure Tg ACM. Values represent mean ± s.e.m from five independent experiments performed at least in triplicate, analyzed by Student's t-test, p-value <0.05.

conditioned medium or wild-type astrocyte-conditioned medium (i.e. non-toxic control) up to 14 days *in vitro* were examined [Figure 2.9a].

This experiment showed the following: Up to 2 days *in vitro*, the number of GFP^+ embryonic stem cell-derived motor neurons exposed to mutant astrocyte-conditioned medium did not differ from the number of neurons exposed to wild-type astrocyte-conditioned medium [Figure 2.9b]. In contrast, after 7 days of exposure to mutant astrocyte-conditioned medium, the number of surviving embryonic stem cell-derived motor neurons was 50 ± 4% (mean ± s.e.m, n=5), lower than that of neurons exposed to wild-type medium [Figure 2.9b]. Interestingly,

thereafter, the number of surviving motor neurons exposed to mutant astrocyte-conditioned medium compared to wild-type astrocyte-conditioned medium plateaued at around 50%, up to 14 days *in vitro* [Figure 2.9b].

Because most of the decline in motor neuron number appeared to occur during the first 7 days of exposure to mutant astrocyte-conditioned medium, the time-course experiment was repeated, but this time with a greater time resolution (i.e. every day) between 0 to 7 days exposure to mutant astrocyte-conditioned medium [Figure 2.9c]. In this study, a similar reduction in number of surviving embryonic stem cell-derived motor neurons up to 48 hours (i.e. 2 days) was found, reaching about 50% loss after 168 hours (i.e. 7 days *in vitro*) [Figure 2.9d]. In addition, after 72 hours of exposure to mutant astrocyte-conditioned medium, the number of surviving embryonic stem cell-derived motor neurons was only 16 ± 4% lower than the number of surviving motor neurons exposed to wild-type astrocyte-conditioned medium [Figure 2.9d]. All of these time-course results were in agreement with previous published findings (Nagai et al., 2007) on non-purified primary and embryonic stem cell-derived motor neurons. This fact provided strong reassurance that purified embryonic stem cell-derived motor neurons do not have altered sensitivities to mutant astrocyte-induced toxicity. Furthermore, since there were no differences in the number of surviving motor neurons exposed to mutant astrocyte-conditioned medium for 7 to 14 days *in vitro*, exposure of cells to mutant medium for 7 days was used for the rest of the characterization experiments.

2.2.3. Purified embryonic stem cell-derived motor neurons are sensitive to mutant astrocyte-conditioned medium regardless of their cell culture age

After assessing the time course of survival of purified embryonic stem cell-derived motor neurons exposed to mutant astrocyte-conditioned medium, we wanted to test whether cell culture age plays any role in the sensitivity of motor neurons to the toxicity emanating from mutant astrocytes. We thought this test was necessary to better understand our *in vitro* model system. Thus, to examine this question, we investigated whether the same magnitude of death is observed in purified embryonic stem cell-derived motor neurons that spend an extra 7 days in fresh medium prior to being exposed to mutant astrocyte-conditioned medium for 7 days, in comparison to motor neurons that are exposed to mutant astrocyte-conditioned medium for 7 days directly after purification [Figure 2.10a]. It was found that, at the end of 7 days of exposure to fresh medium followed by 7 days of exposure to mutant astrocyte-conditioned medium, purified embryonic stem cell-derived motor neurons show a similar loss in number compared to the cells that are directly exposed to mutant astrocyte-conditioned medium [Figure 2.10b]. This result suggested that purified embryonic stem cell-derived motor neurons are equally sensitive to mutant astrocyte-conditioned medium regardless of whether they are a week older. Similar results were found when the experiment was repeated using non-purified primary motor neurons (data not shown), indicating that primary and purified embryonic stem cell-derived motor neurons are equally sensitive to toxicity coming from mutant astrocytes. These results showed the time-independent sensitivity of this *in vitro* model system to mutant astrocytes, which is crucial to study the molecular mechanism underlying mutant astrocyte toxicity for motor neurons.

Figure 2.10: Purified embryonic stem cell-derived motor neurons are sensitive to mutant astrocyte-conditioned medium regardless of their cell culture age

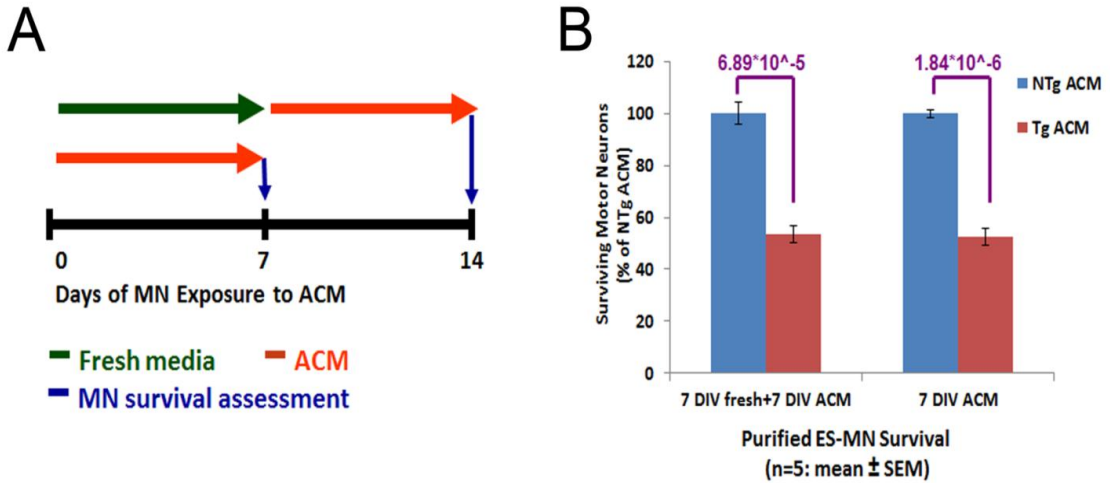

(A) Purified embryonic stem cell-derived motor neurons were put in fresh medium for an extra 7 days prior to being exposed to mutant astrocyte-conditioned medium. (B) However, the motor neurons that were put in fresh medium for an extra 7 days showed a similar loss in number after 7 days of exposure to mutant astrocyte-conditioned medium as motor neurons that were put in mutant medium immediately. Values represent mean ± s.e.m from five independent experiments performed at least in triplicate, analyzed by Student's t-test.

2.2.4. The 50% motor neuron loss upon exposure to mutant astrocyte-conditioned medium is not due to the loss of toxic activity

One of the main questions about the *in vitro* non-cell autonomous ALS model was the maximum 50% cell death observed after exposure to mutant astrocyte-conditioned medium and whether this maximum level of death is due to a time-dependent decline in toxic activity of the mutant medium. To address this question, the potency of mutant astrocyte-derived toxic activity on purified embryonic stem cell-derived motor neurons was investigated by replenishing the medium with a new batch of astrocyte-conditioned medium on the third day of the 7-day incubation [Figure 2.11a] or on the seventh day of the 14-day incubation [Figure 2.11c]. For this, a maximum of about 50% loss in GFP^+ motor neurons was observed in both groups with or

Figure 2.11: The 50% motor neuron loss upon exposure to mutant astrocyte-conditioned medium is not due to the loss of toxic activity

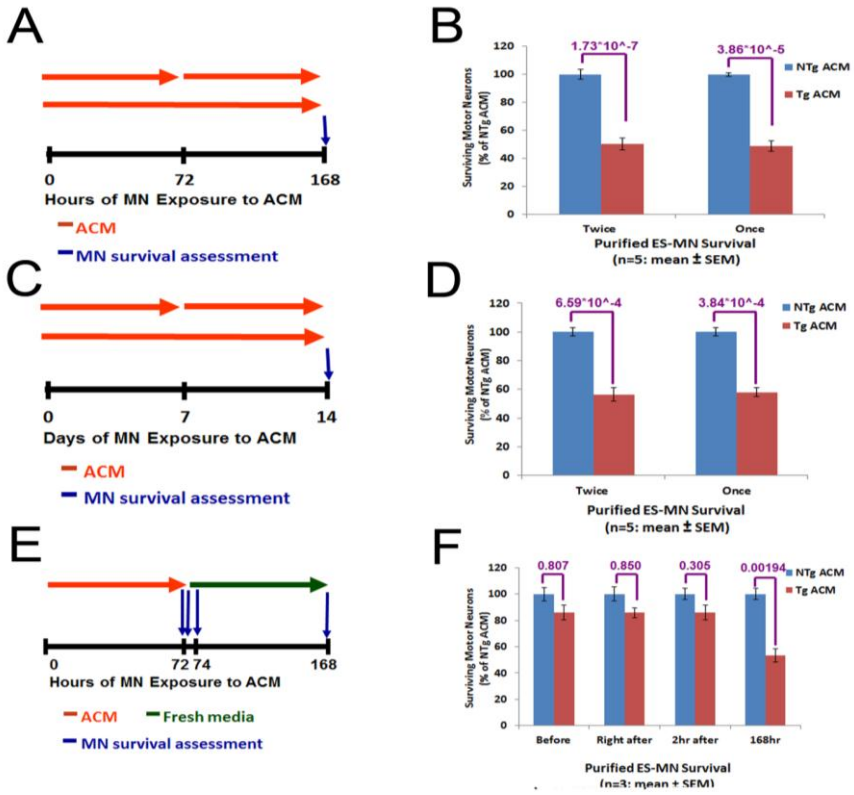

(A) Astrocyte-conditioned medium (ACM) was replenished 72 hours after with a new aliquot from the same batch of ACM. The survival of motor neurons was assessed at the end of 7-day period. (B) Purified embryonic stem cell-derived motor neurons (ES-MNs) showed the same loss in number after 7 days of exposure to mutant ACM with or without replenishment. (C) The study was replicated with longer duration where the media was replenished on the 7th day of exposure and the total ACM exposure was for 14 days. (D) The same results as in (B) were observed. (E) Another study was performed to test the effect of media replenishment on ES-MNs, where the survival of ES-MNs was assessed immediately before, immediately after, and 2 hours after the media replenishment in the 7-day period. (F) There was no difference in the number of ES-MNs that were fixed immediately before, immediately after or 2 hours after their media being replenished. Values represent mean ± s.e.m from five (B, D) and three (F) independent experiments performed at least in triplicate, analyzed by Student's t-test.

without mutant astrocyte-conditioned medium replenishment [Figure 2.11b, d]. These findings suggested that the observed 50% loss in motor neurons is not due to the loss of toxic activity, but is likely reflecting the maximum level of cell loss that can be achieved in this model system under the current experimental conditions. This finding also suggested that, in these cultures, there might be a susceptible and a resistant motor neuron subpopulation. In addition, the medium

replenishment study with the 7-day incubation period was also performed on primary spinal motor neurons and similar results were obtained (data not shown).

While performing the above experiments, it became apparent that replenishing medium might cause a mechanical stress on the embryonic stem cell-derived motor neurons, which could promote cell detachment and spurious alterations in motor neuron numbers. To address this question, purified embryonic stem cell-derived motor neurons were fixed after the third day of incubation immediately before, immediately after and 2 hours after the replenishment with mutant medium [Figure 2.11e]. Regardless of the incubation conditions, the same numbers of GFP^+ embryonic stem cell-derived motor neurons before and after fresh medium additions were noted [Figure 2.11f]. This result indicates that the act of medium replenishment does not cause any alteration in cell numbers in this experimental system, and so, the observed changes in motor neuron number are due to the toxicity emanating from mutant astrocytes.

2.2.5. 72 hours of mutant astrocyte-conditioned medium exposure is the point of no return for embryonic stem cell-derived motor neurons

As discussed in the Introduction, during the degenerating process, neurons, like any other cells, become irreversibly committed to die. Accordingly, it was hypothesized that, in order to develop disease modifying strategies, signaling pathways prior to this point of no return may be the most promising targets. Thus, the next step in this work was to examine when, over the 7-day period, motor neurons exposed to mutant astrocyte-conditioned medium reach a point of no return, i.e. a point when motor neurons become committed to die. To address this question, purified embryonic stem cell-derived motor neurons were exposed to mutant astrocyte-conditioned medium for selected lengths of time and then were put into fresh medium until they reached 7 days *in vitro* [Figure 2.12a].

Figure 2.12: 72 hours of mutant astrocyte-conditioned medium exposure is the point of no return for embryonic stem cell-derived motor neurons

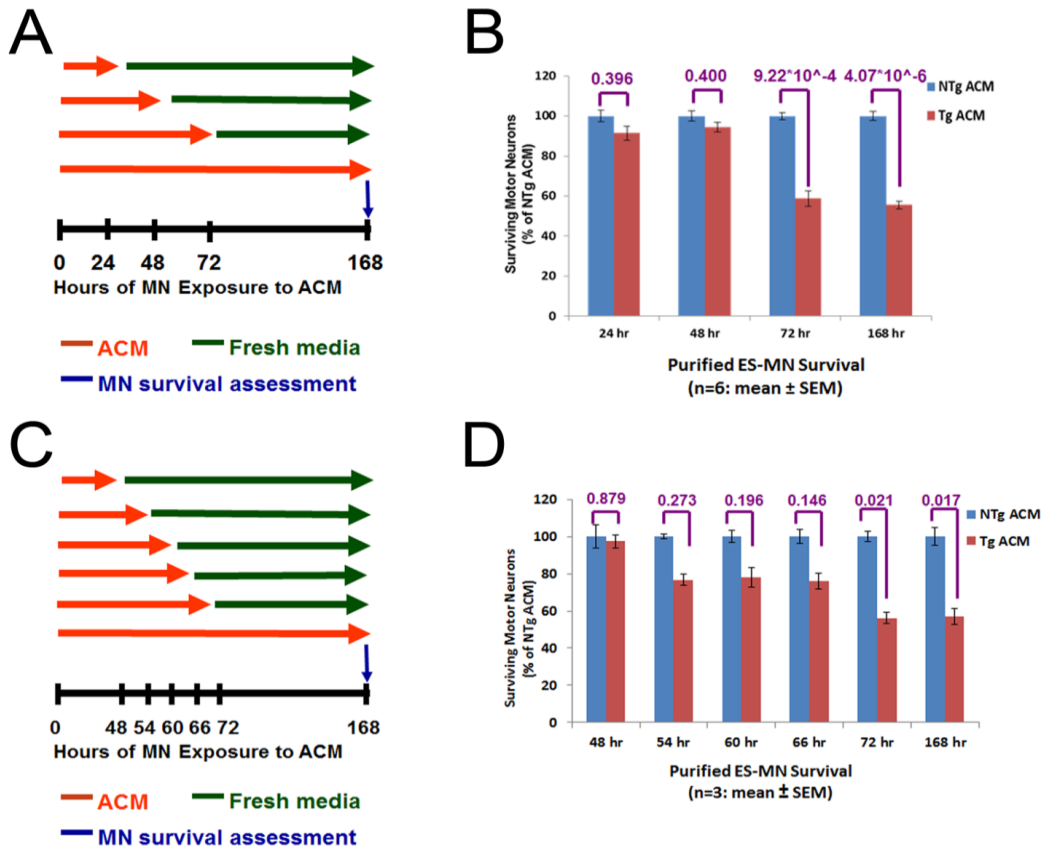

(A) Motor neurons were exposed to astrocyte-conditioned medium for 24, 48, and 72 hours, after which their medium was replaced with fresh medium until they reached 7 days *in vitro*. (B) Motor neurons that were exposed to mutant astrocyte-conditioned medium for 24 and 48 hours, and then being exposed to fresh medium until 7 days *in vitro*, showed almost a full rescue in number. However, the motor neurons that were exposed to mutant astrocyte-conditioned medium for 72 hours, and then put in fresh medium until 7 days *in vitro*, showed the same loss in number as the motor neurons that were exposed to mutant astrocyte-conditioned medium for the whole 7-day period. (C) The study was replicated by extending the exposure durations in between the 48 and 72 hours and adding 54, 60, and 66 hours of exposure to astrocyte-conditioned medium. (D) Purified embryonic stem cell-derived motor neurons that were exposed to mutant astrocyte-conditioned medium for 54, 60, 66, and 72 hours, and then put in fresh medium until they reached 7 days *in vitro*, showed a progressive decay in number until about 50% loss similar to that observed after 168 hours of exposure to mutant astrocyte-conditioned medium. Values represent mean ± s.e.m from six (B) and three (D) independent experiments performed at least in triplicate, analyzed by Student's t-test.

This study revealed that the magnitude of motor neuron loss after 7 days *in vitro*, following 1 or 2 days of exposure to mutant astrocyte-conditioned medium was minimal [Figure 2.12b]. On the other hand, the magnitude of motor neuron loss after 7 days *in vitro*, following 3

days of exposure to mutant astrocyte-conditioned medium was identical to that observed after 7 days of exposure to mutant astrocyte-conditioned medium [Figure 2.12b]. The finding that 3 days of exposure to mutant astrocyte-conditioned medium, followed by the exposure to fresh medium for an additional of 4 days *in vitro*, contrasted with the result found in the survival time course of embryonic stem cell-derived motor neurons discussed in Figure 2.8d, where only about 16% loss was observed in motor neurons after 3 days of exposure to mutant astrocyte-conditioned medium. Taken together, these results indicate that motor neurons exposed to mutant astrocyte-conditioned medium for 3 days do not show an overt degeneration, but their death mechanisms are already turned on and cannot be reversed. This means that 3 days of exposure to mutant astrocyte-conditioned medium is a crucial timepoint at which to study the molecular mechanism underlying mutant astrocyte toxicity for motor neurons. Additionally, the same study was repeated using primary motor neurons, which also showed 3 days of exposure to mutant astrocyte-conditioned medium to be the point of no return for these motor neurons (data not shown).

Since these results indicate that motor neurons are not yet committed to die up to 2 days of exposure to mutant astrocyte-conditioned medium, but by 3 days they are, time frames of exposure were increased for the temporal accuracy of the point of no return to include 54, 60, and 66 hours of astrocyte-conditioned medium exposure [Figure 2.12c]. Results from this aspect of the study show that purified embryonic stem cell-derived motor neurons exhibit a progressive decay in number until they reach about 50% cell loss after 72 hours of exposure to mutant astrocyte-conditioned medium [Figure 2.12d]. Thus, the added timepoints further validated that 72 hours of exposure to mutant astrocyte-conditioned medium is the best estimation of the point of no return for motor neurons under the present experimental conditions.

2.3. Conclusion & Discussion

The studies above enabled us to characterize purified embryonic stem cell-derived motor neurons exposed to mutant astrocyte-conditioned medium as a powerful *in vitro* model to study ALS-linked non-cell autonomous motor neuron degeneration. In these studies, a survival timeline was demonstrated for the purified embryonic stem cell-derived motor neurons upon 7 days of exposure to mutant astrocyte-conditioned medium that is similar to the phenomenon observed in primary motor neurons (Nagai et al., 2007). Interestingly, the 50% motor neuronal loss observed after 7 days of exposure to mutant astrocyte-conditioned medium cannot be due to the loss of toxic activity of the medium, because even if this conditioned medium is changed half-way into the exposure duration, there is no significant further loss of motor neurons. Remarkably, a similar level of motor neuron loss has been reported by Raoul *et al.* (2002) in their study on Fas ligand toxicity in motor neurons (Raoul et al., 2002). Together these studies suggest that the observed 50% of the motor neurons that are spared symbolize a more resistant subpopulation of motor neurons.

Since the purpose of this project is to elucidate the molecular mechanism of non-cell autonomous motor neuron degeneration before neurons become committed to die, a point of no return was identified which will allow the capture of its molecular correlate by the RNA-Seq assay. Accordingly, by testing different exposure times, around 72 hours of exposure to mutant astrocyte-conditioned medium was noted as the time that motor neurons become irreversibly committed to die.

Moreover, compared to the other currently available *in vitro* ALS models, the model system characterized above has multiple advantages: (1) embryonic stem cell-derived motor

neurons combined both the characteristics of postmitotic motor neurons and the fact that they were readily expandable; (2) mutant astrocyte-mediated toxicity was specific for motor neurons; and, (3) this culture system could model disease processes both extrinsic and intrinsic to motor neurons. All of these advantages render embryonic stem cell-derived motor neurons a unique tool to unravel early molecular perturbations that take place in motor neurons in response to ALS-linked astrocyte toxicity.

Before the characterization of this *in vitro* model, there was a question as to whether the purification procedure might render the cells more resistant to the mutant astrocyte-induced toxicity. This was because the isolation method itself caused a physical stress on the cells and could cause or contribute to the demise of the sensitive cell subpopulation in the process. To avoid this scenario, purified embryonic stem cell-derived motor neurons were kept in fresh medium for two days prior to exposing them to mutant astrocyte-conditioned medium. This duration was enough time for the motor neurons to recover from the stress of the purification procedure and to grow processes in culture, suggesting healthy conditions of the cells (data not shown). Furthermore, purified embryonic stem cell-derived motor neurons showed about 50% decline in number after being in fresh medium for 2 days and being exposed to mutant astrocyte-conditioned medium for the following 7 days. This confirmed the stable existence of both the resistant and the sensitive subpopulations in this model system similar to what was observed in the mixed motor neuron cultures.

Following the above-mentioned findings, there are a number of interesting future studies that can be performed to study these subpopulations. For one, another batch of mutant astrocyte-conditioned medium can be added to purified embryonic stem cell-derived motor neurons after

168 hours of exposure to mutant medium to see if a similar molecular mechanism is activated in the resistant subpopulation as was in the sensitive subpopulation. Similarly, the transcriptional alterations that occur in purified embryonic stem cell-derived motor neurons after 168 hours of exposure to mutant astrocyte-conditioned medium, when only the resistant cells survive, can be compared to an earlier exposure time, when sensitive cells are present but are dying. In this manner, the molecular mechanism that is different between the sensitive and resistant subpopulations may be better understood. As of yet, no one has discerned if there are molecular differences between these two motor neuron subpopulations or that the resistant motor neurons merely need more time to become committed to death.

Another interesting future study would be to add the Bax inhibitor, V5, to purified embryonic stem cell-derived motor neurons after 72 hours of exposure to mutant astrocyte-conditioned medium, when motor neurons are already committed to cell death, and to see whether the full rescue of motor neurons can still be observed. If a rescue is not observed, this experiment would further validate that 72 hours of exposure to mutant astrocyte-conditioned medium is the point of no return for motor neurons and their death mechanism cannot be reversed.

Finally, all of the experiments performed on primary motor neurons displayed the same results as those performed on purified embryonic stem cell-derived motor neurons, suggesting strong similarities between these two types of motor neurons. However, even though embryonic stem cell-derived motor neurons are a powerful model system to elucidate the molecular mechanism underlying the ALS-linked astrocyte toxicity for motor neurons *in vitro*, it is still necessary to validate master regulators inferred from the RNA-Seq assay in primary motor

neurons and in transgenic animal models. In the case that a pathway would show pathogenic significance, both *in vitro* and *in vivo*, it would open new doors for therapeutic interventions aimed at targeting deleterious pathways before irreversible damage or commitment to death occurs during ALS-linked motor neuron degeneration.

Chapter 3: Identifying gene alterations germane to the toxicity of mutant astrocytes by elucidating relevant molecular pathways that are dysregulated in motor neurons

3.1. Introduction

Following the initial publication from our laboratory on the effect of mutant SOD1-expressing astrocytes on the survival of spinal motor neurons (Nagai et al., 2007), a number of candidate-based investigations were performed in an attempt to elucidate the molecular underpinning of this *in vitro* neurodegenerative phenotype. Unfortunately, none of our studies have yielded a promising outcome, except for the demonstration that the demise of spinal motor neurons could be mitigated by both the inhibition and the abrogation of the pro-cell death factor Bax. Consequently, we changed our approach by directing our subsequent efforts toward the development and utilization of an unbiased investigation. As a prerequisite for this new research direction, characterization of a modified version of our previous *in vitro* model of ALS using purified embryonic stem cell-derived motor neurons exposed to medium conditioned with mutant SOD1-expressing astrocytes was necessary. This new *in vitro* model represents a much more adaptable system than our primary co-cultures, given the need to enrich the model system in motor neuron molecular signatures.

Following this characterization, an RNA-Seq assay was performed on purified embryonic stem cell-derived motor neurons and then the identified gene expression changes revealed by this assay were subjected to a reverse gene engineering analysis to unravel the molecular networks

engaged in the demise of motor neurons exposed to the toxicity emanating from mutant astrocytes.

As explained in the Introduction, there are a few other groups that have also tried to identify molecular mechanisms underlying ALS-linked astrocyte toxicity for motor neurons using unbiased genomic approaches (Di Giorgio et al., 2008; Ferraiuolo et al., 2011b; Vargas et al., 2008b). However, the majority of these groups focused their attention on the transcriptional changes that occur in mutant astrocytes and on the analysis of what is released from these astrocytes, rather than focusing their attention on the motor neurons themselves, the primary targets of the ALS disease process. Somewhat puzzling is the fact that most of the results generated thus far by these groups turned out to be all different from each other. Furthermore, all of the groups that have reported genomic results have utilized a microarray-based method, which has multiple shortcomings, such as high background noise and limited dynamic range (see below). In their attempt to elucidate the molecular mechanism of non-cell autonomous motor neuron degeneration in ALS, different groups have focused their attention on the differential expression of a selected number of individual genes from their microarray data. This raised the possibility that different prioritizations might have led to different genomic outcomes, even though the studies might have had similar overall genetic expression signatures to begin with.

To gain insights into the molecular underpinning of non-cell autonomous motor neuron degeneration in our model of ALS, our study was designed using: (i) purified embryonic stem cell-derived motor neurons; (ii) the new and powerful genomic technique, RNA-Seq (to be discussed below); and (iii) the bioinformatics algorithms that will allow the interrogation of the whole set of target gene changes to infer the transcription factors (i.e. master regulators) driving

the motor neuron degenerative phenotype triggered by mutant astrocytes. Below is a discussion of the RNA-Seq assay followed by the reverse gene engineering algorithms.

3.1.1. RNA-Seq

RNA-Seq is a high-throughput sequencing-based transcriptome profiling method that directly determines the cDNA sequence. While hybridization-based microarrays are also a high-throughput genomic profiling method, they have several disadvantages in comparison to RNA-Seq assays which render them less potent (Wang et al., 2009): (1) Microarrays have high background signals due to cross-hybridization that need to be normalized using Perfect Match (PM) and MisMatch (MM) signals. (2) They rely heavily on existing knowledge about genome sequence. (3) They have a limited dynamic range of detection due to both background and saturation of signals. (4) Comparing expression levels between experiments is difficult because of complicated normalization methods.

There are also substantial differences in the way these two methods work: In the microarray technique, the extracted total RNA is converted to fragmented cDNA, which is then hybridized with specifically selected microarrays and are read for quantification by fluorescence. In the RNA-Seq assays, on the other hand, the extracted total RNA is converted to a library of cDNA fragments with adaptors attached to one or both ends (Wang et al., 2009). Each molecule is then sequenced in a high-throughput manner to obtain short sequences from one or both ends with 30-400 base pair reads. Following sequencing, the resulting reads are either aligned to a reference genome or reference transcripts, or assembled without the genomic sequence to

produce a genome-scale transcription map that consists of both the transcriptional structure and/or the level of expression for each gene (Wang et al., 2009) [Figure 3.1].

Figure 3.1: Schematic representation of a RNA-Seq assay

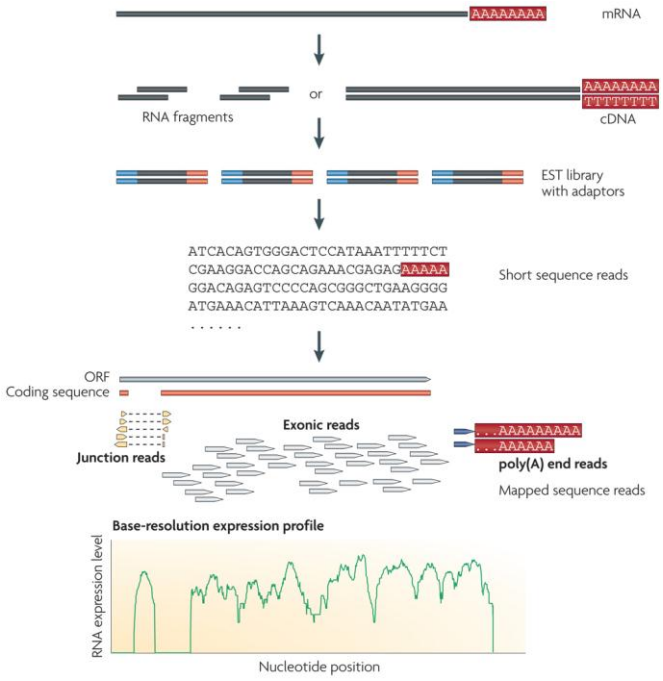

This figure, excerpted from Wang *et al.* (2009) represents how the RNA-Seq assay works. Briefly, long RNAs are first converted into a library of cDNA fragments. Then, sequencing adaptors are added to each cDNA fragment and a short sequence is obtained from each cDNA by high-throughput sequencing technology. The resulting sequence reads are aligned with either a reference genome or a transcriptome, and classified as: junction, exonic or poly(A) end reads. These reads are then used to generate a base-resolution expression profile for each gene.

The following features of the RNA-Seq technology make it much more advantageous over the microarray assay (Wang et al., 2009): (1) RNA-Seq is not limited to detecting transcripts that correspond to existing genomic sequences, making it more desirable for non-model organisms whose genomic sequences are not yet established, in addition to detecting RNA molecules, such as microRNAs, and other non-coding RNAs. (2) While the shorter reads (about 30 base pairs) from RNA-Seq give information about how two exons are connected, longer reads expose connectivity between multiple exons, making RNA-Seq possible to elucidate complex transcriptomes. (3) Compared to microarrays, RNA-Seq assays have very low, if any, background signal. (4) They have no upper limit for quantification, only a number of sequences obtained, which makes analysis much easier and data more robust. (5)

While microarrays are less sensitive for genes expressed either at very low or high levels, and thus have a smaller dynamic range, RNA-Seq has been shown to be highly accurate for quantifying gene expression at any level. (6) RNA-Seq requires less RNA per sample, since it has no amplification step, and costs less, making it a very desirable method over the microarray assay. Please see Table 3.1 for a summary of the comparison of the RNA-Seq to the microarray assay.

Table 3.1: Comparison of RNA-Seq versus microarray

Technology	Microarray	RNA-Seq
Principle	Hybridization	High-throughput sequencing
Resolution	From several to 100 base pairs	Single base
Throughput	High	High
Reliance on genomic sequence	Yes	In some cases
Background noise	High	Low
Dynamic range to quantify gene expression level	Up to a few hundred fold	>8,000 fold
Ability to distinguish different isoforms	Limited	Yes
Ability to distinguish allelic expression	Limited	Yes
Required amount of RNA	High	Low

Cost for mapping transcriptomes to large genomes	High	Relatively low

This table, excerpted and modified from Wang *et al.* (2009) summarizes the technical (in red), applicative (in blue), and practical (in black) differences between the microarray and the RNA-Seq assay. This comparison reveals that the RNA-Seq assay has advantages at every level of transcriptomics, from being high-throughput with low background noise, to having the ability to distinguish allelic expression, to requiring a low amount of RNA with relatively low cost for mapping transcriptomes of large genomes, over microarrays.

Although, as discussed above, RNA-Seq has several advantages over microarrays, it has certain challenges as well. First of all, the cDNA fragmentation step is biased towards the identification of sequences from the 3' ends of transcripts. Secondly, for large transcriptomes, the majority of the sequence reads match multiple locations in the genome, which renders it necessary to proportionally assign the number of multi-matched reads mapped to their neighboring unique sequences (Mortazavi et al., 2008). Finally, there is the challenge of coverage versus cost, where the larger the genome being sequenced, the more complex the transcriptome needs to be and the more sequencing depth is necessary for adequate coverage (Wang et al., 2009). These challenges are currently addressed with the new developments in the field, such as the transcription start site mapping, strand-specific measurements, gene fusion detection, small RNA characterization and detection of alternative splicing events (Ozsolak and Milos, 2011), making the method much more efficient.

Overall, with no probes or primers to design, RNA-Seq provides an unbiased, highly sensitive and powerful high-throughput method that records the numerical frequency of a sequence in a transcriptome.

3.1.2. Reverse gene engineering

As discussed in the preceding chapter, the goal of this thesis was to elucidate the signaling network that is activated in motor neurons in response to the toxic activity from mutant astrocytes before motor neurons become committed to die. To achieve this goal, a traditional bioinformatics approach that focuses on a selected number of genes that are the most differentially expressed was not desirable. Instead, using the whole genomic data to first define particular molecular signatures and then using these signatures to identify transcription factors that most likely regulate them seemed more appropriate. In order to do this, an unbiased reverse gene engineering analysis pioneered by the Califano group was decided upon (Carro et al., 2010).

The rationale for using this reverse gene engineering analysis was the following: if it is assumed that when motor neurons are subjected to the exogenous insult that emanates from mutant astrocytes, then the astrocyte-derived putative soluble factor ligates a surface receptor, thereby triggering a transducing signal. Once this signal is initiated within motor neurons, specific transcription factors are activated, which, in turn, enhance or repress the expression of their target genes. Reverse gene engineering analysis computes the overlap between the expression of target genes of each transcription factor and the differentially expressed gene signatures from the RNA-Seq data to deduce a set of transcription factors that best explain the observed gene profiles. This analysis can be carried forward by utilizing the differential activity of transcription factors as a proxy to determine the activity of signaling molecules upstream to these factors all the way up to the cell surface receptor. Therefore, using this analysis, an entire

signaling network can be inferred instead of limiting the analysis to a restricted number of target genes [Figure 3.2].

Figure 3.2: Inferring transcription factors from the RNA-Seq data

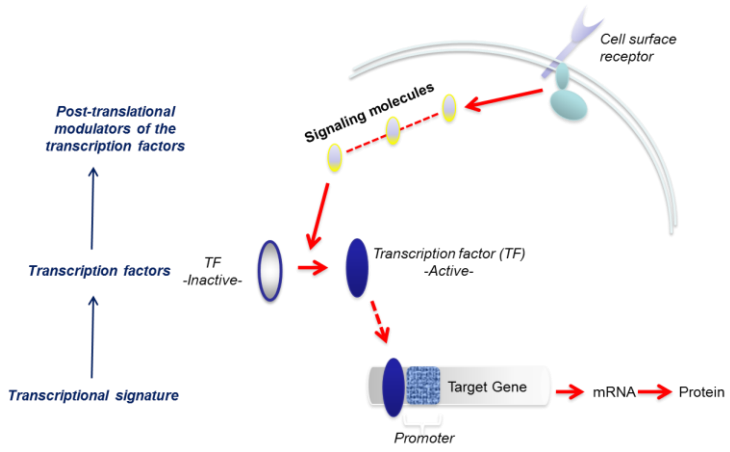

This schematic represents how transcription factors are inferred from the RNA-Seq data. When a cell receives an exogenous signal through its cell surface receptor, it causes the activation of certain signaling molecules, which are responsible from activating specific transcription factors that either enhance or repress the expression of their target genes. Reverse gene engineering analysis computes the overlap between the expression of target genes of each transcription factor and the differentially expressed gene signature from RNA-Seq data and infers a set of transcription factors as the master regulators of the cell phenotype that is being studied.

Consequently, reverse gene engineering analysis consists of two steps (Carro et al., 2010): (1) the estimation of the activity of transcription factors from that of their transcriptional targets using the Algorithm for the Reconstruction of Gene Regulatory Networks in a Mammalian Cellular Context (ARACNe) (Basso et al., 2005; Margolin et al., 2006a; Margolin et al., 2006b); and (2) the identification of transcription factors that are master regulators of the specific phenotype that is being studied, which overlap between their targets and the differential expression signatures extracted from the RNA-Seq (or gene array) data using the Master Regulator Inference algorithm (MARINa) (Lefebvre et al., 2010). Below is an explanation of both of these steps in more detail.

3.1.2.1. ARACNe

Because proteins, which are gene products themselves, regulate gene expression, statistical associations between genes' mRNA levels were thought to be useful to unravel gene regulatory mechanisms (Margolin et al., 2006a). ARACNe, as an information theory-based algorithm for the reverse gene engineering of transcriptional networks using microarray data, predicts potential functional associations among genes by identifying statistical dependencies between gene products (Margolin et al., 2006b). It first identifies statistically significant gene-gene co-regulation by mutual information, which is an information theoretical measure of relatedness, and then eliminates indirect relationships, by applying a well-known staple of data transmission theory called 'data processing inequality', to construct a network (i.e. an interactome) with a high probability of representing either direct regulatory interactions or interactions mediated by post-transcriptional modifiers between transcription factors and their target genes that are undetectable from microarray data (Basso et al., 2005).

One of the main challenges of reverse gene engineering algorithms is the complexity of mammalian networks. ARACNe has been tested on a few synthetic data sets and has proved to be a very powerful algorithm in dealing with these complex networks. For example, ARACNe predictions were validated for the *MYC* protooncogene by chromatin immunoprecipitation assays, which demonstrated that *MYC* binds *in vivo* to the regulatory region of 11 out of 12 genes selected among those inferred by the algorithm (Basso et al., 2005). ARACNe is, however, only the first step in understanding the molecular mechanism of a cellular network and needs to be followed by the MARINa analysis, which is explained next.

3.1.2.2. MARINa

MARINa is designed to infer the differential activity of transcription factors that regulate the cell phenotype that is being studied (Lefebvre et al., 2010). Since differential expression at the mRNA level is a poor indicator of a transcription factor's regulatory activity, Essentially, MARINA is an enrichment algorithm that computes the activity of a transcription factor based on the enrichment of the factor's target genes, whose activity it induces or represses, on a genome-wide expression signature.

In MARINa, first each transcription factor gets associated with a positive and a negative regulon using its activated and repressed targets in the interactome, respectively. Then, the enrichment and activity of each transcription factor is computed by Gene Set Enrichment Analysis and the differentially expressed target odds ratio score. Finally, MARINa is corrected for the transcription factor-regulon overlap to avoid false-positive master regulator inference (Lefebvre et al., 2010). At the end of this step, MARINa computes the statistical significance of the overlap between the regulon of each transcription factor and the differentially expressed gene signature from RNA-Seq data and infers a set of transcription factors as the master regulators of the certain cellular phenotype that is being studied.

One example that combined both the ARACNe and the MARINa algorithms came in 2010, where Carro *et al.* first assembled a glioma-specific regulatory network using ARACNe and then interrogated this interactome using MARINa to reveal a transcriptional network that activates the expression of mesenchymal genes in malignant glioma (Carro et al., 2010). The group then showed that the ectopic expression of two master regulators from the MARINa analysis reprogram neural stem cells into the aberrant mesenchymal signature, and that the

elimination of these regulators in glioma cells lead to the collapse of the mesenchymal signature (Carro et al., 2010).

This study was the first to demonstrate the use of reverse gene engineering algorithms that were generated by the Califano group to successfully elucidate the molecular mechanism of complex mammalian cell phenotypes. While the nature of these algorithms render them applicable to any cell type and/or phenotype (Margolin et al., 2006a), so far the algorithms have primarily been used for *in vivo* tumor samples from patients, such as glioblastoma and neuroblastoma cells, and in phenotypes related to cancer. Thus, this project is the first to utilize these algorithms for cells other than tumor cells, and moreover, in a neurodegeneration context. Below is the presentation of the results gathered from the RNA-Seq data using the reverse gene engineering analysis.

3.2. Results

3.2.1. Experimental design

Given the observations from the previous chapter, it was postulated that the molecular changes linked to the early responses of motor neurons to the toxic activity released from mutant astrocytes are likely to occur at timepoints ≤ 72 hours. Thus, to study these early molecular perturbations that occur in motor neurons after they are exposed to the toxicity emanating from mutant astrocytes, but before they become committed to die, the following timepoints were included in the RNA-Seq assay: 1) 0-hour, the time before any astrocyte-conditioned medium is added to the motor neurons. This was the control timepoint and was used to test for any technical variation that might come from the handling of samples with the same replicate number. 2) 24-

hour, the amount of exposure time to mutant astrocyte-conditioned medium at which motor neurons show a minimal loss in number and their death mechanism is activated, but this can be reversed [Figure 2.12b]. This timepoint was selected for any acute effect of the mutant astrocyte-conditioned medium in conjunction with minimal loss in motor neurons. 3) 72-hour, the time of commitment to death; and 4) 168-hour, the amount of exposure time to mutant medium when the sensitive motor neuron subpopulation dies and the resistant subpopulation remains in culture. This timepoint was selected to subtract the resistant motor neuron subpopulation signature from that of the susceptible subpopulation to better refine the susceptible signature.

During the process of determining the experimental design for the RNA-Seq assay, there were two objectives: (1) to have an adequate number of experimentally independent sample replicates for the assay to be properly powered; and (2) to minimize the non-biological variation that is added during the handling of the samples (i.e. the batch effect). To address the first objective, the number of replicates necessary to do enough permutations in the MARINa analysis needed to estimate random enrichment scores to form a random gene expression signature was computed to be six samples per genotype and per timepoint; please see the *Experimental Methods*.

Consequently, the experimental design for the RNA-Seq assay was set to be the extraction of total RNA samples from purified embryonic stem cell-derived motor neurons exposed to medium conditioned either with non-transgenic, transgenic wild-type SOD1, or transgenic mutant SOD1 astrocytes for either 0, 24, 72 or 168 hours with six sample replicates each [Table 3.2]. Following this design, the total number of RNA samples ended up being 72.

Table 3.2: Replicates per timepoint and treatment for the RNA-Seq assay

Treatment	Time	Replicates
MN	**0**	**18**
NTg	**24**	**6**
Tg	**24**	**6**
WT	**24**	**6**
NTg	**72**	**6**
Tg	**72**	**6**
WT	**72**	**6**
NTg	**168**	**6**
Tg	**168**	**6**
WT	**168**	**6**

The number of experimentally independent replicates obtained per timepoint and treatment samples for the RNA-Seq assay. In total, there were 72 samples. MN: Untreated motor neuron sample; NTg; non-transgenic astrocyte-conditioned medium treatment; Tg: transgenic mutant SOD1 astrocyte-conditioned medium treatment; WT: transgenic wild-type SOD1 astrocyte-conditioned medium treatment.

For the second objective, to minimize potential batch effect, the following steps were taken in the handling of samples before proceeding with the RNA-Seq assay: (1) To minimize any technical variance that could have arisen from astrocyte-conditioned medium, a small portion of every aliquot from different types of astrocyte-conditioned medium was taken out and exposed to purified embryonic stem cell-derived motor neurons. After 7 days of exposure to these small portions of medium, the survival of motor neurons was assessed to validate that the medium does in fact show the desired effect on motor neurons. Once the validation was done for every aliquot, the separate aliquots belonging to the same type of astrocyte-conditioned medium were pooled together to unify their effect on motor neurons [Figure 3.3a]. (2) To minimize the batch effect on motor neurons, embryonic stem cells that came from the same source in 6 different aliquots were thawed, differentiated into motor neurons and purified at the same time and under the same conditions [Figure 3.3b]. (3) All purified motor neurons coming from the same aliquot of embryonic stem cells were plated together, exposed to astrocyte-conditioned medium, and had their RNA extracted at the same time [Figure 3.3c]. Moreover, purified motor neurons for each of the samples were plated on three wells next to each other in a 12-well cell culture dish. Their RNAs were then pooled together as one sample to get enough total RNA for each sample. In the end, RNA samples coming from the same aliquot were considered to have the same replicate number. (4) RNA isolation and quality assessment of each of the 72 samples were also done at the same time. The quality of every total RNA sample was found, using Bioanalyzer, to have an RNA integrity number (i.e. the assessment of RNA integrity determined by the entire electrophoretic trace of the RNA sample) above 9, which represents the highest

Figure 3.3: The RNA-Seq experimental design to minimize technical variance

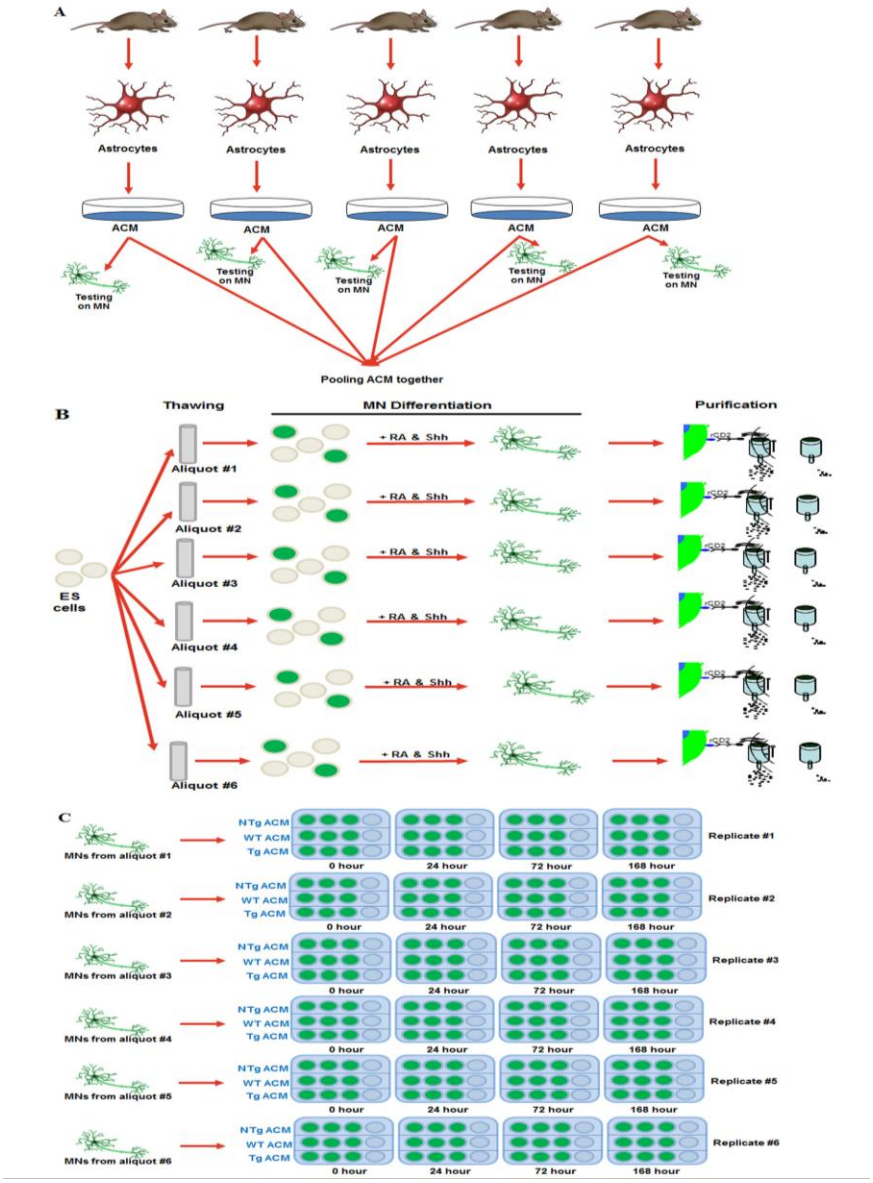

(A) Medium conditioned with separate aliquots belonging to the same type of primary astrocytes were collected and pooled together to unify their effect on motor neurons (MNs), after testing out a proportion of every aliquot on MNs to confirm the effect of the medium; (B) Embryonic stem cells from the same source in 6 different aliquots were thawed, differentiated into MNs, and purified at the same time and under the same conditions; (C) All purified embryonic stem cell-derived MNs from the same replicates and timepoints were exposed to astrocyte-conditioned medium (ACM) and had their RNA extracted at the same time. RNA samples coming from the same aliquot were considered to have the same replicate number. Moreover, purified MNs belonging to the same replicate and timepoint were plated in the same 12-well cell culture dish into 3 consecutive wells per ACM treatment, where their RNAs would be collected and pooled together to have a single RNA sample. ES cells: embryonic stem cells, RA: retinoic acid, Shh: sonic hedgehog, NTg: non-transgenic medium, WT: transgenic wild-type SOD1 medium, Tg: transgenic mutant SOD1 medium.

quality.

At the end of these steps in the experimental design, 72 total RNA samples were extracted from purified embryonic stem cell-derived motor neurons with the highest RNA quality, minimal batch effect, and enough replicate numbers to run an efficient MARINa analysis. These RNA samples were then given to the Genomic Center of Columbia University for the RNA-Seq assay, which consisted of the fragmentation, sequencing, and mapping of the total RNA samples to the mouse genome.

3.2.2. Data pre-processing

The RNA-Seq data was received from the Genomic Center in the format of mapped reads, which consisted of the position of each 100-base long read in the mouse genome. To align the position of each read with a gene on a chromosome, the full mouse genome from the University of California San Diego database, which contained 21,761 genes, was downloaded. This genome was then utilized to align each read from the RNA-Seq data to a gene and the reads were summarized to compute how many reads per gene there were for each sample. From 21,761 genes, 19,179 of them were detected to have at least ten reads across all samples. Ten reads in at least one of the samples was used as a cutoff value for a gene, where the gene that did not make the cutoff was removed from the analysis. This was because ten reads was the value computed by chance in a Poisson distribution, and thus was considered an erroneous read value.

After the selection of the 19,179 genes, their read counts were normalized using Trimmed Mean of M values (TMM) normalization (Robinson and Oshlack, 2010). In this normalization method, the sample with the highest number of read counts was taken as a reference. Then, the

trimmed mean of the log expression ratio between each sample and the reference sample was calculated. Normalization was an important step in the RNA-Seq analysis, because it allowed for comparisons between experiments and the control of extraneous variation among experiments, which could be introduced during sample preparation and processing for the assay.

Following the normalization, the variance in the read counts was stabilized using the negative binomial fit method, which utilizes the linear model: noise variance = mean + deviation (Anders, 2010). This variance stabilization method removed the association between the variance and signal level of the data, making the variance independent of the mean of read counts across all of the genes.

After these pre-processing steps, a scatter plot showing the relationship between the total counts and size-factor was drawn to ensure that the variance was successfully stabilized across all samples. In this scatter plot, a linear relationship between the counts and the samples was observed [Figure 3.4], which confirmed that there is no strong bias in any given gene that can distort the distribution of the read counts. In addition, supervised [Figure 3.5a] and unsupervised [Figure 3.5b] cluster analyses of the data showed successful segregation and clustering of the samples by the treatments they received and their timepoints. These visualization methods further confirmed the lack of technical bias in the samples, which proved the normalization and variance stabilization steps very effective.

Figure 3.4: No strong bias in any of the genes for all of the samples of the RNA-Seq data

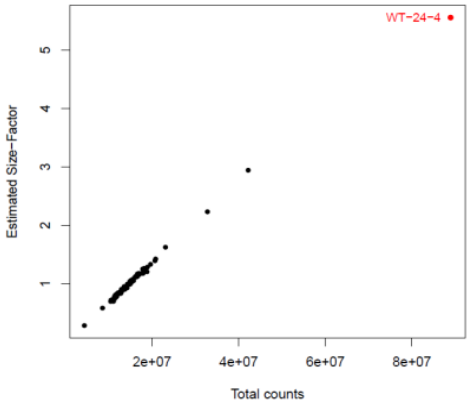

This scatter plot demonstrates the relationship between the total counts and size-factor for all of the samples. The linear plot suggests that there is no strong bias in any given gene in any of the samples that can distort the distribution of the reads. WT-24-4 (in red) is the 24-hour sample that was treated with transgenic wild-type SOD1 astrocyte-conditioned medium whose replicate number was 4. While it is distributed away from the other samples, the fact that it is still linearly associated to them makes it carry minimal variance.

3.2.3. Gene expression signatures

Next in line was the generation of gene expression signatures that made use of all of the timepoints of the RNA-Seq assay, even though the main interest, for the purpose of this project, was in the signature at the time of motor neuron commitment to die. The idea was to use the other signatures for future studies; please see the Conclusion section of this chapter. Consequently, five gene expression signatures were generated.

The initial signature was of the "early response" that takes place in motor neurons at the 24-hour timepoint versus the 0-hour timepoint; before they show any overt degeneration and when their death mechanism can be reversed. The second one was the "commitment to death" signature, where the gene expression of the 72-hour timepoint was compared to that of the 0-hour timepoint. This was followed by the "resistance phenotype" signature comparing the 168-hour timepoint, when the sensitive motor neurons die and the resistant subpopulation remains, to the 0-hour timepoint. The two final signatures were the "commitment vs. early response" signature comparing the differential gene expression between the 72-hour and 24-hour timepoints, and the "resistance vs. commitment" signature comparing the 168-hour to 72-hour timepoints.

Figure 3.5: Cluster analyses based on the RNA-Seq data for different treatments and timepoints

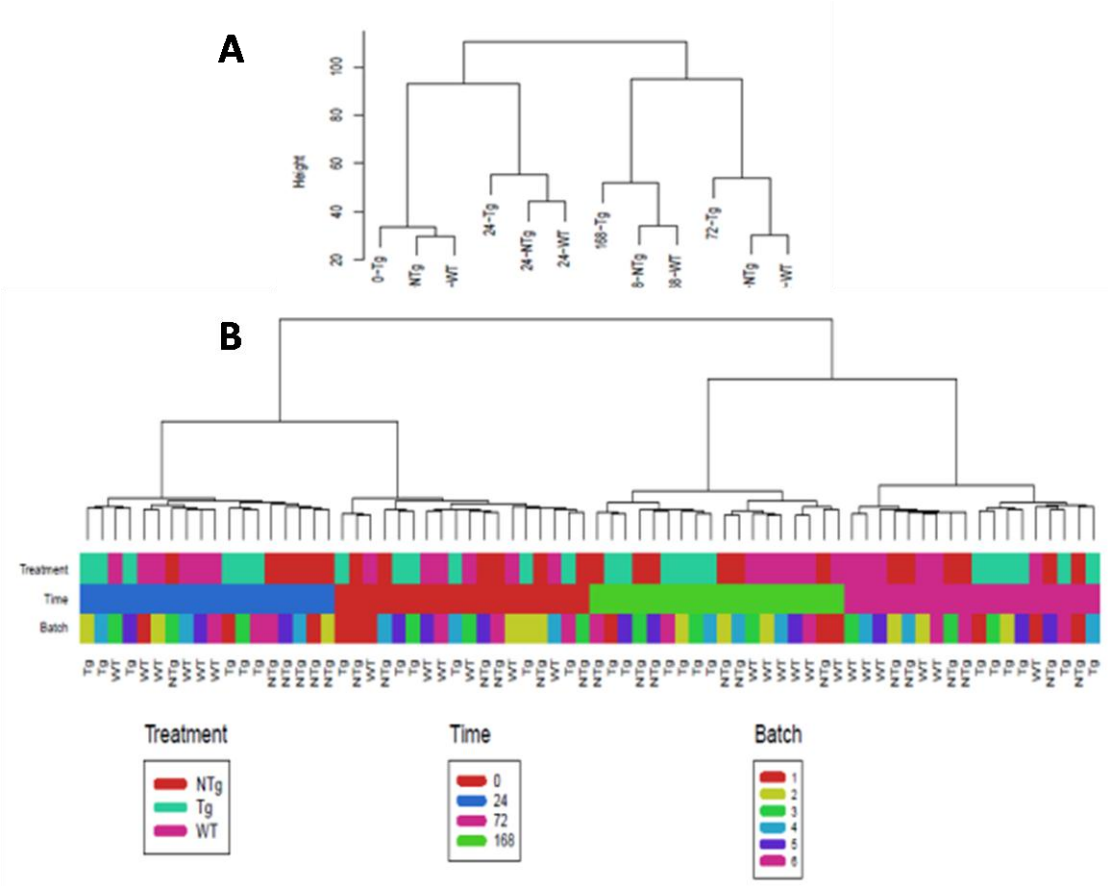

The (A) supervised and the (B) unsupervised cluster analyses on the RNA-Seq data at different treatment and timepoints. These visualizations of samples confirm that experimental variation coming from the replicates is minimal. (Batch stands for the replicate number.) NTg: non-transgenic astrocyte-conditioned medium, WT: transgenic wild-type SOD1 astrocyte-conditioned medium, Tg: transgenic mutant SOD1 astrocyte-conditioned medium

These gene expression signatures were obtained by fitting the read counts per gene across all samples to a linear model using the *limma* package from Bioconductor. The data was fitted to a two-factor linear model: $y = \mu + \alpha T + \beta B + \varepsilon$, where μ was the basal level of read counts for a gene, α was the coefficient of treatment between values 0 and 1, β was the coefficient of batch effect, and ε stood for the error. Using this linear model, a two-way ANOVA test was performed,

per gene across all samples yielding α and β (with no computation of the interaction between the coefficients). Interaction between α and β was not computed because the treatment effect came from the astrocyte-conditioned medium, and the batch effect from the motor neurons being differentiated from the same source of embryonic stem cells, assuming that there is no biological correlation between the treatment and the batch effect.

After computing coefficients for every gene across all of the samples with this linear model fitting, the relevant signatures were obtained below by subtracting the coefficients belonging to the non-transgenic (NTg) and transgenic wild-type SOD1 (WT) astrocyte-conditioned medium treatments from that of the transgenic mutant SOD1 (Tg) astrocyte-conditioned medium. For the 24 vs. 0, 72 vs. 0, and 168 vs. 0 hour signatures, the coefficients of 0-hour timepoint were not subtracted from the other timepoints, because the 0-hour timepoint coefficients for NTg, WT, and Tg treatments were equal (data not shown) and they canceled each other in the equation, as explained below in the 24 vs. 0 hour signature example:

24 vs. 0 hour signature:

(Tg.24 - Tg.0) – [(WT.24 –WT.0 + NTg.24 - NTg.0)/2]

= 2Tg.24 –2Tg.0 – WT.24 + WT.0 – NTg.24 + NTg.0

Since Tg.0 = WT.0 = NTg.0;

= 2Tg.24 ~~–2Tg.0~~ – WT.24 ~~+ WT.0~~ – NTg.24 ~~+ NTg.0~~

= 2Tg.24 – WT.24 – NTg.24

= Tg.24 – [(WT.24 + NTg.24)/2].

:

Thus, the relevant signatures were obtained in the following manner:

1. "Early response" - 24 vs. 0 hour:

   (Tg.24) – [(WT.24 + NTg.24)/2]

2. "Commitment to death" - 72 vs. 0 hour:

   (Tg.72) – [(WT.72 + NTg.72)/2]

3. "Resistance phenotype" - 168 vs. 0 hour:

   (Tg.168) – [(WT.168 + NTg.168)/2]

4. "Commitment vs. early response" - 72 vs. 24 hour:

   (Tg.72 − Tg.24) – [(WT.72 − WT.24 + NTg.72 − NTg.24)/2]

5. "Resistance vs. commitment" - 168 vs. 72 hour:

   (Tg.168 − Tg.72) – [(WT.168 − WT.72 + NTg.168 − NTg.72)/2]

The subtracted coefficients represented the significance of the treatment effect per gene in the signature. The reason why the NTg and WT treatment coefficients were averaged instead of being subtracted separately from the Tg treatment was because no gene was found to be differentially expressed with a false discovery rate corrected p-value less than 0.05 between the NTg and WT treatments (data not shown). This suggested that there is no significant transcriptional difference motor neurons that are exposed to medium conditioned with non-transgenic versus transgenic wild-type SOD1-expressing astrocytes.

Following the selection of gene expression signatures, the number of differentially expressed genes per signature from the two-way ANOVA analysis were examined [Table 3.3].

The 72 vs. 0 and 168 vs. 0 hour signatures were found to be the most powerful, since they had the highest number of significantly differentially expressed genes, which renders them good candidates on which to perform the Master Regulator Analysis.

Table 3.3: Number of differentially expressed genes for each signature

Signature	FDR<0.05	FDR<0.01
24h - 0h	142	80
72h - 0h	1247	420
168h - 0h	1846	952
72h - 24h	394	57
168h - 72h	148	40

The number of differentially expressed genes for each signature with false discover rate (FDR) corrected p-values less than 0.05 or 0.01. In this analysis, the 72 vs. 0 and 168 vs. 0 hour signatures have the highest number of genes, which makes them the most powerful signatures on which to perform the Master Regulator Analysis.

3.2.4. Reverse gene engineering analysis

Next, reverse gene engineering analysis was performed to determine the differential activity of transcription factors that are the candidate master regulators of the molecular mechanism underlying the ALS-linked mutant astrocyte toxicity for motor neurons. In order to do this,

Absolute Enrichment Master Regulator Analysis was performed ignoring the transcription factor mode-of-action on their targets. In this manner, a transcription factor could be identified as differentially active, because of the treatment, without inferring whether the transcription factor is more or less active than the control. This analysis was done independently using seven different transcriptional interactomes that were available from the Califano group. The reason why the analysis was performed using all of the available interactomes was to objectively compare the efficiency of each interactome independently to determine the one that best fits our data. These interactomes were a human prefrontal cortex interactome generated from the Harvard Brain Tissue Resource Center, a human high-grade glioma interactome from The Cancer Genome Atlas (TCGA) consortia, a human glioma interactome from the Philips paper (2006), a human glioma interactome from the Sun paper (2006), a human integrated glioma interactome, a neuroblastoma interactome, and finally a mouse total brain interactome. Below is more detailed information about each of these interactomes.

3.2.4.1. The human prefrontal cortex interactome

The human prefrontal cortex interactome was reverse-engineered from 153 normal pre-frontal cortex tissue samples obtained from the Harvard Brain Tissue Resource Center dataset. This interactome contained 1,432 transcription factors and 20,691 target genes with 267,873 regulatory interactions. The homoloGene database, which is a system for the automated detection of homologs among the annotated genes of several completely sequenced eukaryotic genomes, was used to obtain the murine ortholog genes. Using this database, a 1,176 transcription factors x 15,895 target genes interactome was generated with 198,886 regulatory interactions.

Transcription factors regulating the signatures were inferred with MARINa, weighing the contribution of each target gene according to the number of regulatory interactions each gene has.

3.2.4.2. The human high-grade glioma interactome from TCGA consortia

The TCGA high-grade glioma interactome was reverse-engineered from 319 glioblastoma grade IV samples obtained from TCGA. This interactome contained 885 transcription factors and 9510 target genes with 187,272 regulatory interactions. The homoloGene database was used to obtain the murine ortholog genes and generated a 763 transcription factors x 8,934 target genes interactome, with 164,476 regulatory interactions. Transcription factors regulating the signatures were inferred with MARINa, weighing the contribution of each target gene according to the number of regulatory interactions each gene has.

3.2.4.3. The human glioma interactome from the Philips paper (2006)

The dataset for this interactome consisted of 154 human glioblastoma multiform samples profiled on the HG-U133A Affymetrix arrays. Processing this dataset with reverse engineering produced 8,332 probe-clusters mapping to 8,293 genes. The samples were then classified into 71 mesenchymal, 47 proneural and 36 proliferative gene groups. The Phillips dataset-based transcriptional interactome consisted of 8,240 nodes and 110,979 edges, representing 711 transcription factors for 8,236 target gene interactions.

3.2.4.4. The human glioma interactome from the Sun paper (2006)

The dataset for this interactome consisted of 181 human glioblastoma multiform, 131 astrocytoma and 57 oligodendroglioma samples profiled on the HG-U133 Plus 2 Affymetrix platform. Processing this dataset by reverse engineering produced 14,447 probe-clusters mapping to 13,265 genes. The Sun dataset-based transcriptional interactome consisted of 11,731 nodes and 137,913 edges, representing 1,060 transcription factors for 11,728 target gene interactions.

3.2.4.5. The human integrated glioma interactome

This interactome was built by combining all three human glioma interactomes from the TCGA consortia, Philips (2006) and Sun papers (2006).

3.2.4.6. The human neuroblastoma interactome

The human neuroblastoma interactome was reverse-engineered from 189 samples profiled on Affymetrix exon arrays. This interactome contained 1,360 transcription factors and 14,200 target genes with 175,499 regulatory interactions. The homoloGene database was used to obtain the murine ortholog genes and generated a 1,085 transcription factors x 12,104 target genes interactome, with 138,231 regulatory interactions. Transcription factors regulating the signatures were inferred with MARINa, weighing the contribution of each target gene according to the number of regulatory interactions each gene has.

3.2.4.7. The mouse total brain interactome

The mouse total brain transcriptional interactome was reverse-engineered using ARACNe from a

dataset containing different brain regions from different mouse strains. It represented 1,345 transcription factors regulating 16,527 target genes through 388,550 interactions. MARINa was performed for each of the gene expression signatures, considering only single transcription factor enrichment.

This analysis done on the mouse total brain interactome identified 0 differentially active transcription factors for the 24 vs. 0 hour signature, 120 for the 72 vs. 0 hour signature, 0 for the 168 vs. 0 hour signature, 119 for the 72 vs. 24 hour signature, and 8 for the 168 vs. 72 hour signature for false discovery rate-corrected p-values of less than 0.05.

After performing the Master Regulator Analysis on these seven interactomes, a comparison of these interactomes was made to decide which one would best fit the RNA-Seq data. This was an important selection, since none of the sources of the interactomes exactly matched the *in vitro* model cell type used for the RNA-Seq assay. For the interactome comparison, the absolute enrichment levels of the top 100 transcription factors across the seven transcriptional interactomes were compared for the 24 vs. 0, 72 vs. 0, and 168 vs. 0 hour signatures [Figure 3.6]. The enrichment score is represented as $-\log_{10}$ (p-value) to make it more scalable. In this comparison, the interactome that had the highest number of transcription factors with statistically significant p-values would be the most powerful one and the one that most closely matches the gene expression signatures of the RNA-Seq data.

By this criterion, the mouse total brain interactome outperformed all of the other interactomes. This outperformance was especially obvious for the strongest gene expression signature, the 72 vs. 0 hour signature, which inferred the highest number of differentially active

transcription factors [Figure 3.6b]. Thus, the focus was on the reverse gene engineering analysis results from the mouse total brain interactome with inferred master regulators from the 72 vs. 0

Figure 3.6: The mouse total brain interactome is the most biologically relevant for the RNA-Seq data

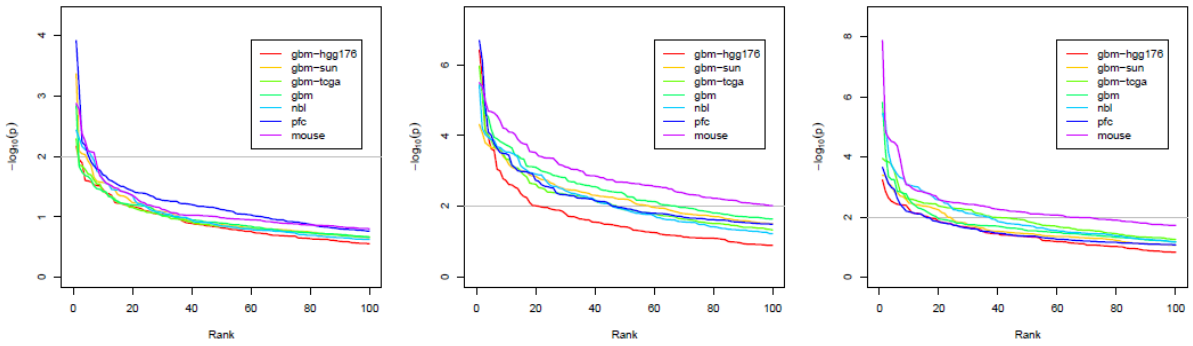

(a) 24h vs. 0h (b) 72h vs. 0h (c) 168h vs. 0h

This figure compares the enrichment score, as $-\log_{10}$ (p-value), of the top 100 transcription factors from the MARINa analyses of the 24 vs. 0, 72 vs. 0, and 168 vs. 0 hour signatures on the seven available interactomes from the Califano group. Rank is the top 100 transcription factors from 1 to 100 and the line, coming from y=2, represents the point of significance, where p-values < 0.01. The most powerful signatures, the 72 vs. 0 and 168 vs. 0 hour, show the mouse total brain interactome to be the most biologically relevant interactome. Gbm-hgg176: the human glioblastoma interactome from the Philips paper, gbm-sun: the human glioblastoma interactome from the Sun paper, gbm-tcga: the human glioblastoma interactome from the TCGA consortia, gbm: the integrated human glioblastoma interactome, nbl: the human neuroblastoma interactome, pfc: the human prefrontal cortex interactome, mouse: the mouse total brain interactome.

hour signature for biological validation, since this signature was the strongest and had the most biological relevance for commitment to death. Please see the Appendix for the complete results on all of the five signatures from this interactome.

3.2.5. Top 25 master regulators

The main purpose of this project after the RNA-Seq assay was to demonstrate the pathological significance of the selected transcriptional regulators. The reverse gene engineering analysis from the 72 vs. 0 signature provided 120 transcription factors, which is a very large number to biologically validate. Therefore, the decision was to focus on the top 25 of these transcription

factors, which consisted of *Psmc3ip, Camta1, Tgif1, Tcf3, Tcf7, Trp53, Zfp503, Zfp235, Hivep2, Mycn, Dennd4a, Zfp36l1, Epas1, App, Irx5, Myb, Cbfa2t3, Smad3, Zfp646, Hmgb2, Nfkb1, Atf5, Zdhhc2, Zfp239, Aatf* with functions mainly involved in the Wnt, JNK, NF-κB, IFN-γ, and transforming growth factor-β (Tgf-β) signaling pathways [Table 3.4].

Table 3.4: The top 25 master regulators from the 72 vs. 0 hour signature

TF Name	p-value	Function
Psmc3ip	5.72e−06	Proteasome ATPase interacting, DNA binding protein
Camta1	2.31e−05	Calmodulin binding transcription activator
Tgif1	2.97e−05	Involved in Tgf-β & JNK signaling, negative regulator of cell proliferation
Tcf3	3.23e−05	T-cell specific TF, involved in Wnt & FoxO pathways
Tcf7	5.56e−05	T-cell specific TF, involved in Wnt pathway, suppresses IFN-γ pathway
Trp53	7.6e−05	Encodes p53, involved in ALS, apoptosis, PI3K, Tgf-β and Wnt pathways
Zfp503	9.35e−05	(=Nolz1), promotes striatal neurogenesis
Zfp235	0.000112	
Hivep2	0.000117	Represses NF-κB for cell survival, modifies Tgf-β signaling
Mycn	0.000123	Inhibits NF-κB & c-Jun, regulated by PI3K
Dennd4a	0.000127	Lowers blood pressure
Zfp36l1	0.000137	Negative regulator of VEGF

Epas1	0.000165	(=Hif2a), opposite effect of Hif1a, Hif1a is found to change in ALS patients and mSOD1 mice, regulates VEGF & hypoxia, regulated by NF-κB & JNK
App	0.000182	Involved in NF-κB & TRAF6 pathways
Irx5	0.000251	Retinal differentiation
Myb	0.000257	Involved in Wnt signaling, might have a similar role as NF-κB
Cbfa2t3	0.000395	
Smad3	0.00052	Involved in Smad/Tgf-β & Wnt signaling pathways
Zfp646	0.000524	
Hmgb2	0.000541	Enhances Wnt signaling, involved in apoptosis
Nfkb1	0.000552	(=p50, p105)
Atf5	0.000675	Represses p53, inhibits apoptosis
Zdhhc2	0.000797	
Zfp239	0.00103	
Aatf	0.00104	(=apoptosis antagonizing TF), anti-apoptotic, involved in Akt, JNK, $p75^{NTR}$ & NGF pathways

The most enriched transcription factors (TFs) from the 72 vs. 0 hour signature extracted from the mouse total brain interactome. The transcription factors are ranked by their p-values. Their known functions, which include the Wnt, JNK, NF-κB, and Tgf-β signaling pathways, are added to the table. Currently the pathological significance of these transcription factors is being investigated by knocking down their expression in purified embryonic stem cell-derived motor neurons exposed to mutant astrocyte-conditioned medium, via shRNA-based lentivirus, and seeing if the knock-down causes any changes in the survival of these motor neurons.

Validation of these transcription factors was decided to be done by knocking down their expression in purified embryonic stem cell-derived motor neurons exposed to mutant astrocyte-conditioned medium using shRNA-based lentivirus and investigating whether a change in the

survival of motor neurons is observed. In this experimental design, an increase or decrease in the survival of motor neurons would suggest the involvement of a transcription factor in the molecular mechanism of motor neuron death in this non-cell autonomous model of ALS and would confirm the transcription factor's role as a master regulator of this mechanism. While in the process of validating the pathological significance of these 25 transcription factors, which is currently in progress, one transcription factor, namely NF-κB, was of particular interest. This was primarily because NF-κB has recently been in the spotlight for its link to different forms of fALS, such as for mutations in TDP-43 (Swarup et al., 2011) and OPTN (Maruyama et al., 2010). In addition, NF-κB has been inferred as one of the top master regulators of the molecular mechanism underlying the ALS-linked astrocyte toxicity for motor neurons. Further investigations into the pathological significance of NF-κB in ALS are discussed in the next chapter.

3.2.6. Gene Set Enrichment Analysis (GSEA)

For an additional analysis of the RNA-Seq data, GSEA, which is for conventional gene class testing, was performed. This analysis statistically compares the number of genes in a class that are 'significant' by using Gene Ontology (GO) or other pathway categories as a source for its gene classes (Allison et al., 2006). Indeed, this analysis allowed the evaluation of how this more traditional bioinformatics approach compares to the reverse gene engineering analysis in the ALS model used in this project. Furthermore, while the primary aim was to perform reverse gene engineering analysis, GSEA would allow the comparison of the data generated here to those from other groups who have often used GSEA (or equivalent) on microarray data to elucidate the

molecular mechanism of non-cell autonomous motor neuron degeneration.

GSEA was performed for the five gene expression signatures using the three most commonly used databases to group genes in related functional annotations: GO biological processes, Kyoto Encyclopedia of Genes and Genomes (KEGG), and Reactome pathways. There are several differences between these functional databases that make their end results slightly different from one another. GO is an ontology of defined terms representing gene product properties under three domains: (1) the cellular component, (2) the molecular function, and (3) the biological process (Consortium, 2008). KEGG, on the other hand, is a collection of online databases dealing with genomes, enzymatic pathways, and biological chemicals (Kanehisa, 2004). It records networks of molecular interactions in the cells including pathways and complexes, information about genes and proteins generated by genome projects, compounds and reactions. However, with KEGG, it is hard to combine all of this information in a unifying manner, since all of the annotations come from different data sets. Finally, Reactome is a species-specific online database of biological pathways (Joshi-Tope G., 2005). What is different with Reactome is that its core unit is the reaction, where entities (e.g. nucleic acids, proteins, complexes and small molecules) participating in reactions form a network of biological interactions that are grouped into pathways. Examples of biological pathways in Reactome include signaling, innate and acquired immune function, transcriptional regulation, translation, apoptosis and classical intermediary metabolism. Moreover, it is organized in a GO-controlled vocabulary, which makes it easier to understand than KEGG identifiers.

Because of the reasons mentioned above, the Reactome database seemed the most compelling one to use for the data from this work. With this information in hand, the list of

molecular pathways deduced from the most differentially expressed target genes (GSEA/Reactome) was compared to those deduced from the most activated master regulators (reverse gene engineering/mouse brain interactome). By looking at the 72 vs. 0 hour signature, which was the primary focus of this work, no agreement was found between the two lists of pathways (data not shown). Similarly, by looking at the 24 vs. 0 hour signature, minimal concurrence between the two lists of pathways was observed (data not shown). However, by looking at the 24 vs. 0 hour signature from the GSEA and the 72 vs. 0 hour signature from the reverse gene engineering analysis, a significant concurrence was noted between the two lists of pathways, such as the IFN-γ and NF-κB pathways [Tables 3.5-6].

Table 3.5: The top 10 most differentially expressed genes in the 24 vs. 0 hour signature

#	Symbol	Fold-change	p-value	Function
1	Ccl2	13.624	3.4e-15	A small cytokine whose knockdown was tested to have no effect on motor neuron survival
2	Usp18	13.123	8.55e-15	A deubiquitinating protease involved in IFN-γ signaling
3	Irf9	12.349	7.34e-14	An interferon regulatory factor that interacts with STAT 2 and STAT1, and involved in IFN-γ signaling
4	Nfkbia	10.387	5.05e-11	Higher activity in MNs exposed to mutant ACM; involved in NF-κB pathway
5	Art3	9.833	3.01e-10	An ecto-ADP-ribosyltransferase
6	Oasl2	9.694	4.18e-10	A 2'-5' oligoadenylate synthetase-like protein

7	Cxcl10	9.575	5.54e-10	A small cytokine belonging to the CXC chemokine family that is regulated by NF-κB and is involved in IFN-γ signaling
8	Trim25	9.127	2.55e-09	A tripartite motif-containing protein involved in NF-κB & TRAF3 pathways
9	Irf1	8.882	5.67e-09	An interferon regulatory factor involved in IFN-γ signaling
10	Stat1	8.787	7.27e-09	A transcription factor involved in JAK/STAT, NF-κB, IFN-γ, and TLR pathways

The top 10 most differentially expressed genes in the 24 vs. 0 hour signature with false discovery rate corrected p-value less than 0.01. The genes are mostly involved in the IFN-γ and NF-κB related pathways. The genes were ranked by their p-values. ACM: astrocyte-conditioned medium; MN: motor neuron; TRAF: tumor necrosis factor receptor associated factor; JAK/STAT: Janus kinase/signal transducers and activators of transcription; TLR: Toll-like receptor.

Table 3.6: The top 10 most enriched pathways in the 24 vs. 0 hour signature

#	Symbol	NES	p-value	Genes
1	Toll Like Receptor 9 (TLR9) Cascade	3.741	0.000183	Nfkbia, Irf7, Nfkb2, Pik3c3, Mapkapk3, Dusp3, Mef2c, Mapk10, Ager, Myd88, Fos, Ikbkg, Ubc, Mapk3, App, Atf1, Map2k6, Nod1, Map2k1, Irak4, Map2k3, Hmg1l1, Ppp2r5d, Pik3r4, Nfkb1, Rps6ka3, Rps6ka2, Tlr7
2	Toll Receptor Cascades	3.468	0.000525	Nfkbia, Irf7, Nfkb2, Pik3c3, Mapkapk3, Dusp3, Mef2c, Lgmn, Mapk10, Ager, Ly96, Tlr2, Myd88, Cd180, Fos, Ikbkg, Sigirr, Ubc, Mapk3, Tlr6, App, Atf1, Map2k6, Nod1, Hspd1, Map2k1, Irak4, Map2k3, Hmg1l1, Ppp2r5d, Ctss, Unc93b1, Irf3, Pik3r4, Lbp, Nfkb1, Rps6ka3, Rps6ka2, Tlr7
3	Toll Like Receptor 4 (TLR4) Cascade	3.434	0.000596	Nfkbia, Irf7, Nfkb2, Mapkapk3, Dusp3, Mef2c, Mapk10, Ager, Ly96, Tlr2, Myd88, Cd180, Fos, Ikbkg, Sigirr, Ubc, Mapk3, Tlr6, App, Atf1,

				Map2k6, Nod1, Hspd1, Map2k1, Irak4, Map2k3, Hmg1l1, Ppp2r5d, Irf3, Lbp, Nfkb1, Rps6ka3, Rps6ka2
4	TRAF6 Mediated Induction of proinflammatory cytokines	3.084	0.00204	Nfkbia, Nfkb2, Mapkapk3, Dusp3, Mef2c, Mapk10, Ager, Fos, Ikbkg, Ubc, Mapk3, App, Atf1, Map2k6, Nod1, Map2k1, Map2k3, Hmg1l1, Ppp2r5d, Nfkb1, Rps6ka3, Rps6ka2
5	TRAF6 mediated NF-kB activation	2.975	0.00293	Nfkbia, Trim25, Ddx58, Ifih1, Nfkb2, Ager
6	MyD88:Mal cascade initiated on plasma membrane	2.949	0.00319	Nfkbia, Nfkb2, Mapkapk3, Dusp3, Mef2c, Mapk10, Ager, Ly96, Tlr2, Myd88, Fos, Ikbkg, Sigirr, Ubc, Mapk3, Tlr6, App, Atf1, Map2k6, Nod1, Hspd1, Map2k1, Irak4, Map2k3, Hmg1l1, Ppp2r5d, Nfkb1, Rps6ka3, Rps6ka2, Ppp2cb, Mapk14, Tirap, Saa3
7	Toll Like Receptor 2 (TLR2) Cascade	2.949	0.00319	Nfkbia, Nfkb2, Mapkapk3, Dusp3, Mef2c, Mapk10, Ager, Ly96, Tlr2, Myd88, Fos, Ikbkg, Sigirr, Ubc, Mapk3, Tlr6, App, Atf1, Map2k6, Nod1, Hspd1, Map2k1, Irak4, Map2k3, Hmg1l1, Ppp2r5d, Nfkb1, Rps6ka3, Rps6ka2, Ppp2cb, Mapk14, Tirap, Saa3
8	Toll Like Receptor TLR1:TLR2 Cascade	2.949	0.00319	Nfkbia, Nfkb2, Mapkapk3, Dusp3, Mef2c, Mapk10, Ager, Ly96, Tlr2, Myd88, Fos, Ikbkg, Sigirr, Ubc, Mapk3, Tlr6, App, Atf1, Map2k6, Nod1, Hspd1, Map2k1, Irak4, Map2k3, Hmg1l1, Ppp2r5d, Nfkb1, Rps6ka3, Rps6ka2, Ppp2cb, Mapk14, Tirap, Saa3
9	Toll Like Receptor TLR6:TLR2 Cascade	2.949	0.00319	Nfkbia, Nfkb2, Mapkapk3, Dusp3, Mef2c, Mapk10, Ager, Ly96, Tlr2, Myd88, Fos, Ikbkg, Sigirr, Ubc, Mapk3, Tlr6, App, Atf1, Map2k6, Nod1, Hspd1, Map2k1, Irak4, Map2k3, Hmg1l1, Ppp2r5d, Nfkb1, Rps6ka3, Rps6ka2, Ppp2cb, Mapk14, Tirap, Saa3
10	MyD88 dependent cascade initiated on endosome	2.876	0.00403	Nfkbia, Irf7, Nfkb2, Mapkapk3, Dusp3, Mef2c, Mapk10, Ager, Myd88, Fos, Ikbkg, Ubc, Mapk3, App, Atf1, Map2k6, Nod1, Map2k1, Irak4, Map2k3, Hmg1l1, Ppp2r5d, Nfkb1, Rps6ka3,

				Rps6ka2, Tlr7

The 10 most enriched pathways in the 24 vs. 0 hour signature using the Reactome pathway database. The pathways were ranked by their normalized enrichment scores (NES) and p-values. The leading-edge genes for each significant gene set at p-value less than 0.05 are also reported. The Toll-like receptor and TRAF6-mediated NF-κB signaling pathways dominate this list.

3.3. Conclusion and Discussion

Unlike the candidate-based approach that was initially tried, using the unbiased RNA-Seq assay to identify gene alterations germane to the toxicity of mutant astrocytes on motor neurons has provided us with many promising molecular hits. This has allowed the use of the gene expression signatures from this assay to infer master regulators of the molecular mechanism of mutant astrocyte-derived motor neuron degeneration and to concentrate efforts on biologically validating the top 25 transcription factors that were inferred as master regulators. Of these transcription factors, the pathological significance of one, NF-κB, has already been confirmed. This will be discussed in more detail in the next chapter.

Interestingly, several of the most differentially expressed target genes of the 24 vs. 0 hour signature, such as *Usp18*, *Irf9*, and *Irf1*, belong to the IFN-γ molecular pathway. This signaling pathway has been shown by Aebischer *et al.* (2011) to be involved in the ALS-linked non-cell autonomous degeneration of motor neurons. Moreover, no significant changes in the activation of any known cell-autonomous motor neuron death mechanisms, such as Fas signaling and ER stress genes at the 24 vs. 0 or 72 vs. 0 hour signatures were noted. However, a change in the activation of Wnt signaling was observed at the 72 vs. 0 hour signature. These comparisons

suggest coherency between the differentially expressed target genes from our data and from the data of other groups on the molecular mechanism underlying non-cell autonomous motor neuron degeneration.

By looking at the differentially expressed target genes and the pathways deduced from these genes, using GSEA, the above comparisons were made. However, the top results from these analyses were limited to the NF-κB and IFN-γ pathways. On the other hand, with the reverse gene engineering analysis, many transcription factors were inferred including, but not limited to NF-κB, that elucidate the upstream signaling underlying this neurodegenerative mechanism that GSEA is not capable of computing. Moreover, with the reverse gene engineering analysis, it was not necessary to select individual target genes, since the analysis utilized the genomic data of target genes as a whole to infer its results. Therefore, it is thought that the results from the reverse gene engineering analysis provide more unbiased mechanistic information at the transcriptional regulation and signalization level than from the results of the GSEA.

Moreover, the comparison of the results from the reverse gene engineering analysis and GSEA showed the consistent involvement of several pathways, such as IFN-γ and NF-κB. But, interestingly, this resemblance arose from different signatures, in that the pathways deduced from differentially expressed target genes were from the 24 vs. 0 hour signature, whereas the pathways deduced from the differentially active transcription factors were from the 72 vs. 0 hour signature. This apparent temporal discrepancy was rather surprising, since the reverse gene engineering analysis infers master regulators that are supposedly upstream to the target genes. Therefore, if not occurring at the same time, it was expected that the results generated by the

reverse gene engineering precede those generated by GSEA. A future study is therefore required to clarify this question.

Additionally, several decisions and observations were made about the experimental design and data analysis processes to perform the RNA-Seq assay and its analysis in the most efficient and unbiased way possible. These decisions and observations are discussed below.

One of the most important decisions made in the experimental design for the RNA-Seq assay was the inclusion of treatment of medium conditioned with transgenic wild-type SOD1 astrocytes, as well as with non-transgenic astrocytes. It was believed that, by doing so, one could control for any gene expression changes that occur in motor neurons merely due to the overexpression of the catalytically active form of SOD1 in astrocytes. Thus, after the completion of the ANOVA analysis for the selected signatures, the non-transgenic astrocyte-conditioned medium treatment effect on motor neurons was compared with that of the transgenic wild-type SOD1 astrocyte-conditioned medium. Interestingly, no differentially expressed gene was found between these two conditions (data not shown), suggesting that the expression of wild-type human SOD1 in astrocytes does not cause detectable gene alterations in motor neurons. This treatment also provided an extra control condition to increase the power of the ANOVA analysis.

During the experimental design process for the RNA-Seq assay, to minimize the technical variation, we thought to perform RNA isolation for all of the 72 total RNA samples at the same time. To do this in the most efficient way, two different methods were compared: (1) the high-throughput MagMax RNA purification kit (Applied Biosystems) using RNA binding magnetic beads with a 96-well plate on a magnetic stand; and (2) the RNAeasy Mini Kit Spin Columns (Qiagen). While the MagMax kit, with the help of the 96-well plate, enabled

purification of RNA for 96 samples at the same time, the RNAeasy columns were for individual sample use which made it difficult to isolate 72 samples at the same time under the same technical and experimental conditions. However, test samples that were isolated using both methods showed very comparable RNA quality and quantity amounts (data not shown). Therefore, since both kits gave comparable RNA quality results, the MagMax RNA purification kit was selected as the preferred RNA isolation method, significantly limiting the technical variations that might have resulted from individual column use in the isolation of the 72 RNA samples.

Once the potentially variation-introducing experimental design steps were fixed, the focus was on the pre-processing of the RNA-Seq data, where the aim was to introduce as little processing to the data as possible. Thus, instead of using the data in the traditional FPKM (i.e. fragments per kilobase of exon per million fragments mapped) format, which cannot be analyzed by methods designed for digital data, the data was received and analyzed in its rawest format, which is the mapped reads format. By normalizing and variance stabilizing the data in this rawest format, the data was kept as little processed as possible so that the results would not be affected by any bias.

While the read counts could only be received in the mapped format from the Genomic center, there were also base reads that were not mapped to the mouse genome, which were not included in the analysis. There could be a few reasons why a read was not mapped to a location in the mouse genome: (1) if the read was mapped to more than one location in the genome, which would make the read non-specific for any gene; (2) if the read was contaminated with DNA or virus; or (3) if the read belonged to an unknown sequence in the genome. The last

option was not very probable, since the mouse genome has been very well sequenced over the years. Thus, the non-mapped reads were most likely either non-specific or contaminated, and were not included in any further analysis of the read count data. However, in case a read belonged to an unknown sequence in the genome that might be sequenced later, the raw non-mapped data is stored for future studies. Indeed, the analysis can be re-run at any time should a more completely sequenced mouse genome become available. This non-mapped read data can also be used to gather read counts on the non-coding RNA, such as microRNAs.

Despite the different strategies adopted in the experimental design to minimize potential batch effect, the samples with the same replicate number still showed a gene expression pattern closer to each other than those with other replicate numbers (data not shown). This suggested that the motor neuron differentiation and purification steps bring undesired technical variation to the data. This effect was reduced by fitting the data to the linear model: $y = \mu + \alpha T + \beta B + \varepsilon$, where β is the coefficient factor for the batch effect. β is additive to α, the coefficient factor for the treatment effect. Therefore, while genes with the highest α values were being computed, genes with the lowest batch effect were also being selected, hence minimizing the batch effect from the gene expression signatures.

Although the reverse gene engineering analysis of the RNA-Seq data has been performed for all of the selected timepoints, the focus was on the 72 vs. 0 hour signature, as discussed in the preceding chapter. This timepoint seemed the most biologically relevant, since 72 hours of exposure to mutant astrocyte-conditioned medium is enough to make motor neurons committed to die and this mechanism cannot be reversed. Thus, by studying the transcriptional network belonging to this timepoint, the hope was to acquire some insight into the molecular mechanism

underlying the commitment to death in motor neurons. Studies on other signatures would also be interesting to pursue further. For instance, the 168 vs. 0 hour signature would be especially interesting to study, since it could elucidate the molecular mechanism that is different between the resistant and sensitive motor neuron subpopulations in this model system of ALS.

One weakness of the reverse gene engineering analysis performed on the RNA-Seq data was the interactomes that have been available, which mostly belonged to the human species and were reverse-engineered from glioblastoma or neuroblastoma cell line samples. While the comparison performed on the seven available interactomes revealed the mouse total brain interactome to be the most relevant to these data, none of the interactomes were motor neuron-specific. Therefore, even though this analysis inferred transcription factors that are differentially active in the model system here, the need to validate the pathological significance of these transcription factors biologically still remains. Moreover, the Califano group is currently generating a mouse motor neuron specific interactome in collaboration with the Wichterle group. We are planning to re-run the reverse gene engineering analysis on the RNA-Seq data using the motor neuron interactome once it is completed.

Another decision that was made about the reverse gene engineering analysis was its absolute enrichment aspect. Since the interactome selected was not an exact fit for the cell type being used, there was a lack of certainty about the enhancement or repression effect of each transcription factor on the expression of their target genes. This was also because it has been shown that certain transcription factors either activate or repress their target genes, depending on their cell types. Thus, Absolute Enrichment Master Regulator Analysis was performed, from which the differential activity of a transcription factor was inferred. However, the direction of the

activity could not be determined. Since the plan was to validate the pathological significance of each of the top 25 transcription factors by biological means, it would be more suitable to use the absolute enrichment analysis. If by knocking-down the expression of a factor, no change in the survival of motor neurons was noted, then we would over-express this factor before reaching a definitive conclusion about its role in the molecular mechanism of motor neuron degeneration. In addition, the number of transcription factors being validated could be expanded; if not enough transcription factors gave conclusive results.

Finally, in the analysis of the RNA-Seq data so far, only transcriptional interactions were calculated. This was because the only available database to run the post-translational analysis was from the human glioblastoma cell line. And, like the transcriptional interactome, the generation of a motor neuron specific post-translational interactome is in progress and will be utilized as soon as it becomes available. This post-translational interactome will provide us with information on the signalization between the entrance of the mutant astrocyte-derived toxic factor to motor neurons and the activation of transcription factors that activate genes that are responsible for the Bax-dependent cell death. Consequently, we will have the ability to complete the signaling network underlying the ALS-linked astrocyte toxicity for motor neurons.

What is unique about the reverse gene engineering method is that it makes use of the whole gene expression signature from the RNA-Seq data rather than selecting a few of the most differentially expressed target genes, which makes it more powerful and unbiased. What makes this project so unique is that this is the first time the reverse gene engineering method has been used in a model of neurodegeneration. In this model of ALS-linked non-cell autonomous motor neuron degeneration, this method was successful in inferring at least one master regulator that is

involved in the molecular mechanism of this degeneration. The results from this part of the project are presented in the next chapter.

Chapter 4: NF-κB regulates the ALS-linked astrocyte toxicity for motor neurons

4.1. Introduction

The Master Regulator Analysis from the RNA-Seq data, as discussed in Chapter 3, inferred NF-κB as one of the top 25 transcription factors driving the ALS-linked astrocyte toxicity for motor neurons. NF-κB is also one of the most differentially expressed target genes and one of the most enriched pathways in this ALS model, as evidenced by GSEA. The interest in this family of transcription factors was further stimulated by the discoveries showing that specific subunits of the NF-κB complex are up-regulated in motor neurons in both sALS cases (Jiang et al., 2005b) and transgenic mutant SOD1 mice (Ferraiuolo et al., 2007), and that the NF-κB subunit p50 modulates the activity of TDP-43, whose mutations give rise to a form of fALS (Swarup et al., 2011).

In light of these findings, the pathological significance of NF-κB in our *in vitro* model of ALS was investigated. However, prior to presenting and discussing any results, a brief review of what is known about NF-κB's signaling, its function in the central nervous system, and its role in ALS is in order to set stage for this chapter.

4.1.1. NF-κB signaling

NF-κB was first identified over 20 years ago as a DNA-binding complex governing transcription at the immunoglobulin light chain gene intronic enhancer (Sen and Baltimore, 1986). Since then,

thousands of papers have been published about this transcription factor being involved in a broad range of biological processes ranging from innate and adaptive immunological responses to cell survival, death, development, stress responses, and maturation (Hayden and Ghosh, 2012). While NF-κB activation in general protects organisms from environmental insults, dysregulated NF-κB activity is observed in various diseases including chronic inflammation, cancer, and neurodegeneration, such as in Huntington's disease and ALS (Shih et al., 2011).

Figure 4.1: Components of the NF-κB pathway

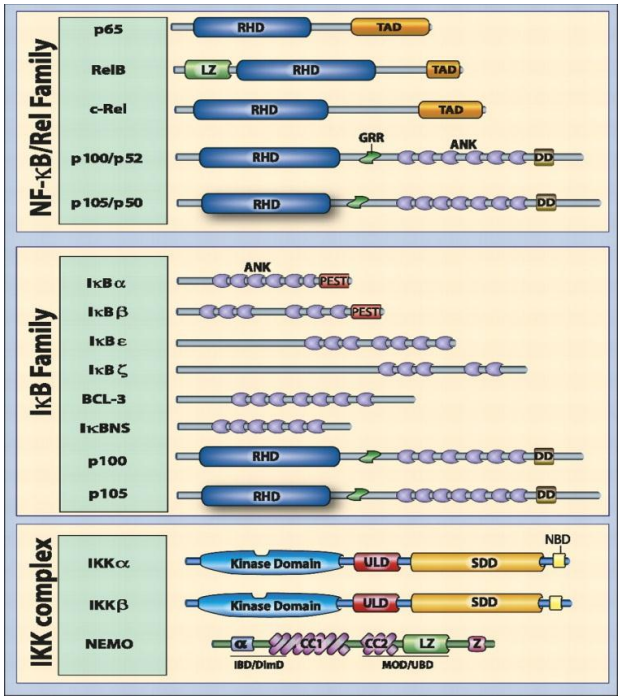

The components of the NF-κB pathway, taken from Hayden and Ghosh (2012). The NF-κB family consists of five members: p65/RelA, RelB, c-Rel, and the precursor proteins p100 and p105 giving rise to p52 and p50, respectively. The IκB family consist of eight members: IκBα, IκBβ, IκBε, IκBζ, BCL-3, IκBNS, p100, and p105. The IKK complex is formed by IKKα, IKKβ, and NEMO. RHD: REL homology domain; TAD: transactivation domain; LZ: leucine zipper domain; GRR: glycine-rich region; ANK: Ankyrin repeat domain; DD: death domain; PEST: proline-rich, glutamic acid-rich, serine-rich, and threonine-rich; ULD: ubiquitin-like domain; SDD: scaffolding and dimerization domain; NBD: NEMO-binding domain; CC: coiled-coil domain; IBD/DimD: IKK-binding domain/dimerization domain; MOD/UBD: minimal oligomerization domain/ubiquitin-binding domain; Z: zinc finger domain.

There are three regulatory components to the NF-κB pathway [Figure 4.1]: (1) the NF-κB/Rel family, (2) the inhibitor of NF-κB (IκB) family, and (3) the IκB kinase (IKK) complex. NF-κB activation is organized by a number of positive and negative regulatory elements (Hayden and Ghosh, 2012). In the dormant state, NF-

Figure 4.2: Activation of the NF-κB signaling pathway

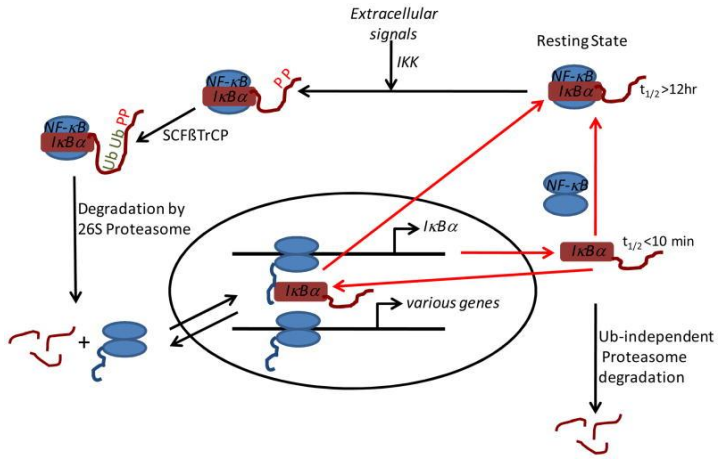

The activation of the NF-κB pathway, excerpted from Ferreiro *et al.* (2010). When inactive, NF-κB dimers are bound to IκB and reside in the cytoplasm. Upon the activation of the IKK complex through extracellular signals, IKK phosphorylates IκB, which then gets ubiquitinated and degraded by the 26S Proteasome. Freed NF-κB dimers, then, are translocated to the nucleus and transcribe new IκB, as well as various other genes. The newly synthesized IκB is either degraded, binds to NF-κB in the cytoplasm, or enters the nucleus and binds to nuclear NF-κB, forming negative feedback loop, indicated by red arrows.

κB dimers are held inactive in the cytoplasm through association with IκB proteins. Inducing stimuli trigger activation of the IKK complex, which then phosphorylates, ubiquitinates, and degrades IκB proteins (Ferreiro and Komives, 2010) [Figure 4.2]. Freed NF-κB dimers translocate to the nucleus, bind to specific DNA sequences, and promote transcription of target genes. One of these target genes is IκB, which then goes back to the cytoplasm and binds to NF-κB in the cytoplasm, forming a negative feedback loop [Figure 4.2].

There are five NF-κB family members in mammals; these are: p65/RelA, RelB, c-Rel, p50/NF-κB1 and p52/NF-κB2 [Figure 4.1]. These proteins are characterized by the presence of an N-terminal Rel homology domain (RHD), which is a protein domain that contains a recognition loop that interacts with DNA bases, and their stoichiometric inhibitor proteins, IκBs. NF-κB family proteins bind to κB sites as either homo- or hetero-dimers and can either turn on or off the transcription of their target genes. The five monomers form 15 potential dimers and the

generation of all monomers is transcriptionally regulated. p50 and p52 are also regulated by the processing of precursor proteins p105 and p100, respectively (Shih et al., 2011).

The main inhibitor proteins of NF-κB are IκBα, IκBβ, and IκBε. However, precursor proteins p100 and p105, in addition to, IκBζ, IκBns, and B-cell lymphoma 3 (Bcl-3) were recently found to have inhibitory roles on NF-κB as well (Hayden and Ghosh, 2012) [Figure 4.1]. IκBs, in general, have an ankyrin repeat domain, which is a 33-residue motif consisting of two alpha helices separated by a loop, which sequesters NF-κB into a dormant state and prevents DNA binding. p100 and p105, on the other hand, mediate NF-κB inhibition only when they are *in trans*, through an activity called IκBδ for p100 (Basak et al., 2007) and IκBγ for p105 (Savinova et al., 2009), respectively.

The NF-κB pathway is subdivided into two pathways which depend on the types of responses they trigger (Sun, 2011): (1) the canonical pathway, which typically activates the rapid and reversible inflammatory and immune responses; and (2) the non-canonical pathway, which is the slower pathway that activates the irreversible developmental responses. The canonical pathway is NF-κB essential modulator (NEMO/IKKγ)-dependent, where the activated IKKα-β complex phosphorylates IκBα. The NF-κB dimers involved in this pathway are mostly p65, p50 and c-Rel [Figure 4.3]. IKKs can be phosphorylated through autophosphorylation or by upstream kinases. Moreover, since the canonical pathway is usually activated by inflammatory stimuli, the known receptors that activate this signaling pathway include the Toll-like, Tumor Necrosis Factor, B-cell and T-cell receptors. The non-canonical pathway, on the other hand, is NEMO-independent where the IKK complex consists of IKKα and the NF-κB-inducing kinase (NIK). In addition, in the non-canonical pathway, new synthesis of p100 and RelB allows for the

generation of NF-κB dimers RelB and p52 (Shih et al., 2011). Finally, the known receptors of the non-canonical pathway are the B-cell activating factor receptor, CD40, lymptotoxin β receptor and receptor activator of NF-κB [Figure 4.3].

Figure 4.3: The canonical and non-canonical pathways of NF-κB

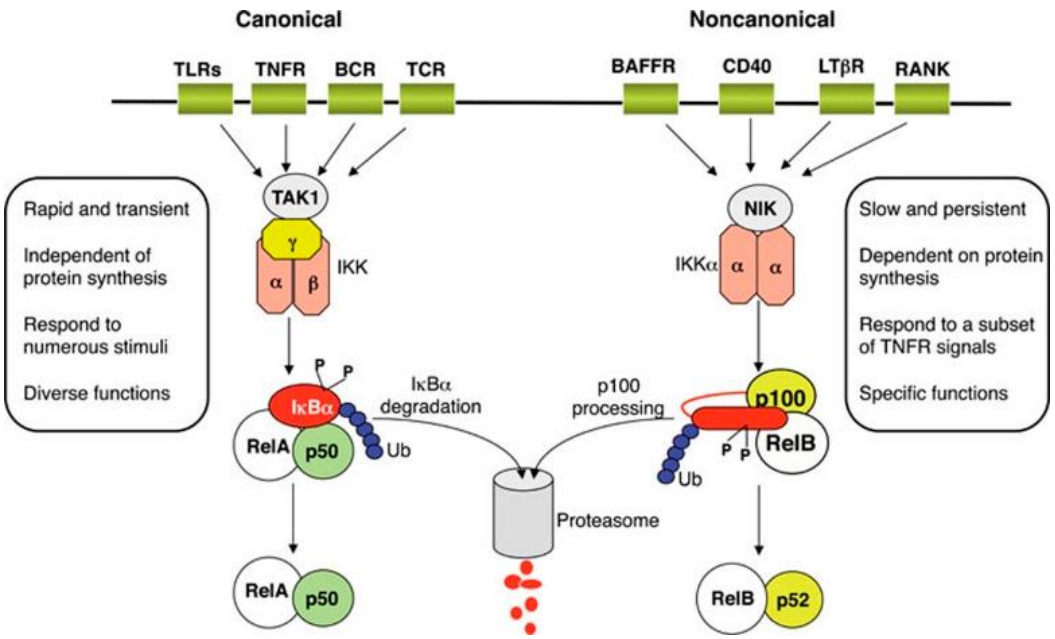

The canonical and non-canonical pathways of NF-κB, extracted from Sun *et al.* (2011). There are major differences between the pathways. While the canonical pathway, which responds to numerous inflammatory and immune stimuli, is rapid and transient, the non-canonical pathway responds to developmental signals and is slow and persistent. Moreover, some of the main receptors that activate the canonical pathway are the Toll-like (TLR), Tumor Necrosis Factor (TNF), B-cell (BCR) and T-cell (TCR) receptors that turn on TAK1, which then phosphorylates the IKKα, β, and γ (NEMO) complex. This pathway also constitutes of IκBα, RelA (p65) and p50. The non-canonical pathway is activated by B-cell activating factor receptor (BAFFR), CD40, lymptotoxin-β receptor (LTβR) and receptor activator of NF-κB (RANK), which then turns on the NF-κB-inducing kinase (NIK) and IKKα complex. The non-canonical pathway consists of RelB and p52.

Even though the canonical and non-canonical pathways are generally distinct from one another, recent studies have revealed cross-talk between them. One example of this is the functional overlap found between p50/NF-κB1 and p52/NF-κB2 through the NF-κB gene deletion studies. Biochemical analysis of mutant cells showed that the loss of canonical p50

results in the formation of p65/p52 dimers and near normal p65 activation in response to inflammatory stimuli (Hoffmann et al., 2003). Moreover, lymph node organogenesis, which is a developmental phenotype normally seen under the conditions of weakened activity of the non-canonical NF-κB pathway, has also been observed in *NF-κB1*$^{-/-}$ mice which are characterized by the inhibition of the activity of the canonical pathway (Basak and Hoffmann, 2008). These results indicate functional overlap and interdependencies between the canonical and non-canonical pathways.

Although the activating cell surface receptors may vary, research on NF-κB signaling discovered a convergence of signaling intermediates upstream to the IKK complex. These intermediates include Receptor-interacting protein (RIP) and tumor necrosis factor receptor associated factor (TRAF) families of proteins. In most cases, both RIP and TRAF family proteins lead to the activation of IKK (Hayden and Ghosh, 2012). However, while the TRAF family proteins are required in both the canonical and non-canonical pathways, the RIP family is selectively used in the canonical pathway. Similarly, Tgf-β-activated kinase 1 (TAK1) is generally accepted as an IKK kinase of the canonical pathway. All of these regulatory aspects of NF-κB signaling are to control for the multiple functions of NF-κB, which are discussed in the next section.

4.1.2. Functions of NF-κB in the nervous system

NF-κB has a wide array of cellular functions, including stress and immune responses, differentiation, proliferation, apoptosis and cell survival. Moreover, its diverse functions extend to the nervous system spanning from development and activity, including control of cell growth,

synaptic plasticity, behavior, and cognition. In addition, recent literature in the field has revealed NF-κB's role in various neurodegenerative diseases, such as Alzheimer's, Parkinson's, and Huntington's diseases, proving it to be a highly versatile molecule.

A wide array of stimuli activate NF-κB in the immune system as well as in the nervous system, such as cytokines (e.g. tumor necrosis factor alpha [TNFα] and interleukin-1), chemokines, lipopolysaccharide, HIV, oxidative stress caused by SOD, and nitric oxide (Memet, 2006). Additionally, certain stimuli activate NF-κB only in the nervous system. These stimuli are neurotrophins (NGF and S100β), neurotransmitters (glutamate, metabotropic glutamate receptor type 5 agonists), membrane depolarization, synaptic activity, amyloid β peptide, neural cell adhesion molecule, and sleep deprivation (Memet, 2006).

For the activation of NF-κB, types of host cells, dimers, and the specificity of stimulus all play an important role. For example, while interleukin-1β induces activity only in astrocytes (Srinivasan et al., 2004), glutamate activates NF-κB p65/p50 only in neurons (Kaltschmidt et al., 1995). Activation of NF-κB in neurons is also triggered by several cascades including the p21/ras phosphatidylinositol-3-kinase (PI3K) AKT, protein kinase C and calcium-calmodulin-dependent kinase II (Memet, 2006). NF-κB activity in the nervous system, on the other hand, can be negatively regulated by a number of molecules, such as Tgf-β, glycogen synthase kinase-3, interleukin-4, interleukin-10, and glucocorticoids. Subsequently, some of the well-known target genes of NF-κB in the nervous system are the neural cell adhesion molecule, inducible nitric oxide synthase, amyloid β precursor protein (APP), β-secretase (BACE, which is the first and rate-limiting enzyme for APP cleavage), BDNF, inducible cyclooxygenase-2, and calcium/calmodulin-dependent kinase II δ (Memet, 2006).

One of the main associations of NF-κB in the nervous system has been in neurodevelopment. In fact, increase in NF-κB binding activity has been reported to occur during nervous system development. During embryogenesis, NF-κB activity was detected in the central nervous system as early as E12.5 in the spinal cord and certain nuclei of the rhombencephalon (i.e. portions of the central nervous system that includes the medulla, pons, and cerebellum) of transgenic mice expressing the reporter gene lacZ under the control of κB sites from the p105 gene (Schmidt-Ullrich et al., 1996). Moreover, during neural development, NF-κB signaling has been found to promote neurogenesis (Denis-Donini et al., 2008) and the growth of neuronal processes of maturing neurons (Gutierrez et al., 2005; Koulich et al., 2001; Lezoualc'h et al., 1998; Maggirwar et al., 1998; Middleton et al., 2000), as well as cell differentiation and survival (Bhakar et al., 2002; Chiarugi, 2002; Koulich et al., 2001; Maggirwar et al., 1998; Middleton et al., 2000) through regulation of Bcl-2-family antiapoptotic genes (Bhakar et al., 2002; Chiarugi, 2002). Signaling via CNTF- and NGF-$p75^{NTR}$-, but not BDNF-mediated signaling, has been shown to be responsible for the NF-κB-dependent survival of developing embryonic neurons (Hamanoue et al., 1999; Middleton et al., 2000).

In addition to having a role in neurodevelopment, NF-κB is considered to be a participant in synaptic plasticity. It has been proposed that synaptic plasticity leads to information storage as a result of glutamate release from the presynaptic site followed by a modification of the presynaptic release process (Routtenberg, 2000). This process requires a retrograde messenger that travels along the axon to turn on gene expression in order to replenish the presynaptic protein supply. NF-κB is thought to be involved in this process of synaptic plasticity. Evidence that supports this hypothesis includes: (1) inducible forms of NF-κB found in synaptosomes,

which contain presynaptic proteins that are sealed and stabilized by postsynaptic density (Kaltschmidt et al., 1993); (2) NF-κB activation in mouse hippocampus by long-term potentiation, in rat amygdala by fear-potentiated startle, and in crab brain after retrieval (Memet, 2006); and (3) blocking long-term potentiation induction in the hippocampus and amygdala through inhibition of NF-κB using a κB decoy DNA, as well as ablation of TNF signaling pathway in $TNFR^{-/-}$ mice (Collister and Albensi, 2005).

Research in the field suggests that NF-κB also plays a role in memory formation, cognition, and behavior. Use of κB decoy DNA indicated the involvement of NF-κB in long-term retention of fear memory in rats, inhibitory avoidance long-term memory and spatial long-term memory in the Morris water maze task in mice (Memet, 2006). More specifically, deficits of contextual fear memory were found in mice lacking c-Rel. These deficits impaired anxiety responses seen in p50-deficient mice, while mice lacking p65 demonstrated deficits in spatial memory (Marini et al., 2007). Altogether, these various studies indicate that NF-κB activation is essential for the mechanisms of long-term memory formation, especially those requiring the hippocampus.

Besides its role in synaptic plasticity and memory, NF-κB has been shown to promote neuronal death as well as to protect against it. For example, global ischemia was demonstrated to activate p50/p65 dimers in neurons of rats, mice, and humans, where this activation of dimers has been shown to promote cell death (Memet, 2006). Similarly, NF-κB was found to modulate the response of the tumor suppressor protein p53 in neurons with DNA damage and to be involved in the cell death process (Aleyasin et al., 2004). TNF pretreatment, on the other hand, has also been associated with increased production of the anti-apoptotic proteins Bcl-2 and Bcl-

X_L, and the expression of a dominant negative form of IκB has been shown to inhibit the ability of TNF to protect hippocampal neurons (Tamatani et al., 1999). A pro-survival role for NF-κB has also been seen in the increased neurotoxin-induced damage to neuronal cells of mice lacking p50 (Yu et al., 1999).

Alternatively, activation of NF-κB in glial cells (especially in microglia and astrocytes) has been suggested to indirectly promote neuronal death, since NF-κB activation in both astrocytes and microglia results in the production of inflammatory mediators, including chemokines and cytokines, such as TNFα, interleukin-1, interleukin-6, and matrix metalloproteinase-9. Interestingly, NF-κB has a prosurvival role in oligodendrocytes and promotes maturation of oligodendrocyte progenitor cells (Memet, 2006). Similarly, NF-κB has been shown to play a major role in the differentiation of Schwann cells into cells exhibiting the myelinating phenotype in the peripheral nervous system (Nickols et al., 2003).

All of these studies suggest that NF-κB's role in cell survival or death is cell-context and stimulus specific. In fact, it is suggested that while p50/65 dimers are more responsive to environmental neurotoxic signals and can drive gene programs leading to neuronal cell death, the activation of c-Rel-containing dimers is triggered by neuroprotective signals and increases neuronal resistance to stressful conditions by inducing the expression of anti-apoptotic genes (Pizzi and Spano, 2006) [Figure 4.4].

Finally, the NF-κB signaling pathway is altered in several chronic neurodegenerative diseases, including Alzheimer's, Parkinson's, and Huntington's diseases, as well as ALS. For example, increased p65 immunoreactivity has been found in both neurons and glial cells of postmortem brains, as well as in cholinergic neurons of the basal forebrain and hippocampi of

Alzheimer's disease patients (Memet, 2006), suggesting increased NF-κB activation in those cells. Similarly, a significant increase in the nuclear NF-κB staining in cholinergic neurons from Alzheimer's disease patients was also observed (Boissiere et al., 1997), indicating an association between NF-κB activation and the process of cholinergic degeneration in Alzheimer's disease. Moreover, exposure of cultured neurons to amyloid β-peptide or a secreted form of APP has been found to induce NF-κB activation, indicating a role for proteolytic products of APP in NF-κB activation in Alzheimer's disease brain cells (Mattson and Meffert, 2006). Inhibition of NF-κB transcriptional activity with decoy DNA resulted in increased vulnerability of neurons to death induced by APP (Mattson and Guo, 1997). All of these studies suggest that the activation of neuronal NF-κB in Alzheimer's disease may be a neuroprotective response against death induced by APP.

Figure 4.4: Diverse NF-κB complexes can be involved in opposite effects on neuronal survival

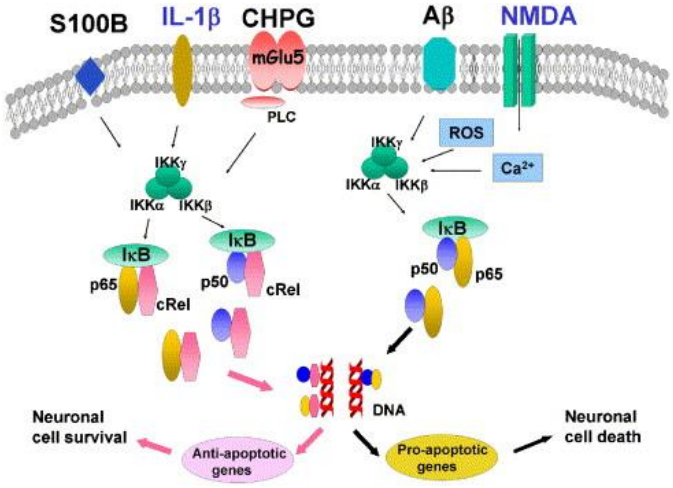

The activation of different NF-κB dimers may have opposite effects on neuronal survival by either promoting or protecting against degeneration, taken from Pizzi and Spano (2006). While p50/65 dimers are necessary for glutamate-(NMDA) and amyloid β (Aβ)-induced cell death program, c-Rel containing dimers (p50/c-Rel and p65/c-Rel) have been shown to mediate pro-survival effects of interleukin-1β (IL-1β), mGlu5 receptor agonist CHPG, and S100B. The c-Rel dependent anti-apoptotic pathway includes the expression of anti-apoptotic genes, such as MnSOD and Bcl-X_L, which are responsible for neuroprotection. ROS: reactive oxygen species; PLC: phospholipase C.

A role for NF-κB in Parkinson's disease has also been proposed. For example, a 70-fold increase in dopaminergic neurons exhibiting p65 immunoreactivity was observed postmortem in

the brains of Parkinson's disease patients. Moreover, NF-κB has been described as either promoting or delaying dopamine-induced apoptosis in PC12 cells (Memet, 2006). On the other hand, contrary to Alzheimer's disease, in Huntington's disease, NF-κB was found to regulate the polyglutamine-induced neurodegeneration (Memet, 2006). Wild-type Huntingtin protein, whose loss of normal function caused by the expansion of a polyglutamine tract results in Huntington's disease, has been shown to stimulate the transport of NF-κB out of dendritic spines and supports a high level of active NF-κB in neuronal nuclei (Marcora and Kennedy, 2010). Marcora *et al.* (2010) have further shown that this NF-κB-related function of Huntingtin is impaired by its polyglutamine tract expansion, which suggest that NF-κB activation might contribute to neurodegeneration observed in Huntington's disease. Similar to other cellular contexts in the nervous system regarding neuronal survival or death, NF-κB is involved in the pathogenesis of different neurological disorders, either by mitigating or promoting these disorders. Thus, in order to find therapeutic solutions to these diseases, the perspective agents should be cell-type selective in their actions.

4.1.3. NF-κB's role in ALS

In addition to Alzheimer's, Parkinson's, and Huntington's diseases, NF-κB has also been associated with ALS in numerous studies. For example, NF-κB was found to be among the most up-regulated genes in a gene expression profile of degenerating spinal motor neurons isolated from autopsied patients with sALS (Jiang et al., 2005a). This finding was confirmed by several other groups studying motor neurons autopsied from human ALS patients, as well as motor neurons laser-captured from transgenic mutant SOD1 rodent models [Table 4.1]. However so far

the findings on NF-κB related to ALS have been somewhat conflicting on whether NF-κB has a pro-survival or pro-death role on motor neurons. Some of these findings are discussed below.

Table 4.1: Expression of NF-κB in existing motor neuron gene array data

Study	Species/ System	Platform	Comparison	NF-κB expression
(Jiang et al., 2005b)	Human MN LCM	4.8K Array	sALS vs. Ctrl	NF-κB p65 is one of the most up-regulated genes in ALS MNs (18^{th}, w/ 4.52 fc)
(Kirby et al., 2005)	NSC34 Cells	Affy U74Av2A Array	WT SOD1 vs. G93A SOD1	IκBα is one of the most down-regulated genes in G93A SOD1 cells (w/ -2.90 fc)
(Lobsiger et al., 2007)	Rat E14 SC MN LCM	Affy Rat 230 v 2.0	WT SOD1 vs. G93A SOD1	NF-κB p65 is slightly higher in G93A SOD1 MNs
(Ferraiuolo et al., 2007)	Mouse MN LCM	Affy Mouse Genome 430 2.0	G93A vs. WT SOD1 at 60, 90, 120 days	NF-κB p65 expression is about the same at 60 days, 20% higher at 90 days, 50% higher at 120 days in G93A MNs
(Rabin et al., 2010)	Human MN LCM	Affy Human Exon 1.0 ST	sALS vs. Ctrl	NF-κB p65 expression is 40% higher in sALS MNs
(Cox et al., 2010)	Human MN LCM CHMP2B	Affy Hu133 2.0 Plus	fALS vs. Ctrl	NF-κB p65 expression is about the same
(Kirby, 2011)	Human MN LCM SOD1	Affy Hu133 2.0 Plus	fALS vs. Ctrl	NF-κB p65 expression is about the same

The expression of NF-κB in existing gene array studies that were performed on motor neurons either from human ALS patients or transgenic rodents expressing mutant SOD1. Overall, NF-κB p65 expression is slightly higher in ALS motor neurons. MN: motor neuron; LCM: laser capture microscopy; SC: spinal cord; Affy: Affymetrix; sALS: sporadic ALS; fALS: famial ALS; WT: wild-type, fc: fold-change.

Evidence suggesting the pro-survival role of NF-κB is the following: In riluzole-treated mutant SOD1 mice, increased nuclear expression of NF-κB was observed. Moreover, a pharmacological histone deactylase inhibitor, sodium phenylbutyrate, which was shown to significantly extend survival of mutant SOD1 mice, was also shown to induce the nuclear expression of NF-κB, the phosphorylated IκB, and the anti-apoptotic Bcl-2 (Ryu et al., 2005). This suggests that the pharmacological induction of NF-κB-dependent transcription is neuroprotective in mutant SOD1 mice. Similarly, the administration of another neuroprotective agent, EGCG, to mutant transgenic mice also caused an increase in the expression of nuclear NF-κB. These findings propose a pro-survival role for NF-κB, especially given its known anti-apoptotic target genes, such as the X-linked inhibitor of apoptosis (Xiap) and Bcl-2. However, all of these data were found through pharmacological means and do not allow one to conclude with certainty that NF-κB is neuroprotective in ALS.

On the other hand, the data supporting the pro-death role of NF-κB appear more compelling. First of all, motor neuron-neuroblastoma hybrid cells that express mutant SOD1 were found to be more vulnerable to glutamate excitotoxicity and to show higher NF-κB activity and nuclear c-Rel expression in comparison to the hybrid cells that express wild-type SOD1 (Pyo et al., 2010). Furthermore, this same group demonstrated that glutamate treatment decreased Xiap expression and increased caspase-3 activity in mutant SOD1 hybrid cells (Pyo et al., 2010). Others have reported that treatment with a pharmacological peroxisome proliferators-activated receptor gamma agonist, pioglitazone, which is thought to block NF-κB, extended survival in mutant SOD1 mice, as well as reducing the expression of induced nitric oxide synthase, NF-κB, and 3-nitrotyrosine in the spinal cords of these mice (Kiaei et al., 2005). Finally, NF-κB was

shown to be involved in the glutamate-induced spinal cord motor neuron death through TNFα potentiation in ALS, where increased extracellular glutamate levels caused by co-exposure to TNFα and glutamate-uptake inhibitor threohydroxyaspartate were prevented by NF-κB inhibition in spinal cord motor neurons (Tolosa et al., 2011).

More importantly, NF-κB has been associated with motor neuron death in the context of different forms of ALS. Maruyama *et al.* (2010) identified mutations in OPTN in patients with fALS or sALS. The authors demonstrated that nonsense and missense mutations of OPTN eliminated the inhibition of NF-κB, indicating that NF-κB inhibitors might be useful to treat ALS. Moreover, in patients with sALS or OPTN-ALS, the expression pattern of NF-κB was altered when compared to that of normal controls, where NF-κB immunoreactivity tended to be absent from neuronal nucleus and was increased in microglia (Sako et al., 2012). Similarly, a recent study by Swarup *et al.* (2011) showed that TDP-43 and p65 expression is higher in spinal cords of ALS patients. Moreover, the group demonstrated that TDP-43 interacts and co-localizes with p65 in glial and neuronal cells from ALS patients, as well as in mice expressing wild-type and mutant TDP-43, but not in cells from healthy individuals or non-transgenic mice (Swarup et al., 2011). Interestingly, this group showed that when the mutant TDP-43 mice were treated with an NF-κB activity inhibitor, they observed reduced denervation in the neuromuscular junction and delayed ALS disease symptoms, suggesting that TDP-43 deregulation contributes to the ALS pathogenesis by enhancing NF-κB activity. Furthermore, FUS has been found to be a co-activator of NF-κB (Uranishi et al., 2001) and mutant VCP increase NF-κB activity (Custer et al., 2010).

Finally, an *in vivo* study has been performed by knocking-down the expression of NF-κB in astrocytes and studying the effects in mutant SOD1 mice. Because astrocytes become reactive in transgenic mice expressing mutant SOD1, and hence, supposedly, release cytokines and nitric oxide, it was suggested that NF-κB might be mediating some of the inflammatory events seen in these mice. To test this hypothesis, Crosio *et al.* (2011) generated double transgenic mice expressing the mutant $SOD1^{G93A}$ ubiquitously and the dominant negative form of IκBα in GFAP-expressing cells only. These investigators found no effect on the age of onset of disease manifestations or disease progression (Crosio et al., 2011).

While this study suggests that NF-κB expression in astrocytes might not be involved in the ALS disease process, it may be prudent to take this conclusion with caution for the following reasons: (1) the GFAP promoter, which was used here to drive the expression of mutant IκBα, is known to be a weak promoter, unless astrocytes are activated, which does not occur in a conspicuous manner in asymptomatic mutant SOD1 mice. Instead, Aldh1l1 might have been a better promoter to use in this study. (2) The study never showed how much inhibition in the activity of NF-κB was observed in the animals and which subunits were specifically targeted. The latter is especially important, since compensatory pathways (e.g. non-canonical versus canonical) might have been recruited, e.g. the activation of p52 instead of p50 to form a dimer with p65, which is a very common phenomenon. (3) Since the toxic stimulus through mutant SOD1 is persistent, alternative inflammatory pathways might have been activated in mice that caused the disease to occur in its usual progression.

All of these data suggest that NF-κB may constitute a therapeutic target for different forms of fALS, as well as sALS. However, due to the cell- and stimulus-selective responses and

functions of NF-κB, it is important to investigate its differential activity and pathological significance in the well-controlled model system that is used here and to see which dimers and pathways are specifically activated. Results for this are discussed below.

4.2. Results

4.2.1. The canonical NF-κB pathway is activated in motor neurons exposed to mutant astrocyte-conditioned medium

As indicated above, the NF-κB pathway is subdivided into two different pathways, the canonical and non-canonical pathways, which are composed of specific dimer groups that are related to different functions associated with the particular pathway. Therefore, it is important, in the investigation of the differential activity of NF-κB in our model system, to know which pathway and which subunits are specifically activated. Accordingly, the first step was to quantify the DNA-binding activity of different NF-κB subunits in purified embryonic stem cell-derived motor neurons exposed to mutant versus wild-type astrocyte-conditioned medium for different lengths of time using the TransAM assay (Active Motif), which is a highly sensitive enzyme-linked ELISA-based assay.

Unlike other methods that are used to study the activity of NF-κB, such as gel-shift assays, immunostaining and Western blot, the TransAM assay does not limit its investigation of NF-κB subunit activity to the subunit nuclear localization, but instead looks specifically for the active form of transcription factor in the nuclear extract of cells through antibody binding. Specifically, when the nuclear extracts of motor neurons are added to the assay, which essentially is a 96-well plate pre-coated with consensus NF-κB binding sites, activated

transcription factors bind the oligonucleotides at their consensus binding sites and are quantified using the included antibodies that are specific to the bound and active form of the transcription factors. This aspect of the TransAM assay makes it a more precise method to measure NF-κB subunit DNA-binding activity, since it has been shown that NF-κB may sometimes be bound to IκB and be inactive, even if it is located in the nucleus (Hayden and Ghosh, 2012). Moreover, the Ghosh group has also recently found that the translocation of NF-κB to the nucleus is not sufficient to drive the transcription of target genes. The specific phosphorylation of p65 is also required for both efficient DNA-binding and transcription activity of nuclear NF-κB (Hayden and Ghosh, 2012). Thus, nuclear localization of NF-κB does not directly correspond to its binding activity.

Consequently, the TransAm assay was performed on motor neurons exposed to mutant versus wild-type astrocyte-conditioned medium for 0, 24, 48, 72, and 168 hours for four NF-κB subunits: p65, p50, p52, and RelB; an antibody for c-Rel was not available for mouse and thus could not be tested. Following this assay, a significantly higher binding activity for p65 was found in nuclear extracts of purified embryonic stem cell-derived motor neurons exposed to mutant astrocyte-conditioned medium for 24, 48, and 72 hours [Figure 4.5a]. Similarly, a significantly higher binding activity was observed for p50 in nuclear extracts of purified embryonic stem cell-derived motor neurons exposed to mutant medium for 24 hours [Figure 4.5a]. Interestingly, after 168 hours of exposure to mutant medium, this binding activity went down to levels similar to that in nuclear extracts of motor neurons exposed to wild-type astrocyte-conditioned medium [Figure 4.5a], a time when all of the sensitive cells had died. This suggests that the differential activity of p65 and p50 is a response of motor neurons as they are

dying or that they are activated only in the subpopulation of motor neurons that are vulnerable. Finally, no significant binding activity was observed for NF-κB subunits p52 and RelB [Figure 4.5b], which belong to the non-canonical pathway. These results imply that the canonical pathway is activated in motor neurons exposed to mutant astrocyte-conditioned medium, in a time-dependent manner. As shown in Figure 4.5, p65 especially responds to the toxic signal emanating from mutant astrocytes.

Figure 4.5: The canonical NF-κB pathway is activated in motor neurons exposed to mutant astrocyte-conditioned medium

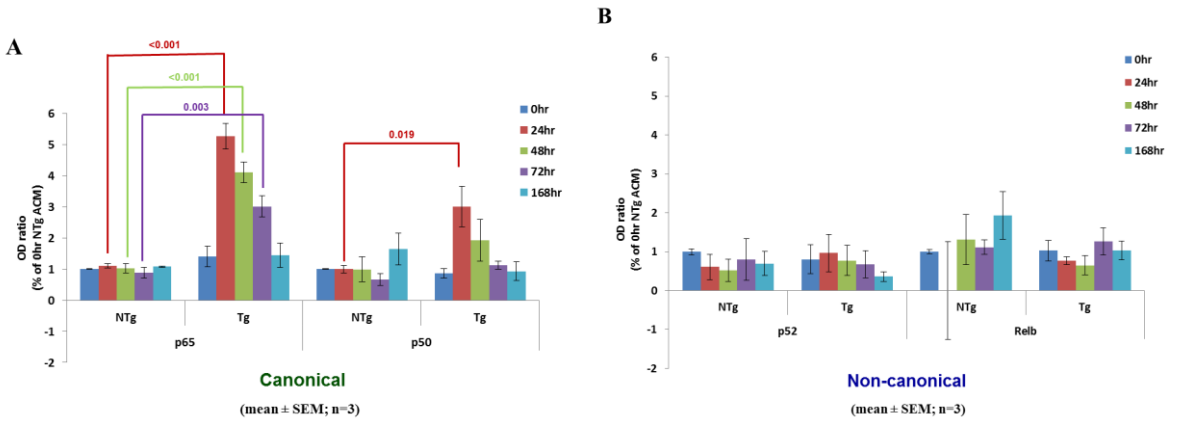

The TransAM assay demonstrates that the NF-κB subunits belonging to (A) the canonical pathway (p65 and p50) have a significantly higher DNA-binding activity in motor neurons that were exposed to transgenic (Tg) mutant SOD1 astrocyte-conditioned medium vs. non-transgenic (NTg) medium for 24, 48, and 72 hours. The NF-κB subunits belonging to (B) the non-canonical pathway, p52 and RelB, on the other hand, did not show any significant DNA-binding activity. The optical density (OD) values were normalized to the OD of motor neurons exposed to NTg astrocyte-conditioned medium for 0 hours. Values represent mean ± s.e.m from three independent experiments, analyzed by Student's t-test.

4.2.2. NF-κB is localized more in the nuclei of motor neurons exposed to mutant astrocyte-conditioned medium

Next, came the confirmation of the differential activity of p65 in motor neurons by performing subcellular fractionation on motor neurons exposed to mutant versus wild-type astrocyte-conditioned medium and testing to see whether an increased nuclear localization of p65 is observed using Western blot. In three independent experiments, an increase in the nuclear content of p65 was observed in motor neurons exposed to mutant astrocyte-conditioned medium for 24, 48, and 72 hours [Figure 4.6]. While this experiment confirmed what was observed in the

Figure 4.6: Increase in nuclear NF-κB expression in motor neurons exposed to mutant astrocyte-conditioned medium

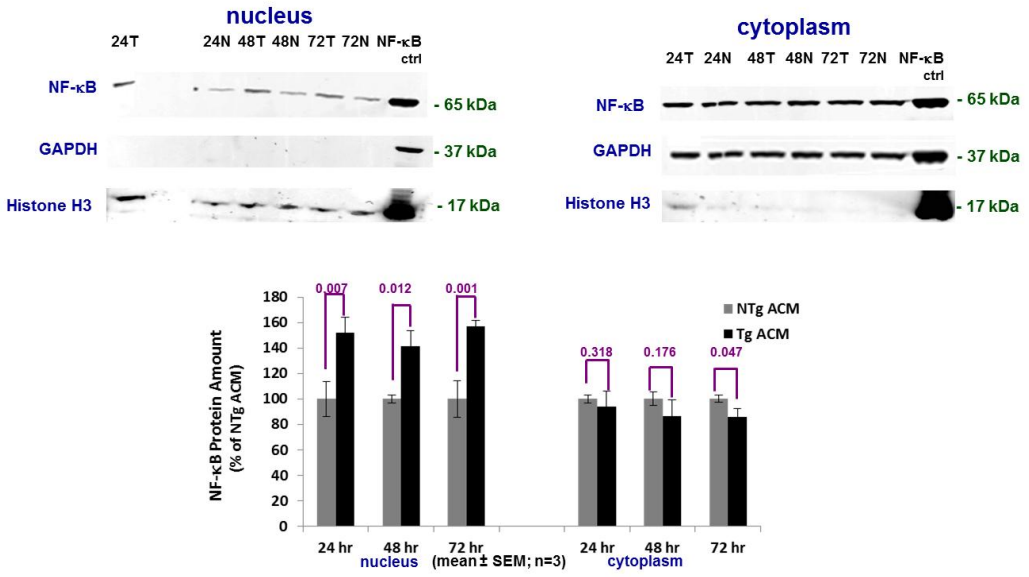

There is an increase in the nuclear expression of NF-κB p65 in motor neurons exposed to mutant transgenic (T-Tg) vs. non-transgenic (N-NTg) astrocyte-conditioned medium (ACM) for 24, 48 and 72 hours, using Western blot. In this study, GAPDH is used as a cytoplasmic and Histone H3 as a nuclear marker. The NF-κB protein amount expression was measured by normalizing each value to its corresponding amount of NTg ACM. NF-κB ctrl was a cell extract provided from Cell Signaling to test the p65 antibody. Values represent mean ± s.e.m from three independent experiments, analyzed by Student's t-test. The values in pink represent the p-value.

TransAM assay, the amount of increase in nuclear p65 in motor neurons exposed to mutant medium was not the same as the amount of increase in the p65 binding activity in nuclear extracts of motor neurons exposed to mutant medium (about 1.5 fold increase in Western blot versus 4 fold in the TransAM assay). This may be due to the greater sensitivity of the TransAm assay versus Western blot, as well as the possibility that there is a certain amount of inactive p65 in the nuclei of motor neurons that were exposed to wild-type astrocyte-conditioned medium that was not detected by the TransAM assay, since the assay specifically measures the binding activity, which was not the case with Western blot.

4.2.3. Phosphorylated IκB is increased in motor neurons exposed to mutant astrocyte-conditioned medium

After the demonstration that the NF-κB canonical pathway is differentially activated in motor neurons exposed to mutant astrocyte-conditioned medium, as evidenced by the TransAM assay and p65 nuclear localization, the question of how much phosphorylated IκBα was present in purified embryonic stem cell-derived motor neurons exposed to mutant astrocyte-conditioned medium arose. This was an important to know for validation, because IκBα is the main inhibitor of NF-κB dimers in the canonical pathway and its phosphorylation is key to its ubiquitination and degradation, which is necessary for the nuclear localization and activation of NF-κB dimers. Therefore, the amount of phosphorylated IκBα is an upstream marker for active NF-κB canonical pathway.

Figure 4.7: Increase in expression of phosphorylated IκB in motor neurons exposed to mutant astrocyte-conditioned medium

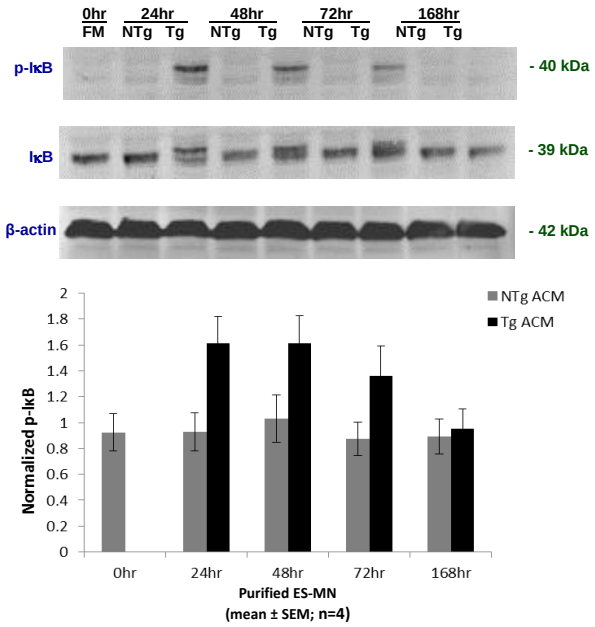

There is an increase in the expression of phosphorylated IκB (p- IκB) in motor neurons exposed to mutant (Tg) vs. non-transgenic (NTg) astrocyte-conditioned medium (ACM) for 24, 48 and 72 hours, using Western blot. In this study, β-actin is used as a loading control. The phosphorylated IκB protein expression was measured by normalizing each value to its corresponding amount of IκB. FM: motor neurons in fresh media used as a negative control. Values represent mean ± s.e.m from four independent experiments, analyzed by Student's t-test.

Using Western blots of motor neuron extracts, in three independent experiments, it was observed that there is an increase in phosphorylated IκBα in purified embryonic stem cell-derived motor neurons that are exposed to mutant astrocyte-conditioned medium for 24, 48, and 72 hours in comparison to motor neurons exposed to wild-type medium [Figure 4.7]. Similar to what was observed in the TransAm assay, this increase was slightly higher after 24 hours versus 72 hours of mutant medium exposure, and the expression was completely absent after 168 hours of exposure to mutant astrocyte-conditioned medium [Figure 4.7]. These results suggested one more time that the canonical pathway of NF-κB activity is up-regulated in the mutant astrocyte-induced motor neuron death process.

4.2.4. IKK inhibitor rescues motor neurons exposed to mutant astrocyte-conditioned medium

Even though we confirmed that the NF-κB canonical pathway is differentially activated in purified embryonic stem cell-derived motor neurons exposed to mutant astrocyte-conditioned medium, more needed to be done to reach a firm conclusion about the pathological significance of NF-κB in this model system of ALS. Therefore, the effect of inhibiting NF-κB activity was investigated in purified embryonic stem cell-derived motor neurons exposed to mutant astrocyte-conditioned medium by blocking the upstream IKK activity with a pharmacological inhibitor of IKK, and then assessing the change this inhibition causes in the survival of motor neurons. In doing so, depending on the changes in the number of motor neurons after the cell survival assessment, we could determine whether NF-κB promotes or protects against motor neuron death.

To do this investigation, Wedelolactone (Calbiochem), a cell-permeable, selective, and irreversible inhibitor of IKKα and β kinase activity, that inhibits NF-κB-mediated gene transcription by blocking the phosphorylation and degradation of IκBα, was used at concentrations ranging from 50 nM to 5 μM. Starting at concentrations from 500 nM, the addition of Wedelolactone to purified embryonic stem cell-derived motor neurons exposed to mutant astrocyte-conditioned medium rescued these neurons fully in our *in vitro* model [Figure 4.8]. Similarly, the addition of 1 μM Wedelolactone to purified embryonic stem cell-derived motor neurons exposed to mutant astrocyte-conditioned medium also fully rescued these neurons (data not shown). All of these results were confirmed by five independent experiments. While the addition of 50 nM Wedelolactone displayed no effect, at 50 nM, Wedelolactone showed a

mild rescue effect on motor neurons exposed to mutant astrocyte-conditioned medium [Figure 4.8], suggesting a half maximal inhibitory concentration of the pharmacological inhibitor compound in our culture model. Overall, this experiment showed that the loss of NF-κB activity rescues motor neurons exposed to mutant astrocyte-conditioned medium, indicating that increase in NF-κB activity regulates the ALS-linked mutant astrocyte toxicity for motor neurons.

Figure 4.8: IKK inhibitor rescues motor neurons exposed to mutant astrocyte-conditioned medium

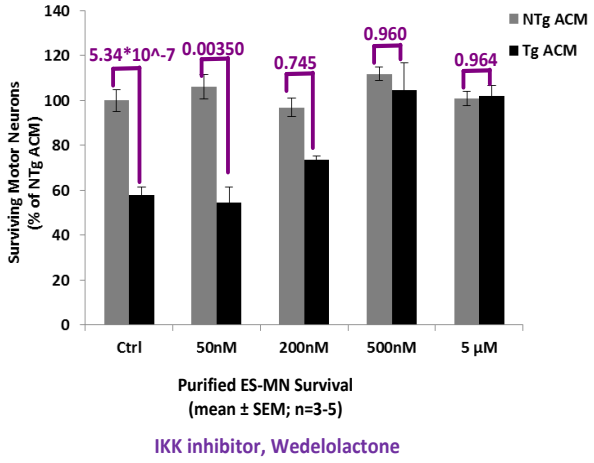

The treatment with IKK inhibitor, Wedelolactone, rescues motor neurons exposed to mutant astrocyte-conditioned medium (ACM) starting from 500 nM. In this study, purified embryonic stem cell-derived motor neurons exposed to either mutant (Tg) or non-transgenic (NTg) ACM were treated with Wedelolactone at concentrations 50 nM, 200 nM, 500 nM, and 5 µM at their first day *in vitro*. After seven days *in vitro*, the motor neurons were fixed and their survival was assessed using immunostaining. This experiment was repeated five times for the Wedelolactone concentrations 50 nM, 500 nM, and 5 µM, and three times for the 200 nM concentration. All the values represent the number of neurons as percentage of NTg ACM, with mean ± s.e.m from at least three independent experiments, analyzed by Student's t-test. The values in pink are the p-values.

4.2.5. IKK inhibitor does not rescue motor neurons from other toxicities

Using a pharmacological inhibitor to investigate the pathological significance of NF-κB brought up a concern about the specificity of its effect on motor neurons, since pharmacological agents often exert non-specific effects. Wedelolactone was previously shown to have no effect on non-NF-κB pathways, such as p38, MAPK, and AKT pathways (Kobori et al., 2004). However, to ensure that the protection of Wedelolactone against motor neuron degeneration is specific to the NF-κB-linked mutant

astrocyte-induced toxicity, motor neurons were exposed to two other death stimuli that are known to kill motor neurons, namely Fas ligand and domoic acid, via a non-NF-κB-dependent mechanism.

As explained in the Introduction, Raoul *et al.* (2002) found that 48 hours after treatment with Fas ligand primary motor neurons showed 50% loss *in vitro*. This cell-autonomous motor neuron death was mediated by Ask1, p38, and neuronal nitric oxide synthase signaling (Raoul et al., 2002). Similarly, domoic acid, an excitotoxin that is an agonist of the non-*N*-methyl-$_D$-aspartate (non-NMDA) AMPA kainate receptor, was also shown to cause about 40% loss in motor neurons through an increase in reactive oxygen species, but not through NF-κB signaling (Xu et al., 2008).

To perform this investigation, first tested was the effectiveness of Wedelolactone on primary motor neurons, from E12.5 mice, that were exposed to mutant astrocyte-conditioned medium, since Fas receptor (to which Fas ligand binds to) is not completely formed in embryonic stem cell-derived motor neurons. We found that, similar to its effect on purified embryonic stem cell-derived motor neurons, Wedelolactone showed a full rescue on primary motor neurons that were exposed to mutant astrocyte-conditioned medium [Figure 4.9a].

Once the effect of Wedelolactone was established on primary motor neurons exposed to mutant astrocyte-conditioned medium, primary motor neurons were treated next, in fresh motor neuron medium, with Fas ligand and domoic acid, with or without Wedelolactone. We found that, by 48 hours of exposure, motor neurons treated with Fas ligand or domoic acid showed about 40% loss in comparison to the neurons kept in fresh medium with no treatment [Figure 4.9b]. This validated what other groups had observed on the effect of other toxicities on motor

neurons. Next, we showed that there was no rescue effect on motor neurons that were treated with Wedelolactone once Fas ligand or domoic acid was added to them [Figure 4.9b]. This study was repeated for three independent experiments, all with the same results, suggesting that Wedelolactone has a motor neuron rescue effect specific to mutant astrocyte-derived toxicity.

Figure 4.9: IKK inhibitor does not rescue motor neurons from other toxicities

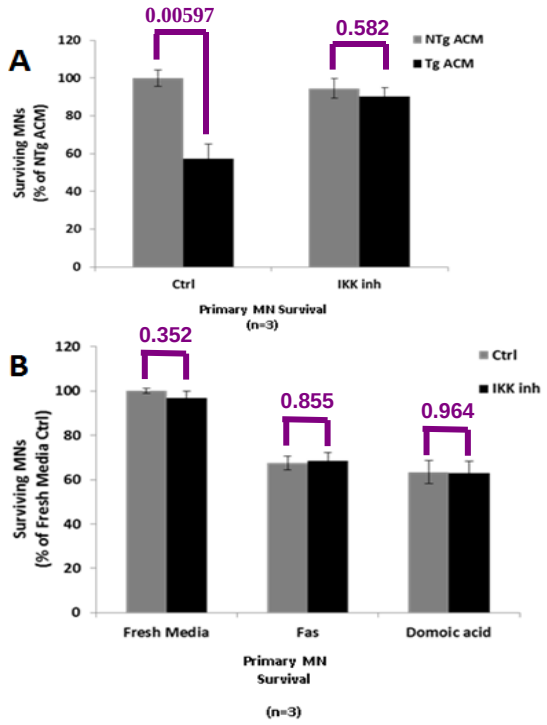

The IKK inhibitor does not protect motor neurons (MNs) from other toxicities whose mechanisms do not include NF-κB. For this study, primary MNs were used, (A) where first tested was the protective effect of Wedelolactone (5μM) on MNs that were exposed to mutant (Tg) vs. non-transgenic (NTg) astrocyte-conditioned medium (ACM). (B) Once the effect was confirmed, primary MNs, kept in fresh medium for five days *in vitro*, were either treated with Fas ligand (10ng/ml) or domoic acid (1μM), where after 48 hours; they showed about 40% demise in comparison to the MNs that were kept in fresh medium without treatment. The MNs that were treated with Fas ligand or domoic acid, in addition to Wedelolactone at four days *in vitro*, were fully rescued. Ctrl: control where Wedelolactone is not added. All the values represent number of surviving MNs as percentage of NTg ACM or fresh media control with mean ± s.e.m from three independent experiments, analyzed by Student's t-test. The values in pink are the p-values.

4.2.6. Super repressive IκB viral vector rescues motor neurons exposed to mutant astrocyte-conditioned medium

Since Wedelolactone is a pharmacological inhibitor and can have non-specific effects, even though the specificity of its motor neuron rescue effect on other toxicities was tested, we wanted to investigate further the effect of loss of NF-κB activity on motor neurons using another method: a dominant negative adeno-associated viral vector expressing super repressive IκB. Mutations in IκBα serines 32 and 36 have been shown to prevent both the

phosphorylation and the degradation of the IκB, where the infected mutant IκB competes with endogenous IκB molecules in the cell to block NF-κB activation (Magne et al., 2006). This mutant molecule is therefore referred to as a super repressive IκB. By infecting motor neurons with the viral vector expressing this mutant molecule, the aim was to block NF-κB activity in motor neurons.

For an efficient infection of purified embryonic stem cell-derived motor neurons with proper inhibition of NF-κB activity, different titrations of the adenovirus at varying multiplicities of infection (MOI) were tested first using an adenovirus titration kit (Clontech). This kit was designed around a hexon-specific antibody, which was used to label infected cells. The hexon protein is encoded by the adenoviral genome and is an essential component of the adenoviral capsid required for adenoviral replication. Thus, only the infected cells produce the hexon protein, which is then labeled and utilized to count infected cells. Using this kit, purified embryonic stem cell-derived motor neurons were found to exhibit about a 100% infection rate starting from 50 MOI (data not shown). The virus was toxic to the cells starting from 150 MOI (data not shown), providing us with a very narrow infection window to work with.

Making use of this titration data, next tested was the effect of the super repressive viral vector on the amount of phosphorylated NF-κB in motor neurons, since a decrease in the NF-κB activity would result in the decrease in the amount of phosphorylated NF-κB. Infection with the viral vector (at 50 and 100 MOIs) showed a significant decrease in the amount of phosphorylated NF-κB in purified embryonic stem cell-derived motor neurons exposed to mutant astrocyte-conditioned medium in comparison to those infected with viral vectors expressing green fluorescent protein only [Figure 4.10]. Additionally, the viral vector at 25 MOI showed a mild

decrease in the amount of phosphorylated NF-κB in motor neurons [Figure 4.10], corresponding to the partial viral vector infection observed in the cells. This study confirmed the functional effect of the super repressive IκB viral vector blockade of NF-κB activity in motor neurons.

Figure 4.10: Super repressive IκB viral vector decreases the amount of phosphorylated NF-κB in motor neurons

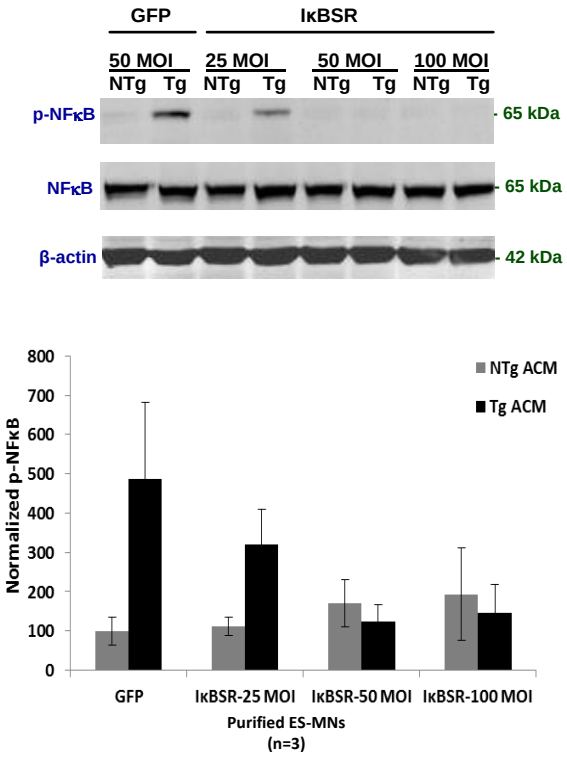

The adeno-associated viral vector expressing super repressive IκB (IκBSR) blocks NF-κB activity by decreasing the amount of phosphorylated NF-κB (p-NF-κB) in purified embryonic stem cell-derived motor neurons exposed to mutant (Tg) vs. non-transgenic (NTg) astrocyte-conditioned medium (ACM) for 24 hours in comparison to motor neurons infected by viral vector expressing green fluorescent protein (GFP) only, using Western blot. In this study, β-actin is used as a loading control. The phosphorylated NF-κB protein expression was measured by normalizing each value to its corresponding amount of NF-κB. Values represent mean ± s.e.m from three independent experiments, analyzed by Student's t-test.

Finally, the effect of this viral vector on the survival of motor neurons was tested to see whether the loss of NF-κB activity would rescue motor neurons exposed to mutant astrocyte-derived toxicity as shown using Wedelolactone. To test this hypothesis, we infected purified embryonic stem cell-derived motor neurons exposed to mutant astrocyte-conditioned medium with viral vectors expressing either green fluorescent protein only or with super repressive IκB. In three independent experiments, we observed an almost full rescue effect on motor neurons that were exposed to mutant astrocyte-conditioned

medium and infected with viral vectors expressing super repressive IκB (at 50 MOI) [Figure 4.11]. Similar to what was observed in the study with the Wedelolactone treatment, this study showed that the loss of NF-κB activity via the infection with super repressive IκB viral vector rescues motor neurons from toxicity emanating from mutant astrocytes, indicating that NF-κB regulates the mutant astrocyte-derived motor neuron death in this model system of ALS.

Figure 4.11: Super repressive IκB viral vector rescues motor neurons exposed to mutant astrocyte-conditioned medium

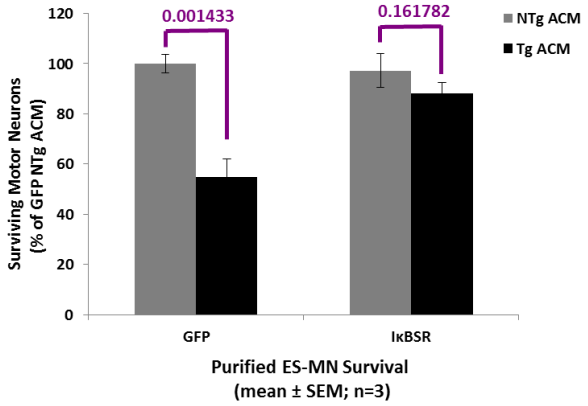

The infection with the adeno-associated viral vector expressing super repressive IκB (IκBSR) vs. green fluorescent protein (GFP) rescues motor neurons exposed to mutant (Tg) vs. non-transgenic (NTg) astrocyte-conditioned medium (ACM). In this study, motor neurons were infected with the viral vector one day after the addition of ACM, and cell survival was assessed after seven days *in vitro*. All the values represent number of surviving motor neurons as percentage of NTg ACM with mean ± s.e.m from three independent experiments, analyzed by Student's t-test. The values in pink are p-values.

4.3. Conclusion & Discussion

This section of the thesis confirmed that NF-κB, which was one of the top 25 transcription factors inferred by the Master Regulator Analysis performed on the 72 vs. 0 hour signature from the RNA-Seq data, regulates the ALS-linked mutant astrocyte toxicity for motor neurons. Despite its complex regulatory and stimulus-selective response mechanisms, an increase in NF-κB activity was demonstrated in purified embryonic stem cell-derived motor neurons exposed to mutant astrocyte-conditioned medium before they become committed to die. Moreover, it was shown that this increase in NF-κB activity promotes motor neuron death and that this activity is specific to the canonical pathway of NF-κB involving

p65, and to some extent p50. One additional experiment that could be performed is to test the super repressive IκB viral vector on motor neurons with another stressor, just like we have done with Wedelolactone, to test the specificity of the rescue effect of the viral vector on motor neurons.

Even though we saw that NF-κB differential activity occurs in motor neurons specifically in the canonical pathway through the involvement of p65, p50, and IκBα in our model system, we cannot fully exclude the possibility of the involvement of the non-canonical NF-κB pathway. That is because there is evidence of cross-talk between the canonical and non-canonical pathways involving p65 forming dimers with p52, instead of p50, as a compensatory mechanism. Also, while observing no differential activity of p52 and RelB in the TransAM assay, we could not measure the binding activity for c-Rel. Thus, no conclusive statement can be made about the involvement of c-Rel in the mechanism of non-cell autonomous motor neuron degeneration in our model system. However, overall, the canonical pathway seems to be the main pathway that is activated in motor neurons exposed to mutant astrocyte-conditioned medium.

Since it is known that the canonical pathway is involved in mutant astrocyte-derived motor neuron death, it would be interesting to investigate the involvement of known molecules that are upstream to the IKK complex that activate the canonical NF-κB pathway, such as TAK1, TRAF6, interleukin-1 receptor associated kinase-1 (IRAK1), and RIP1. The immunology field is vast with knowledge on the signalization of the NF-κB pathway and this knowledge can be used to decipher what is upstream to NF-κB in our model system. This is especially true with the help of the RNA-Seq data where one can check the presence of candidates in the genomic data as a

preliminary checkpoint to see whether these upstream mediators are present in the RNA-Seq data.

Furthermore, one could use the literature from the immunology field to link NF-κB with the downstream signalization leading to programmed cell death, which Nagai *et al.* has shown to be activated in motor neurons that are exposed to mutant astrocyte-conditioned medium, such as Bax and caspase 3 (Nagai et al., 2007). For example, it has been shown that when the cell receives inflammatory stimuli, activated nuclear NF-κB transcribes anti-apoptotic Bcl-2 and Bcl-X_L, which then inhibit Bax activation (Hayden and Ghosh, 2012). This finding suggests that NF-κB activation inhibits Bax activation in cell survival-promoting circumstances. However, since in our model system, NF-κB promotes cell death, its activation might have the opposite effect on Bax activation, which needs to be investigated. One way to investigate this hypothesis would be to treat motor neurons, exposed to mutant astrocyte-conditioned medium, with Wedelolactone and see if the neurons still show increased Bax activation, which can be measured by the increase in the translocation of Bax to mitochondria. Similarly, motor neurons could be treated with a Bax inhibitor to see if an increase in NF-κB activity is still observed. This study may help us demonstrate whether or not Bax and NF-κB are on the same linear molecular pathway and to confirm that NF-κB is upstream to Bax in this death cascade.

Another question that would be interesting to address would be whether NF-κB gets activated upon exposure to mutant astrocyte-conditioned medium only in sensitive motor neurons or also in the resistant subpopulation. In order to investigate this question, we could add mutant astrocyte-conditioned medium to motor neurons that are already exposed to mutant medium for 168 hours and test, either by Western blot or the TransAM assay, whether NF-κB is

differentially activated in these cells in comparison to those exposed to wild-type astrocyte conditioned-medium. This study would help our understanding of how specific the NF-κB response is in motor neurons exposed to mutant astrocyte-conditioned medium.

So far, the pathological significance of NF-κB in ALS has been shown only *in vitro* (Swarup et al., 2011). However, it is also important, as a future study, to validate NF-κB's role in motor neuron death *in vivo*. For this, four approaches could be followed: (1) performing a longitudinal immunohistochemistry study to look at nuclear NF-κB motor neuron expression in spinal cords of mutant $SOD1^{G93A}$ mice at pre-symptomatic (i.e. P30, P60), symptomatic (i.e. P90), and end-stage (i.e. P120); (2) performing a similar immunohistochemistry study in postmortem spinal cords of ALS patients; and (3) generating transgenic mice expressing mutant $SOD1^{G93A}$, which also carry motor neuron-specific null mutations for *p65* or *NEMO* gene, either by using the Cre-lox system or gene therapy methods. These double-engineered mice would then be used to assess the impact of the *p65* or *NEMO* deletion, only within motor neurons, on the survival, onset of disease manifestations, and disease duration caused by mutant SOD1. (4) Finally, known inhibitors of NF-κB activity, such as celastrol or Withaferin A, can be administered to mutant SOD1 mice before the onset of disease symptoms (i.e. P30) and their effect on disease duration and survival in these mice could be studied. Performing these *in vivo* studies would further validate the involvement of NF-κB in ALS-linked motor neuron degeneration.

Finally, NF-κB was only one of the top transcription factors inferred by the Master Regulator Analysis. While this endeavor was a success in validating NF-κB as a master regulator, in order to understand the complete signalization that takes place in motor neurons, the

pathological significance of the other transcription factors needs to be investigated, as well. Only in doing so, the molecular mechanism underlying the ALS-linked mutant astrocyte toxicity for motor neurons might eventually be fully elucidated.

Chapter 5: Conclusion and Discussion

ALS, like many other prominent adult-onset neurodegenerative diseases, such as Alzheimer's and Parkinson's diseases, is characterized by the demise of specific subsets of neurons. Although ALS is essentially a sporadic disorder, the investigations of the rare ALS-causing genetic mutations, which have been discussed in the Introduction, have led to several breakthroughs in our understanding of the neurobiology of this fatal paralytic disorder including, but not limited to, protein misfolding, ER stress, and the recruitment of the apoptotic machinery.

Another key advance in the pathogenesis of ALS is linked to our growing recognition of the importance played by non-neuronal cells, such as glia, in the demise of motor neurons. Although thus far, this line of investigation relies on mutant SOD1 and *in vitro* studies, the consensus in the field of ALS research is that insights gained via this particular disease model system might provide important clues into the pathogenesis of the prominent sALS. In support of this idea is the recent work done with human cells from sALS patients, which produced very similar results as those generated with mouse mutant SOD1-expressing cells (see below).

Probably, the most salient results published thus far about the role of glial cells in the ALS neurodegenerative process in experimental models are the following. It has been shown that the selective reduction of mutant SOD1 by a Cre-Lox system in motor neurons, microglia, or astrocytes, prolongs survival in transgenic $SOD1^{G37R}$ mice compared to their germ-line littermates (Boillee et al., 2006; Yamanaka et al., 2008b). It has also been shown that transgenic mice in which mutant SOD1 is restricted to both motor neurons and astrocytes develop a severe overt ALS phenotype (Wang et al., 2005b). Furthermore, using a neuron/glia co-culture system,

Nagai *et al.* and others (Di Giorgio et al., 2007; Nagai et al., 2007; Vargas et al., 2006) have found that astrocytes expressing mutant SOD1 trigger the death of primary and embryonic stem cell-derived motor neurons, regardless of whether or not they express mutant SOD1. Nagai *et al.* further showed that the contribution of the mutant astrocytes to the death of motor neurons *in vitro* is caused by a soluble factor (Nagai et al., 2007). Interestingly, medium conditioned with mutant SOD1-expressing astrocytes impairs motor neuron survival whereas medium conditioned with mutant microglia does not (Nagai et al., 2007). Moreover, Nagai *et al.* also showed that motor neurons are selectively vulnerable to this mutant astrocyte-derived toxic activity, since GABAergic interneurons cultured on astrocyte layers or dorsal root ganglion neurons cultured in astrocyte-conditioned medium are not affected (Nagai et al., 2007).

Extending these *in vitro* mouse cell findings, it has been shown that astrocytes derived from neural progenitor cells obtained from postmortem spinal cords of human sALS patients are also toxic to spinal motor neurons (Haidet-Phillips et al., 2011). We have confirmed this result using human primary astrocytes from sALS patients (data not shown). It has also been reported that mutant SOD1-expressing glial-restricted precursors grafted into spinal cords of wild-type rats produce motor neuron loss in living animals (Papadeas et al., 2011). Thus, as indicated above, these observations provide substantial support to the idea that the toxic phenotype caused by ALS astrocytes is not restricted to *in vitro* systems, to mouse cells, or to fALS. Given these facts, we thought that the mutant SOD1 model of non-cell autonomous degeneration of motor neurons may be ideal to shed more light into how and why motor neurons degenerate in ALS.

The goal of this thesis work has thus been to exploit this unique *in vitro* ALS model of spontaneous motor neuron degeneration to acquire insights into the molecular mediators of the

non-cell autonomous components of ALS pathogenesis. However, given the minimal success we had in addressing this outstanding question using a candidate-based approach, employed here was a combination of genomic and bioinformatics methodologies to try to **elucidate the molecular underpinning of the mutant astrocyte toxicity for motor neurons, especially before these neurons become committed to die.**

As shown and discussed in Chapter 2, prior to embarking on the actual genomic analyses, it was necessary to further characterize the planned *in vitro* model to assure that the work could be conducted under the most suitable conditions. Since the aim was to study the transcriptional alterations that take place in motor neurons in response to the toxic insult emanating from mutant astrocytes, it was crucial to use only motor neurons for this work. Nagai *et al.* has found that motor neurons exposed to mutant astrocyte-conditioned medium display the same amount of degeneration as the motor neurons co-cultured on mutant astrocyte monolayers (Nagai et al., 2007). Therefore, it sufficed to expose motor neurons to mutant astrocyte-conditioned medium to bring about the toxic phenotype and, as such, to eliminate glial cells from the culture setting. Yet, this was not sufficient to assure that we were dealing with motor neurons only, since embryonic stem cells differentiated by current protocols only produced about 30% motor neurons; the rest being other types of neurons and even non-neuronal cells. Thus, for the efficient purification of embryonic stem cell-derived motor neurons, two different methods were tested, namely FACS and MACS. Through the work presented in Chapter 2, we found MACS to be the more efficient method of the two. Thus, the combination of the mutant astrocyte-conditioned medium and the MACS purification method allowed obtaining cultures made up of more than 90% of motor neurons to be used as a non-cell autonomous model of motor neuron degeneration in ALS.

Next, we asked what would be the most relevant timepoints, after exposure to mutant astrocyte-conditioned medium, to harvest motor neurons and extract their RNA. First, we found the timeline of motor neuron degeneration to be quite similar to that previously reported for primary non-purified motor neurons (Nagai et al., 2007). Indeed, the number of purified embryonic stem cell-derived motor neurons exposed to mutant astrocyte-conditioned medium declines by about 50% after 7 days *in vitro* without further changes up to 14 days *in vitro*. Worth noting is the fact that the incomplete neuronal loss observed after 7 days of exposure to mutant astrocyte-conditioned medium cannot be due to the loss of toxic activity of the medium, since we found that even if this conditioned medium is changed at 7 days and the motor neurons are allowed to remain in culture for an additional 7 days, there is no significant further loss of motor neurons. Interestingly, a similar (about 50%) loss of motor neurons was reported by Raoul and collaborators (2002) in their study on Fas ligand toxicity in motor neurons. Based on what is currently known about the toxic mechanisms driving mutant astrocytes and Fas ligand, these two models do not intersect and thus may well operate by very different signaling pathways, at least at the proximal level of their respective death cascades. Therefore, it is surmised that about 50% of the spared motor neurons epitomize a more resilient subpopulation of motor neurons. Perhaps, it may be valuable to design future studies to explore the molecular basis of this differential sensitivity, which could be readily extracted from some of the already available genomic signatures that have generated during this work.

Since the purpose of this project has been to elucidate the molecular mechanisms of non-cell autonomous motor neuron degeneration before motor neurons become committed to die, it was necessary to define the timeframe within which this point of no return is reached so that

experiments could be designed to properly capture the intended early molecular events. Accordingly, by testing different exposure times, ranging from 24 to 168 hours, we found that at around 72 hours of exposure to mutant astrocyte-conditioned medium, motor neurons become irreversibly committed to die. Therefore, in light of this information, it was assumed that the most significant signatures of early perturbations had to take place in motor neurons no later than 72 hours of exposure to mutant astrocyte-conditioned medium.

With the above-mentioned information and the RNA-Seq data for different selected timepoints, the early event signatures linked to motor neuron degeneration were extracted by performing a reverse gene engineering analysis. This powerful bioinformatics algorithm is inferential in nature, since it is based on interrogation of a database which is ideally constructed with the information generated from the same species and cell type as the ones used in RNA-Seq experiments. Unfortunately, at this time, a mouse motor neuron interactome is not available, although we are aware that such an interactome is in development (data not shown). Thus, for the time being, all seven interactomes that are available from the Califano group were interrogated. As shown in Figure 3.6, of these seven interactomes, the mouse brain interactome was found to be the most trustworthy for analyzing the RNA-Seq data. Also, the 72 vs. 0 hour signature was found to be the "strongest" signature, because it yielded the highest number of transcription factors and differentially expressed genes. These findings were assuring given the fact that the aim was to focus on molecular events up to 72 hours.

Next, to validate the significance of the master regulators inferred by the mouse brain interactome using the 72 vs. 0 hour signature in Chapter 3, particular attention was given to the 25 most differentially dysregulated master regulators. (These master regulators are listed in

Table 3.4.) Of the 25 selected master regulators, NF-κB was especially intriguing. This was not only because NF-κB was one of the top master regulators, most differentially expressed genes, and most enriched pathways, but also recent discoveries in ALS research have hinted at its dysregulation in the disease process. For example, NF-κB was found to be up-regulated in sALS patients (Jiang et al., 2005b) and in transgenic mutant SOD1 mice (Ferraiuolo et al., 2007). Moreover, NF-κB has been found to be involved in the TDP-43- and OPTN-linked ALS pathogenesis (Maruyama et al., 2010; Swarup et al., 2011). All of these findings render NF-κB a very interesting master regulator candidate to investigate in relation to its pathological significance in ALS.

Thus, as shown in Chapter 4, the significance of NF-κB was validated in our *in vitro* ALS model of non-cell autonomous motor neuron degeneration. Using a DNA binding assay, subcellular fractionation and Western blot, a time-dependent increase of NF-κB activity was noted in purified embryonic stem cell-derived motor neurons exposed to mutant astrocyte-conditioned medium. This activity culminated prior to 72 hours of exposure to mutant medium and involved the canonical pathway of the NF-κB complex, as evidenced by the nuclear localization of the p65 subunit. Even more important, we found that, by inhibiting NF-κB through both pharmacological and genetic means, the toxicity of mutant astrocyte-conditioned medium for motor neurons was abrogated. These results indicated that NF-κB is indeed instrumental in our non-cell autonomous scenario of ALS pathogenesis. Based on the above findings, it can be concluded that this overall approach represents a proof of principle that, with such methodology as used in this work, one may unravel programmed cell death.

This finding on the involvement of NF-κB in the mutant SOD1-linked non-cell autonomous model of motor neuron degeneration coincided with the previous discoveries on the TDP-43 and OPTN ALS models. Until now, it has been a mystery, in the field, of how genetic mutations in fALS, as well as in sALS, which are so different from one another, can result in such a similar clinical and pathological phenotype. And, it has been suggested that perhaps distinct preliminary molecular mechanisms may intersect at a common point. Can it be that NF-κB is that common point between the molecular mechanisms of different genetic mutations of fALS and sALS?

While not much is known about the molecular machinery involved in NF-κB in these ALS models, it has been shown that TDP-43 acts as a co-activator of p65 (Swarup et al., 2011), which is a subunit of the canonical NF-κB pathway. Similarly, it has been suggested that the ALS-related OPTN mutations lack inhibitory effects toward NEMO, the IKK complex member specific to the canonical NF-κB pathway, resulting in a subsequent increase in the ubiquitination of RIP and in the activity of the canonical NF-κB pathway (Maruyama et al., 2010). These findings, taken together, suggest the involvement of the canonical pathway of NF-κB in the motor neuron degeneration of ALS for the TDP-43 and OPTN models, which matches with the findings which used the mutant SOD1 non-cell autonomous model.

Since NF-κB is a highly studied molecule in the field of immunology, the activation of the NF-κB canonical pathway can shed light on what is upstream to this signaling. For example, as described in Chapter 4, TAK1 is a kinase that selectively phosphorylates the IKK complex of the canonical NF-κB pathway. Similarly, RIP family proteins, which form a complex with the receptor-associated factors, such as TNF receptor type 1-associated DEATH domain (TRADD)

and TRAF, and subsequently phosphorylate the IKK kinases of the canonical pathway, are also specific to the canonical pathway. Although these results on the molecular machinery responsible for the activation of the NF-κB pathway comes mostly from the field of immunology, it would be an interesting future study to target some of the molecules mentioned above to test their involvement in our model system, by inhibiting their activity in motor neurons through pharmacological or genetic means, and investigating their effects on the survival of these neurons. Furthermore, to understand the complete molecular mechanism underlying the ALS-linked astrocyte toxicity for motor neurons, it would be important to investigate the rest of the top 25 master regulators from the 72 vs. 0 hour signature for their pathological significance in motor neuron death. This investigation is currently on going.

Finally, one of the interesting observations made from the analysis of the RNA-Seq data was that the pathways that were activated early on in motor neurons exposed to mutant astrocyte-conditioned medium primarily belonged to the NF-κB and IFN-γ signaling pathways. Remarkably, an increase in IFN-γ-dependent signaling has also been observed by other groups, such as by the groups of Raoul (Aebischer et al., 2011) and Maniatis (unpublished work), in motor neurons exposed to the toxicity emanating from mutant astrocytes. Moreover, IFN-γ has been found to induce DNA binding of NF-κB in a STAT1-independent manner (Deb et al., 2001), suggesting a potential link between the two pathways. Similarly, PI3K pathway, which is also one of the signaling pathways activated early on in motor neurons exposed to mutant astrocyte-conditioned medium, has been found to be activated by IFN-γ signaling (Nguyen et al., 2001). This pathway, upon activation, has been shown to activate the canonical NF-κB pathway (Memet, 2006), strengthening further the potential link between IFN-γ and NF-κB pathways.

In addition, of the pathways activated early in motor neurons exposed to mutant astrocyte-conditioned medium, a cross talk between Wnt and NF-κB signaling has also been reported. In the nucleus of breast and colon cancer cells that express β-catenin aberrantly, the ability of NF-κB to bind DNA has been shown to be suppressed by its association with β-catenin (Deng et al., 2002). Furthermore, through screening deubiquinating enzymes involved in Wnt signaling, CYLD, a negative regulator of NF-κB signaling, has been identified as an important regulator of the β-catenin pathway (Tauriello et al., 2010). Moreover, the cross talk between NF-κB and Wnt signaling has also been demonstrated in the β-catenin-independent pathway, mainly through Wnt5a. In endothelial cells, Wnt5a has been found to induce translocation of NF-κB into the nucleus through the Ca^{2+}/PKC pathway to cause inflammation (Kim et al., 2010).

Similarly, recent data suggest that there is also a cross talk between JNK and NF-κB signaling, where TAK1 and TRAF6 are the common upstream activators of these pathways through the involvement of either Toll-like, TNF, $p75^{NTR}$, interleukin-1, or Tgf-β receptors (Landstrom, 2010). Furthermore, it has been found that, in murine embryonic fibroblasts, an NF-κB target gene, Xiap, inhibits JNK activation (Tang et al., 2001). On the other hand, inhibition of JNK by overexpression of a dominant negative SEK1 has been shown to impair degradation of IκBα and activation of NF-κB induced by vanadate in macrophages (Chen and Davis, 1999). Moreover, in Jurkat T cells, Xiap and Siva bound to TAK1 have been found to be the switch between NF-κB and JNK pathways (Resch et al., 2009). All of these data on NF-κB and JNK signaling indicate a strong interaction between these two pathways. However, it is difficult to determine which of the pathways regulate the other. Moreover, since none of the findings on these pathways are on motor neurons, it would be worthwhile to test the interaction of IFN-γ,

PI3K, Wnt and JNK pathways with NF-κB by inhibiting the activation of NF-κB in motor neurons exposed to mutant astrocyte-conditioned medium and examining the changes in the activity of the other pathways, and vice versa. This way, we could determine more accurately whether these pathways interact with NF-κB signaling, and if they do, which pathway acts upstream to the other.

While the published and unpublished results discussed above are consistent with our findings, some of the data generated here diverge from those of some other groups. For example, we did not find Fas to be differentially regulated in the RNA-Seq data, which was found to be involved in the cell autonomous motor neuron degeneration in ALS by Raoul *et al.* (2002). We also did not observe any increase in the activity of ER stress, which has been found to be involved early in the ALS disease process *in vivo* in motor neurons of mutant SOD1 mice by Saxena *et al.* (2009). One possible explanation as to why we did not observe any changes in these molecular pathways might pertain to the fact that they may belong primarily to the cell autonomous mechanisms and not to the non-cell autonomous mechanisms involved in the demise of motor neurons. It is well established in the field that motor neurons in ALS may die through many pathogenic processes. Therefore, it is possible that the non-cell autonomous mechanism is involved in the more inflammatory-linked NF-κB and IFN-γ pathways, whereas the cell autonomous mechanism is involved in the pathogenic processes affecting the ER among other cellular systems. Thus, depending of the experimental conditions, one may see evidence of some pathways over others. If this is the correct assumption, then one should expect to see, for example, evidence for the involvement of both NF-κB and ER stress pathways if both mutant

SOD1-expressing motor neurons and mutant SOD1-expressing astrocyte-conditioned medium are used in this model system.

If NF-κB is validated as a significant regulator of human ALS, then it would be a promising, but not necessarily straightforward therapeutic target for the disease. The reason is that NF-κB is a critical regulator involved in the homeostasis of a host of vital functions. Therefore, for the treatment of ALS, the chronic inhibition of NF-κB cannot be generalized. Instead, strategies to deliver treatments specifically to motor neurons of patients may need to be developed. Perhaps, one such targeted delivery could be achieved by gene therapy using viral vectors expressing super repressive IκB under the Hb9 promoter. Since ALS is a chronic disease, it is also possible that a mild inhibition of NF-κB might suffice to modify the natural course of the disease and to prolong survival beyond the effect of riluzole. Along this line, it is worth noting that achieving a mild inhibition of NF-κB could be feasible by using a natural compound, such as *Withania somnifera*, which is a plant also known as Indian ginseng or wild cherry. In this case, enough NF-κB inhibition may be achieved to slow the progression of the disease without triggering major side effects in patients. This idea has been tested by the Julien group, where the group administered the natural compound to mutant $SOD1^{G93A}$ and $SOD1^{G37R}$ mice before the onset of disease symptoms, and found the treatment to improve the disease phenotype, as well as to extend the life span of these animals (data not shown).

In conclusion, early diagnosis of ALS is difficult and is often delayed by the subtle onset of manifestations that mimic other conditions. Moreover, clinical trials are still very slow in determining whether a treatment is effective. All of these difficulties necessitate the discovery of early motor neuron degeneration markers that can be used as biomarkers for the early diagnosis

of ALS, as well as to develop new therapies aimed at mitigating motor neuron degeneration. An increasing body of evidence suggests that non-cell autonomous processes play critical roles during the initiation and progression of ALS pathology. **Therefore, it may be extremely important to discover, not only early cell autonomous, but also early non-cell autonomous pathogenic mechanisms in order to acquire a deeper understanding of the neurobiology of ALS and to be able to devise effective therapeutic approaches for preventing or reversing the progression of ALS.** We believe that, by using well-controlled *in vitro* models and reverse gene engineering analysis, we have come closer to the discovery of these mechanisms.

Chapter 6: Experimental Methods

Primary cultures of rodent astrocytes and preparation of astrocyte-conditioned medium

Astrocyte monolayers were prepared from spinal cords or cortices of newborn mouse and rat pups, obtained from the matings of transgenic SOD^{G93A} and SOD^{WT} rodents with wild-type animals. For each pup, tail DNA was extracted for genotyping by PCR, and spinal cord and cortex were dissected. Basically, meninges were removed, and spinal cords and cortices were dissociated mechanically (20 passages through 18G needles). Cell suspensions were plated individually on 75 or 25 cm^2 flasks in glial medium: Dubelco Modified Eagle's medium (DMEM; Invitrogen, Carlsbad, CA) containing 10% fetal bovine serum (Invitrogen), 100 U/mL penicillin and 100 µg/mL streptomycin (Invitrogen). Cultures were, then, maintained for two weeks in a humidified incubator at 37°C under 5% CO_2. Medium was changed twice a week. After 2 weeks, these primary glial cultures contained 95% $GFAP^+$ astrocytes, 5% of $CD11b^+$ microglia, and no neurons or oligodendrocytes as indicated by the lack of respectively MAP2 or 2'-3'-cyclic nucleotide phosphohydrolase immunoreactivity. To eliminate microglia, 2-week-old flasks were agitated on a rotary shaker (200 rpm; 6 h) and carefully washed twice with PBS before being placed with motor neuron medium: Neurobasal medium (Invitrogen) containing 2% horse serum (heat inactivated; Invitrogen), B27 supplement, 0.5 mM glutamine (Invitrogen), 25 µM β-mercaptoethanol, 100 U/mL penicillin, and 100 µg/mL streptomycin supplemented with 0.5 ng/mL glia-derived neurotrophic factor (GDNF), 1 ng/mL brain-derived neurotrophic factor (BDNF), and 10 ng/mL ciliary neurotrophic factor (CNTF), all trophic factors from R&D systems. After 7 days, the conditioned medium was collected and centrifuged (500xg, 10 min) to

eliminate floating cells. Supernatants from different genotypically-matched astrocyte cultures were collected mixed together and frozen in several aliquots. On the day of assay, conditioned medium was supplemented with 4.5 g/mL D-glucose (final concentration), penicillin/streptomycin, and trophic factors (as described above) and filtered through a 0.22 μm filter before being added to the motor neuron cultures.

Embryonic stem cell-derived motor neuron cultures

Embryonic stem cells were derived from Tg *Hlxb9-GFP1Tmj* mice expressing eGFP or eGFP and CD2 driven by the mouse HB9 promoter (Wichterle et al., 2002) and were differentiated into motor neurons as described previously (Wichterle et al., 2002) with some modifications. To form embryoid bodies, embryonic stem cells were first grown for 2 days in 1:1 (v/v) DMEM (Invitrogen)/Ham's F-12 media (Invitrogen) medium containing the B27 supplement (Invitrogen), 100 U/mL penicillin, 100 μg/mL streptomycin, and 0.1 mM β-mercaptoethanol (Sigma, Saint Louis, MO). They were then treated with 1 μM retinoic acid (Sigma) and 400 nM sonic hedgehog agonist (Hh-Ag1.3, Curis Inc., Cambridge, MA) for 5 days before being dissociated with a papain solution (Worthington, Lakewood, NJ). The produced cell suspensions were washed with the motor neuron medium described above and resuspended in PBS containing 1% BSA at the concentration of ~ 20 x 10^6 cells per mL to be processed by FACS or MACS (see methods below) to purify GFP-positive motor neurons from the rest of the cells.

Sorting of GFP-positive motor neurons by FACS

Prior to sorting, cell suspensions (~20 x 10^6 cells per mL, in 1% BSA PBS) were filtered through filter top tubes (Falcon 12X75mm Cat#2235). Cell sorting was performed using a Becton Dickinson FACS Aria cytometer (BD Biosciences) at the Flow Cytometry Core Facility of Columbia University (http://www.ccc.columbia.edu/FCCF/flow_cytometry.html). Forward scatter (FS) and side scatter (SSC) were collected through a filter. The GFP signal was collected in the FL1 channel. A light scatter gate was drawn in the SSC versus FS plot to exclude debris and include the viable cells. Cells in the gate were displayed in a single-parameter histogram for GFP and final gate settings determined to collect the GFP-positive cells. Post-sorting, the cells were collected in motor neuron medium supplemented with 20% FBS. Before plating, the pure motor neuron suspension were collected by centrifugation (300xg, 5 min) and resuspended in motor neuron medium.

Sorting of CD2-positive motor neurons by MACS

Upon dissociation and wash with L15 medium consisting of L15 solution (Sigma), 50 µM EDTA, 4% BSA (Sigma), 25 mM glucose, 2% Horse Serum (Sigma), 40 µg/mL DNAse, 500 µg/mL Insulin (Sigma), 0.01M Putrecine (Sigma), 10 mg/mL Conalbumin (Sigma), 30 µM Sodium Selenite (Sigma), cell suspensions were incubated with 80 µl of L15 medium and 10 µl of anti-rat CD2 antibody (Invitrogen; per 15 million dissociated cells) for 20 minutes at 4^0C. After washing again with L15 medium, cells were then incubated with anti-mouse magnetic microbeads (Miltenyi Biotec) for 20 minutes at 4^0C. Finally, cells were passed through a

magnetic column to separate CD2-GFP-positive cells from the other types. Post-sorting, the cells were collected in motor neuron medium and were plated for culture.

Primary motor neuron cultures

Spinal neuronal cultures were performed from E12.5 Hlxb9-GFP1Tmj transgenic rodents as previously described (Raoul et al., 2002) with some modifications. Cells were plated at 1,500 $eGFP^+$ cells cm^{-2} for Hlxb9::eGFP either on coverslips coated with 0.01% poly-D-lysine and 10 µg ml^{-1} laminin (poly-D-lysine/laminin) or on astrocyte monolayers. The culture medium was either motor neuron medium supplemented with a cocktail of trophic factors composed of 0.5 ng ml^{-1} GDNF, 1 ng ml^{-1} BDNF and 10 ng ml^{-1} CNTF (trophic factor cocktail, R&D Systems); or astrocyte-conditioned motor neuron medium.

Immunocytochemistry

For immunocytochemistry, cells were processed as we previously described (Nagai et al., 2007; Przedborski et al., 1996). Primary antibodies used were: rabbit polyclonal anti–eGFP (1:1000; Molecular Probes), rabbit anti–HB9 (1:1000, Abcam); goat polyclonal anti–ChAT (1:100; Chemicon, Temecula, CA), and mouse monoclonal anti–MAP–2 (1:1000; Chemicon), rabbit anti–GFAP (1:200; DAKO Z0334), and mouse anti–Islet 1 (1:100; from Dr. Jessell's lab).

Verification of astrocyte-conditioned medium toxicity

Prior to their use for the RNA-Seq assay, the toxicity of transgenic $SOD1^{G93A}$ astrocyte-conditioned medium versus non-transgenic and transgenic $SOD1^{WT}$ astrocyte-conditioned media

were confirmed. For that, embryonic stem cell-derived motor neurons plated (1500 cells per cm^2) on laminin-coated coverslips were incubated with the conditioned medium for 7 days, and, at that time, the number of GFP-positive surviving cells were counted as described below. Only transgenic $SOD1^{G93A}$ conditioned medium that generated the expected 50 ± 10 % motor neuron loss after 7 days incubation compared to transgenic $SOD1^{WT}$ or non-transgenic conditioned medium were used.

Handling of the samples for the RNA-Seq assay

At the specified timepoints, total mRNA samples from purified embryonic stem cell-derived motor neurons were extracted using TRI Reagent Solution (Ambion) and isolated with MagMAX-96 total RNA Isolation kit (Ambion). Total RNA samples were, then, quantified by Nanodrop (Thermo Scientific) and their RNA integrity was assessed using a 2100 Bioanalyzer (Agilent Technologies, Palo Alto, CA); only those RNAs with an integrity number >9 were used for the RNA-seq. Then, high quality total RNA samples were sent to the Columbia Genome Center, where sequencing libraries were prepared, 20 million raw 100 base pair Single End reads were sequenced on Illumina HiSeq2000 instruments, the reads were mapped on reference genomes and the normalized expression level of known genes and transcripts were estimated.

Sample size estimation for the *in vitro* studies and Master Regulator Analysis

6 biological replicates per timepoint and treatment were used based on the following argument: if the false positive rate was fixed at 0.01, then 10,000 permutations would be needed to estimate the nominal p-values for master regulator analysis. The number of combinations of *n* elements

in groups of *k* elements with reposition is $\binom{n+k-1}{k}$. Thus, by using 5 biological replicates, we cannot get enough combinations: $\binom{10+5-1}{5}$ = 2,002, but with 6 we d:o $\binom{12+6-1}{6}$ = 12,376. The variance of the RNA-seq data was stabilized by log transformation and gene expression signatures was obtained by Student's t-test and ANOVA. Gene expression signatures were obtained by Student's *t*-test and ANOVA. Expression data transformation and analysis were performed on the R-system platform.

Master Regulator Inference algorithm (MARINa)

MARINa was developed to identify transcriptional regulators (i.e. transcription factors) controlling a specific gene expression signature. It was used previously to identify the regulatory module controlling the mesenchymal phenotype in human high grade glioma (Carro et al., 2010), and to identify the transcription factors controlling the gene expression program for the differentiation of naïve human B-cells in the germinal center reaction (Lefebvre et al., 2010). A modified version of Gene Set Enrichment Analysis (GSEA) was used to compute the enrichment of the targets for each transcription factor (its regulon) on the susceptibility and commitment gene expression signatures. Transcription factor regulons (i.e. the set of target genes transcriptionally regulated by a transcription factor) were obtained from related, previously assembled transcriptional networks, which were constructed by reverse engineering of large gene expression datasets using ARACNe (Basso et al., 2005). Spearman correlation was used to infer whether a transcription factor activated or repressed an inferred target gene and this information was used in the modified GSEA to estimate the relative activity of each transcription factor in association with the gene expression signature; i.e. the differential activity of each transcription

factor was estimated in association with a given gene expression signature based on the enrichment of its regulon among genes belonging to the tails of the gene expression signature. Nominal p-values for differential enrichment/activity were computed by uniformly shuffling the samples 10,000 times. Transcription factors, whose activity was significantly associated with the commitment and susceptibility signatures, were prioritized according to the level of enrichment.

Nuclear/ cytoplasmic subcellular fractionation

Harvested cells were homogenized in buffer A (250 mM sucrose, 20mM Hepes, 10 mM KCl, 1.5 mM Mg Cl_2, 2 mM EDTA, pH 7.4) supplemented with a protease inhibitor cocktail (Complete mini, Roche Applied Science, Indianapolis, IN). For each preparation, an aliquot of cell homogenate was saved and the rest was centrifuged. The pellet (P1) was used for nuclear purification, whereas the supernatant (S1) was used for the cytosolic purification. To purify nuclei, P1 was re-homogenized in buffer B (2 M sucrose, 50 mM Tris-HCl, 5 mM $MgCl_2$, 1 mM DTT and 1 mM PMSF, pH 7.4) supplemented with the protease inhibitor cocktail and then centrifuged through a cushion of buffer B. The resulting pellet was enriched with nuclei and was designated as *nuclear fraction*. As S1, it was centrifuged. The resulting supernatant was further centrifuged. The supernatant of the latter centrifugation was designated as the *cytosolic fraction*. After each preparation and prior to using, the purities of the subcelluar fractions were confirmed by Western blot using the following antibodies: anti-Histone H3 (Cell Signaling) for nuclei and anti-GAPDH (Cell Signaling) for cytosol. These antibodies were also used to assure equivalent protein loading within a given subcellular fraction.

TransAM NF-κB binding assay

Using the TransAM NF-κB transcription factor assay kit (Active Motif, Carlsbad, California), 20 μg of nuclear extract was added per sample diluted with Complete Lysis Buffer per well in a 96-well cell culture plate with 30 μl Complete Binding Buffer provided with the kit. Then, the plate was incubated for 1 hour at room temperature with mild agitation, followed by three washes with 200 μl of 1X Wash Buffer. 100 μl of diluted NF-κB antibody was added (1:1000) to each well being used in the plate and the plate was incubated again for 1 hour at room temperature without agitation, followed by three washes with 200 μl of 1X Wash Buffer. This step was repeated this time with the 100 μl HRP-conjugated antibody (1:1000). Finally, 100 μl Developing Solution was added to the wells being used. The plate was incubated for 1 minute away from the light and 100 μl Stop Solution was added, where the blue color turned yellow depending on the binding activity of the transcription factor. This activity was read using a spectrophotometer at 450 nm after 5 minutes. Every sample had three replicates and all values were expressed as mean ± s.e.m.

Western blots of total and phosphorylated proteins

After exposure to astrocyte-conditioned medium or infection with viral vector, motor neurons were harvested in lysis buffer containing sodium orthovanadate and sodium fluoride to avoid dephosphorylation. The following primary antibodies were used: rabbit anti-phosphorylated NF-κB p65 antibody (Cell Signaling) anti-NF-κB p65 antibody (Cell Signaling), anti-GAPDH antibody (Cell Signaling), anti-Histone H3 (Cell Signaling), anti-phosphotylated IκB (Cell Signaling), anti-IκB (Cell Signaling), and mouse anti-β-actin (Sigma). The concentration used

for all the antibodies was 1:1000, except for β-actin, for which the concentration was 1:20,000. Western blots using antibodies raised against the cytosolic and nuclear markers cited above were used as loading controls. All bands were quantified by Odyssey Infrared Imaging system using IRDye dye-labeled secondary antibodies (LI-COR). Results were expressed as ratios of arbitrary fluorescence units for the protein of interest over arbitrary fluorescence units for loading controls or as ratios of phosphorylated protein of interest over total protein of interest.

Pharmacological treatments

Wedelolactone (Calbiochem) was dissolved in DMSO and added to motor neurons, to final concentrations ranging from 50 nM –5 μM, 1 day after addition of astrocyte-conditioned medium to motor neurons. Fas ligand (Sigma) and domoic acid (Sigma) were added to motor neurons at concentrations 10 ng/ml and 1 μM, respectively, after five days *in vitro* of being in fresh medium. Cell survival was evaluated at 7 days *in vitro* by counting $eGFP^{+}$ neurons as described below.

Adeno-associated viral vector titration and infection

The adeno-associated viral vectors expressing GFP and GFP + super repressive IκB were obtained from Dr. David Park's group in University of Ottawa, Canada. Motor neurons were infected with GFP-expressing viral vectors one day after being plated, at concentrations ranging from 25-250 μM and their titration was tested using the Adenovirus Titration Kit (Clontech) five days after infection with the viral vectors. Similarly, for Western blot and cell counting, motor neurons were infected with viral vectors at concentrations ranging from 25-100 μM one day after

astrocyte-conditioned medium addition and their survival was assessed or protein were extracted six and five days after the infection, respectively.

Statistics for cell counting and Western blot

Each experiment was repeated at least 3-5 times. Results for the cell counting were the average of 3-6 coverslips. Each coverslip was counted in its entirety at x100 under fluorescent examination. All values were expressed as mean ± s.e.m unless stated otherwise. Differences between means were analyzed using a two-tailed Student's t test. Differences among means were analyzed using a two-way ANOVA with the different genotypes and times after exposure to the conditioned medium as the independent factors. When ANOVA showed significant differences, pair-wise comparisons among means were tested by Newman-Keuls post-hoc testing. All data sets were tested for normality and equality of variance and, when either or both criteria were violated, the appropriate nonparametric test was used. In all analyses, the null hypothesis was rejected at the 0.05 level. All statistical analyses were performed using SigmaStat or R.

Chapter 7: References

1. Aebischer, J., Cassina, P., Otsmane, B., Moumen, A., Seilhean, D., Meininger, V., Barbeito, L., Pettmann, B., and Raoul, C. (2011). IFNgamma triggers a LIGHT-dependent selective death of motoneurons contributing to the non-cell-autonomous effects of mutant SOD1. Cell Death Differ *18*, 754-768.

2. Aebischer, J., Moumen, A., Sazdovitch, V., Seilhean, D., Meininger, V., and Raoul, C. (2012). Elevated levels of IFNgamma and LIGHT in the spinal cord of patients with sporadic amyotrophic lateral sclerosis. Eur J Neurol *19*, 752-759, e745-756.

3. Alexander, G.M., Deitch, J.S., Seeburger, J.L., Del, V.L., and Heiman-Patterson, T.D. (2000). Elevated cortical extracellular fluid glutamate in transgenic mice expressing human mutant (G93A) Cu/Zn superoxide dismutase. J Neurochem *74*, 1666-1673.

4. Aleyasin, H., Cregan, S.P., Iyirhiaro, G., O'Hare, M.J., Callaghan, S.M., Slack, R.S., and Park, D.S. (2004). Nuclear factor-(kappa)B modulates the p53 response in neurons exposed to DNA damage. J Neurosci *24*, 2963-2973.

5. Allison, D.B., Cui, X., Page, G.P., and Sabripour, M. (2006). Microarray data analysis: from disarray to consolidation and consensus. NatRevGenet *7*, 55-65.

6. Anders, S. (2010). Analysin RNA-Seq data with the "DESeq" package (Heidelberg, Germany).

7. Andersen, P.M., and Al-Chalabi, A. (2011). Clinical genetics of amyotrophic lateral sclerosis: what do we really know? Nat Rev Neurol *7*, 603-615.

8. Arai, T., Hasegawa, M., Akiyama, H., Ikeda, K., Nonaka, T., Mori, H., Mann, D., Tsuchiya, K., Yoshida, M., Hashizume, Y., *et al.* (2006). TDP-43 is a component of ubiquitin-positive tau-negative inclusions in frontotemporal lobar degeneration and amyotrophic lateral sclerosis. BiochemBiophysResCommun *351*, 602-611.

9. Barbeito, L.H., Pehar, M., Cassina, P., Vargas, M.R., Peluffo, H., Viera, L., Estevez, A.G., and Beckman, J.S. (2004). A role for astrocytes in motor neuron loss in amyotrophic lateral sclerosis. Brain ResBrain ResRev *47*, 263-274.

10. Basak, S., and Hoffmann, A. (2008). Crosstalk via the NF-kappaB signaling system. Cytokine Growth Factor Rev *19*, 187-197.

11. Basak, S., Kim, H., Kearns, J.D., Tergaonkar, V., O'Dea, E., Werner, S.L., Benedict, C.A., Ware, C.F., Ghosh, G., Verma, I.M., *et al.* (2007). A fourth IkappaB protein within the NF-kappaB signaling module. Cell *128*, 369-381.

12. Basso, K., Margolin, A.A., Stolovitzky, G., Klein, U., la-Favera, R., and Califano, A. (2005). Reverse engineering of regulatory networks in human B cells. Nat Genet *37*, 382-390.

13. Bhakar, A.L., Tannis, L.L., Zeindler, C., Russo, M.P., Jobin, C., Park, D.S., MacPherson, S., and Barker, P.A. (2002). Constitutive nuclear factor-kappa B activity is required for central neuron survival. The Journal of neuroscience : the official journal of the Society for Neuroscience *22*, 8466-8475.

14. Boillee, S., Yamanaka, K., Lobsiger, C.S., Copeland, N.G., Jenkins, N.A., Kassiotis, G., Kollias, G., and Cleveland, D.W. (2006). Onset and Progression in Inherited ALS Determined by Motor Neurons and Microglia. Science *312*, 1389-1392.

15. Boissiere, F., Hunot, S., Faucheux, B., Duyckaerts, C., Hauw, J.J., Agid, Y., and Hirsch, E.C. (1997). Nuclear translocation of NF-kappaB in cholinergic neurons of patients with Alzheimer's disease. Neuroreport *8*, 2849-2852.

16. Bosco, D.A., Lemay, N., Ko, H.K., Zhou, H., Burke, C., Kwiatkowski, T.J., Jr., Sapp, P., McKenna-Yasek, D., Brown, R.H., Jr., and Hayward, L.J. (2010). Mutant FUS proteins that cause amyotrophic lateral sclerosis incorporate into stress granules. Human Molecular Genetics *19*, 4160-4175.

17. Bowling, A.C., Schulz, J.B., Brown, R.H., Jr., and Beal, M.F. (1993). Superoxide dismutase activity, oxidative damage, and mitochondrial energy metabolism in familial and sporadic amyotrophic lateral sclerosis. JNeurochem *61*, 2322-2325.

18. Browne, S.E., Yang, L., DiMauro, J.P., Fuller, S.W., Licata, S.C., and Beal, M.F. (2006). Bioenergetic abnormalities in discrete cerebral motor pathways presage spinal cord pathology in the G93A SOD1 mouse model of ALS. Neurobiology of disease *22*, 599-610.

19. Bruening, W., Roy, J., Giasson, B., Figlewicz, D.A., Mushynski, W.E., and Durham, H.D. (1999). Up-regulation of protein chaperones preserves viability of cells expressing toxic Cu/Zn-superoxide dismutase mutants associated with amyotrophic lateral sclerosis. JNeurochem *72*, 693-699.

20. Bruijn, L.I., Becher, M.W., Lee, M.K., Anderson, K.L., Jenkins, N.A., Copeland, N.G., Sisodia, S., Rothstein, J.D., Borchelt, D.R., Price, D.L., *et al.* (1997). ALS-linked SOD1 mutant G85R mediated damage to astrocytes and promotes rapidly progressive disease with SOD1-containing inclusions. Neuron *18*, 327-338.

21. Bruijn, L.I., Houseweart, M.K., Kato, S., Anderson, K.L., Anderson, S.D., Ohama, E., Reaume, A.G., Scott, R.W., and Cleveland, D.W. (1998). Aggregation and motor neuron toxicity of an ALS-linked SOD1 mutant independent from wild-type SOD1. Science *281*, 1851-1854.

22. Burke, R.E., Levine, D.N., Tsairis, P., and Zajac, F.E., 3rd (1973). Physiological types and histochemical profiles in motor units of the cat gastrocnemius. The Journal of physiology *234*, 723-748.

23. Cahoy, J.D., Emery, B., Kaushal, A., Foo, L.C., Zamanian, J.L., Christopherson, K.S., Xing, Y., Lubischer, J.L., Krieg, P.A., Krupenko, S.A., *et al.* (2008). A transcriptome database for astrocytes, neurons, and oligodendrocytes: a new resource for understanding brain development and function. JNeurosci *28*, 264-278.

24. Carro, M.S., Lim, W.K., Alvarez, M.J., Bollo, R.J., Zhao, X., Snyder, E.Y., Sulman, E.P., Anne, S.L., Doetsch, F., Colman, H., *et al.* (2010). The transcriptional network for mesenchymal transformation of brain tumours. Nature *463*, 318-325.

25. Cassina, P., Cassina, A., Pehar, M., Castellanos, R., Gandelman, M., de Leon, A., Robinson, K.M., Mason, R.P., Beckman, J.S., Barbeito, L., *et al.* (2008). Mitochondrial dysfunction in S0D1(G93A)-bearing astrocytes promotes motor neuron degeneration: Prevention by mitochondrial-targeted antioxidants. J Neurosci *28*, 4115-4122.

26. Cassina, P., Pehar, M., Vargas, M.R., Castellanos, R., Barbeito, A.G., Estevez, A.G., Thompson, J.A., Beckman, J.S., and Barbeito, L. (2005). Astrocyte activation by fibroblast growth factor-1 and motor neuron apoptosis: implications for amyotrophic lateral sclerosis. J Neurochem *93*, 38-46.

27. Chang-Hong, R., Wada, M., Koyama, S., Kimura, H., Arawaka, S., Kawanami, T., Kurita, K., Kadoya, T., Aoki, M., Itoyama, Y., *et al.* (2005). Neuroprotective effect of oxidized galectin-1 in a transgenic mouse model of amyotrophic lateral sclerosis. Experimental Neurology *194*, 203-211.

28. Chen, A., and Davis, B.H. (1999). UV irradiation activates JNK and increases alphaI(I) collagen gene expression in rat hepatic stellate cells. J Biol Chem *274*, 158-164.

29. Chen, Y.Z., Bennett, C.L., Huynh, H.M., Blair, I.P., Puls, I., Irobi, J., Dierick, I., Abel, A., Kennerson, M.L., Rabin, B.A., *et al.* (2004). DNA/RNA helicase gene mutations in a form of juvenile amyotrophic lateral sclerosis (ALS4). AmJHumGenet *74*, 1128-1135.

30. Chiarugi, A. (2002). Characterization of the molecular events following impairment of NF-kappaB-driven transcription in neurons. Brain Res Mol Brain Res *109*, 179-188.

31. Chow, C.Y., Landers, J.E., Bergren, S.K., Sapp, P.C., Grant, A.E., Jones, J.M., Everett, L., Lenk, G.M., McKenna-Yasek, D.M., Weisman, L.S., *et al.* (2009). Deleterious variants of FIG4, a phosphoinositide phosphatase, in patients with ALS. American Journal of Human Genetics *84*, 85-88.

32. Clement, A.M., Nguyen, M.D., Roberts, E.A., Garcia, M.L., Boillee, S., Rule, M., McMahon, A.P., Doucette, W., Siwek, D., Ferrante, R.J., *et al.* (2003). Wild-Type Nonneuronal Cells Extend Survival of SOD1 Mutant Motor Neurons in ALS Mice. Science *302*, 113-117.

33. Cleveland, D.W., and Rothstein, J.D. (2001). From Charcot to Lou Gehrig: deciphering selective motor neuron death in ALS. NatRevNeurosci *2*, 806-819.

34. Collister, K.A., and Albensi, B.C. (2005). Potential therapeutic targets in the NF-kappaB pathway for Alzheimer's disease. Drug News Perspect *18*, 623-629.

35. Consortium, T.G.O. (2008). The Gene Ontology project in 2008. Nucleic Acids Res *36*, D440-444.

36. Corbo, M., and Hays, A.P. (1992). Peripherin and neurofilament protein coexist in spinal spheroids of motor neuron disease. JNeuropatholExpNeurol *51*, 531-537.

37. Cox, L.E., Ferraiuolo, L., Goodall, E.F., Heath, P.R., Higginbottom, A., Mortiboys, H., Hollinger, H.C., Hartley, J.A., Brockington, A., Burness, C.E., *et al.* (2010). Mutations in CHMP2B in lower motor neuron predominant amyotrophic lateral sclerosis (ALS). PloS one *5*, e9872.

38. Crosio, C., Valle, C., Casciati, A., Iaccarino, C., and Carri, M.T. (2011). Astroglial inhibition of NF-kappaB does not ameliorate disease onset and progression in a mouse model for amyotrophic lateral sclerosis (ALS). PloS one *6*, e17187.

39. Cudkowicz, M.E., McKenna-Yasek, D., Sapp, P.E., Chin, W., Geller, B., Hayden, D.L., Schoenfeld, D.A., Hosler, B.A., Horvitz, H.R., and Brown, R.H. (1997). Epidemiology of mutations in superoxide dismutase in amyotrophic lateral sclerosis. Annals of Neurology *41*, 210-221.

40. Custer, S.K., Neumann, M., Lu, H., Wright, A.C., and Taylor, J.P. (2010). Transgenic mice expressing mutant forms VCP/p97 recapitulate the full spectrum of IBMPFD including degeneration in muscle, brain and bone. Hum Mol Genet *19*, 1741-1755.

41. Dal Canto, M.C., and Gurney, M.E. (1995). Neuropathological changes in two lines of mice carrying a transgene for mutant human Cu,Zn SOD, and in mice overexpressing wild type human SOD: A model of familial amyotrophic lateral sclerosis (FALS). Brain Res *676*, 25-40.

42. Deb, A., Haque, S.J., Mogensen, T., Silverman, R.H., and Williams, B.R. (2001). RNA-dependent protein kinase PKR is required for activation of NF-kappa B by IFN-gamma in a STAT1-independent pathway. J Immunol *166*, 6170-6180.

43. DeJesus-Hernandez, M., Mackenzie, I.R., Boeve, B.F., Boxer, A.L., Baker, M., Rutherford, N.J., Nicholson, A.M., Finch, N.A., Flynn, H., Adamson, J., *et al.* (2011). Expanded GGGGCC hexanucleotide repeat in noncoding region of C9ORF72 causes chromosome 9p-linked FTD and ALS. Neuron *72*, 245-256.

44. Deng, H.X., Chen, W., Hong, S.T., Boycott, K.M., Gorrie, G.H., Siddique, N., Yang, Y., Fecto, F., Shi, Y., Zhai, H., *et al.* (2011). Mutations in UBQLN2 cause dominant X-linked juvenile and adult-onset ALS and ALS/dementia. Nature *477*, 211-215.

45. Deng, H.X., Shi, Y., Furukawa, Y., Zhai, H., Fu, R., Liu, E., Gorrie, G.H., Khan, M.S., Hung, W.Y., Bigio, E.H., *et al.* (2006). Conversion to the amyotrophic lateral sclerosis phenotype is associated with intermolecular linked insoluble aggregates of SOD1 in mitochondria. Proceedings of the National Academy of Sciences of the United States of America *103*, 7142-7147.

46. Deng, J., Miller, S.A., Wang, H.Y., Xia, W., Wen, Y., Zhou, B.P., Li, Y., Lin, S.Y., and Hung, M.C. (2002). beta-catenin interacts with and inhibits NF-kappa B in human colon and breast cancer. Cancer Cell *2*, 323-334.

47. Denis-Donini, S., Dellarole, A., Crociara, P., Francese, M.T., Bortolotto, V., Quadrato, G., Canonico, P.L., Orsetti, M., Ghi, P., Memo, M., *et al.* (2008). Impaired adult neurogenesis associated with short-term memory defects in NF-kappaB p50-deficient mice. The Journal of neuroscience : the official journal of the Society for Neuroscience *28*, 3911-3919.

48. Di Giorgio, F.P., Boulting, G.L., Bobrowicz, S., and Eggan, K.C. (2008). Human embryonic stem cell-derived motor neurons are sensitive to the toxic effect of glial cells carrying an ALS-causing mutation. Cell Stem Cell *3*, 637-648.

49. Di Giorgio, F.P., Carrasco, M.A., Siao, M.C., Maniatis, T., and Eggan, K. (2007). Non-cell autonomous effect of glia on motor neurons in an embryonic stem cell-based ALS model. NatNeurosci *10*, 608-614.

50. Durham, H.D., Roy, J., Dong, L., and Figlewicz, D.A. (1997). Aggregation of mutant Cu/Zn superoxide dismutase proteins in a culture model of ALS. JNeuropatholExpNeurol *56*, 523-530.

51. Ekblom, J., Jossan, S.S., Oreland, L., Walum, E., and Aquilonius, S.M. (1994). Reactive gliosis and monoamine oxidase B. Journal of neural transmission Supplementum *41*, 253-258.

52. Elden, A.C., Kim, H.J., Hart, M.P., Chen-Plotkin, A.S., Johnson, B.S., Fang, X., Armakola, M., Geser, F., Greene, R., Lu, M.M., *et al.* (2010). Ataxin-2 intermediate-length polyglutamine expansions are associated with increased risk for ALS. Nature *466*, 1069-1075.

53. Estevez, A.G., Crow, J.P., Sampson, J.B., Reiter, C., Zhuang, Y., Richardson, G.J., Tarpey, M.M., Barbeito, L., and Beckman, J.S. (1999). Induction of nitric oxide-dependent apoptosis in motor neurons by zinc-deficient superoxide dismutase. Science *286*, 2498-2500.

54. Facchinetti, F., Sasaki, M., Cutting, F.B., Zhai, P., MacDonald, J.E., Reif, D., Beal, M.F., Huang, P.L., Dawson, T.M., Gurney, M.E., *et al.* (1999). Lack of involvement of neuronal nitric oxide synthase in the pathogenesis of a transgenic mouse model of familial amyotrophic lateral sclerosis. Neuroscience *90*, 1483-1492.

55. Ferraiuolo, L., Heath, P.R., Holden, H., Kasher, P., Kirby, J., and Shaw, P.J. (2007). Microarray analysis of the cellular pathways involved in the adaptation to and progression of motor neuron injury in the SOD1 G93A mouse model of familial ALS. J Neurosci *27*, 9201-9219.

56. Ferraiuolo, L., Higginbottom, A., Heath, P.R., Barber, S., Greenald, D., Kirby, J., and Shaw, P.J. (2011a). Dysregulation of astrocyte-motoneuron cross-talk in mutant superoxide dismutase 1-related amyotrophic lateral sclerosis. Brain : a journal of neurology *134*, 2627-2641.

57. Ferraiuolo, L., Kirby, J., Grierson, A.J., Sendtner, M., and Shaw, P.J. (2011b). Molecular pathways of motor neuron injury in amyotrophic lateral sclerosis. Nat Rev Neurol *7*, 616-630.

58. Ferrante, R.J., Browne, S.E., Shinobu, L.A., Bowling, A.C., Baik, M.J., MacGarvey, U., Kowall, N.W., Brown, R.H., Jr., and Beal, M.F. (1997). Evidence of increased oxidative damage in both sporadic and familial amyotrophic lateral sclerosis. Journal of Neurochemistry *69*, 2064-2074.

59. Ferreiro, D.U., and Komives, E.A. (2010). Molecular mechanisms of system control of NF-kappaB signaling by IkappaBalpha. Biochemistry *49*, 1560-1567.

60. Fischer, L.R., Culver, D.G., Tennant, P., Davis, A.A., Wang, M., Castellano-Sanchez, A., Khan, J., Polak, M.A., and Glass, J.D. (2004). Amyotrophic lateral sclerosis is a distal axonopathy: evidence in mice and man. ExpNeurol *185*, 232-240.

61. Forsberg, K., Jonsson, P.A., Andersen, P.M., Bergemalm, D., Graffmo, K.S., Hultdin, M., Jacobsson, J., Rosquist, R., Marklund, S.L., and Brannstrom, T. (2010). Novel antibodies reveal inclusions containing non-native SOD1 in sporadic ALS patients. PloS one *5*, e11552.

62. Frey, D., Schneider, C., Xu, L., Borg, J., Spooren, W., and Caroni, P. (2000). Early and selective loss of neuromuscular synapse subtypes with low sprouting competence in motoneuron diseases. J Neurosci *20*, 2534-2542.

63. Gonatas, N.K., Gonatas, J.O., and Stieber, A. (1998). The involvement of the Golgi apparatus in the pathogenesis of amyotrophic lateral sclerosis, Alzheimer's disease, and ricin intoxication. Histochem Cell Biol *109*, 591-600.

64. Goto, J.J., Zhu, H., Sanchez, R.J., Nersissian, A., Gralla, E.B., Valentine, J.S., and Cabelli, D.E. (2000). Loss of in vitro metal ion binding specificity in mutant copper-zinc superoxide dismutases associated with familial amyotrophic lateral sclerosis. The Journal of biological chemistry *275*, 1007-1014.

65. Gould, T.W., Buss, R.R., Vinsant, S., Prevette, D., Sun, W., Knudson, C.M., Milligan, C.E., and Oppenheim, R.W. (2006). Complete dissociation of motor neuron death from motor dysfunction by Bax deletion in a mouse model of ALS. JNeurosci *26*, 8774-8786.

66. Greenway, M.J., Andersen, P.M., Russ, C., Ennis, S., Cashman, S., Donaghy, C., Patterson, V., Swingler, R., Kieran, D., Prehn, J., *et al.* (2006). ANG mutations segregate with familial and 'sporadic' amyotrophic lateral sclerosis. Nature Genetics *38*, 411-413.

67. Guégan, C., and Przedborski, S. (2003). Programmed cell death in amyotrophic lateral sclerosis. JClinInvest *111*, 153-161.

68. Guégan, C., Vila, M., Rosoklija, G., Hays, A.P., and Przedborski, S. (2001). Recruitment of the mitochondrial-dependent apoptotic pathway in amyotrophic lateral sclerosis. JNeurosci *21*, 6569-6576.

69. Guo, H., Lai, L., Butchbach, M.E., Stockinger, M.P., Shan, X., Bishop, G.A., and Lin, C.L. (2003). Increased expression of the glial glutamate transporter EAAT2 modulates excitotoxicity and delays the onset but not the outcome of ALS in mice. Human Molecular Genetics *12*, 2519-2532.

70. Gurney, M.E., Pu, H., Chiu, A.Y., Dal Canto, M.C., Polchow, C.Y., Alexander, D.D., Caliendo, J., Hentati, A., Kwon, Y.W., Deng, H.-X., *et al.* (1994). Motor neuron degeneration in mice that express a human Cu, Zn superoxide dismutase mutation. Science *264*, 1772-1775.

71. Gutierrez, H., Hale, V.A., Dolcet, X., and Davies, A. (2005). NF-kappaB signalling regulates the growth of neural processes in the developing PNS and CNS. Development *132*, 1713-1726.

72. Hadano, S., Hand, C.K., Osuga, H., Yanagisawa, Y., Otomo, A., Devon, R.S., Miyamoto, N., Showguchi-Miyata, J., Okada, Y., Singaraja, R., *et al.* (2001). A gene encoding a putative GTPase regulator is mutated in familial amyotrophic lateral sclerosis 2. NatGenet *29*, 166-173.

73. Haidet-Phillips, A.M., Hester, M.E., Miranda, C.J., Meyer, K., Braun, L., Frakes, A., Song, S., Likhite, S., Murtha, M.J., Foust, K.D., *et al.* (2011). Astrocytes from familial and sporadic ALS patients are toxic to motor neurons. Nat Biotechnol *29*, 824-828.

74. Hall, E.D., Oostveen, J.A., and Gurney, M.E. (1998). Relationship of microglial and astrocytic activation to disease onset and progression in a transgenic model of familial ALS. Glia *23*, 249-256.

75. Halliwell, B., and Gutteridge, J.M. (1991). Free radicals in biology and medicine, 2 edn (Oxford: Clarendon Press).

76. Hamanoue, M., Middleton, G., Wyatt, S., Jaffray, E., Hay, R.T., and Davies, A.M. (1999). p75-mediated NF-kappaB activation enhances the survival response of developing sensory neurons to nerve growth factor. Molecular and cellular neurosciences *14*, 28-40.

77. Hand, C.K., and Rouleau, G.A. (2002). Familial amyotrophic lateral sclerosis. Muscle Nerve *25*, 135-159.

78. Hayden, M.S., and Ghosh, S. (2012). NF-kappaB, the first quarter-century: remarkable progress and outstanding questions. Genes Dev *26*, 203-234.

79. He, C.Z., and Hays, A.P. (2004). Expression of peripherin in ubiquinated inclusions of amyotrophic lateral sclerosis. JNeurolSci *217*, 47-54.

80. Hegedus, J., Putman, C.T., and Gordon, T. (2007). Time course of preferential motor unit loss in the SOD1 G93A mouse model of amyotrophic lateral sclerosis. NeurobiolDis *28*, 154-164.

81. Hirano, A. (1996). Neuropathology of ALS: an overview. Neurology *47*, S63-S66.

82. Hoffmann, A., Leung, T.H., and Baltimore, D. (2003). Genetic analysis of NF-kappaB/Rel transcription factors defines functional specificities. The EMBO journal *22*, 5530-5539.

83. Hosler, B.A., Siddique, T., Sapp, P.C., Sailor, W., Huang, M.C., Hossain, A., Daube, J.R., Nance, M., Fan, C., Kaplan, J., *et al.* (2000). Linkage of familial amyotrophic lateral sclerosis with frontotemporal dementia to chromosome 9q21-q22. JAMA : the journal of the American Medical Association *284*, 1664-1669.

84. Hutton, M., Lendon, C.L., Rizzu, P., Baker, M., Froelich, S., Houlden, H., Pickering-Brown, S., Chakraverty, S., Isaacs, A., Grover, A., *et al.* (1998). Association of missense and 5'-splice-site mutations in tau with the inherited dementia FTDP-17. Nature *393*, 702-705.

85. Ilieva, H., Polymenidou, M., and Cleveland, D.W. (2009). Non-cell autonomous toxicity in neurodegenerative disorders: ALS and beyond. J Cell Biol *187*, 761-772.

86. Ince, P.G., Highley, J.R., Kirby, J., Wharton, S.B., Takahashi, H., Strong, M.J., and Shaw, P.J. (2011). Molecular pathology and genetic advances in amyotrophic lateral sclerosis: an emerging molecular pathway and the significance of glial pathology. Acta Neuropathologica *122*, 657-671.

87. Israelson, A., Arbel, N., Da Cruz, S., Ilieva, H., Yamanaka, K., Shoshan-Barmatz, V., and Cleveland, D.W. (2010). Misfolded mutant SOD1 directly inhibits VDAC1 conductance in a mouse model of inherited ALS. Neuron *67*, 575-587.

88. Jessell, T.M. (2000). Neuronal specification in the spinal cord: inductive signals and transcriptional codes. Nat Rev Genet *1*.

89. Jiang, Y.M., Yamamoto, M., Kobayashi, Y., Yoshihara, T., Liang, Y., Terao, S., Takeuchi, H., Ishigaki, S., Katsuno, M., Adachi, H., *et al.* (2005a). Gene expression

profile of spinal motor neurons in sporadic amyotrophic lateral sclerosis. Annals of Neurology *57*, 236-251.

90. Jiang, Y.M., Yamamoto, M., Kobayashi, Y., Yoshihara, T., Liang, Y., Terao, S., Takeuchi, H., Ishigaki, S., Katsuno, M., Adachi, H., *et al.* (2005b). Gene expression profile of spinal motor neurons in sporadic amyotrophic lateral sclerosis. AnnNeurol *57*, 236-251.

91. Johnston, J.A., Dalton, M.J., Gurney, M.E., and Kopito, R.R. (2000). Formation of high molecular weight complexes of mutant Cu, Zn-superoxide dismutase in a mouse model for familial amyotrophic lateral sclerosis. ProcNatlAcadSciUSA *97*, 12571-12576.

92. Jonsson, P.A., Ernhill, K., Andersen, P.M., Bergemalm, D., Brannstrom, T., Gredal, O., Nilsson, P., and Marklund, S.L. (2004). Minute quantities of misfolded mutant superoxide dismutase-1 cause amyotrophic lateral sclerosis. Brain : a journal of neurology *127*, 73-88.

93. Jonsson, P.A., Graffmo, K.S., Andersen, P.M., Brannstrom, T., Lindberg, M., Oliveberg, M., and Marklund, S.L. (2006). Disulphide-reduced superoxide dismutase-1 in CNS of transgenic amyotrophic lateral sclerosis models. Brain : a journal of neurology *129*, 451-464.

94. Joshi-Tope G., G.M., Vastrik I., D'Eustachio P., Schmidt E., de Bono B., Gopinath G. R., Wu G. R., Matthews L., Lewis S., Birney E., Stein L. (2005). Reactome: a knowledgebase of biological pathways. Nucleic Acids Res *33*, D428-432.

95. Kaltschmidt, C., Kaltschmidt, B., and Baeuerle, P.A. (1993). Brain synapses contain inducible forms of the transcription factor NF-kappa B. Mech Dev *43*, 135-147.

96. Kaltschmidt, C., Kaltschmidt, B., and Baeuerle, P.A. (1995). Stimulation of ionotropic glutamate receptors activates transcription factor NF-kappa B in primary neurons. Proceedings of the National Academy of Sciences of the United States of America *92*, 9618-9622.

97. Kanehisa, M.G., S;Kawashima, S; Okuno, Y; Hattori, M (2004). The KEGG resource for deciphering the genome. Nucleic Acids Res *32*, D277-280.

98. Kato, S., Horiuchi, S., Liu, J., Cleveland, D.W., Shibata, N., Nakashima, K., Nagai, R., Hirano, A., Takikawa, M., Kato, M., *et al.* (2000). Advanced glycation endproduct-modified superoxide dismutase-1 (SOD1)-positive inclusions are common to familial amyotrophic lateral sclerosis patients with SOD1 gene mutations and transgenic mice expressing human SOD1 with a G85R mutation. Acta Neuropathologica *100*, 490-505.

99. Kawamata, T., Akiyama, H., Yamada, T., and McGeer, P.L. (1992). Immunologic reactions in amyotrophic lateral sclerosis brain and spinal cord tissue. Am J Pathol *140*, 691-707.

100. Kawashima, T., Kikuchi, H., Takita, M., Doh-ura, K., Ogomori, K., Oda, M., and Iwaki, T. (1998). Skein-like inclusions in the neostriatum from a case of amyotrophic lateral sclerosis with dementia. Acta Neuropathologica *96*, 541-545.

101. Kiaei, M., Kipiani, K., Chen, J., Calingasan, N.Y., and Beal, M.F. (2005). Peroxisome proliferator-activated receptor-gamma agonist extends survival in transgenic mouse model of amyotrophic lateral sclerosis. Experimental Neurology *191*, 331-336.

102. Kikuchi, H., Almer, G., Yamashita, S., Guegan, C., Nagai, M., Xu, Z., Sosunov, A.A., McKhann, G.M., and Przedborski, S. (2006). Spinal cord endoplasmic reticulum stress associated with a microsomal accumulation of mutant superoxide dismutase-1 in an ALS model. ProcNatl AcadSciUSA *103*, 6025-6030.

103. Kim, J., Kim, J., Kim, D.W., Ha, Y., Ihm, M.H., Kim, H., Song, K., and Lee, I. (2010). Wnt5a induces endothelial inflammation via beta-catenin-independent signaling. J Immunol *185*, 1274-1282.

104. Kirby, J. (2011).

105. Kirby, J., Halligan, E., Baptista, M.J., Allen, S., Heath, P.R., Holden, H., Barber, S.C., Loynes, C.A., Wood-Allum, C.A., Lunec, J., *et al.* (2005). Mutant SOD1 alters the motor neuronal transcriptome: implications for familial ALS. Brain : a journal of neurology *128*, 1686-1706.

106. Kobori, M., Yang, Z., Gong, D., Heissmeyer, V., Zhu, H., Jung, Y.K., Gakidis, M.A., Rao, A., Sekine, T., Ikegami, F., *et al.* (2004). Wedelolactone suppresses LPS-induced caspase-11 expression by directly inhibiting the IKK complex. Cell Death Differ *11*, 123-130.

107. Kostic, V., Jackson-Lewis, V., De Bilbao, F., Dubois-Dauphin, M., and Przedborski, S. (1997). Bcl-2: Prolonging life in a transgenic mouse model of familial amyotrophic lateral sclerosis. Science *277*, 559-562.

108. Koulich, E., Nguyen, T., Johnson, K., Giardina, C., and D'Mello, S. (2001). NF-kappaB is involved in the survival of cerebellar granule neurons: association of IkappaBbeta [correction of Ikappabeta] phosphorylation with cell survival. J Neurochem *76*, 1188-1198.

109. Kukigawa, K., Nankano, R. , Otaku, M., Takashi, I. (2000). Generation of Mutant SOD1-expressing Mice (Program for Societas Neurologica Japonica), pp. 200.

110. Kunst, C.B., Mezey, E., Brownstein, M.J., and Patterson, D. (1997). Mutations in SOD1 associated with amyotrophic lateral sclerosis cause novel protein interactions. NatGenet *15*, 91-94.

111. Kuo, J.J., Schonewille, M., Siddique, T., Schults, A.N., Fu, R., Bar, P.R., Anelli, R., Heckman, C.J., and Kroese, A.B. (2004). Hyperexcitability of cultured spinal motoneurons from presymptomatic ALS mice. JNeurophysiol *91*, 571-575.

112. Kusaka, H. (1999). [Neuropathology of the motor neuron disease--Bunina body]. Rinsho Shinkeigaku *39*, 65-66.

113. Kwiatkowski, T.J., Jr., Bosco, D.A., LeClerc, A.L., Tamrazian, E., Vanderburg, C.R., Russ, C., Davis, A., Gilchrist, J., Kasarskis, E.J., Munsat, T., *et al.* (2009). Mutations in the FUS/TLS gene on chromosome 16 cause familial amyotrophic lateral sclerosis. Science *323*, 1205-1208.

114. Landstrom, M. (2010). The TAK1-TRAF6 signalling pathway. Int J Biochem Cell Biol *42*, 585-589.

115. Lee, Y., Morrison, B.M., Li, Y., Lengacher, S., Farah, M.H., Hoffman, P.N., Liu, Y., Tsingalia, A., Jin, L., Zhang, P.W., *et al.* (2012). Oligodendroglia metabolically support axons and contribute to neurodegeneration. Nature *487*, 443-448.

116. Lefebvre, C., Rajbhandari, P., Alvarez, M.J., Bandaru, P., Lim, W.K., Sato, M., Wang, K., Sumazin, P., Kustagi, M., Bisikirska, B.C., *et al.* (2010). A human B-cell interactome identifies MYB and FOXM1 as master regulators of proliferation in germinal centers. MolSystBiol *6*, 377.

117. Leigh, P.N., Whitwell, H., Garofalo, O., Buller, J., Swash, M., Martin, J.E., Gallo, J.M., Weller, R.O., and Anderton, B.H. (1991). Ubiquitin-immunoreactive intraneuronal inclusions in amyotrophic lateral sclerosis. Morphology, distribution, and specificity. Brain : a journal of neurology *114 (Pt 2)*, 775-788.

118. Lepore, A.C., O'Donnell, J., Kim, A.S., Williams, T., Tuteja, A., Rao, M.S., Kelley, L.L., Campanelli, J.T., and Maragakis, N.J. (2011). Human glial-restricted progenitor transplantation into cervical spinal cord of the SOD1 mouse model of ALS. PloS one *6*, e25968.

119. Lepore, A.C., Rauck, B., Dejea, C., Pardo, A.C., Rao, M.S., Rothstein, J.D., and Maragakis, N.J. (2008). Focal transplantation-based astrocyte replacement is neuroprotective in a model of motor neuron disease. Nature Neurosci *11*, 1294-1301.

120. Lezoualc'h, F., Sagara, Y., Holsboer, F., and Behl, C. (1998). High constitutive NF-kappaB activity mediates resistance to oxidative stress in neuronal cells. The Journal of neuroscience : the official journal of the Society for Neuroscience *18*, 3224-3232.

121. Li, J., Johnson, D., Calkins, M., Wright, L., Svendsen, C., and Johnson, J. (2005). Stabilization of Nrf2 by tBHQ confers protection against oxidative stress-induced cell death in human neural stem cells. Toxicol Sci *83*, 313-328.

122. Lino, M.M., Schneider, C., and Caroni, P. (2002). Accumulation of SOD1 mutants in postnatal motoneurons does not cause motoneuron pathology or motoneuron disease. JNeurosci *22*, 4825-4832.

123. Liu, J., Lillo, C., Jonsson, P.A., Vande Velde, C., Ward, C.M., Miller, T.M., Subramaniam, J.R., Rothstein, J.D., Marklund, S., Andersen, P.M., *et al.* (2004). Toxicity of familial ALS-linked SOD1 mutants from selective recruitment to spinal mitochondria. Neuron *43*, 5-17.

124. Lobsiger, C.S., Boillee, S., and Cleveland, D.W. (2007). Toxicity from different SOD1 mutants dysregulates the complement system and the neuronal regenerative response in ALS motor neurons. ProcNatlAcadSciUSA *104*, 7319-7326.

125. Locatelli, F., Corti, S., Papadimitriou, D., Fortunato, F., Del Bo, R., Donadoni, C., Nizzardo, M., Nardini, M., Salani, S., Ghezzi, S., *et al.* (2007). Fas small interfering RNA reduces motoneuron death in amyotrophic lateral sclerosis mice. Annals of Neurology *62*, 81-92.

126. Longo, V.D., Gralla, E.B., and Valentine, J.S. (1996). Superoxide dismutase activity is essential for stationary phase survival in Saccharomyces cerevisiae. Mitochondrial production of toxic oxygen species in vivo. The Journal of biological chemistry *271*, 12275-12280.

127. Luty, A.A., Kwok, J.B., Dobson-Stone, C., Loy, C.T., Coupland, K.G., Karlstrom, H., Sobow, T., Tchorzewska, J., Maruszak, A., Barcikowska, M., *et al.* (2010). Sigma nonopioid intracellular receptor 1 mutations cause frontotemporal lobar degeneration-motor neuron disease. Annals of Neurology *68*, 639-649.

128. Maggirwar, S.B., Sarmiere, P.D., Dewhurst, S., and Freeman, R.S. (1998). Nerve growth factor-dependent activation of NF-kappaB contributes to survival of sympathetic neurons. The Journal of neuroscience : the official journal of the Society for Neuroscience *18*, 10356-10365.

129. Magne, N., Toillon, R.A., Bottero, V., Didelot, C., Houtte, P.V., Gerard, J.P., and Peyron, J.F. (2006). NF-kappaB modulation and ionizing radiation: mechanisms and future directions for cancer treatment. Cancer Lett *231*, 158-168.

130. Magrane, J., Hervias, I., Henning, M.S., Damiano, M., Kawamata, H., and Manfredi, G. (2009). Mutant SOD1 in neuronal mitochondria causes toxicity and mitochondrial dynamics abnormalities. HumMolGenet *18*, 4552-4564.

131. Magrane, J., Sahawneh, M.A., Przedborski, S., Estevez, A.G., and Manfredi, G. (2012). Mitochondrial dynamics and bioenergetic dysfunction is associated with synaptic alterations in mutant SOD1 motor neurons. The Journal of neuroscience : the official journal of the Society for Neuroscience *32*, 229-242.

132. Marcora, E., and Kennedy, M.B. (2010). The Huntington's disease mutation impairs Huntingtin's role in the transport of NF-kappaB from the synapse to the nucleus. Hum Mol Genet *19*, 4373-4384.

133. Margolin, A.A., Nemenman, I., Basso, K., Wiggins, C., Stolovitzky, G., Dalla Favera, R., and Califano, A. (2006a). ARACNE: an algorithm for the reconstruction of gene regulatory networks in a mammalian cellular context. BMC Bioinformatics *7 Suppl 1*, S7.

134. Margolin, A.A., Wang, K., Lim, W.K., Kustagi, M., Nemenman, I., and Califano, A. (2006b). Reverse engineering cellular networks. Nat Protoc *1*, 662-671.

135. Marini, A.M., Jiang, X., Wu, X., Pan, H., Guo, Z., Mattson, M.P., Blondeau, N., Novelli, A., and Lipsky, R.H. (2007). Preconditioning and neurotrophins: a model for brain adaptation to seizures, ischemia and other stressful stimuli. Amino Acids *32*, 299-304.

136. Maruyama, H., Morino, H., Ito, H., Izumi, Y., Kato, H., Watanabe, Y., Kinoshita, Y., Kamada, M., Nodera, H., Suzuki, H., *et al.* (2010). Mutations of optineurin in amyotrophic lateral sclerosis. Nature *465*, 223-226.

137. Masu, K., Beppu, T., Fujiwara, S., Kizawa, H., Kashimura, H., Kurose, A., Ogasawara, K., and Sasaki, M. (2009). Proton magnetic resonance spectroscopy and diffusion-weighted imaging of tumefactive demyelinating plaque. Neurol Med Chir (Tokyo) *49*, 430-433.

138. Matsumoto, S., Goto, S., Kusaka, H., Imai, T., Murakami, N., Hashizume, Y., Okazaki, H., and Hirano, A. (1993). Ubiquitin-positive inclusion in anterior horn cells in subgroups of motor neuron diseases: a comparative study of adult-onset amyotrophic lateral sclerosis, juvenile amyotrophic lateral sclerosis and Werdnig-Hoffmann disease. Journal of the Neurological Sciences *115*, 208-213.

139. Mattiazzi, M., D'Aurelio, M., Gajewski, C.D., Martushova, K., Kiaei, M., Beal, M.F., and Manfredi, G. (2002). Mutated human SOD1 causes dysfunction of oxidative phosphorylation in mitochondria of transgenic mice. JBiolChem *277*, 29626-29633.

140. Mattson, M.P., and Guo, Q. (1997). Cell and molecular neurobiology of presenilins: a role for the endoplasmic reticulum in the pathogenesis of Alzheimer's disease? Journal of Neuroscience Research *50*, 505-513.

141. Mattson, M.P., and Meffert, M.K. (2006). Roles for NF-kappaB in nerve cell survival, plasticity, and disease. Cell Death Differ *13*, 852-860.

142. Maxwell, M.M., Pasinelli, P., Kazantsev, A.G., and Brown, R.H., Jr. (2004). RNA interference-mediated silencing of mutant superoxide dismutase rescues cyclosporin A-induced death in cultured neuroblastoma cells. ProcNatlAcadSciUSA *101*, 3178-3183.

143. Memet, S. (2006). NF-kappaB functions in the nervous system: from development to disease. Biochem Pharmacol *72*, 1180-1195.

144. Meyer, T., Fromm, A., Munch, C., Schwalenstocker, B., Fray, A.E., Ince, P.G., Stamm, S., Gron, G., Ludolph, A.C., and Shaw, P.J. (1999). The RNA of the glutamate transporter EAAT2 is variably spliced in amyotrophic lateral sclerosis and normal individuals. J Neurol Sci *170*, 45-50.

145. Middleton, G., Hamanoue, M., Enokido, Y., Wyatt, S., Pennica, D., Jaffray, E., Hay, R.T., and Davies, A.M. (2000). Cytokine-induced nuclear factor kappa B activation promotes the survival of developing neurons. The Journal of cell biology *148*, 325-332.

146. Miles, G.B., Yohn, D.C., Wichterle, H., Jessell, T.M., Rafuse, V.F., and Brownstone, R.M. (2004). Functional properties of motoneurons derived from mouse embryonic stem cells. JNeurosci *24*, 7848-7858.

147. Mizutani, T., Sakamaki, S., Tsuchiya, N., Kamei, S., Kohzu, H., Horiuchi, R., Ida, M., Shiozawa, R., and Takasu, T. (1992). Amyotrophic lateral sclerosis with ophtalmoplegia and multisystem degeneration in patiens on long-term use of respirators. Acta Neuropathol(Berl) *84*, 372-377.

148. Moreira, M.C., Klur, S., Watanabe, M., Nemeth, A.H., Le Ber, I., Moniz, J.C., Tranchant, C., Aubourg, P., Tazir, M., Schols, L., *et al.* (2004). Senataxin, the ortholog of a yeast RNA helicase, is mutant in ataxia-ocular apraxia 2. Nature Genetics *36*, 225-227.

149. Morris, H.R., Waite, A.J., Williams, N.M., Neal, J.W., and Blake, D.J. (2012). Recent advances in the genetics of the ALS-FTLD complex. Curr Neurol Neurosci Rep *12*, 243-250.

150. Mortazavi, A., Williams, B.A., McCue, K., Schaeffer, L., and Wold, B. (2008). Mapping and quantifying mammalian transcriptomes by RNA-Seq. Nature methods *5*, 621-628.

151. Mourelatos, Z., Gonatas, N.K., Stieber, A., Gurney, M.E., and Dal Canto, M.C. (1996). The Golgi apparatus of spinal cord motor neurons in transgenic mice expressing mutant Cu,Zn superoxide dismutase becomes fragmented in early, preclinical stages of the disease. ProcNatlAcadSciUSA *93*, 5472-5477.

152. Mu, X., He, J., Anderson, D.W., Trojanowski, J.Q., and Springer, J.E. (1996). Altered expression of bcl-2 and bax mRNA in amyotrophic lateral sclerosis spinal cord motor neurons. AnnNeurol *40*, 379-386.

153. Murayama, S., Inoue, K., Kawakami, H., Bouldin, T.W., and Suzuki, K. (1991). A unique pattern of astrocytosis in the primary motor area in amyotrophic lateral sclerosis. Acta Neuropathologica *82*, 456-461.

154. Nagai, M., Re, D.B., Nagata, T., Chalazonitis, A., Jessell, T.M., Wichterle, H., and Przedborski, S. (2007). Astrocytes expressing ALS-linked mutated SOD1 release factors selectively toxic to motor neurons. NatNeurosci *10*, 615-622.

155. Nguyen, H., Ramana, C.V., Bayes, J., and Stark, G.R. (2001). Roles of phosphatidylinositol 3-kinase in interferon-gamma-dependent phosphorylation of STAT1 on serine 727 and activation of gene expression. J Biol Chem *276*, 33361-33368.

156. Nickols, J.C., Valentine, W., Kanwal, S., and Carter, B.D. (2003). Activation of the transcription factor NF-kappaB in Schwann cells is required for peripheral myelin formation. Nature neuroscience *6*, 161-167.

157. Nishimura, A.L., Mitne-Neto, M., Silva, H.C., Richieri-Costa, A., Middleton, S., Cascio, D., Kok, F., Oliveira, J.R., Gillingwater, T., Webb, J., *et al.* (2004). A mutation in the vesicle-trafficking protein VAPB causes late-onset spinal muscular atrophy and amyotrophic lateral sclerosis. American Journal of Human Genetics *75*, 822-831.

158. Nishimura, A.L., Zupunski, V., Troakes, C., Kathe, C., Fratta, P., Howell, M., Gallo, J.M., Hortobagyi, T., Shaw, C.E., and Rogelj, B. (2010). Nuclear import impairment causes cytoplasmic trans-activation response DNA-binding protein accumulation and is associated with frontotemporal lobar degeneration. Brain : a journal of neurology *133*, 1763-1771.

159. Okamoto, K., Hirai, S., Amari, M., Watanabe, M., and Sakurai, A. (1993). Bunina bodies in amyotrophic lateral sclerosis immunostained with rabbit anti-cystatin C serum. Neuroscience Letters *162*, 125-128.

160. Okamoto, K., Hirai, S., Shoji, M., Senoh, Y., and Yamazaki, T. (1990). Axonal swellings in the corticospinal tracts in amyotrophic lateral sclerosis. Acta Neuropathol(Berl) *80*, 222-226.

161. Orlacchio, A., Babalini, C., Borreca, A., Patrono, C., Massa, R., Basaran, S., Munhoz, R.P., Rogaeva, E.A., St George-Hyslop, P.H., Bernardi, G., *et al.* (2010). SPATACSIN mutations cause autosomal recessive juvenile amyotrophic lateral sclerosis. Brain : a journal of neurology *133*, 591-598.

162. Ozdinler, P.H., Benn, S., Yamamoto, T.H., Guzel, M., Brown, R.H., Jr., and Macklis, J.D. (2011). Corticospinal motor neurons and related subcerebral projection neurons undergo early and specific neurodegeneration in hSOD1G(9)(3)A transgenic ALS mice. The Journal of neuroscience : the official journal of the Society for Neuroscience *31*, 4166-4177.

163. Ozsolak, F., and Milos, P.M. (2011). RNA sequencing: advances, challenges and opportunities. Nature reviews Genetics *12*, 87-98.

164. Papadeas, S.T., Kraig, S.E., O'Banion, C., Lepore, A.C., and Maragakis, N.J. (2011). Astrocytes carrying the superoxide dismutase 1 (SOD1G93A) mutation induce

wild-type motor neuron degeneration in vivo. Proc Natl Acad Sci U S A *108*, 17803-17808.

165. Pardo, A.C., Wong, V., Benson, L.M., Dykes, M., Tanaka, K., Rothstein, J.D., and Maragakis, N.J. (2006). Loss of the astrocyte glutamate transporter GLT1 modifies disease in SOD1(G93A) mice. ExpNeurol *201*, 120-130.

166. Pasinelli, P., Belford, M.E., Lennon, N., Bacskai, B.J., Hyman, B.T., Trotti, D., and Brown, R.H., Jr. (2004). Amyotrophic lateral sclerosis-associated SOD1 mutant proteins bind and aggregate with Bcl-2 in spinal cord mitochondria. Neuron *43*, 19-30.

167. Pasinelli, P., Borchelt, D.R., Houseweart, M.K., Cleveland, D.W., and Brown, R.H., Jr (1998). Caspase-1 is activated in neural cells and tissue with amyotrophic lateral sclerosis-associated mutations in copper-zinc superoxide dismutase. ProcNatlAcadSciUSA *95*, 15763-15768.

168. Pasinelli, P., and Brown, R.H. (2006). Molecular biology of amyotrophic lateral sclerosis: insights from genetics. NatRevNeurosci *7*, 710-723.

169. Peljto, M., Dasen, J.S., Mazzoni, E.O., Jessell, T.M., and Wichterle, H. (2010). Functional diversity of ESC-derived motor neuron subtypes revealed through intraspinal transplantation. Cell Stem Cell *7*, 355-366.

170. Peterson, A., and Seed, B. (1987). Monoclonal antibody and ligand binding sites of the T cell erythrocyte receptor (CD2). Nature *329*, 842-846.

171. Phillips, H.S., Kharbanda, S., Chen, R., Forrest, W.F., Soriano, R.H., Wu, T.D., Misra, A., Nigro, J.M., Colman, H., Soroceanu, L., *et al.* (2006). Molecular subclasses of high-grade glioma predict prognosis, delineate a pattern of disease progression, and resemble stages in neurogenesis. Cancer Cell *9*, 157-173.

172. Pizzi, M., and Spano, P. (2006). Distinct roles of diverse nuclear factor-kappaB complexes in neuropathological mechanisms. Eur J Pharmacol *545*, 22-28.

173. Plaitakis, A., and Caroscio, J.T. (1987). Abnormal glutamate metabolism in amyotrophic lateral sclerosis. AnnNeurol *22*, 575-579.

174. Przedborski, S., Khan, U., Kostic, V., Carlson, E., Epstein, C.J., and Sulzer, D. (1996). Increased superoxide dismutase activity improves survival of cultured postnatal midbrain neurons. JNeurochem *67*, 1383-1392.

175. Przedborski, S., Mitsumoto, H., and Rowland, L.P. (2003). Recent advances in amyotrophic lateral sclerosis research. CurrNeurolNeurosciRep *3*, 70-77.

176. Pun, S., Santos, A.F., Saxena, S., Xu, L., and Caroni, P. (2006). Selective vulnerability and pruning of phasic motoneuron axons in motoneuron disease alleviated by CNTF. NatNeurosci *9*, 408-419.

177. Pyo, J.S., Ko, Y.S., Kim, W.H., Kim, M., Lee, K.W., Nam, S.Y., Chung, H.Y., Cho, S.J., Baik, T.K., and Lee, B.L. (2010). Impairment of nuclear factor-kappaB activation increased glutamate excitotoxicity in a motoneuron-neuroblastoma hybrid cell line expressing mutant (G93A) Cu/Zn-superoxide dismutase. Journal of Neuroscience Research *88*, 2494-2503.

178. Rabin, S.J., Kim, J.M., Baughn, M., Libby, R.T., Kim, Y.J., Fan, Y., La Spada, A., Stone, B., and Ravits, J. (2010). Sporadic ALS has compartment-specific aberrant exon splicing and altered cell-matrix adhesion biology. Human Molecular Genetics *19*, 313-328.

179. Raoul, C., Buhler, E., Sadeghi, C., Jacquier, A., Aebischer, P., Pettmann, B., Henderson, C.E., and Haase, G. (2006). Chronic activation in presymptomatic amyotrophic lateral sclerosis (ALS) mice of a feedback loop involving Fas, Daxx, and FasL. ProcNatl AcadSciUSA *103*, 6007-6012.

180. Raoul, C., Estevez, A., Nishimune, H., Cleveland, D., deLapeyriere, O., Henderson, C., Haase, G., and Pettmann, B. (2002). Motoneuron Death Triggered by a Specific Pathway Downstream of Fas. Potentiation by ALS-Linked SOD1 Mutations. Neuron *35*, 1067-1083.

181. Reaume, A.G., Elliott, J.L., Hoffman, E.K., Kowall, N.W., Ferrante, R.J., Siwek, D.F., Wilcox, H.M., Flood, D.G., Beal, M.F., Brown, R.H., Jr., *et al.* (1996). Motor neurons in Cu/Zn superoxide dismutase-deficient mice develop normally but exhibit enhanced cell death after axonal injury. NatGenet *13*, 43-47.

182. Renton, A.E., Majounie, E., Waite, A., Simon-Sanchez, J., Rollinson, S., Gibbs, J.R., Schymick, J.C., Laaksovirta, H., van Swieten, J.C., Myllykangas, L., *et al.* (2011). A hexanucleotide repeat expansion in C9ORF72 is the cause of chromosome 9p21-linked ALS-FTD. Neuron *72*, 257-268.

183. Resch, U., Schichl, Y.M., Winsauer, G., Gudi, R., Prasad, K., and de Martin, R. (2009). Siva1 is a XIAP-interacting protein that balances NFkappaB and JNK signalling to promote apoptosis. J Cell Sci *122*, 2651-2661.

184. Reyes, N.A., Fisher, J.K., Austgen, K., VandenBerg, S., Huang, E.J., and Oakes, S.A. (2010). Blocking the mitochondrial apoptotic pathway preserves motor neuron viability and function in a mouse model of amyotrophic lateral sclerosis. The Journal of clinical investigation *120*, 3673-3679.

185. Ripps, M.E., Huntley, G.W., Hof, P.R., Morrison, J.H., and Gordon, J.W. (1995). Transgenic mice expressing an altered murine superoxide dismutase gene provide an animal model of amyotrophic lateral sclerosis. ProcNatlAcadSciUSA *92*, 689-693.

186. Robinson, M.D., and Oshlack, A. (2010). A scaling normalization method for differential expression analysis of RNA-seq data. Genome Biol *11*, R25.

187. Rosen, D.R., Siddique, T., Patterson, D., Figlewicz, D.A., Sapp, P., Hentati, A., Donaldson, D., Goto, J., O'Regan, J.P., Deng, H.-X., *et al.* (1993). Mutations in Cu/Zn superoxide dismutase gene are associated with familial amyotrophic lateral sclerosis. Nature *362*, 59-62.

188. Rothstein, J.D., Martin, L.J., and Kuncl, R.W. (1992). Decreased glutamate transport by the brain and spinal cord in amyotrophic lateral sclerosis. NEnglJMed *326*, 1464-1468.

189. Rothstein, J.D., Tsai, G., Kuncl, R.W., Clawson, L., Cornblath, D.R., Drachman, D.B., Pestronk, A., Stauch, B.L., and Coyle, J.T. (1990). Abnormal excitatory amino acid metabolism in amyotrophic lateral sclerosis. AnnNeurol *28*, 18-25.

190. Routtenberg, A. (2000). It's about time. In Memory Consolidation, P.E. Gold, Greenough W.T., ed. (American Pyschological Association), pp. 17-34.

191. Rowland, L.P. (1998). Diagnosis of amyotrophic lateral sclerosis. Journal of the Neurological Sciences *160 Suppl 1*, S6-24.

192. Rowland, L.P.P., T. A., ed. (2010). Merritt's Neurology, Twelfth Edition edn (New York, New York: Wolters Kluwer, Lippincott Williams & Wilkins).

193. Ryu, H., Smith, K., Camelo, S.I., Carreras, I., Lee, J., Iglesias, A.H., Dangond, F., Cormier, K.A., Cudkowicz, M.E., Brown, R.H., Jr., *et al.* (2005). Sodium phenylbutyrate prolongs survival and regulates expression of anti-apoptotic genes in transgenic amyotrophic lateral sclerosis mice. Journal of Neurochemistry *93*, 1087-1098.

194. Sako, W., Ito, H., Yoshida, M., Koizumi, H., Kamada, M., Fujita, K., Hashizume, Y., Izumi, Y., and Kaji, R. (2012). Nuclear factor kappa B expression in patients with sporadic amyotrophic lateral sclerosis and hereditary amyotrophic lateral sclerosis with optineurin mutations. Clinical neuropathology *31*, 418-423.

195. Sapp, P.C., Hosler, B.A., McKenna-Yasek, D., Chin, W., Gann, A., Genise, H., Gorenstein, J., Huang, M., Sailer, W., Scheffler, M., *et al.* (2003). Identification of two novel loci for dominantly inherited familial amyotrophic lateral sclerosis. American Journal of Human Genetics *73*, 397-403.

196. Sasaki, S., and Iwata, M. (1996). Ultrastructural study of synapses in the anterior horn neurons of patients with amyotrophic lateral sclerosis. NeurosciLett *204*, 53-56.

197. Sasaki, S., and Maruyama, S. (1994). Immunocytochemical and ultrastructural studies of the motor cortex in amyotrophic lateral sclerosis. Acta Neuropathologica *87*, 578-585.

198. Sathasivam, S., and Shaw, P.J. (2005). Apoptosis in amyotrophic lateral sclerosis--what is the evidence? Lancet Neurol *4*, 500-509.

199. Savinova, O.V., Hoffmann, A., and Ghosh, G. (2009). The Nfkb1 and Nfkb2 proteins p105 and p100 function as the core of high-molecular-weight heterogeneous complexes. Molecular cell *34*, 591-602.

200. Sawada, M., Sun, W., Hayes, P., Leskov, K., Boothman, D.A., and Matsuyama, S. (2003). Ku70 suppresses the apoptotic translocation of Bax to mitochondria. NatCell Biol *5*, 320-329.

201. Saxena, S., Cabuy, E., and Caroni, P. (2009). A role for motoneuron subtype-selective ER stress in disease manifestations of FALS mice. Nature neuroscience *12*, 627-636.

202. Schiffer, D., Cordera, S., Cavalla, P., and Migheli, A. (1996). Reactive astrogliosis of the spinal cord in amyotrophic lateral sclerosis. JNeurolSci *139*, 27-33.

203. Schmidt-Ullrich, R., Memet, S., Lilienbaum, A., Feuillard, J., Raphael, M., and Israel, A. (1996). NF-kappaB activity in transgenic mice: developmental regulation and tissue specificity. Development *122*, 2117-2128.

204. Sen, R., and Baltimore, D. (1986). Inducibility of kappa immunoglobulin enhancer-binding protein Nf-kappa B by a posttranslational mechanism. Cell *47*, 921-928.

205. Shaw, P.J., Forrest, V., Ince, P.G., Richardson, J.P., and Wastell, H.J. (1995). CSF and plasma amino acid levels in motor neuron disease: elevation of CSF glutamate in a subset of patients. Neurodegeneration *4*, 209-216.

206. Shibata, N., Hirano, A., Kobayashi, M., Sasaki, S., Kato, T., Matsumoto, S., Shiozawa, Z., Komori, T., Ikemoto, A., Umahara, T., *et al.* (1994). Cu/Zn superoxide dismutase-like immunoreactivity in Lewy body-like inclusions of sporadic amyotrophic lateral sclerosis. NeurosciLett *179*, 149-152.

207. Shih, V.F., Tsui, R., Caldwell, A., and Hoffmann, A. (2011). A single NFkappaB system for both canonical and non-canonical signaling. Cell Res *21*, 86-102.

208. Sojka, P., Andersen, P.M., and Forsgren, L. (1997). Effects of riluzole on symptom progression in amyotrophic lateral sclerosis. Lancet *349*, 176-177.

209. Soundararajan, P., Miles, G.B., Rubin, L.L., Brownstone, R.M., and Rafuse, V.F. (2006). Motoneurons derived from embryonic stem cells express transcription factors and develop phenotypes characteristic of medial motor column neurons. J Neurosci *26*, 3256-3268.

210. Spalloni, A., Albo, F., Ferrari, F., Mercuri, N., Bernardi, G., Zona, C., and Longone, P. (2004). Cu/Zn-superoxide dismutase (GLY93-->ALA) mutation alters AMPA receptor subunit expression and function and potentiates kainate-mediated toxicity in motor neurons in culture. NeurobiolDis *15*, 340-350.

211. Spreux-Varoquaux, O., Bensimon, G., Lacomblez, L., Salachas, F., Pradat, P.F., Le, F.N., Marouan, A., Dib, M., and Meininger, V. (2002). Glutamate levels in cerebrospinal fluid in amyotrophic lateral sclerosis: a reappraisal using a new HPLC method with coulometric detection in a large cohort of patients. J NeurolSci *193*, 73-78.

212. Sreedharan, J., Blair, I.P., Tripathi, V.B., Hu, X., Vance, C., Rogelj, B., Ackerley, S., Durnall, J.C., Williams, K.L., Buratti, E., *et al.* (2008). TDP-43 mutations in familial and sporadic amyotrophic lateral sclerosis. Science *319*, 1668-1672.

213. Srinivasan, D., Yen, J.H., Joseph, D.J., and Friedman, W. (2004). Cell type-specific interleukin-1beta signaling in the CNS. J Neurosci *24*, 6482-6488.

214. Subramaniam, J.R., Lyons, W.E., Liu, J., Bartnikas, T.B., Rothstein, J., Price, D.L., Cleveland, D.W., Gitlin, J.D., and Wong, P.C. (2002). Mutant SOD1 causes motor neuron disease independent of copper chaperone-mediated copper loading. NatNeurosci *5*, 301-307.

215. Sun, L., Hui, A.M., Su, Q., Vortmeyer, A., Kotliarov, Y., Pastorino, S., Passaniti, A., Menon, J., Walling, J., Bailey, R., *et al.* (2006). Neuronal and glioma-derived stem cell factor induces angiogenesis within the brain. Cancer Cell *9*, 287-300.

216. Sun, S.C. (2011). Non-canonical NF-kappaB signaling pathway. Cell Res *21*, 71-85.

217. Swarup, V., Phaneuf, D., Dupre, N., Petri, S., Strong, M., Kriz, J., and Julien, J.P. (2011). Deregulation of TDP-43 in amyotrophic lateral sclerosis triggers nuclear factor kappaB-mediated pathogenic pathways. The Journal of experimental medicine *208*, 2429-2447.

218. Tamatani, M., Che, Y.H., Matsuzaki, H., Ogawa, S., Okado, H., Miyake, S., Mizuno, T., and Tohyama, M. (1999). Tumor necrosis factor induces Bcl-2 and Bcl-x expression through NFkappaB activation in primary hippocampal neurons. The Journal of biological chemistry *274*, 8531-8538.

219. Tang, G., Minemoto, Y., Dibling, B., Purcell, N.H., Li, Z., Karin, M., and Lin, A. (2001). Inhibition of JNK activation through NF-kappaB target genes. Nature *414*, 313-317.

220. Tauriello, D.V., Haegebarth, A., Kuper, I., Edelmann, M.J., Henraat, M., Canninga-van Dijk, M.R., Kessler, B.M., Clevers, H., and Maurice, M.M. (2010). Loss of the tumor suppressor CYLD enhances Wnt/beta-catenin signaling through K63-linked ubiquitination of Dvl. Mol Cell *37*, 607-619.

221. Tikka, T.M., Vartiainen, N.E., Goldsteins, G., Oja, S.S., Andersen, P.M., Marklund, S.L., and Koistinaho, J. (2002). Minocycline prevents neurotoxicity induced by cerebrospinal fluid from patients with motor neurone disease. Brain : a journal of neurology *125*, 722-731.

222. Tobisawa, S., Hozumi, Y., Arawaka, S., Koyama, S., Wada, M., Nagai, M., Aoki, M., Itoyama, Y., Goto, K., and Kato, T. (2003). Mutant SOD1 linked to familial amyotrophic lateral sclerosis, but not wild-type SOD1, induces ER stress in COS7 cells and transgenic mice. BiochemBiophysResCommun *303*, 496-503.

223. Tolosa, L., Caraballo-Miralles, V., Olmos, G., and Llado, J. (2011). TNF-alpha potentiates glutamate-induced spinal cord motoneuron death via NF-kappaB. Molecular and cellular neurosciences *46*, 176-186.

224. Troost, D., Das, P.K., van den Oord, J.J., and Louwerse, E.S. (1992). Immunohistological alterations in muscle of patients with amyotrophic lateral sclerosis: mononuclear cell phenotypes and expression of MHC products. ClinNeuropathol *11*, 115-120.

225. Trotti, D., Aoki, M., Pasinelli, P., Berger, U.V., Danbolt, N.C., Brown, R.H., Jr., and Hediger, M.A. (2001). Amyotrophic lateral sclerosis-linked glutamate transporter mutant has impaired glutamate clearance capacity. JBiolChem *276*, 576-582.

226. Tu, P.H., Raju, P., Robinson, K.A., Gurney, M.E., Trojanowski, J.Q., and Lee, V.M.Y. (1996). Transgenic mice carrying a human mutant superoxide dismutase transgene develop neuronal cytoskeletal pathology resembling human amyotrophic lateral sclerosis lesions. ProcNatlAcadSciUSA *93*, 3155-3160.

227. Turner, B.J., and Talbot, K. (2008). Transgenics, toxicity and therapeutics in rodent models of mutant SOD1-mediated familial ALS. ProgNeurobiol *85*, 94-134.

228. Uranishi, H., Tetsuka, T., Yamashita, M., Asamitsu, K., Shimizu, M., Itoh, M., and Okamoto, T. (2001). Involvement of the pro-oncoprotein TLS (translocated in liposarcoma) in nuclear factor-kappa B p65-mediated transcription as a coactivator. J Biol Chem *276*, 13395-13401.

229. Van Damme, P., Bogaert, E., Dewil, M., Hersmus, N., Kiraly, D., Scheveneels, W., Bockx, I., Braeken, D., Verpoorten, N., Verhoeven, K., *et al.* (2007). Astrocytes regulate GluR2 expression in motor neurons and their vulnerability to excitotoxicity. ProcNatlAcadSciUSA *104*, 14825-14830.

230. Van Deerlin, V.M., Leverenz, J.B., Bekris, L.M., Bird, T.D., Yuan, W.X., Elman, L.B., Clay, D., Wood, E.M., Chen-Plotkin, A.S., Martinez-Lage, M., *et al.* (2008). TARDBP mutations in amyotrophic lateral sclerosis with TDP-43 neuropathology: a genetic and histopathological analysis. Lancet Neurol *7*, 409-416.

231. Vance, C., Rogelj, B., Hortobagyi, T., De Vos, K.J., Nishimura, A.L., Sreedharan, J., Hu, X., Smith, B., Ruddy, D., Wright, P., *et al.* (2009). Mutations in FUS, an RNA processing protein, cause familial amyotrophic lateral sclerosis type 6. Science *323*, 1208-1211.

232. Vargas, M.R., Johnson, D.A., Sirkis, D.W., Messing, A., and Johnson, J.A. (2008a). Nrf2 activation in astrocytes protects against neurodegeneration in mouse models of familial amyotrophic lateral sclerosis. J Neurosci *28*, 13574-13581.

233. Vargas, M.R., Pehar, M., Cassina, P., Beckman, J.S., and Barbeito, L. (2006). Increased glutathione biosynthesis by Nrf2 activation in astrocytes prevents p75NTR-dependent motor neuron apoptosis. JNeurochem *97*, 687-696.

234. Vargas, M.R., Pehar, M., Diaz-Amarilla, P.J., Beckman, J.S., and Barbeito, L. (2008b). Transcriptional profile of primary astrocytes expressing ALS-linked mutant SOD1. Journal of Neuroscience Research *86*, 3515-3525.

235. Veglianese, P., Lo Coco, D., Bao Cutrona, M., Magnoni, R., Pennacchini, D., Pozzi, B., Gowing, G., Julien, J.P., Tortarolo, M., and Bendotti, C. (2006). Activation of the p38MAPK cascade is associated with upregulation of TNF alpha receptors in the spinal motor neurons of mouse models of familial ALS. Molecular and cellular neurosciences *31*, 218-231.

236. Vukosavic, S., Dubois-Dauphin, M., Romero, N., and Przedborski, S. (1999). Bax and Bcl-2 interaction in a transgenic mouse model of familial amyotrophic lateral sclerosis. JNeurochem *73*, 2460-2468.

237. Wang, J., Slunt, H., Gonzales, V., Fromholt, D., Coonfield, M., Copeland, N.G., Jenkins, N.A., and Borchelt, D.R. (2003). Copper-binding-site-null SOD1 causes ALS in transgenic mice: aggregates of non-native SOD1 delineate a common feature. HumMolGenet *12*, 2753-2764.

238. Wang, J., Xu, G., Li, H., Gonzales, V., Fromholt, D., Karch, C., Copeland, N.G., Jenkins, N.A., and Borchelt, D.R. (2005a). Somatodendritic accumulation of misfolded SOD1-L126Z in motor neurons mediates degeneration: alphaB-crystallin modulates aggregation. Human Molecular Genetics *14*, 2335-2347.

239. Wang, J., Xu, G., Slunt, H.H., Gonzales, V., Coonfield, M., Fromholt, D., Copeland, N.G., Jenkins, N.A., and Borchelt, D.R. (2005b). Coincident thresholds of mutant protein for paralytic disease and protein aggregation caused by restrictively expressed superoxide dismutase cDNA. NeurobiolDis *20*, 943-952.

240. Wang, L.J., Lu, Y.Y., Muramatsu, S., Ikeguchi, K., Fujimoto, K., Okada, T., Mizukami, H., Matsushita, T., Hanazono, Y., Kume, A., *et al.* (2002). Neuroprotective effects of glial cell line-derived neurotrophic factor mediated by an adeno-associated virus vector in a transgenic animal model of amyotrophic lateral sclerosis. J Neurosci *22*, 6920-6928.

241. Wang, Z., Gerstein, M., and Snyder, M. (2009). RNA-Seq: a revolutionary tool for transcriptomics. Nature reviews Genetics *10*, 57-63.

242. Watanabe, Y., Yasui, K., Nakano, T., Doi, K., Fukada, Y., Kitayama, M., Ishimoto, M., Kurihara, S., Kawashima, M., Fukuda, H., *et al.* (2005). Mouse motor neuron disease caused by truncated SOD1 with or without C-terminal modification. Brain Res Mol Brain Res *135*, 12-20.

243. Wegorzewska, I., and Baloh, R.H. (2011). TDP-43-based animal models of neurodegeneration: new insights into ALS pathology and pathophysiology. Neurodegener Dis *8*, 262-274.

244. Wegorzewska, I., Bell, S., Cairns, N.J., Miller, T.M., and Baloh, R.H. (2009). TDP-43 mutant transgenic mice develop features of ALS and frontotemporal lobar degeneration. Proc Natl Acad Sci U S A *106*, 18809-18814.

245. Wengenack, T.M., Holasek, S.S., Montano, C.M., Gregor, D., Curran, G.L., and Poduslo, J.F. (2004). Activation of programmed cell death markers in ventral horn motor neurons during early presymptomatic stages of amyotrophic lateral sclerosis in a transgenic mouse model. Brain Res *1027*, 73-86.

246. Wichterle, H., Lieberam, I., Porter, J.A., and Jessell, T.M. (2002). Directed differentiation of embryonic stem cells into motor neurons. Cell *110*, 385-397.

247. Wichterle, H., Peljto, M., and Nedelec, S. (2009). Xenotransplantation of embryonic stem cell-derived motor neurons into the developing chick spinal cord. Methods Mol Biol *482*, 171-183.

248. Wiedau-Pazos, M., Goto, J.J., Rabizadeh, S., Gralla, E.B., Roe, J.A., Lee, M.K., Valentine, J.S., and Bredesen, D.E. (1996). Altered reactivity of superoxide dismutase in familial amyotrophic lateral sclerosis. Science *271*, 515-518.

249. Williamson, T.L., Corson, L.B., Huang, L., Burlingame, A., Liu, J., Bruijn, L.I., and Cleveland, D.W. (2000). Toxicity of ALS-linked SOD1 mutants. Science *288*, 399.

250. Wong, P.C., Pardo, C.A., Borchelt, D.R., Lee, M.K., Copeland, N.G., Jenkins, N.A., Sisodia, S.S., Cleveland, D.W., and Price, D.L. (1995). An adverse property of a familial ALS-linked SOD1 mutation causes motor neuron disease characterized by vacuolar degeneration of mitochondria. Neuron *14*, 1105-1116.

251. Xiao, Q., Zhao, W., Beers, D.R., Yen, A.A., Xie, W., Henkel, J.S., and Appel, S.H. (2007). Mutant SOD1(G93A) microglia are more neurotoxic relative to wild-type microglia. JNeurochem *102*, 2008-2019.

252. Xu, R., Tao, Y., Wu, C., Yi, J., Yang, Y., Yang, R., and Hong, D. (2008). Domoic acid induced spinal cord lesions in adult mice: evidence for the possible molecular pathways of excitatory amino acids in spinal cord lesions. Neurotoxicology *29*, 700-707.

253. Yamanaka, K., Boillee, S., Roberts, E.A., Garcia, M.L., onis-Downes, M., Mikse, O.R., Cleveland, D.W., and Goldstein, L.S. (2008a). Mutant SOD1 in cell types other

than motor neurons and oligodendrocytes accelerates onset of disease in ALS mice. ProcNatlAcadSciUSA *105*, 7594-7599.

254. Yamanaka, K., Chun, S.J., Boillee, S., Fujimori-Tonou, N., Yamashita, H., Gutmann, D.H., Takahashi, R., Misawa, H., and Cleveland, D.W. (2008b). Astrocytes as determinants of disease progression in inherited amyotrophic lateral sclerosis. NatNeurosci *11*, 251-253.

255. Yim, M.B., Kang, J.H., Yim, H.S., Kwak, H.S., Chock, P.B., and Stadtman, E.R. (1996). A gain-of-function of an amyotrophic lateral sclerosis- associated Cu,Zn-superoxide dismutase mutant: An enhancement of free radical formation due to a decrease in K_m for hydrogen peroxide. ProcNatlAcadSciUSA *93*, 5709-5714.

256. Yohn, D.C., Miles, G.B., Rafuse, V.F., and Brownstone, R.M. (2008). Transplanted mouse embryonic stem-cell-derived motoneurons form functional motor units and reduce muscle atrophy. J Neurosci *28*, 12409-12418.

257. Yu, Z., Zhou, D., Bruce-Keller, A.J., Kindy, M.S., and Mattson, M.P. (1999). Lack of the p50 subunit of nuclear factor-kappaB increases the vulnerability of hippocampal neurons to excitotoxic injury. J Neurosci *19*, 8856-8865.

258. Zhao, W., Beers, D.R., Henkel, J.S., Zhang, W., Urushitani, M., Julien, J.P., and Appel, S.H. (2010). Extracellular mutant SOD1 induces microglial-mediated motoneuron injury. Glia *58*, 231-243.

259. Zhu, S., Stavrovskaya, I., Drozda, M., Kim, B., Ona, V., Li, M., Sarang, S., Liu, A., Hartley, D., Wu, D., *et al.* (2002). Minocycline inhibits cytochrome c release and delays progression of amyotrophic lateral sclerosis in mice. Nature *417*, 74-78.

Chapter 8: Appendix

8.1. The master regulators inferred by the mouse brain interactome

Symbol	24h-0h(NES)	72h-0h(NES)	168h-0h(NES)	72h-24h(NES)	168h-72h(NES)	24h-0h(p-value)	72h-0h(p-value)	168h-0h(p-value)	72h-24h(p-value)	168h-72h(p-value)
Camta1	0.45	4.233	1.846	3.61	2.426	0.653	2.31e-05	0.065	0.000306	0.0152
Zbtb48	1.317	1.785	1.371	1.908	1.714	0.188	0.0743	0.17	0.0564	0.0865
Zmym6	0.558	0.546	1.074	0.636	1.91	0.577	0.585	0.283	0.525	0.0562
Akna	0.225	0.038	0.479	0.117	0.105	0.822	0.97	0.632	0.907	0.916
Zfand2a	0.313	0.67	0.121	0.934	0.821	0.754	0.503	0.904	0.35	0.412
Zfp518b	1.088	1.467	1.123	1.344	1.169	0.277	0.142	0.261	0.179	0.242
Nfxl1	0.637	1.814	3.053	0.91	0.257	0.524	0.0696	0.00227	0.363	0.797
Zfp513	0.433	0.001	0.279	0.026	0.733	0.665	0.999	0.78	0.979	0.463
Zfp282	1.553	2.556	1.896	2.182	1.489	0.121	0.0106	0.058	0.0291	0.137
Tada3	0.023	0.219	0.135	0.176	1.064	0.982	0.827	0.893	0.86	0.287
Taf5l	1.522	0.226	0.502	0.517	1.391	0.128	0.821	0.616	0.605	0.164
Zdhhc7	0.602	0.393	1.152	0.54	1.341	0.547	0.694	0.249	0.589	0.18
Snapc2	0.965	0.832	0.1	1.152	2.126	0.334	0.405	0.92	0.249	0.0335
Hinfp	0.26	0.141	0.366	0.061	0.523	0.795	0.888	0.714	0.951	0.601
Dennd4a	0.751	3.832	1.55	4.389	1.464	0.453	0.000127	0.121	1.14e-05	0.143
Zc3h10	0.67	0.098	0.141	0.148	0.69	0.503	0.922	0.888	0.882	0.49
Zfp692	0.717	0.369	1.456	0.631	0.341	0.474	0.712	0.145	0.528	0.733
Hoxb2	0.871	0.84	0.628	0.279	0.404	0.384	0.401	0.53	0.78	0.686
Etv5	0.524	2.52	2.768	1.639	0.935	0.6	0.0118	0.00565	0.101	0.35
Isl2	0.9	0.304	0.51	0.224	0.928	0.368	0.761	0.61	0.823	0.353
Barhl2	1.158	1.744	1.618	1.049	0.999	0.247	0.0811	0.106	0.294	0.318
Rcor2	0.778	0.857	0.916	1.005	2.5	0.436	0.391	0.36	0.315	0.0124
Rhox9	1.417	1.122	1.065	1.909	0.211	0.157	0.262	0.287	0.0562	0.833
E2f4	0.72	1.931	0.239	1.265	0.371	0.471	0.0535	0.811	0.206	0.711
Cggbp1	0.01	0.123	1.685	0.009	1.254	0.992	0.902	0.0919	0.993	0.21
Zc3h7a	0.089	0.745	1.627	0.27	1.537	0.929	0.456	0.104	0.787	0.124
Rrn3	0.202	0.221	0.129	0.132	0.422	0.84	0.825	0.897	0.895	0.673
Tcf19	1.017	1.574	1.448	1.045	1.264	0.309	0.116	0.148	0.296	0.206
Btaf1	0.116	0.393	0.824	0.116	0.188	0.908	0.694	0.41	0.908	0.851
Atf5	0.679	3.4	0.901	2.686	1.716	0.497	0.000675	0.368	0.00723	0.0863

Ovol2	2.192	2.061	0.403	1.533	0.696	0.0284	0.0393	0.687	0.125	0.486
Prrxl1	1.308	0.697	0.376	0.577	0.43	0.191	0.486	0.707	0.564	0.667
Ankrd1	0.041	1.001	0.061	0.783	0.601	0.967	0.317	0.951	0.434	0.548
Bmyc	1.064	2.519	2.996	2.165	0.864	0.287	0.0118	0.00274	0.0304	0.387
Scml2	0.978	0.485	0.129	1.088	0.064	0.328	0.628	0.897	0.276	0.949
Whsc1	0.389	1.613	1.906	1.291	1.389	0.697	0.107	0.0567	0.197	0.165
Gcm2	0.281	0.516	0.204	0.593	1.246	0.779	0.606	0.838	0.553	0.213
Taf9	0.249	0.529	0.107	0.03	0.211	0.803	0.597	0.915	0.976	0.833
Foxp1	1.147	0.786	1.18	1.051	1.336	0.251	0.432	0.238	0.293	0.182
Zdhhc15	0.305	2.272	0.269	1.002	0.607	0.76	0.0231	0.788	0.316	0.544
Zzz3	0.768	0.305	2.51	0.15	1.307	0.442	0.76	0.0121	0.881	0.191
E2f8	0.836	1.485	0.803	1.219	1.159	0.403	0.137	0.422	0.223	0.247
Slc30a9	0.598	1.039	0.244	1.171	1.034	0.55	0.299	0.807	0.241	0.301
Rlf	0.965	0.021	1.42	0.838	0.734	0.335	0.983	0.156	0.402	0.463
Tbx10	0.753	0.118	0.346	0.231	0.058	0.451	0.906	0.729	0.817	0.954
Lmo1	0.243	0.489	1.269	0.211	0.613	0.808	0.625	0.204	0.833	0.54
Mzf1	0.426	0.874	1.14	0.68	0.775	0.67	0.382	0.254	0.496	0.438
Zfp91	1.821	1.115	1.489	1.02	0.592	0.0686	0.265	0.136	0.308	0.554
Zbtb25	0.166	0.116	0.004	0.09	0.18	0.868	0.908	0.997	0.928	0.857
Hivep1	1.029	1.43	1.975	0.884	1.866	0.304	0.153	0.0482	0.377	0.0621
Lmx1a	0.654	0.004	0.018	0.094	0.167	0.513	0.997	0.986	0.925	0.867
Nr3c2	0.24	0.324	0.14	0.338	0.709	0.81	0.746	0.889	0.735	0.478
Tshz1	0.502	2.479	1.935	1.482	2.205	0.616	0.0132	0.053	0.138	0.0275
Foxp2	1.211	1.361	2.621	2.502	1.26	0.226	0.174	0.00877	0.0124	0.208
Zfp295	0.599	0.131	0.275	0.3	0.859	0.549	0.896	0.783	0.764	0.39
Zmynd10	0.51	0.315	0.04	0.131	0.753	0.61	0.753	0.968	0.896	0.452
Prdm15	0.095	2.497	2.593	1.789	2.357	0.924	0.0125	0.00951	0.0736	0.0184
Gtf2ird2	0.972	0.735	1.34	0.662	0.984	0.331	0.462	0.18	0.508	0.325
Ferd3l	0.35	0.546	0.181	0.161	0.715	0.726	0.585	0.856	0.872	0.475
Vsx1	1.147	0.41	0.183	1.052	0.466	0.251	0.682	0.855	0.293	0.641
Adnp	1.018	0.362	0.444	0.775	0.938	0.309	0.717	0.657	0.439	0.348
Aebp1	0.838	1.441	0.826	1.655	1.452	0.402	0.15	0.409	0.0979	0.147
Aebp2	0.698	0.026	0.229	0.395	0.256	0.485	0.979	0.819	0.693	0.798
Nr0b1	0.008	0.313	0.063	0.118	0.392	0.994	0.754	0.95	0.906	0.695
Ahr	1.407	1.637	1.912	1.289	0.381	0.16	0.102	0.0558	0.197	0.703
Aire	0.43	0.116	0.102	0.748	0.412	0.667	0.908	0.919	0.454	0.68
Foxn4	0.493	0.03	0.478	0.44	0.74	0.622	0.976	0.633	0.66	0.459
Baz2a	0.948	0.142	0.392	0.719	0.387	0.343	0.887	0.695	0.472	0.699

Mta1	0.846	0.864	0.679	1.283	2.025	0.398	0.388	0.497	0.199	0.0429
Mta3	0.253	1.593	1.36	1.491	0.948	0.8	0.111	0.174	0.136	0.343
Alx3	0.749	1.573	1.27	1.635	1.139	0.454	0.116	0.204	0.102	0.255
Alx4	0.917	1.706	0.308	1.718	1.932	0.359	0.0881	0.758	0.0857	0.0534
Nr2f2	0.809	1.41	1.766	1.483	0.953	0.418	0.158	0.0773	0.138	0.341
App	0.616	3.743	1.542	3.313	1.147	0.538	0.000182	0.123	0.000924	0.251
Ar	1.088	2.999	2.444	2.423	0.802	0.277	0.00271	0.0145	0.0154	0.423
Klf16	0.381	1.529	1.054	0.598	1.12	0.703	0.126	0.292	0.55	0.263
Phox2a	0.277	0.417	2.139	0.147	1.268	0.782	0.677	0.0324	0.883	0.205
Arnt	1.165	2.422	1.732	2.214	1.718	0.244	0.0154	0.0832	0.0269	0.0857
Arnt2	0.335	0.779	0.677	0.202	0.103	0.738	0.436	0.498	0.84	0.918
Arntl	0.628	0.837	0.746	1.096	0.592	0.53	0.402	0.456	0.273	0.554
Arx	0.828	1.509	0.856	0.909	1.105	0.408	0.131	0.392	0.363	0.269
Zfhx3	1.011	1.125	0.152	1.053	0.66	0.312	0.261	0.879	0.292	0.509
Atf1	1.143	2.524	2.569	1.548	0.871	0.253	0.0116	0.0102	0.122	0.384
Atf2	1.289	1.915	1.431	2.705	2.815	0.197	0.0555	0.152	0.00683	0.00487
Atf3	0.192	0.356	0.533	0.561	0.092	0.848	0.722	0.594	0.575	0.927
Atf4	0.282	0.458	1.249	0.396	1.439	0.778	0.647	0.212	0.692	0.15
Atoh1	0.667	0.015	0.111	0.434	0.02	0.505	0.988	0.912	0.664	0.984
Neurod6	0.781	2.747	1.369	1.963	0.986	0.435	0.00602	0.171	0.0497	0.324
Neurog2	0.718	1.23	1.17	0.22	0.719	0.473	0.219	0.242	0.826	0.472
Neurog3	0.604	0.294	3.176	0.392	1.405	0.546	0.769	0.00149	0.695	0.16
Bach1	0.475	0.581	1.868	0.247	1.683	0.635	0.561	0.0618	0.805	0.0924
Nkx3-2	0.109	0.135	0.043	0.243	0.126	0.913	0.893	0.966	0.808	0.9
Barx2	0.411	0.058	0.04	0.332	0.298	0.681	0.954	0.968	0.74	0.766
Bcl6b	1.026	2.367	1.097	1.305	1.233	0.305	0.0179	0.273	0.192	0.218
Bcl3	0.166	1.392	1.389	1.191	2.504	0.868	0.164	0.165	0.234	0.0123
Bcl6	0.991	0.817	1.926	0.757	1.874	0.321	0.414	0.0541	0.449	0.0609
Prdm1	0.739	1.834	1.162	1.169	1.041	0.46	0.0667	0.245	0.242	0.298
Bnc1	0.537	2.469	2.418	0.983	0.552	0.591	0.0135	0.0156	0.326	0.581
Zfp36l1	1.273	3.813	0.863	2.018	2.07	0.203	0.000137	0.388	0.0436	0.0384
Zfp36l2	0.619	0.008	0.142	0.011	0.816	0.536	0.994	0.887	0.991	0.415
Klf5	0.338	1.469	0.468	1.07	0.698	0.735	0.142	0.64	0.284	0.485
Nr1i3	0.325	0.178	0.016	0.331	0.147	0.745	0.859	0.987	0.741	0.883
Ctnnb1	0.75	0.461	0.844	0.41	0.358	0.453	0.645	0.399	0.682	0.72
Runx2	0.727	1.841	1.463	0.899	0.947	0.467	0.0657	0.144	0.369	0.344
Runx1	1.048	1.416	0.968	1.417	0.368	0.295	0.157	0.333	0.157	0.713
Runx1t1	0.787	1.382	1.923	2.214	2.258	0.431	0.167	0.0544	0.0268	0.0239

Cbfa2t3	0.116	3.544	2.504	1.464	1.141	0.908	0.000395	0.0123	0.143	0.254
Runx3	1.148	0.059	0.068	0.669	0.299	0.251	0.953	0.946	0.503	0.765
Cbfb	0.38	0.217	1.419	0.207	0.392	0.704	0.828	0.156	0.836	0.695
Cbl	0.38	0.288	0.476	0.183	0.514	0.704	0.773	0.634	0.855	0.607
Cbx2	0.691	0.019	0.004	0.053	0.122	0.489	0.985	0.997	0.958	0.903
Ccrn4l	0.174	1.445	0.702	0.141	0.522	0.862	0.148	0.482	0.888	0.602
Cdkn2a	0.476	0.758	0.372	0.403	0.719	0.634	0.448	0.71	0.687	0.472
Cdx1	0.701	0.298	0.021	0.671	0.207	0.484	0.766	0.983	0.502	0.836
Cdx2	1.199	0.05	0.108	0.385	0.078	0.23	0.96	0.914	0.7	0.938
Cdx4	0.513	0.001	0.429	0.004	0.425	0.608	0.999	0.668	0.997	0.671
Cebpa	0.231	0.286	1.192	0.041	0.724	0.817	0.775	0.233	0.967	0.469
Cebpz	1.043	0.809	1.806	0.48	0.688	0.297	0.418	0.0709	0.631	0.492
Cebpb	0.377	1.214	1.787	0.406	2.44	0.706	0.225	0.0739	0.685	0.0147
Cebpd	1.085	1.368	0.784	1.303	1.222	0.278	0.171	0.433	0.193	0.222
Cebpg	0.281	0.354	0.206	0.414	0.206	0.779	0.723	0.837	0.679	0.837
Vsx2	0.217	0.14	0.349	0.064	0.264	0.828	0.889	0.727	0.949	0.792
Cited1	0.645	0.693	0.38	0.987	0.248	0.519	0.488	0.704	0.324	0.804
Clock	1.165	0.996	1.003	1.86	2.412	0.244	0.319	0.316	0.0628	0.0159
Cnbp	0.196	1.632	1.139	0.465	0.542	0.845	0.103	0.255	0.642	0.588
Creb1	0.035	0.599	1.997	0.399	2.073	0.972	0.549	0.0458	0.69	0.0381
Creb3	0.783	0.425	0.147	0.855	0.726	0.434	0.671	0.883	0.392	0.468
Crebbp	0.921	0.102	0.444	0.093	0.088	0.357	0.919	0.657	0.926	0.93
Atf6b	0.415	1.019	2.183	0.76	1.418	0.678	0.308	0.029	0.447	0.156
Crem	2.215	0.866	1.666	2.211	0.927	0.0267	0.386	0.0957	0.027	0.354
Crx	0.354	0.131	0.192	0.069	0.57	0.723	0.896	0.848	0.945	0.569
Ctbp1	1.634	0.809	0.896	0.895	0.984	0.102	0.419	0.37	0.371	0.325
Ctbp2	1.201	1.032	1.364	1.217	0.91	0.23	0.302	0.173	0.224	0.363
Ctcf	0.193	0.982	1.536	0.249	0.041	0.847	0.326	0.124	0.803	0.967
Cux1	0.243	0	0.545	0.121	0.05	0.808	1	0.586	0.904	0.96
Cux2	0.818	1.79	1.383	1.578	0.337	0.414	0.0735	0.167	0.115	0.736
Dach1	0.112	0.61	0.559	0.089	0.962	0.911	0.542	0.576	0.929	0.336
Dbp	0.656	1.225	3.232	1.349	1.024	0.512	0.22	0.00123	0.177	0.306
Dbx1	0.38	0.671	1.841	1.778	1.748	0.704	0.502	0.0657	0.0754	0.0805
Ddit3	0.188	0.876	0.313	0.105	1.87	0.851	0.381	0.754	0.916	0.0615
Twist2	0.98	1.214	1.528	0.255	1.459	0.327	0.225	0.126	0.799	0.145
Dlx1	1.086	1.548	2.732	1.191	1.878	0.277	0.122	0.0063	0.233	0.0604
Dlx2	0.871	1.378	2.218	0.712	1.648	0.384	0.168	0.0265	0.476	0.0993
Dlx3	0.356	0.415	0.682	0.562	0.872	0.722	0.678	0.495	0.574	0.383

Dlx4	0.229	0.507	0.72	0.132	0.418	0.819	0.612	0.472	0.895	0.676
Dlx5	0.881	2.129	1.694	2.537	2.111	0.378	0.0332	0.0902	0.0112	0.0348
Dlx6	1.791	2.276	1.488	2.945	2.535	0.0733	0.0229	0.137	0.00323	0.0112
Dnmt3a	0.437	0.415	0.151	0.809	1.307	0.662	0.678	0.88	0.419	0.191
Dnmt3b	1.187	0.801	0.095	0.441	0.548	0.235	0.423	0.924	0.659	0.584
Slc26a3	0.599	0.06	0.019	0.539	0.281	0.549	0.952	0.985	0.59	0.779
Arid3a	0.763	0.036	0.159	0.909	0.175	0.445	0.971	0.874	0.364	0.861
E2f1	0.772	1.483	0.327	0.399	0.558	0.44	0.138	0.744	0.69	0.577
E2f3	0.653	1.804	1.338	2.388	2.461	0.514	0.0713	0.181	0.0169	0.0139
E2f5	1.235	0.349	1.23	0.16	1.291	0.217	0.727	0.219	0.873	0.197
E4f1	0.751	0.775	0.559	1.767	2.13	0.453	0.439	0.576	0.0773	0.0331
Ebf1	0.895	0.708	1.636	0.74	0.619	0.371	0.479	0.102	0.46	0.536
Ebf2	0.59	0.331	1.71	1.086	0.187	0.555	0.741	0.0872	0.277	0.852
Ebf3	0.219	0.253	2.214	0.124	1.237	0.827	0.8	0.0268	0.901	0.216
Egr1	0.555	2.366	2.161	1.402	2.206	0.579	0.018	0.0307	0.161	0.0274
Egr2	0.51	1.225	0.772	1.037	0.492	0.61	0.221	0.44	0.3	0.623
Egr3	0.164	0.173	0.604	0.056	0.982	0.87	0.863	0.546	0.955	0.326
Egr4	1.144	2.423	1.585	2.417	0.887	0.253	0.0154	0.113	0.0157	0.375
Ehf	0.598	0.009	0.004	0.089	0.031	0.55	0.993	0.997	0.929	0.975
Elf1	0.84	1.114	1.303	0.934	0.578	0.401	0.265	0.192	0.35	0.563
Elf3	0.48	0.684	0.639	0.312	0.173	0.631	0.494	0.523	0.755	0.863
Elf5	1.065	0.108	0.436	0.512	0.174	0.287	0.914	0.663	0.609	0.862
Elk1	0.965	1.053	1.162	1.081	0.626	0.334	0.292	0.245	0.28	0.531
Elk3	0.421	1.145	2.212	0.519	1.061	0.674	0.252	0.027	0.604	0.289
Elk4	0.688	0.036	0.243	0.156	0.536	0.491	0.971	0.808	0.876	0.592
Emx1	0.01	0.221	1.204	0.074	0.499	0.992	0.825	0.229	0.941	0.618
Emx2	0.19	2.443	2.224	1.329	0.565	0.849	0.0145	0.0262	0.184	0.572
En1	1.192	2.042	1.397	1.212	1.329	0.233	0.0411	0.162	0.226	0.184
En2	1.133	0.024	0.902	0.9	1.695	0.257	0.981	0.367	0.368	0.09
Eomes	1.661	0.117	1.678	0.07	1.568	0.0968	0.907	0.0933	0.944	0.117
Epas1	0.645	3.768	1.788	2.364	0.822	0.519	0.000165	0.0737	0.0181	0.411
Nr2f6	1.254	0.698	2.009	0.923	1.702	0.21	0.485	0.0445	0.356	0.0887
Nr2f1	0.744	2.461	1.912	1.721	1.109	0.457	0.0139	0.0559	0.0852	0.267
Erf	0.282	0.51	0.246	0.366	0.295	0.778	0.61	0.806	0.714	0.768
Erg	0.809	0.432	0.291	0.986	0.716	0.418	0.666	0.771	0.324	0.474
Esr1	1.165	1.392	0.365	1.052	1.14	0.244	0.164	0.715	0.293	0.254
Esr2	0.98	0.008	0.21	0.104	0.079	0.327	0.994	0.834	0.917	0.937
Esx1	0.645	0	0.026	0.141	0.085	0.519	1	0.979	0.888	0.932

Etv2	0.426	0.229	0.509	0.625	0.858	0.67	0.819	0.611	0.532	0.391
Etv1	0.589	1.207	2.413	1.164	1.442	0.556	0.227	0.0158	0.244	0.149
Mecom	0.161	0.04	0.093	0.064	0.457	0.872	0.968	0.926	0.949	0.648
Bcl11a	0.543	1.669	2.749	1.098	1.377	0.587	0.0951	0.00598	0.272	0.169
Evx1	0.485	0.246	0.21	0.884	1.156	0.628	0.806	0.834	0.377	0.248
Evx2	0.138	0.003	0.029	0.005	0.054	0.89	0.998	0.977	0.996	0.957
Ewsr1	0.578	0.617	1.761	0.303	0.208	0.563	0.537	0.0782	0.762	0.835
Dmbx1	0.389	0.011	0.026	0.256	0.152	0.697	0.991	0.979	0.798	0.879
Zfp358	0.325	0.716	2.002	0.385	0.898	0.745	0.474	0.0453	0.7	0.369
Bhlhe23	0.198	0.018	1.852	0.494	1.896	0.843	0.986	0.0641	0.621	0.058
Foxh1	0.855	0.04	0.281	0.418	0.411	0.393	0.968	0.779	0.676	0.681
Foxi1	0.019	1.008	0.503	0.173	0.964	0.985	0.313	0.615	0.863	0.335
Foxc2	0.934	1.908	1.351	1.072	0.947	0.35	0.0564	0.177	0.284	0.344
Foxm1	0.973	0.008	0.02	0.084	0.878	0.331	0.994	0.984	0.933	0.38
Foxn2	0.299	0.098	0.073	0.045	0.116	0.765	0.922	0.942	0.964	0.908
Foxd4	0.04	0.224	0.561	0.792	0.066	0.968	0.823	0.575	0.428	0.947
Foxf2	0.549	1.23	0.124	1.084	0.899	0.583	0.219	0.901	0.278	0.369
Foxs1	0.251	0.21	0.045	0.537	0.503	0.802	0.834	0.964	0.591	0.615
Foxb2	0.353	0.102	0.503	0.571	0.039	0.724	0.919	0.615	0.568	0.969
Fli1	0.454	0.068	0.636	0.187	0.166	0.65	0.946	0.525	0.852	0.868
Zcchc14	0.21	1.007	1.095	1.275	1.025	0.834	0.314	0.274	0.202	0.305
Fos	0.935	1.572	0.796	0.239	0.513	0.35	0.116	0.426	0.811	0.608
Fosb	1.31	0.529	3.004	0.266	1.439	0.19	0.597	0.00266	0.79	0.15
Fosl1	1.413	1.097	1.019	1.997	0.787	0.158	0.273	0.308	0.0458	0.431
Fosl2	1.01	0.506	0.129	0.234	0.415	0.313	0.613	0.897	0.815	0.678
Gabpa	0.722	0.373	2.169	0.026	1.113	0.471	0.709	0.0301	0.979	0.266
Gabpb1	1.029	2.332	1.013	1.453	0.592	0.304	0.0197	0.311	0.146	0.554
Gas7	0.643	1.835	0.278	1.303	0.436	0.52	0.0666	0.781	0.193	0.663
Gata1	0.285	0.237	0.356	0.053	0.157	0.776	0.813	0.722	0.958	0.875
Gata2	2.975	0.197	0.011	0.093	0.911	0.00293	0.844	0.991	0.926	0.362
Gata3	0.539	2.058	1.543	1.367	0.743	0.59	0.0396	0.123	0.171	0.458
Gata4	0.43	0.19	0.305	0.533	0.329	0.667	0.849	0.76	0.594	0.742
Gata5	1.225	0.462	0.004	0.617	0.114	0.221	0.644	0.997	0.537	0.909
Gata6	0.948	1.697	1.767	1.753	0.871	0.343	0.0897	0.0773	0.0796	0.384
Gbx2	0.675	0.546	0.458	1.522	0.335	0.5	0.585	0.647	0.128	0.738
Gcm1	0.574	0.015	0.402	0.024	0.332	0.566	0.988	0.688	0.981	0.74
Nr6a1	0.161	0.828	0.111	0.687	0.998	0.872	0.407	0.912	0.492	0.318
Gfi1	1.031	0.993	1.244	1.043	0.235	0.303	0.32	0.213	0.297	0.814

Gfi1b	0.077	0.387	0.516	0.15	0.008	0.939	0.699	0.606	0.881	0.994
Tsc22d3	0.432	0.671	1.767	1.552	0.789	0.666	0.502	0.0773	0.121	0.43
Gli1	0.504	0.014	0.221	0.349	0.312	0.614	0.989	0.825	0.727	0.755
Gli2	0.024	0.975	1.359	0.278	0.772	0.981	0.33	0.174	0.781	0.44
Gli3	0.368	1.735	1.041	0.826	1.443	0.713	0.0827	0.298	0.409	0.149
Nr3c1	0.53	0.614	1.354	0.924	1.884	0.596	0.539	0.176	0.355	0.0596
Gsc	0.586	1.856	2.149	1.73	0.695	0.558	0.0634	0.0316	0.0836	0.487
Gsx1	0.908	0.008	0.1	0.053	0.217	0.364	0.994	0.92	0.958	0.828
Gsx2	1.854	0.57	1.005	1.047	1.226	0.0637	0.569	0.315	0.295	0.22
Nkx6-2	0.041	0.936	2.672	0.373	0.909	0.967	0.349	0.00753	0.709	0.363
Hand1	0.166	0.673	0.961	0.546	1.158	0.868	0.501	0.337	0.585	0.247
Hand2	0.157	0.033	2.235	0.031	0.909	0.875	0.974	0.0254	0.975	0.363
Hcfc1	1.446	0.513	0.87	0.886	1.253	0.148	0.608	0.384	0.376	0.21
Hcls1	0.448	0.523	0.942	0.264	0.147	0.654	0.601	0.346	0.792	0.883
Hdac2	0.265	1.578	0.313	0.377	1.097	0.791	0.115	0.754	0.706	0.273
Hdgf	0.228	2.442	0.728	1.475	1.507	0.82	0.0146	0.466	0.14	0.132
Hes1	0.901	0.729	1.79	1.191	2.174	0.367	0.466	0.0735	0.234	0.0297
Hes2	0.45	0.244	0.131	0.376	0.282	0.653	0.807	0.896	0.707	0.778
Hes3	0.251	0.55	0.27	0.212	0.266	0.802	0.582	0.787	0.832	0.79
Hes5	0.183	0.598	0.88	0.369	1.39	0.855	0.55	0.379	0.712	0.165
Hesx1	0.238	0.006	0.338	0.02	0.233	0.812	0.995	0.735	0.984	0.816
Hey1	0.678	3.075	1.282	1.263	1.155	0.498	0.00211	0.2	0.206	0.248
Hey2	0.338	2.406	1.823	1.123	1.276	0.735	0.0161	0.0683	0.261	0.202
Foxn1	0.432	0.567	0.034	0.846	0.773	0.666	0.571	0.973	0.397	0.439
Foxq1	1.002	0.248	0.66	0.384	0.138	0.316	0.804	0.509	0.701	0.89
Foxd3	1.004	1.357	1.772	0.55	0.66	0.315	0.175	0.0764	0.582	0.509
Foxj1	0.392	0.329	0.013	0.81	0.114	0.695	0.742	0.99	0.418	0.909
Foxf1a	0.112	0.695	1.318	0.217	0.206	0.911	0.487	0.187	0.828	0.837
Foxg1	0.542	2.076	1.872	0.913	0.611	0.588	0.0379	0.0613	0.361	0.541
Foxd1	1.244	1.284	0.487	0.832	2.356	0.214	0.199	0.626	0.406	0.0185
Hhex	0.53	0.642	0.369	0.721	0.482	0.596	0.521	0.712	0.471	0.63
Hic1	0.84	0.362	0.112	0.384	0.716	0.401	0.717	0.911	0.701	0.474
Hif1a	0.243	0.792	2.189	0.565	0.295	0.808	0.428	0.0286	0.572	0.768
Hira	0.192	0.596	0.292	0.288	0.349	0.848	0.551	0.77	0.773	0.727
Hivep2	0.487	3.852	1.63	4.193	1.019	0.626	0.000117	0.103	2.75e-05	0.308
Hlx	1.163	1.152	0.423	1.311	2.059	0.245	0.249	0.672	0.19	0.0395
Mnx1	0.371	0.021	0.118	0.104	0.18	0.711	0.983	0.906	0.917	0.857
Hmg20b	1.007	0.084	0.003	0.305	0.608	0.314	0.933	0.998	0.76	0.543

Hmga1	0.422	3.271	1.255	2.657	2.349	0.673	0.00107	0.21	0.0079	0.0188
Hmga2	0.381	0.253	0.135	0.459	0.331	0.703	0.8	0.893	0.646	0.741
Nr4a1	0.291	2.093	0.077	0.686	0.697	0.771	0.0363	0.939	0.493	0.486
Hmx1	0.167	0.147	0.951	0.071	0.331	0.867	0.883	0.342	0.943	0.741
Hmx2	0.234	0.436	0.118	0.479	0.862	0.815	0.663	0.906	0.632	0.389
Hmx3	0.197	0.151	0.114	0.174	0.24	0.844	0.88	0.909	0.862	0.81
Foxa1	0.479	0.097	0.345	0.197	0.493	0.632	0.923	0.73	0.844	0.622
Foxa2	0.22	0.197	0.549	0.437	0.517	0.826	0.844	0.583	0.662	0.605
Foxa3	0.357	0.129	0.088	0.286	0.249	0.721	0.897	0.93	0.775	0.803
Hnf4a	0.183	0.693	0.722	0.799	0.229	0.855	0.489	0.47	0.424	0.819
Onecut1	0.204	0.028	0.005	0.005	0.762	0.838	0.978	0.996	0.996	0.446
Hnrnpab	0.349	2.113	0.622	1.469	1.162	0.727	0.0346	0.534	0.142	0.245
Hoxa1	0.646	0.197	0.55	0.522	0.83	0.518	0.844	0.582	0.602	0.406
Hoxa10	1.144	1.307	1.433	1.532	0.633	0.253	0.191	0.152	0.126	0.527
Hoxa11	0.396	0.572	0.423	1.994	1.201	0.692	0.567	0.672	0.0461	0.23
Hoxa13	0.118	0.112	0.003	0.026	0.129	0.906	0.911	0.998	0.979	0.897
Hoxa2	0.198	0.179	0.129	0.411	0.761	0.843	0.858	0.897	0.681	0.447
Hoxa3	0.43	0.642	0.599	1.075	0.197	0.667	0.521	0.549	0.282	0.844
Hoxa4	0.111	0.077	0.176	0.371	0.698	0.912	0.939	0.86	0.711	0.485
Hoxa5	0.555	0.497	0.321	0.533	0.295	0.579	0.619	0.748	0.594	0.768
Hoxa6	0.344	0.385	0.681	0.85	0.305	0.731	0.7	0.496	0.395	0.76
Hoxa7	0.468	0.132	0.066	0.14	0.353	0.64	0.895	0.947	0.889	0.724
Hoxa9	0.765	2.106	1.757	1.343	1.279	0.445	0.0352	0.079	0.179	0.201
Hoxb1	0.755	0.135	1.1	0.233	0.179	0.45	0.893	0.271	0.816	0.858
Hoxb13	0.943	1.018	1.608	1.065	0.654	0.345	0.309	0.108	0.287	0.513
Hoxb3	0.873	2.249	0.238	1.351	2.275	0.383	0.0245	0.812	0.177	0.0229
Hoxb4	1.147	0.1	0.034	0.871	0.102	0.251	0.92	0.973	0.384	0.919
Hoxb5	0.09	0.059	1.855	0.001	0.188	0.928	0.953	0.0636	0.999	0.851
Hoxb6	1.096	0.05	0.188	0.198	0.781	0.273	0.96	0.851	0.843	0.435
Hoxb8	0.798	0.83	0.05	1.761	0.272	0.425	0.407	0.96	0.0782	0.786
Hoxb9	0.868	0.752	0.243	1.666	0.705	0.386	0.452	0.808	0.0957	0.481
Hoxc12	0.693	0.07	0.213	0.327	0.3	0.488	0.944	0.831	0.744	0.764
Hoxc13	0.433	0.728	1.143	0.341	0.028	0.665	0.466	0.253	0.733	0.978
Hoxc4	0.014	0.868	0.23	0.74	1.03	0.989	0.386	0.818	0.46	0.303
Hoxc5	0.333	1.043	0.478	0.415	0.739	0.739	0.297	0.633	0.678	0.46
Hoxc6	0.393	2.486	0.514	1.585	0.948	0.694	0.0129	0.607	0.113	0.343
Hoxc8	1.615	1.297	0.476	1.168	0.121	0.106	0.195	0.634	0.243	0.904
Hoxc9	0.89	0.605	0.448	1.674	0.44	0.374	0.545	0.654	0.0942	0.66

Hoxd1	0.611	0.395	0.601	0.208	0.555	0.541	0.693	0.548	0.835	0.579
Hoxd10	0.324	0.1	0.705	0.08	0.772	0.746	0.92	0.481	0.936	0.44
Hoxd11	0.094	0.048	0.634	0.075	0.61	0.925	0.962	0.526	0.94	0.542
Hoxd12	1.239	0.758	0.114	0.925	1.199	0.215	0.448	0.909	0.355	0.231
Hoxd13	1.385	1.21	1.206	1.266	0.148	0.166	0.226	0.228	0.205	0.882
Hoxd3	0.404	0.013	0.366	0.238	0.167	0.686	0.99	0.714	0.812	0.867
Hoxd4	1.88	0.171	0	1.07	0.142	0.0601	0.864	1	0.284	0.887
Hoxd8	1.009	0.448	0.904	0.94	1.009	0.313	0.654	0.366	0.347	0.313
Hoxd9	0.607	3.217	0.412	2.288	0.268	0.544	0.0013	0.68	0.0221	0.789
Hr	1.282	1.495	3.235	1.632	1.191	0.2	0.135	0.00122	0.103	0.234
Hsf1	0.796	1.351	0.421	0.464	1.411	0.426	0.177	0.674	0.643	0.158
Hsf2	0.625	0.02	0.895	0.116	0.166	0.532	0.984	0.371	0.908	0.868
Irf8	1.071	1.035	0.216	0.371	0.946	0.284	0.301	0.829	0.711	0.344
Id1	0.687	3.209	0.841	1.975	2.363	0.492	0.00133	0.4	0.0483	0.0181
Id3	0.396	0.869	1.198	1.306	3.242	0.692	0.385	0.231	0.192	0.00119
Ilf3	0.073	0.844	0.784	0.656	0.44	0.942	0.399	0.433	0.512	0.66
Irf1	0.648	1.529	0.593	1.416	1.02	0.517	0.126	0.553	0.157	0.308
Irf2	0.556	0.561	1.553	0.724	1.955	0.578	0.575	0.121	0.469	0.0506
Irf4	0.575	1.608	0.598	1.759	0.933	0.565	0.108	0.55	0.0785	0.351
Irx1	0.628	0.751	1.542	0.836	0.013	0.53	0.453	0.123	0.403	0.99
Irx2	0.944	0.324	0.104	0.18	0.931	0.345	0.746	0.917	0.857	0.352
Irx3	0.482	0.159	0.119	0.665	0.836	0.63	0.874	0.905	0.506	0.403
Irf9	0.637	0.137	0.155	0.06	0.769	0.524	0.891	0.877	0.952	0.442
Isl1	0.281	1.424	2.343	1.227	1.507	0.779	0.154	0.0191	0.22	0.132
Jarid2	0.073	2.328	1.859	0.882	1.506	0.942	0.0199	0.063	0.378	0.132
Jun	0.387	1.13	1.608	1.675	0.868	0.699	0.258	0.108	0.094	0.385
Junb	0.231	1.454	1.479	0.387	3.527	0.817	0.146	0.139	0.699	0.00042
Jund	0.279	0.078	0.684	0.113	0.897	0.78	0.938	0.494	0.91	0.37
Klf1	0.589	0.069	0.073	0.524	0.229	0.556	0.945	0.942	0.6	0.819
Klf12	0.639	2.928	1.12	2.627	0.843	0.523	0.00341	0.263	0.0086	0.399
Klf2	1.16	0.849	1.076	1.138	1.898	0.246	0.396	0.282	0.255	0.0577
Klf3	0.317	2.173	0.902	1.708	1.607	0.751	0.0298	0.367	0.0877	0.108
Klf4	0.841	1.646	1.893	1.477	1.497	0.4	0.0998	0.0584	0.14	0.135
Klf9	0.665	1.672	0.903	1.025	1.628	0.506	0.0945	0.367	0.305	0.104
Hivep3	0.266	0.654	1.328	0.038	0.636	0.79	0.513	0.184	0.97	0.525
Mafb	1.028	0.229	0.668	0.675	0.886	0.304	0.819	0.504	0.5	0.376
Aff3	1.697	3.058	2.472	3.079	0.81	0.0898	0.00223	0.0134	0.00208	0.418
Lbx1	0.194	0.399	1.668	0.136	1.08	0.846	0.69	0.0953	0.892	0.28

Lbx2	0.102	0.079	0.038	0.396	0.454	0.919	0.937	0.97	0.692	0.65
Lef1	0.439	1.316	0.379	0.662	1.086	0.661	0.188	0.705	0.508	0.277
Lhx1	1.188	1.257	0.892	0.788	0.667	0.235	0.209	0.372	0.431	0.505
Lhx2	0.795	1.942	2.308	1.575	1.125	0.426	0.0522	0.021	0.115	0.261
Lhx3	0.485	0.45	0.033	0.941	0.668	0.628	0.653	0.974	0.347	0.504
Lhx4	0.127	1.849	1.734	1.468	0.628	0.899	0.0645	0.0829	0.142	0.53
Lhx5	0.357	0.278	0.971	0.132	1.437	0.721	0.781	0.331	0.895	0.151
Lhx6	0.4	0.222	0.028	0.336	0.804	0.689	0.824	0.978	0.737	0.422
Lhx8	0.671	0.183	0.055	0.307	0.507	0.502	0.855	0.956	0.759	0.612
Lhx9	0.774	1.041	0.974	0.789	0.71	0.439	0.298	0.33	0.43	0.478
Lmo4	0.77	1.538	1.885	1.107	0.64	0.441	0.124	0.0594	0.268	0.522
Lmx1b	0.672	1.248	0.928	0.513	0.238	0.502	0.212	0.354	0.608	0.812
Mycl1	0.7	1.677	0.759	1.909	2.263	0.484	0.0935	0.448	0.0563	0.0236
Zbtb7a	1.692	0.944	0.412	2.418	1.201	0.0907	0.345	0.68	0.0156	0.23
Sp7	0.601	0.083	0.372	0.174	1.005	0.548	0.934	0.71	0.862	0.315
Ubn1	0.604	0.399	1.023	1.723	0.79	0.546	0.69	0.306	0.0849	0.429
Scrt1	0.542	0.155	0.957	0.307	0.562	0.588	0.877	0.338	0.759	0.574
Zscan5b	0.061	0.433	0.294	0.124	0.835	0.951	0.665	0.769	0.901	0.404
Zfp287	2.029	0.17	0.084	1.334	0.4	0.0424	0.865	0.933	0.182	0.689
Zfp704	0.536	1.684	3.191	1.449	3.047	0.592	0.0922	0.00142	0.147	0.00231
Rfxap	0.105	0.104	0.244	0.024	0.246	0.916	0.917	0.807	0.981	0.806
Lyl1	0.357	0.213	0.148	0.118	0.454	0.721	0.831	0.882	0.906	0.65
Mxd1	0.154	1.777	1.092	1.68	0.754	0.878	0.0756	0.275	0.093	0.451
Mxd3	1.669	1.811	0.704	3.41	0.668	0.095	0.0702	0.482	0.000648	0.504
Mxd4	0.802	0.595	1.493	0.817	0.908	0.423	0.552	0.136	0.414	0.364
Smad1	0.642	1.04	1.733	0.337	0.755	0.521	0.298	0.083	0.736	0.45
Smad3	0.571	3.47	2.165	2.471	1.706	0.568	0.00052	0.0304	0.0135	0.0881
Smad4	1.783	1.717	1.867	1.703	1.959	0.0746	0.0859	0.0619	0.0885	0.0501
Smad5	0.903	0.812	3.901	1.582	0.461	0.366	0.417	9.59e-05	0.114	0.645
Smad6	1.698	2.304	0.522	2.977	3.246	0.0895	0.0212	0.602	0.00291	0.00117
Smad7	1.139	1.44	0.953	0.97	0.975	0.255	0.15	0.341	0.332	0.329
Maf	0.524	1.32	1.34	0.981	1.303	0.6	0.187	0.18	0.327	0.193
Maff	0.069	0.329	0.404	0.234	0.142	0.945	0.742	0.686	0.815	0.887
Mafg	0.397	0.548	0.921	0.485	1.319	0.691	0.584	0.357	0.628	0.187
Mafk	0.221	1.015	0.543	0.753	1.559	0.825	0.31	0.587	0.452	0.119
Ascl1	0.614	0.673	1.765	0.204	1.255	0.539	0.501	0.0775	0.838	0.21
Ascl2	0.616	1.332	1.861	0.445	1.126	0.538	0.183	0.0627	0.656	0.26
Max	0.758	1.063	1.525	0.305	0.179	0.449	0.288	0.127	0.76	0.858

Maz	0.459	1.23	2.501	0.72	0.097	0.646	0.219	0.0124	0.472	0.923
Mbd1	1.166	1.51	1.191	0.836	0.281	0.244	0.131	0.234	0.403	0.779
Mecp2	0.876	0.706	1.757	0.571	1.898	0.381	0.48	0.0789	0.568	0.0577
Mef2a	0.423	0.667	1.059	0.546	1.624	0.672	0.505	0.289	0.585	0.104
Mef2b	0.303	1.713	0.689	2.234	1.871	0.762	0.0867	0.491	0.0255	0.0613
Mef2c	0.741	2.871	2.699	2.407	1.018	0.459	0.00409	0.00696	0.0161	0.309
Mef2d	1.108	0.013	0.673	0.014	0.099	0.268	0.99	0.501	0.989	0.921
Meis1	1.289	0.082	0.665	0.748	0.033	0.198	0.935	0.506	0.454	0.974
Meox1	0.16	0.011	0.092	0.003	0.092	0.873	0.991	0.927	0.998	0.927
Meox2	1.881	0.361	1.242	1.402	0.701	0.0599	0.718	0.214	0.161	0.483
Mesp1	0.352	0.774	0.208	0.53	0.282	0.725	0.439	0.835	0.596	0.778
Mesp2	0.656	0.162	0.184	0.426	0.034	0.512	0.871	0.854	0.67	0.973
Foxc1	1.127	1.289	0.964	1.098	1.21	0.26	0.198	0.335	0.272	0.226
Foxd2	0.981	0.325	0.159	0.833	2.28	0.327	0.745	0.874	0.405	0.0226
Bhlha15	0.103	0.678	0.513	0.48	0.841	0.918	0.498	0.608	0.631	0.4
Mitf	1.834	0.237	1.814	0.455	0.656	0.0667	0.813	0.0696	0.649	0.512
Mllt10	0.034	0.604	0.568	0.357	0.02	0.973	0.546	0.57	0.721	0.984
Aff1	0.344	0.005	0.014	0.238	0.201	0.731	0.996	0.989	0.812	0.841
Mmp14	0.482	0.966	0.828	0.757	1.349	0.63	0.334	0.408	0.449	0.177
Foxk1	0.26	0.201	0.198	0.251	0.082	0.795	0.841	0.843	0.802	0.935
Mnt	0.59	0.119	0.1	0.461	0.206	0.555	0.905	0.92	0.645	0.837
Morc1	0.715	0.796	0.141	0.788	0.369	0.475	0.426	0.888	0.431	0.712
Meis2	1.249	1.206	2.086	1.22	1.438	0.212	0.228	0.037	0.223	0.15
Meis3	0.303	0.443	0.107	0.183	0.054	0.762	0.658	0.915	0.855	0.957
Msc	1.407	1.147	0.03	2.252	0.111	0.16	0.252	0.976	0.0243	0.912
Cited2	0.486	1.71	2.765	0.63	0.578	0.627	0.0872	0.00569	0.529	0.563
Msl3	0.324	1.604	1.395	0.95	0.662	0.746	0.109	0.163	0.342	0.508
Msx1	0.722	0.003	0.003	0.05	0.171	0.471	0.998	0.998	0.96	0.864
Msx2	0.311	0.141	0.496	0.097	0.259	0.756	0.888	0.62	0.923	0.796
Msx3	0.48	0.099	0.299	0.065	0.003	0.631	0.921	0.765	0.948	0.998
Mtf1	0.164	0.762	0.196	0.122	0.189	0.87	0.446	0.845	0.903	0.85
Mtf2	1.293	0.52	1.809	0.816	2.077	0.196	0.603	0.0705	0.414	0.0378
Myb	0.014	3.655	0.751	1.72	1.021	0.989	0.000257	0.453	0.0854	0.307
Mybl1	0.395	0.143	0.184	0.599	0.509	0.693	0.886	0.854	0.549	0.611
Mybl2	1.312	0.479	0.269	0.253	0.097	0.19	0.632	0.788	0.8	0.923
Myc	0.202	2.808	2.623	1.585	0.156	0.84	0.00499	0.00872	0.113	0.876
Mycs	0.219	0.315	0.281	0.26	0.396	0.827	0.753	0.779	0.795	0.692
Myf5	0.762	1.051	0.715	0.742	0.043	0.446	0.293	0.474	0.458	0.966

Myf6	0.457	0.234	0.135	0.502	0.344	0.648	0.815	0.893	0.616	0.731
Myod1	0.61	0.312	1.081	0.141	1.046	0.542	0.755	0.28	0.888	0.296
Myog	0.448	0.872	0.257	0.381	0.981	0.654	0.383	0.797	0.703	0.327
Myt1	0.999	1.306	0.815	1.788	1.62	0.318	0.191	0.415	0.0738	0.105
Myt1l	0.785	3.069	2.01	3.274	1.57	0.433	0.00215	0.0444	0.00106	0.116
Neurod2	1.271	2.612	1.492	2.604	1.682	0.204	0.00901	0.136	0.00923	0.0926
Neurog1	0.371	0.015	0.014	0.309	0.102	0.711	0.988	0.989	0.757	0.919
Nfatc1	0.439	1.463	0.685	0.841	0.897	0.661	0.143	0.493	0.4	0.37
Nfatc2	0.791	0.755	0.991	1.457	0.608	0.429	0.45	0.322	0.145	0.543
Nfatc3	1.096	1.387	2.219	2.075	1.997	0.273	0.165	0.0265	0.038	0.0459
Nfe2	0.473	0.279	0.138	0.141	0.233	0.636	0.78	0.89	0.888	0.816
Nfe2l1	0.804	0.589	2.068	0.744	0.989	0.422	0.556	0.0386	0.457	0.323
Nfe2l2	0.47	2.529	0.959	1.81	1.464	0.638	0.0114	0.338	0.0702	0.143
Nfe2l3	1.25	1.153	0.919	1.212	0.614	0.211	0.249	0.358	0.226	0.539
Nfia	0.273	0.244	0.972	0.036	0.887	0.785	0.807	0.331	0.971	0.375
Nfib	0.084	1.468	3.168	0.259	1.114	0.933	0.142	0.00154	0.796	0.265
Nfic	0.639	0.827	2.272	0.58	1.642	0.523	0.408	0.0231	0.562	0.101
Nfil3	1.139	1.556	2.153	1.759	0.972	0.254	0.12	0.0313	0.0787	0.331
Nfix	0.699	0.845	1.662	1.259	2.385	0.485	0.398	0.0966	0.208	0.0171
Nfkb1	0.387	3.454	1.365	2.006	1.387	0.699	0.000552	0.172	0.0448	0.165
Nfkb2	0.452	2.848	2.291	1.365	1.619	0.651	0.0044	0.022	0.172	0.106
Nfya	1.132	1.953	0.596	2.1	0.897	0.257	0.0508	0.551	0.0358	0.369
Nfyb	0.822	0.23	0.653	0.774	1.01	0.411	0.818	0.514	0.439	0.312
Nfyc	0.278	1.202	1.375	0.97	1.176	0.781	0.23	0.169	0.332	0.24
Nhlh1	1.086	0.296	0.436	0.683	0.593	0.277	0.767	0.663	0.495	0.553
Nhlh2	0.286	0.372	0.381	0.493	0.026	0.775	0.71	0.703	0.622	0.979
Nkx2-2	1.49	1.815	1.833	0.506	0.448	0.136	0.0695	0.0669	0.613	0.654
Nkx2-3	0.206	0.023	0.09	0.199	0.179	0.837	0.982	0.928	0.842	0.858
Nkx2-5	1.047	1.338	0.337	1.393	1.302	0.295	0.181	0.736	0.164	0.193
Nkx2-6	0.358	0.051	0.269	0.782	0.105	0.72	0.959	0.788	0.435	0.916
Nkx2-9	0.259	0.166	0.068	0.259	0.296	0.796	0.868	0.946	0.796	0.767
Nkx3-1	1.84	0.995	0.348	1.103	0.533	0.0658	0.32	0.728	0.27	0.594
Nkx6-1	0.674	0.147	0.117	0.433	0.135	0.5	0.883	0.907	0.665	0.893
Nme2	0.604	1.771	0.079	1.779	1.06	0.546	0.0765	0.937	0.0752	0.289
Mycn	0.66	3.839	2.424	2.475	0.646	0.509	0.000123	0.0154	0.0133	0.518
Nr4a3	0.138	2.76	1.422	2.408	1.197	0.89	0.00578	0.155	0.016	0.231
Notch1	0.126	1.126	1.505	0.342	2.57	0.9	0.26	0.132	0.732	0.0102
Notch2	0.399	1.096	0.441	0.914	1.295	0.69	0.273	0.659	0.361	0.195

Notch3	0.332	0.504	0.114	1.314	0.662	0.74	0.614	0.909	0.189	0.508
Notch4	0.3	1.232	0.527	2.502	0.941	0.764	0.218	0.598	0.0123	0.347
Zfml	0.611	0.545	0.691	0.826	2.253	0.541	0.586	0.49	0.409	0.0242
Uhrf1	0.34	0.238	1.196	0.754	0.503	0.734	0.812	0.232	0.451	0.615
Npas1	0.202	1.386	2.005	0.679	0.849	0.84	0.166	0.0449	0.497	0.396
Npas2	0.288	1.561	1.269	0.907	0.54	0.773	0.118	0.204	0.364	0.589
Nr1i2	1.637	0.064	0.093	0.257	0.213	0.102	0.949	0.926	0.797	0.831
Nrf1	0.492	0.282	0.558	0.767	0.108	0.623	0.778	0.577	0.443	0.914
Nrl	0.311	0.295	0.212	0.662	0.004	0.756	0.768	0.832	0.508	0.997
Nr4a2	0.601	1.955	2.83	1.188	1.638	0.548	0.0505	0.00465	0.235	0.101
Nobox	0.887	0.279	0.568	0.222	0.155	0.375	0.78	0.57	0.824	0.877
Sebox	0.159	0.061	0.353	0.231	1.045	0.874	0.951	0.724	0.817	0.296
Otp	0.193	0.304	0.294	0.181	0.527	0.847	0.761	0.769	0.856	0.598
Otx1	1.18	0.328	0.794	0.141	0.623	0.238	0.743	0.427	0.888	0.533
Otx2	1.542	0.729	0.084	0.298	1.377	0.123	0.466	0.933	0.766	0.169
Ovol1	0.07	0.354	0.648	0.381	0.071	0.944	0.723	0.517	0.703	0.943
Pax1	0.701	0.066	0.126	0.019	0.265	0.484	0.947	0.9	0.985	0.791
Pax2	1.026	0.005	0.249	0.055	0.502	0.305	0.996	0.803	0.956	0.616
Pax3	1.36	2.225	0.871	2.432	0.631	0.174	0.0261	0.384	0.015	0.528
Pax4	1.024	0.222	1.34	0.295	1.189	0.306	0.824	0.18	0.768	0.235
Pax5	0.207	0.751	2.47	0.098	0.845	0.836	0.452	0.0135	0.922	0.398
Pax6	0.494	0.559	0.786	0.459	1.082	0.621	0.576	0.432	0.646	0.279
Pax7	0.05	0	0.058	0.011	0.041	0.96	1	0.954	0.991	0.967
Pax8	0.868	1.121	1.387	1.073	0.526	0.385	0.262	0.166	0.283	0.599
Pax9	0.348	0.299	0.192	0.577	0.073	0.728	0.765	0.848	0.564	0.942
Pbx1	0.611	1.767	1.371	1.149	1.174	0.541	0.0772	0.17	0.251	0.241
Pbx2	0.396	1.863	0.664	1.141	1.479	0.692	0.0625	0.507	0.254	0.139
Pbx3	1.041	1.438	2.458	1.292	1.81	0.298	0.151	0.014	0.197	0.0703
Pdx1	0.278	0.099	0.715	1.298	1.807	0.781	0.921	0.475	0.194	0.0708
Etv4	0.472	0.015	0.031	0.025	0.437	0.637	0.988	0.975	0.98	0.662
Peg3	0.938	0.112	0.005	1.362	0.17	0.348	0.911	0.996	0.173	0.865
Rhox5	0.982	1.131	2.406	0.782	1.273	0.326	0.258	0.0161	0.434	0.203
Pgr	0.295	0.54	0.699	1.011	0.486	0.768	0.589	0.485	0.312	0.627
Phf2	0.5	1.963	0.741	1.319	0.779	0.617	0.0497	0.459	0.187	0.436
Phtf1	1.837	0.013	0.58	0.094	0.274	0.0662	0.99	0.562	0.925	0.784
Pou1f1	0.244	1.678	0.345	0.03	0.026	0.807	0.0934	0.73	0.976	0.979
Pitx1	1.487	0.023	0.1	0.287	0.152	0.137	0.982	0.92	0.774	0.879
Pitx2	0.792	1.087	0.769	0.44	0.371	0.428	0.277	0.442	0.66	0.711

Pitx3	0.572	0.045	0.167	0.418	0.265	0.567	0.964	0.867	0.676	0.791
Pknox1	0.546	0.429	0.074	0.033	0.452	0.585	0.668	0.941	0.974	0.651
Pa2g4	0.593	2.379	0.567	2.16	1.974	0.553	0.0174	0.571	0.0308	0.0484
Pml	0.795	1.271	1.897	0.372	1.568	0.427	0.204	0.0578	0.71	0.117
Prrx1	1.279	0.504	0.242	1.843	1.67	0.201	0.614	0.809	0.0654	0.095
Phox2b	0.295	0.049	0.102	0.044	0.317	0.768	0.961	0.919	0.965	0.751
Cnot7	0.174	0.146	0.799	0.262	1.798	0.862	0.884	0.424	0.793	0.0722
Pou2f1	0.905	0.622	2.193	0.596	0.636	0.366	0.534	0.0283	0.551	0.525
Pou2f2	0.274	0.013	0.132	0.01	0.051	0.784	0.99	0.895	0.992	0.959
Pou2f3	1.353	0.393	2.559	1.326	0.504	0.176	0.694	0.0105	0.185	0.614
Pou3f1	0.968	0.592	1.838	1.214	0.949	0.333	0.554	0.066	0.225	0.343
Pou3f2	0.127	0.187	0.132	0.466	0.798	0.899	0.852	0.895	0.641	0.425
Pou3f3	0.787	1.905	1.906	2.014	0.779	0.431	0.0568	0.0566	0.044	0.436
Pou3f4	0.353	1.438	1.244	0.288	0.637	0.724	0.15	0.214	0.773	0.524
Pou4f1	0.829	1.943	2.312	1.043	0.674	0.407	0.052	0.0208	0.297	0.5
Pou4f2	0.024	0.509	1.388	1.002	1.962	0.981	0.611	0.165	0.316	0.0498
Pou4f3	0.662	0.128	0.683	0.558	0.465	0.508	0.898	0.494	0.577	0.642
Pou5f1	0.765	0.316	0.239	0.613	0.324	0.444	0.752	0.811	0.54	0.746
Pou6f1	0.188	0.767	1.131	0.151	0.512	0.851	0.443	0.258	0.88	0.609
Ppara	0.419	0.562	0.199	1.676	0.253	0.675	0.574	0.842	0.0937	0.8
Ppard	0.211	2.293	1.547	1.902	1.978	0.833	0.0219	0.122	0.0572	0.0479
Pparg	0.201	0.152	0.126	0.145	1.268	0.841	0.879	0.9	0.885	0.205
Prkdc	0.752	0.277	2.014	0.015	1.263	0.452	0.782	0.044	0.988	0.207
Mapk8ip1	0.344	1.34	2.179	0.74	0.519	0.731	0.18	0.0294	0.459	0.604
Prop1	1.092	0.048	0.026	1.135	0.113	0.275	0.962	0.979	0.256	0.91
Prox1	0.291	0.065	2.186	0.194	0.982	0.771	0.948	0.0288	0.846	0.326
Psmc3ip	0.864	4.536	2.39	2.228	1.687	0.388	5.72e-06	0.0168	0.0259	0.0915
Rhox6	0.116	0.354	0.279	0.281	0.637	0.908	0.723	0.78	0.779	0.524
Ptf1a	0.768	0.73	2.247	0.457	0.865	0.443	0.465	0.0246	0.648	0.387
Ash1l	0.208	2.753	1.744	2.081	2.002	0.835	0.0059	0.0812	0.0374	0.0453
Zfp286	0.689	1.199	1.474	1.482	2.094	0.491	0.23	0.14	0.138	0.0362
Pura	0.278	1.181	1.322	1.003	1.699	0.781	0.237	0.186	0.316	0.0894
Purb	0.758	2.33	1.203	1.336	1.309	0.448	0.0198	0.229	0.182	0.19
Zfp3	0.937	0.764	0.898	1.513	1.466	0.349	0.445	0.369	0.13	0.143
Zfp184	0.36	0.083	1.187	0.038	0.303	0.719	0.934	0.235	0.97	0.762
Zbtb12	0.166	1.896	0.145	0.509	0.273	0.868	0.058	0.885	0.611	0.785
Rara	0.571	1.314	1.647	1.648	0.918	0.568	0.189	0.0996	0.0994	0.359
Rarg	0.396	0.936	0.656	0.894	0.273	0.692	0.349	0.512	0.371	0.785

Rax	0.249	1.086	0.235	0.559	1.08	0.803	0.278	0.814	0.576	0.28
Klf11	0.651	0.028	0.553	0.061	0.584	0.515	0.978	0.58	0.951	0.559
Rhox4e	0.235	0.723	0.233	0.233	0.206	0.814	0.469	0.816	0.816	0.837
Zzef1	0.14	0.073	0.391	0.039	0.16	0.889	0.942	0.696	0.969	0.873
Gsc2	0.975	0	0	0.235	0.119	0.33	1	1	0.814	0.905
Grhl1	0.493	1.374	2.421	1.072	1.455	0.622	0.169	0.0155	0.284	0.146
Rb1	0.035	0.927	2.01	0.643	0.06	0.972	0.354	0.0445	0.52	0.952
Rbl1	1.084	3.03	1.363	1.794	0.893	0.278	0.00245	0.173	0.0729	0.372
Rbl2	0.169	1.322	1.766	0.457	0.626	0.866	0.186	0.0774	0.648	0.531
Rbpj	0.693	1.857	0.581	0.916	1.143	0.488	0.0633	0.561	0.359	0.253
Rbpjl	0.114	0.08	0.773	0.253	0.202	0.909	0.936	0.439	0.8	0.84
Rel	0.327	0.137	0.879	0.107	0.141	0.744	0.891	0.38	0.915	0.888
Rela	0.761	2.38	0.8	2.548	2.539	0.447	0.0173	0.424	0.0108	0.0111
Relb	0.731	0.823	0.388	0.225	0.112	0.465	0.41	0.698	0.822	0.911
Rest	1.35	1.951	0.885	2.647	1.763	0.177	0.051	0.376	0.00811	0.0779
Trim27	0.879	1.116	0.861	1.295	2.077	0.379	0.264	0.389	0.195	0.0378
Rfx1	0.752	0.353	0.06	0.921	0.605	0.452	0.724	0.952	0.357	0.545
Rfx2	0.337	0.073	0.283	0.044	0.823	0.736	0.942	0.777	0.965	0.411
Rfx3	1.339	1.732	1.347	1.303	0.786	0.181	0.0832	0.178	0.192	0.432
Rfxank	0.375	0.001	0.061	0.053	0.255	0.708	0.999	0.951	0.958	0.799
Rnf4	0.121	1.71	0.262	1.168	0.67	0.904	0.0873	0.793	0.243	0.503
Rora	0.425	0.859	4.569	0.502	3.25	0.671	0.39	4.89e-06	0.616	0.00116
Rorc	0.459	0.421	1.86	0.362	0.548	0.646	0.674	0.0628	0.717	0.584
Rpl7	0.228	2.176	0.341	1.592	1.052	0.82	0.0295	0.733	0.111	0.293
Rxra	0.261	0.028	0.217	0.226	0.166	0.794	0.978	0.828	0.821	0.868
Rxrb	0.215	1.462	1.851	1.71	0.739	0.83	0.144	0.0641	0.0873	0.46
Rxrg	1.124	1.955	1.914	1.788	1.234	0.261	0.0505	0.0556	0.0737	0.217
Ncor1	0.04	1.207	0.722	0.559	1.141	0.968	0.227	0.47	0.576	0.254
Nr1h4	0.768	0.088	0.138	0.534	0.83	0.442	0.93	0.89	0.593	0.407
Prrx2	0.211	0.685	2.699	0.634	0.783	0.833	0.493	0.00695	0.526	0.434
Satb1	1.281	2.526	1.434	2.602	0.999	0.2	0.0115	0.152	0.00926	0.318
Nkx1-2	0.251	0.225	0.676	0.324	0.224	0.802	0.822	0.499	0.746	0.823
Scx	0.18	0.67	0.832	0.188	0.395	0.857	0.503	0.405	0.851	0.693
Foxp3	0.499	1.694	1.404	1.236	0.543	0.618	0.0902	0.16	0.216	0.587
Sfpi1	0.65	0.837	1.008	0.524	0.709	0.516	0.403	0.314	0.6	0.478
Zfp106	0.181	0.726	0.255	0.789	0.492	0.856	0.468	0.799	0.43	0.623
Shox2	0.388	1.659	0.308	1.387	1.36	0.698	0.0971	0.758	0.166	0.174
Sim1	0.357	1.711	0.52	1.622	0.598	0.721	0.0871	0.603	0.105	0.55

Sim2	0.65	0.188	0.046	0.312	0.159	0.516	0.851	0.963	0.755	0.874
Sin3a	1.497	1.992	1.401	3.696	1.205	0.134	0.0464	0.161	0.000219	0.228
Six1	0.141	2.002	1.069	2.458	1.951	0.888	0.0453	0.285	0.014	0.051
Six2	1.456	0.256	0.504	0.828	0.021	0.145	0.798	0.614	0.408	0.983
Six3	0.302	0.164	0	0.113	0.234	0.763	0.87	1	0.91	0.815
Six4	0.73	3.074	1.68	1.072	0.949	0.466	0.00211	0.093	0.284	0.343
Six5	0.098	0.328	0.794	0.059	0.018	0.922	0.743	0.427	0.953	0.986
Six6	0.277	0.114	0.308	0.337	0.725	0.782	0.909	0.758	0.736	0.469
Snai2	0.52	0.558	0.989	0.976	1.136	0.603	0.577	0.323	0.329	0.256
Hltf	1.644	1.868	0.7	1.06	2.081	0.1	0.0617	0.484	0.289	0.0374
Smarca4	0.798	1.082	0.623	1.012	1.586	0.425	0.279	0.533	0.312	0.113
Kdm5c	0.133	1.69	1.239	1.809	2.777	0.894	0.0911	0.215	0.0705	0.00549
Snai1	0.43	2.33	0.985	1.849	1.291	0.667	0.0198	0.325	0.0645	0.197
Sox1	0.17	0.033	0.061	0.132	0.04	0.865	0.974	0.951	0.895	0.968
Sox10	0.52	1.012	2.546	0.593	0.806	0.603	0.311	0.0109	0.553	0.42
Sox11	0.833	1.403	2.718	0.946	1.245	0.405	0.161	0.00657	0.344	0.213
Sox13	1.078	0.815	1.471	0.792	1.094	0.281	0.415	0.141	0.428	0.274
Sox14	0.408	0.043	0.311	0.048	0.727	0.683	0.966	0.756	0.962	0.467
Sox15	0.732	0.29	0.344	0.251	0.519	0.464	0.772	0.731	0.802	0.604
Sox17	0.616	0.331	0.034	0.517	0.337	0.538	0.741	0.973	0.605	0.736
Sox18	0.084	2.059	3.248	0.3	0.806	0.933	0.0395	0.00116	0.764	0.42
Sox2	1.001	2.49	0.803	2.148	0.667	0.317	0.0128	0.422	0.0317	0.505
Sox4	0.523	1.655	2.626	1.798	1.01	0.601	0.0979	0.00864	0.0722	0.312
Sox5	2.46	2.054	1.837	3.029	0.346	0.0139	0.04	0.0662	0.00245	0.729
Sox6	0.008	0.901	0.024	0.036	0.206	0.994	0.368	0.981	0.971	0.837
Sox7	0.09	0.221	0.403	0.087	0.183	0.928	0.825	0.687	0.931	0.855
Sox8	0.421	1.49	0.759	1.316	1.845	0.674	0.136	0.448	0.188	0.0651
Sox9	0.941	1.068	0.317	0.9	1.35	0.347	0.286	0.751	0.368	0.177
Sp1	0.534	2.515	2.742	1.274	0.65	0.593	0.0119	0.0061	0.203	0.516
Sp3	0.023	0.147	2.149	0.016	0.64	0.982	0.883	0.0316	0.987	0.522
Sp4	2.297	0.365	0.18	0.068	0.21	0.0216	0.715	0.857	0.946	0.834
Zbtb7c	0.113	0.092	0.434	0.029	0.17	0.91	0.927	0.664	0.977	0.865
Spic	1.68	0.063	0.617	0.365	0.084	0.0929	0.95	0.537	0.715	0.933
Csrnp2	1.093	0.426	1.121	1.019	0.45	0.274	0.67	0.262	0.308	0.653
Srebf1	0.497	3.192	1.681	3.196	2.419	0.619	0.00142	0.0928	0.0014	0.0156
Srebf2	0.953	0.664	1.532	0.972	1.386	0.341	0.507	0.125	0.331	0.166
Srf	0.979	0.375	1.198	0.908	1.203	0.327	0.708	0.231	0.364	0.229
Pknox2	0.503	0.465	0.458	0.601	0.79	0.615	0.642	0.647	0.548	0.429

Mlxip	1.129	1.33	2.031	0.877	1.097	0.259	0.183	0.0423	0.38	0.272
Stat1	0.898	1.77	1.147	3.48	2.088	0.369	0.0767	0.251	0.000502	0.0368
Stat2	0.395	1.312	1.591	0.685	0.986	0.693	0.189	0.112	0.493	0.324
Stat3	0.77	0.001	0.029	0.415	0.233	0.441	0.999	0.977	0.678	0.816
Stat4	3.917	0.842	0.458	1.743	0.303	8.97e-05	0.4	0.647	0.0813	0.762
Stat5a	0.031	0.899	1.325	0.16	1.003	0.975	0.369	0.185	0.873	0.316
Stat5b	1.08	1.76	1.964	1.372	1.573	0.28	0.0785	0.0496	0.17	0.116
Stat6	0.433	3.015	0.176	3.782	1.473	0.665	0.00257	0.86	0.000155	0.141
Creb3l2	1.11	1.318	1.526	1.605	1.102	0.267	0.187	0.127	0.109	0.27
Creb3l3	0.41	0.005	0.181	0.059	0.333	0.682	0.996	0.856	0.953	0.739
Zdhhc9	1.445	0.377	1.02	0.59	0.581	0.148	0.706	0.308	0.555	0.561
Bhlhe40	1.049	1.071	2.556	1.298	1.533	0.294	0.284	0.0106	0.194	0.125
Zfp280c	0.348	0.269	2.091	0.175	1.79	0.728	0.788	0.0365	0.861	0.0735
Zc3hav1l	0.581	0.602	0.712	0.745	1.04	0.561	0.547	0.477	0.456	0.298
Supt4h1	0.758	0.59	0.331	0.646	0.999	0.449	0.555	0.741	0.518	0.318
Zfp710	0.213	1.278	0.294	0.659	1.642	0.831	0.201	0.769	0.51	0.101
Supt6h	0.578	0.776	0.67	0.472	0.999	0.563	0.438	0.503	0.637	0.318
Tcfe3	0.104	0.671	1.046	0.77	1.53	0.917	0.502	0.295	0.441	0.126
Hoxc10	0.904	0.465	0.643	1.859	0.69	0.366	0.642	0.52	0.063	0.49
T	1.477	0.261	1.497	0.936	0.886	0.14	0.794	0.134	0.349	0.376
Zfp719	0.598	0.23	2.46	0.497	0.935	0.55	0.818	0.0139	0.619	0.35
Zfp180	0.988	1.149	0.503	0.55	1.589	0.323	0.25	0.615	0.582	0.112
Zkscan2	0.436	1.802	0.967	1.357	1.019	0.663	0.0715	0.334	0.175	0.308
Zfp526	0.991	0.264	0.519	0.369	0.084	0.322	0.792	0.604	0.712	0.933
Zfp677	1.069	0.23	1.454	0.43	1.324	0.285	0.818	0.146	0.667	0.186
Mkx	1.203	1.484	0.328	0.335	0.4	0.229	0.138	0.743	0.738	0.689
Kcnh8	0.682	1.322	0.688	0.324	1.684	0.495	0.186	0.491	0.746	0.0921
Tfdp2	0.926	1.145	2.248	2.45	1.502	0.354	0.252	0.0246	0.0143	0.133
Zfyve26	0.639	1.572	0.261	0.561	0.025	0.523	0.116	0.794	0.575	0.98
Cc2d1a	0.315	0.015	1.128	0.061	0.1	0.753	0.988	0.259	0.951	0.92
Zswim4	0.71	0.119	0.176	0.38	0.368	0.478	0.905	0.86	0.704	0.713
Lcor	0.57	0.537	1.022	0.645	2.057	0.569	0.591	0.307	0.519	0.0397
Satb2	0.99	1.458	1.208	1.2	1.312	0.322	0.145	0.227	0.23	0.19
Gabpb2	1.159	0.5	5.073	0.243	1.436	0.247	0.617	3.92e-07	0.808	0.151
Zbbx	0.035	0.155	0.832	0.273	0.014	0.972	0.877	0.405	0.785	0.989
Taf1b	0.058	0.151	0.305	0.024	0.112	0.954	0.88	0.76	0.981	0.911
Zcchc5	0.243	1.05	0.667	0.315	1.675	0.808	0.294	0.505	0.753	0.094

Tal1	0.845	0.021	0.138	0.117	0.187	0.398	0.983	0.89	0.907	0.852
Tal2	0.349	0.213	0.075	0.478	0.08	0.727	0.831	0.94	0.633	0.936
Tbl1x	1.035	0.261	0.261	1.548	1.096	0.301	0.794	0.794	0.122	0.273
Tbp	0.199	0.762	0.979	0.674	0.244	0.842	0.446	0.328	0.5	0.807
Tbr1	0.97	3.079	1.413	2.167	0.946	0.332	0.00208	0.158	0.0302	0.344
Zfp598	1.207	2.969	1.853	1.626	1.355	0.228	0.00298	0.0639	0.104	0.175
Tbx1	1.248	0.155	0.23	0.165	0.298	0.212	0.877	0.818	0.869	0.766
Tbx15	0.279	1.097	1.157	1.516	1.81	0.78	0.272	0.247	0.129	0.0703
Tbx2	1.232	0.72	0	0.194	1.325	0.218	0.471	1	0.846	0.185
Tbx3	0.944	0.805	1.145	1.072	1.4	0.345	0.421	0.252	0.284	0.162
Tbx4	0.327	0.239	0.472	0.469	0.685	0.744	0.811	0.637	0.639	0.493
Tbx5	0.454	0.169	0.059	0.217	0.063	0.65	0.866	0.953	0.828	0.95
Tbx6	0.533	0.545	0.285	0.668	0.756	0.594	0.586	0.776	0.504	0.45
Hnf1a	0.507	0.179	0.319	0.878	0.228	0.612	0.858	0.75	0.38	0.82
Tcf12	0.659	1.912	2.614	0.891	0.426	0.51	0.0558	0.00895	0.373	0.67
Tcf15	0.536	0.961	1.034	0.145	0.457	0.592	0.336	0.301	0.885	0.648
Zfp354a	0.604	2.761	1.9	2.286	1.614	0.546	0.00576	0.0575	0.0222	0.107
Hnf1b	1.189	0.473	0.504	0.419	0.787	0.234	0.636	0.614	0.675	0.431
Sox30	0.73	0.636	0.876	1.342	0.718	0.465	0.525	0.381	0.18	0.473
Tcf20	0.83	0.368	0.294	0.008	0.198	0.406	0.713	0.769	0.994	0.843
Tcf21	0.493	0.634	0.003	0.464	0.196	0.622	0.526	0.998	0.643	0.845
Tcf4	0.651	3.078	1.128	3.457	1.223	0.515	0.00209	0.259	0.000546	0.221
Tcf7	0.316	4.031	1.257	3.736	1.923	0.752	5.56e-05	0.209	0.000187	0.0545
Tcf7l1	0.303	0.714	0.108	0.862	0.735	0.762	0.476	0.914	0.388	0.462
Tcf7l2	0.788	1.184	1.593	2.007	1.209	0.431	0.237	0.111	0.0447	0.227
Mll1	1.179	0.015	0.891	0.203	1.584	0.238	0.988	0.373	0.839	0.113
Zeb1	0.077	0.213	0.71	0.02	0.794	0.939	0.831	0.478	0.984	0.427
Tcfap2a	2.475	0.628	1.431	0.631	0.224	0.0133	0.53	0.152	0.528	0.823
Tcfap2b	0.53	0.626	1.352	0.354	1.089	0.596	0.531	0.176	0.723	0.276
Tcfap2c	0.321	1.936	2.098	0.622	1.216	0.748	0.0528	0.0359	0.534	0.224
Tcfcp2	0.587	0.005	1.162	0.03	1.42	0.557	0.996	0.245	0.976	0.156
Tcf3	0.34	4.157	1.668	2.364	1.264	0.734	3.23e-05	0.0954	0.0181	0.206
Tcfeb	0.797	0.155	1.231	0.552	1.385	0.426	0.877	0.218	0.581	0.166
Tcfec	0.643	0.17	0.305	0.141	0.082	0.52	0.865	0.76	0.888	0.935
Vps72	1.051	0.113	0.185	0.447	1.685	0.293	0.91	0.853	0.655	0.092
Mlx	0.969	0.479	0.745	0.888	1.529	0.333	0.632	0.456	0.374	0.126
Zcchc6	0.226	0.131	0.344	0.286	0.069	0.821	0.896	0.731	0.775	0.945
Zfp609	0.304	0.244	0.137	0.468	0.749	0.761	0.807	0.891	0.64	0.454

Kdm5a	1.611	0.003	1.988	0.238	1.292	0.107	0.998	0.0468	0.812	0.196
Csrnp1	0.251	0.475	0.451	0.008	0.21	0.802	0.635	0.652	0.994	0.834
Zmat1	0.204	0.653	0.927	0.867	2.098	0.838	0.514	0.354	0.386	0.0359
Zfp365	0.526	2.042	2.425	1.328	1.064	0.599	0.0411	0.0153	0.184	0.288
Alx1	1.175	0.184	0.099	0.033	0.088	0.24	0.854	0.921	0.974	0.93
Phf1	0.451	1.142	2.347	0.879	1.979	0.652	0.254	0.0189	0.379	0.0478
Tead1	0.951	1.432	1.131	1.118	0.196	0.342	0.152	0.258	0.263	0.845
Tead2	0.984	1.803	0.676	1.709	1.701	0.325	0.0714	0.499	0.0875	0.0889
Tead3	1.119	1.756	0.113	1.077	0.824	0.263	0.079	0.91	0.281	0.41
Tead4	0.797	0.044	0.094	0.038	0.298	0.426	0.965	0.925	0.97	0.766
Tef	0.466	2.3	1.888	1.463	0.636	0.641	0.0214	0.059	0.144	0.525
Tada2a	0.729	0.368	0.465	0.496	2.08	0.466	0.713	0.642	0.62	0.0375
Trim25	0.766	3.154	2.961	1.483	0.705	0.444	0.00161	0.00307	0.138	0.481
Hlf	0.664	2.581	1.962	1.793	0.871	0.507	0.00986	0.0498	0.073	0.384
Myst2	0.264	0.683	0.738	0.626	0.202	0.792	0.494	0.46	0.531	0.84
Nr1d1	0.545	0.766	1.138	0.65	0.763	0.586	0.443	0.255	0.516	0.446
Baz1a	0.555	1.58	1.867	1.052	1.017	0.579	0.114	0.0619	0.293	0.309
Zfand3	1.201	0.19	0.079	0.617	0.937	0.23	0.849	0.937	0.537	0.349
Zfyve1	0.274	1.37	1.584	1.356	0.41	0.784	0.171	0.113	0.175	0.682
Tfam	0.203	1.619	0.01	0.998	0.238	0.839	0.105	0.992	0.318	0.812
Tfdp1	0.656	1.941	2.503	1.424	0.759	0.512	0.0522	0.0123	0.155	0.448
Pou6f2	0.16	0.383	0.06	0.673	0.704	0.873	0.702	0.952	0.501	0.481
Tsc22d1	0.586	1.037	0.78	0.35	0.549	0.558	0.3	0.436	0.726	0.583
Zfp322a	0.572	0.167	0.57	1.041	1.367	0.567	0.867	0.569	0.298	0.171
Tgif1	0.662	4.176	3.72	3.936	1.629	0.508	2.97e-05	2e-04	8.27e-05	0.103
Thra	0.677	2.52	2.726	1.757	1.134	0.499	0.0117	0.00641	0.079	0.257
Thrb	0.464	1.811	1.059	1.225	1.207	0.643	0.0702	0.29	0.221	0.228
Zfyve16	0.189	1.034	1.701	0.992	0.389	0.85	0.301	0.0889	0.321	0.697
Klf10	0.522	1.177	0.952	0.598	1.266	0.602	0.239	0.341	0.55	0.206
Trim28	1.254	1.361	1.284	1.489	2.281	0.21	0.173	0.199	0.136	0.0226
Mier3	0.278	0.251	1.51	0.164	1.053	0.781	0.802	0.131	0.87	0.292
Nkx2-1	1.096	1.109	1.172	1.804	0.077	0.273	0.267	0.241	0.0713	0.939
Rarb	0.584	1.836	1.729	2.923	1.401	0.559	0.0664	0.0839	0.00347	0.161
Zfp503	0.391	3.907	0.61	2.586	1.587	0.696	9.35e-05	0.542	0.0097	0.113
Tle4	0.727	1.57	1.245	1.665	1.577	0.467	0.116	0.213	0.096	0.115
Nr2e1	0.634	1.028	2.294	0.914	0.338	0.526	0.304	0.0218	0.36	0.735
Tlx1	0.698	0.187	0.345	0.561	0.64	0.485	0.852	0.73	0.575	0.522
Tlx2	1.137	0.001	0.157	0.178	0.128	0.255	0.999	0.875	0.859	0.898

Zmym5	0.464	0.854	1.441	0.809	1.937	0.643	0.393	0.149	0.418	0.0528
Hmbox1	0.116	0.156	0.324	0.124	0.523	0.908	0.876	0.746	0.901	0.601
Top2a	0.451	3.263	0.485	3.683	1.833	0.652	0.0011	0.628	0.000231	0.0668
Top2b	1.078	0.309	1.669	0.553	1.486	0.281	0.757	0.0952	0.58	0.137
Nr2c1	0.665	0.253	0.811	0.167	0.485	0.506	0.8	0.418	0.867	0.628
Nr2c2	0.875	2.694	1.529	2.119	1.965	0.382	0.00706	0.126	0.0341	0.0494
Trp53	0.242	3.957	0.478	2.811	1.716	0.809	7.6e-05	0.633	0.00493	0.0861
Trp63	0.121	0.084	0.019	0.473	0.364	0.904	0.933	0.985	0.636	0.716
Trp73	0.565	0	0.231	0.088	0.29	0.572	1	0.817	0.93	0.772
Twist1	1.105	3.233	1.291	3.214	0.863	0.269	0.00123	0.197	0.00131	0.388
Zrsr2	0.732	0.328	0.377	0.455	0.559	0.464	0.743	0.706	0.649	0.576
Ubp1	0.414	0.169	2.096	0.425	1.232	0.679	0.866	0.0361	0.671	0.218
Uncx	1.407	0.098	1.384	0.147	0.912	0.16	0.922	0.166	0.883	0.362
Nr1h3	0.118	0.203	0.025	0.192	1.02	0.906	0.839	0.98	0.848	0.308
Nr1h2	0.68	0.212	0.499	1.298	2.571	0.497	0.832	0.618	0.194	0.0101
Usf1	1.427	0.395	0.058	0.493	1.695	0.154	0.693	0.954	0.622	0.09
Usf2	0.286	1.241	2.592	0.723	1.305	0.775	0.215	0.00954	0.47	0.192
Utf1	0.366	0.104	0.206	0.252	1.375	0.714	0.917	0.837	0.801	0.169
Sox21	0.029	0.809	0.954	0.375	1.417	0.977	0.418	0.34	0.708	0.156
Vav1	0.596	1.574	0.482	1.74	1.7	0.551	0.115	0.63	0.0818	0.0891
Vax1	1.031	0	0.019	0.03	0.009	0.302	1	0.985	0.976	0.993
Vdr	0.371	0.117	0.193	0.64	0.377	0.711	0.907	0.847	0.522	0.706
Zc3h3	0.162	0.025	0.123	0.069	0.596	0.871	0.98	0.902	0.945	0.551
Zfp7	0.489	1.1	1.469	1.482	0.987	0.625	0.271	0.142	0.138	0.324
Zbed4	0.27	0.802	1.373	0.102	0.183	0.787	0.423	0.17	0.919	0.855
Dbx2	1.025	1.426	0.866	0.753	0.892	0.305	0.154	0.387	0.451	0.372
Baz1b	1.195	0.543	0.667	0.397	1.685	0.232	0.587	0.505	0.691	0.092
Atf7	0.88	0.628	1.568	0.637	2.345	0.379	0.53	0.117	0.524	0.019
Zmat3	0.27	0.426	0.533	0.412	0.567	0.787	0.67	0.594	0.68	0.571
Wiz	0.589	1.295	0.903	1.324	1.06	0.556	0.195	0.366	0.185	0.289
Dzip3	0.905	2.048	0.204	3.866	1.469	0.365	0.0405	0.838	0.000111	0.142
Wt1	0.714	1.334	1.607	0.986	0.572	0.475	0.182	0.108	0.324	0.567
Xbp1	0.939	2.861	0.941	1.814	1.256	0.347	0.00423	0.347	0.0697	0.209
Zdhhc14	0.727	1.369	2.641	0.897	0.851	0.467	0.171	0.00826	0.37	0.395
Flywch1	0.844	0.95	0.718	0.936	1.098	0.399	0.342	0.473	0.349	0.272
Zfp523	0.813	1.43	2.744	0.749	0.599	0.416	0.153	0.00608	0.454	0.549
Trerf1	0.608	0.354	0.151	0.357	0.029	0.543	0.723	0.88	0.721	0.977
Thoc1	0.806	0.126	1.637	0.373	2.14	0.42	0.9	0.102	0.709	0.0324

Zfp521	1.915	0.63	2.077	0.699	1.807	0.0555	0.529	0.0378	0.485	0.0708
Onecut2	1.157	0.873	1.314	1.108	1.934	0.247	0.383	0.189	0.268	0.0531
Npas4	1.054	1.758	2.5	0.532	0.749	0.292	0.0787	0.0124	0.595	0.454
Gm98	0.373	0.085	0.009	0.098	0.162	0.709	0.932	0.993	0.922	0.871
Rorb	0.425	1.047	0.166	0.861	0.006	0.671	0.295	0.868	0.389	0.995
Dmrt2	0.713	0.099	0.586	0.189	0.327	0.476	0.921	0.558	0.85	0.744
Glis3	0.021	0.016	0.068	0.204	0	0.983	0.987	0.946	0.838	1
Ybx1	0.51	2.7	2.793	1.205	0.919	0.61	0.00694	0.00523	0.228	0.358
Taf5	1.41	0.536	0.287	0.459	0.542	0.159	0.592	0.774	0.646	0.588
Yy1	0.248	0.962	0.095	1.107	0.43	0.804	0.336	0.924	0.268	0.667
Zfp1	0.693	1.016	0.795	0.443	1.692	0.488	0.31	0.426	0.658	0.0907
Zranb3	0.534	0.011	1.993	0.102	0.181	0.593	0.991	0.0462	0.919	0.856
Zbtb17	0.151	0.034	1.341	0.05	0.489	0.88	0.973	0.18	0.96	0.625
Zfp281	0.73	0.636	0.927	1.579	0.536	0.465	0.525	0.354	0.114	0.592
Zfp105	0.329	0.423	1.185	0.653	0.693	0.742	0.672	0.236	0.514	0.488
Zbtb41	0.447	0.112	1.291	0.034	1.527	0.655	0.911	0.197	0.973	0.127
Zfp11	0.066	0.507	0.147	0.146	0.38	0.947	0.612	0.883	0.884	0.704
Zfp13	0.775	0.313	0.054	0.054	0.419	0.439	0.754	0.957	0.957	0.675
Pcgf2	0.222	0.415	0.524	0.441	0.556	0.824	0.678	0.6	0.659	0.578
Zfp148	0.384	0.104	0.877	0.025	1.748	0.701	0.917	0.381	0.98	0.0805
Atf6	0.483	0.482	1.002	0.328	1.145	0.629	0.63	0.316	0.743	0.252
Zfp161	0.797	0.006	0.268	0.444	0.673	0.425	0.995	0.789	0.657	0.501
Ahctf1	0.412	1.684	2.953	0.917	0.905	0.68	0.0922	0.00315	0.359	0.365
Zfp2	0.643	2.699	2.483	3.028	2.061	0.52	0.00695	0.013	0.00247	0.0393
Zfp207	0.018	1.746	1.703	0.785	0.208	0.986	0.0808	0.0885	0.432	0.835
Zfand5	0.373	1.206	0.728	0.639	1.79	0.709	0.228	0.466	0.523	0.0735
Zfp239	0.731	3.281	1.685	2.8	1.417	0.465	0.00103	0.0919	0.00511	0.157
Zfp26	0.909	0.184	0.567	0.421	1.94	0.363	0.854	0.571	0.674	0.0524
Tcfap2d	0.239	1.056	2.159	1.603	0.377	0.811	0.291	0.0309	0.109	0.706
Zfp28	0.617	0.006	1.138	0.087	1.548	0.537	0.995	0.255	0.931	0.122
Zscan2	0.178	0.387	0.035	0.478	0.251	0.859	0.699	0.972	0.633	0.802
Zfp30	0.749	1.427	1.705	1.17	1.006	0.454	0.154	0.0882	0.242	0.314
Zfp36	0.696	2.957	1.426	1.888	1.286	0.486	0.0031	0.154	0.059	0.198
Zfp37	0.219	0.256	0.292	0.421	0.434	0.827	0.798	0.77	0.674	0.664
Zscan21	0.976	1.371	1.765	0.754	0.645	0.329	0.171	0.0776	0.451	0.519
Zfp42	0.523	0.331	0.346	0.216	1.971	0.601	0.741	0.729	0.829	0.0487
Zfp46	0.61	0.181	0.051	0.388	0.189	0.542	0.856	0.959	0.698	0.85
Zfp51	0.019	0.381	2.067	0.233	1.701	0.985	0.703	0.0388	0.816	0.0889

Zfp57	0.08	1.299	1.019	0.162	0.604	0.936	0.194	0.308	0.871	0.546
Zfp62	0.156	0.26	1.419	0.366	2.059	0.876	0.795	0.156	0.714	0.0395
Zfp64	1.143	3.254	1.042	2.23	1.7	0.253	0.00114	0.297	0.0258	0.0892
Zbtb7b	0.451	0.006	0.157	0.197	0.229	0.652	0.995	0.875	0.844	0.819
Zcchc2	0.596	1.984	2.488	1.425	0.55	0.551	0.0473	0.0128	0.154	0.582
Zfp9	1.425	0.207	0.534	0.52	1.455	0.154	0.836	0.593	0.603	0.146
Zfp90	0.234	0.099	0.324	0.377	0.736	0.815	0.921	0.746	0.706	0.462
Zfp92	0.657	0.221	0.001	0.358	0.185	0.511	0.825	0.999	0.72	0.853
Zkscan5	0.568	0.124	0.113	0.124	0.145	0.57	0.901	0.91	0.901	0.885
Zscan12	0.239	1.788	1.202	1.874	2.409	0.811	0.0739	0.229	0.0609	0.016
Zfpm1	0.982	0.9	1.531	0.798	1.032	0.326	0.368	0.126	0.425	0.302
Zfpm2	0.999	2.106	1.843	1.483	1.179	0.318	0.0352	0.0653	0.138	0.238
Zfr	0.194	1.303	0.943	0.741	1.06	0.846	0.193	0.346	0.459	0.289
Zfx	0.216	0.261	0.181	0.275	1.397	0.829	0.794	0.856	0.783	0.162
Snapc4	0.377	0.019	0.864	0.103	1.047	0.706	0.985	0.388	0.918	0.295
Rexo4	0.574	0.35	0.344	0.668	1	0.566	0.726	0.731	0.504	0.317
Zhx1	0.417	0.004	0.962	0.044	1.608	0.677	0.997	0.336	0.965	0.108
Zic1	0.656	1.949	1.758	1.473	1.296	0.512	0.0513	0.0788	0.141	0.195
Zic2	0.229	0.178	0.123	0.479	1.477	0.819	0.859	0.902	0.632	0.14
Zic3	0.404	1.344	1.372	1.101	1.994	0.686	0.179	0.17	0.271	0.0461
Zik1	0.083	0.83	1.636	0.733	1.73	0.934	0.407	0.102	0.464	0.0836
Ikzf1	1.116	1.705	1.706	1.371	0.637	0.264	0.0882	0.088	0.17	0.524
Ikzf2	0.803	0.151	0.147	0.287	1.052	0.422	0.88	0.883	0.774	0.293
Ikzf3	0.519	0.028	0.425	0.26	0.911	0.604	0.978	0.671	0.795	0.362
Ikzf4	0.07	0	0	0.197	0.14	0.944	1	1	0.844	0.889
Zdhhc5	0.623	2.17	2.185	2.062	0.968	0.533	0.03	0.0289	0.0392	0.333
Zfp770	0.053	0.16	0.358	0.014	1.228	0.958	0.873	0.72	0.989	0.219
Ebf4	0.009	1.234	0.434	0.407	0.054	0.993	0.217	0.664	0.684	0.957
Nkx2-4	0.277	0.024	0.054	0.256	0.239	0.782	0.981	0.957	0.798	0.811
Zfp341	1.628	0.02	0.237	0.335	2.63	0.104	0.984	0.813	0.738	0.00854
Phf20	0.268	1.242	1.134	0.696	0.412	0.789	0.214	0.257	0.487	0.68
Tgif2	0.869	2.628	0.834	1.8	1.066	0.385	0.00859	0.404	0.0718	0.286
Zfp334	0.813	1.181	0.574	1.199	0.558	0.416	0.237	0.566	0.231	0.577
Zmynd8	0.058	0.406	1.142	0.396	0.344	0.954	0.685	0.253	0.692	0.731
Tshz2	0.608	1.668	1.286	0.194	0.711	0.543	0.0954	0.199	0.846	0.477
Zfp217	0.213	0.659	0.321	0.526	0.85	0.831	0.51	0.748	0.599	0.395
Zgpat	2.445	0.162	0.917	0.49	0.713	0.0145	0.871	0.359	0.624	0.476
Gatad2b	1.155	0.411	1.394	0.137	0.439	0.248	0.681	0.163	0.891	0.661

Znhit6	0.58	0.739	0.204	1.24	0.572	0.562	0.46	0.838	0.215	0.567
Prdm13	0.523	1.016	0.237	0.723	1.541	0.601	0.31	0.813	0.469	0.123
Zbtb5	0.015	2.592	0.995	2.17	2.051	0.988	0.00955	0.32	0.03	0.0403
Zfp189	0.604	0.093	0.354	0.519	0.137	0.546	0.926	0.723	0.604	0.891
Glis1	0.197	0.029	0.213	0.726	0.162	0.844	0.977	0.831	0.468	0.871
Zcchc11	0.512	0.602	1.922	0.571	1.06	0.609	0.547	0.0546	0.568	0.289
Zfyve9	0.055	0.004	0.008	0.003	0.27	0.956	0.997	0.994	0.998	0.787
Foxj3	1.107	2.57	2.179	2.384	1.62	0.269	0.0102	0.0294	0.0171	0.105
Zc3h12a	0.396	0.011	0.102	0.113	0.348	0.692	0.991	0.919	0.91	0.728
Zbtb40	0.509	0.272	0.66	0.308	0.428	0.611	0.786	0.509	0.758	0.669
Tardbp	0.593	1.685	2.217	1.462	0.369	0.553	0.0919	0.0266	0.144	0.712
Gbx1	0.365	0.516	0.818	0.523	0.894	0.715	0.606	0.413	0.601	0.371
Zfyve28	0.58	2.255	1.45	1.884	1.098	0.562	0.0241	0.147	0.0596	0.272
Trafd1	0.252	0.929	1.424	0.671	0.315	0.801	0.353	0.154	0.502	0.753
Zfp12	0.1	0.443	1.076	0.5	1.32	0.92	0.658	0.282	0.617	0.187
Jazf1	0.43	3.066	1.382	1.803	1.593	0.667	0.00217	0.167	0.0713	0.111
Creb5	0.383	0.667	0.756	0.465	0.068	0.702	0.505	0.449	0.642	0.946
Zfp637	0.929	0.184	0.948	0.199	1.345	0.353	0.854	0.343	0.842	0.179
Zc3hc1	0.155	0.01	0.073	0.078	0.117	0.877	0.992	0.942	0.938	0.907
Zfp212	1.39	0.679	0.35	0.657	1.31	0.164	0.497	0.726	0.511	0.19
Zfp628	0.024	1.309	1.239	1.324	0.476	0.981	0.191	0.215	0.186	0.634
Zfp418	0.335	0.793	1.614	0.86	0.89	0.738	0.428	0.107	0.39	0.374
Zscan22	1.304	0.217	0.104	0.839	0.761	0.192	0.828	0.917	0.401	0.446
Grlf1	0.133	1.068	0.193	0.468	0.132	0.894	0.285	0.847	0.64	0.895
Mypop	0.383	1.171	1.972	1.153	1.011	0.702	0.242	0.0486	0.249	0.312
Zfp428	0.665	0.876	1.984	0.744	1.01	0.506	0.381	0.0473	0.457	0.312
Zfp574	0.681	0.105	0.083	0.444	0.265	0.496	0.916	0.934	0.657	0.791
Zfp790	1.628	0.815	0.909	1.792	1.298	0.103	0.415	0.363	0.0732	0.194
Zfp592	0.233	0.112	0.371	0.039	0.296	0.816	0.911	0.711	0.969	0.767
Crebzf	0.561	0.89	1.461	1.511	2.643	0.575	0.373	0.144	0.131	0.00823
Zfp553	0.775	0.173	0.732	0.01	0.559	0.438	0.863	0.464	0.992	0.576
Zfp768	0.07	0.794	0.589	0.237	1.323	0.944	0.427	0.556	0.813	0.186
Zfp764	0.099	0.118	0.668	0	0.317	0.921	0.906	0.504	1	0.751
Zfp646	0.758	3.468	1.747	0.936	1.742	0.448	0.000524	0.0806	0.349	0.0815
Gatad2a	0.883	1.333	0.838	2.003	0.733	0.377	0.183	0.402	0.0452	0.463
Zfp612	0.118	2.306	2.132	2.869	3.053	0.906	0.0211	0.033	0.00412	0.00226
Zfp426	1.292	0.307	0.239	0.476	0.608	0.197	0.759	0.811	0.634	0.543
Zbtb44	0.483	0.332	0.147	0.51	0.626	0.629	0.74	0.883	0.61	0.531

Nfrkb	0.665	0.253	1.544	0.097	1.827	0.506	0.8	0.123	0.923	0.0677
Zbtb16	0.131	0.014	0.143	0.141	0.291	0.896	0.989	0.886	0.888	0.771
Zfp280d	0.225	0.169	1.665	0.485	1.977	0.822	0.866	0.096	0.628	0.0481
Zfp445	0.824	0.66	0.66	1.335	1.41	0.41	0.509	0.509	0.182	0.159
Zfp825	0.929	0.194	0.81	0.754	1.148	0.353	0.846	0.418	0.451	0.251
Zfp709	0.345	0.377	0.212	0.734	0.344	0.73	0.706	0.832	0.463	0.731
Zc3h12d	0.812	1.268	0.063	1.671	1.664	0.417	0.205	0.95	0.0946	0.0961
Zfp454	0.49	0.616	1.26	0.315	1.596	0.624	0.538	0.208	0.753	0.111
Ash2l	1.004	1.47	0.082	1.061	0.428	0.315	0.141	0.935	0.289	0.669
Arid4a	0.493	0.294	0.823	0.302	0.634	0.622	0.769	0.41	0.763	0.526
C130039O16Rik	0.457	0.194	0.02	0.064	0.68	0.648	0.846	0.984	0.949	0.497
Klf6	0.348	1.286	0.983	0.714	0.35	0.728	0.198	0.325	0.476	0.726
Dmtf1	1.074	0.063	1.031	0.412	1.179	0.283	0.95	0.303	0.68	0.239
Zfp367	0.422	0.92	1.823	0.934	0.908	0.673	0.357	0.0684	0.35	0.364
Ets1	0.951	0.499	1.775	1.378	0.845	0.342	0.618	0.0759	0.168	0.398
Ets2	0.388	1.889	1.719	1.387	0.844	0.698	0.0589	0.0855	0.165	0.399
Fiz1	0.66	0.907	0.493	0.492	1.309	0.509	0.364	0.622	0.623	0.191
Mta2	0.03	0.773	0.053	0.494	1.902	0.976	0.44	0.958	0.621	0.0572
Zfp647	1.494	0.063	0.317	0.224	0.934	0.135	0.95	0.751	0.823	0.35
Nr0b2	0.708	0.331	0.377	0.286	0.073	0.479	0.741	0.706	0.775	0.942
Nr2e3	0.882	0.146	0.356	0.432	0.36	0.378	0.884	0.722	0.666	0.719
Zfp641	0.313	0.376	0.128	0.036	0.01	0.754	0.707	0.898	0.971	0.992
Zfp799	0.524	0.141	0.439	0.27	0.737	0.6	0.888	0.661	0.787	0.461
Zfp563	0.239	0.918	0.176	1.036	0.847	0.811	0.359	0.86	0.3	0.397
Zfp438	0.58	0.001	0.041	0.019	0.365	0.562	0.999	0.967	0.985	0.715
Adnp2	0.373	1.091	1.289	0.476	1.74	0.709	0.275	0.197	0.634	0.0818
Zfp407	0.577	0.221	0.157	0.307	0.548	0.564	0.825	0.875	0.759	0.584
St18	0.754	2.403	1.444	1.539	0.987	0.451	0.0163	0.149	0.124	0.324
Taf7	1.441	0.029	1.47	0.58	0.529	0.15	0.977	0.142	0.562	0.597
Zbtb37	0.333	0.192	0.217	0.128	0.225	0.739	0.848	0.828	0.898	0.822
Rbck1	1.209	0.061	0.17	0.94	0.575	0.227	0.951	0.865	0.347	0.565
Carf	0.399	0.634	0.184	0.251	0.053	0.69	0.526	0.854	0.802	0.958
Vax2	0.407	0.238	0.136	0.52	0.406	0.684	0.812	0.892	0.603	0.685
Zbtb6	0.753	0.727	0.225	0.441	0.273	0.452	0.467	0.822	0.659	0.785
Zeb2	0.754	1.798	1.033	1.036	0.558	0.451	0.0723	0.302	0.3	0.577
Lass6	0.282	1.283	0.415	0.814	1.122	0.778	0.199	0.678	0.416	0.262
Zfp385b	0.924	1.703	1.928	1.597	1.606	0.355	0.0887	0.0538	0.11	0.108
Zfp804a	0.833	1.937	1.271	2.612	1.574	0.405	0.0527	0.204	0.00899	0.115

L3mbtl1	0.906	1.715	0.761	2.55	1.423	0.365	0.0864	0.447	0.0108	0.155
Zfp697	0.73	0.586	0.277	0.441	0.215	0.465	0.558	0.782	0.659	0.83
Zfp462	1.302	1.346	1.489	1.966	1.463	0.193	0.178	0.137	0.0493	0.143
Bnc2	0.958	0.469	0.261	0.384	0.021	0.338	0.639	0.794	0.701	0.983
Dmrta1	0.406	0.202	0.049	0.192	0.069	0.685	0.84	0.961	0.848	0.945
Dmrta2	0.642	0.84	1.206	0.327	0.795	0.521	0.401	0.228	0.744	0.426
E2f2	1.157	1.682	2.438	2.375	0.939	0.247	0.0925	0.0148	0.0176	0.347
Zfp128	0.826	0.233	1.068	0.517	0.278	0.409	0.816	0.285	0.605	0.781
Zfp324	0	1.006	2.445	0.307	1.26	1	0.314	0.0145	0.759	0.208
Zfp14	0.577	1.931	1.645	2.604	0.069	0.564	0.0535	0.1	0.00922	0.945
Tshz3	2.675	1.177	2.268	1.4	1.07	0.00747	0.239	0.0233	0.162	0.285
Zfp536	0.567	1.681	2.771	0.646	1.034	0.571	0.0927	0.00559	0.518	0.301
Zfp473	0.107	0.138	0.21	0.026	1.548	0.915	0.89	0.834	0.979	0.122
Zdhhc13	1.19	0.433	0.754	0.164	1.656	0.234	0.665	0.451	0.87	0.0977
Zfp771	0.251	0.529	2.601	0.411	0.987	0.802	0.597	0.00929	0.681	0.324
Zfp668	0.399	0.473	0.715	0.821	0.436	0.69	0.636	0.475	0.412	0.663
Zfp317	0.197	0.127	1.085	0.556	0.126	0.844	0.899	0.278	0.578	0.9
Zfp846	0.226	1.241	2.101	1.386	3.156	0.821	0.215	0.0356	0.166	0.0016
Npat	1.344	1.845	1.597	1.874	2.106	0.179	0.065	0.11	0.061	0.0352
Zbtb38	0.454	2.332	0.292	2.81	1.855	0.65	0.0197	0.77	0.00496	0.0636
Zfp300	0.23	0.437	0.044	0.58	0.36	0.818	0.662	0.965	0.562	0.719
Hsf3	1.126	0.543	0.403	0.529	0.851	0.26	0.587	0.687	0.597	0.395
Tbx22	0.308	0.183	0.084	0.111	0.092	0.758	0.855	0.933	0.912	0.927
Tgif2lx1	1.401	0.713	1.706	1.213	0.61	0.161	0.476	0.0879	0.225	0.542
Zfp711	0.628	1.62	0.36	2.426	1.19	0.53	0.105	0.719	0.0153	0.234
Hdx	1.468	1.172	0.457	1.133	1.416	0.142	0.241	0.648	0.257	0.157
Klf8	1.074	0.507	0.23	0.244	1.024	0.283	0.612	0.818	0.807	0.306
Onecut3	0.581	0.371	1.795	0.226	0.235	0.561	0.711	0.0727	0.821	0.814
Zfp277	0.317	0.152	0.249	0.014	0.082	0.751	0.879	0.803	0.989	0.935
Obox3	1.267	0.336	0.282	0.126	1.896	0.205	0.737	0.778	0.9	0.0579
Grhl2	0.379	0.639	0.422	0.879	0.542	0.705	0.523	0.673	0.38	0.588
Fev	0.451	0.493	0.689	0.851	0.844	0.652	0.622	0.491	0.395	0.399
Ciao1	0.595	0.44	0.485	0.381	0.634	0.552	0.66	0.628	0.703	0.526
Esrra	0.68	0.864	1.072	0.468	1.404	0.496	0.388	0.284	0.64	0.16
Esrrb	0.814	1.325	1.472	0.678	0.698	0.415	0.185	0.141	0.498	0.485
Esrrg	0.813	0.59	0	1.137	0.078	0.416	0.555	1	0.256	0.938
Hsf4	0.519	0.8	2.895	0.29	0.369	0.604	0.423	0.00379	0.772	0.712
Nr5a1	0.575	0.7	0.35	0.514	0.662	0.565	0.484	0.726	0.607	0.508

Nr5a2	1.126	0.492	0.208	0.602	0.157	0.26	0.623	0.835	0.547	0.875
Creb3l1	0.558	0.977	0	0.935	0.141	0.577	0.329	1	0.35	0.888
Zfp146	0.188	0.001	0.996	0.003	0.051	0.851	0.999	0.319	0.998	0.959
Zfp260	0.939	0.777	1.561	0.907	1.622	0.348	0.437	0.118	0.364	0.105
Scml4	0.071	0.105	0.188	0.07	0.537	0.943	0.916	0.851	0.944	0.591
Zkscan17	0.884	2.95	2.007	1.97	1.553	0.377	0.00318	0.0447	0.0488	0.121
Zbtb1	0.743	0.571	0.704	0.035	0.281	0.458	0.568	0.482	0.972	0.779
Zfp608	0.902	0.999	1.285	1.479	0.691	0.367	0.318	0.199	0.139	0.49
Zfp346	0.066	0.536	0.741	0.016	0.458	0.947	0.592	0.459	0.987	0.647
Foxl2	0.503	0.058	0.041	0.273	0.084	0.615	0.954	0.967	0.785	0.933
Ecsit	0.94	0.946	1.319	1.001	1.148	0.347	0.344	0.187	0.317	0.251
Zscan20	0.75	0.03	0.05	0.499	0.288	0.453	0.976	0.96	0.618	0.773
Chd5	1.148	2.306	4.042	2.163	0.975	0.251	0.0211	5.3e-05	0.0305	0.33
Zfp512	1.331	1.689	0.523	1.334	1.008	0.183	0.0912	0.601	0.182	0.314
Zfp384	1.085	0	0.457	0.041	0.362	0.278	1	0.648	0.967	0.717
Nat14	0.746	2.275	2.565	1.585	0.786	0.456	0.0229	0.0103	0.113	0.432
Zfp446	1.052	0.059	0.815	1.085	1.479	0.293	0.953	0.415	0.278	0.139
Foxi2	0.323	0.084	0.136	0.143	0.464	0.747	0.933	0.892	0.886	0.643
Etv3	0.393	0.026	0.302	0.087	0.476	0.694	0.979	0.763	0.931	0.634
Irf5	1.033	0.711	0.613	1.22	2.081	0.302	0.477	0.54	0.222	0.0374
Zbtb11	1.344	1.602	0.371	1.187	1.281	0.179	0.109	0.711	0.235	0.2
Tlx3	0.319	0.103	0.275	0.08	0.512	0.75	0.918	0.783	0.936	0.609
Nrk	1.558	0.008	0.366	0.206	0.414	0.119	0.994	0.714	0.837	0.679
Mixl1	0.548	0.503	0.075	1.474	1.275	0.584	0.615	0.94	0.141	0.202
Arntl2	0.165	2.444	0.559	0.567	0.48	0.869	0.0145	0.576	0.571	0.631
Zfp398	0.251	2.925	2.268	1.935	0.08	0.802	0.00344	0.0233	0.053	0.936
Spib	0.853	0.154	0.083	0.228	0.085	0.394	0.878	0.934	0.82	0.932
Zfp354b	1.226	0.57	2.865	0.818	0.55	0.22	0.569	0.00417	0.414	0.582
Npas3	1.03	0.252	1.087	0.458	1.127	0.303	0.801	0.277	0.647	0.26
Zdhhc8	0.222	0.751	1.273	0.556	0.49	0.824	0.452	0.203	0.578	0.624
Znhit2-ps	0.838	0.35	0.466	0.536	0.962	0.402	0.726	0.641	0.592	0.336
Mga	0.407	0.52	0.772	0.348	0.974	0.684	0.603	0.44	0.728	0.33
Zfp385a	0.252	0.225	0.337	0.883	0.023	0.801	0.822	0.736	0.377	0.982
Scmh1	0.108	0.06	0.192	0.466	0.43	0.914	0.952	0.848	0.641	0.667
Zfp292	0.105	0.389	0.617	0.55	1.724	0.916	0.697	0.537	0.582	0.0847
Spdef	0.522	0.198	1.164	0.281	1.334	0.602	0.843	0.244	0.779	0.182
Foxe3	0.499	0.62	0.583	0.888	1.319	0.618	0.535	0.56	0.374	0.187
Snai3	1.244	0.011	1.49	0.225	1.199	0.213	0.991	0.136	0.822	0.231

Zfp238	0.614	2.424	1.866	1.196	0.887	0.539	0.0153	0.062	0.232	0.375
Zfp330	0.407	0.275	0.137	0.379	0.01	0.684	0.783	0.891	0.705	0.992
Pttg1	0.48	3.027	0.861	2.505	1	0.631	0.00247	0.39	0.0123	0.317
Hnf4g	0.876	0.055	0.296	0.046	0.003	0.381	0.956	0.767	0.963	0.998
Zfp354c	0.448	1.731	1.891	0.971	1.465	0.654	0.0834	0.0587	0.332	0.143
Zfp672	0.88	0.745	0.648	0.277	0.869	0.379	0.456	0.517	0.782	0.385
Zfp750	0.622	0.016	0.226	0.497	0.01	0.534	0.987	0.821	0.619	0.992
Zfp182	0.228	1.465	0.303	0.288	1.62	0.82	0.143	0.762	0.773	0.105
Zfp653	0.507	0.766	0.436	0.466	1.328	0.612	0.444	0.663	0.641	0.184
Zfyve27	0.567	0.727	1.913	0.485	0.688	0.571	0.467	0.0557	0.628	0.491
Rfx7	0.422	0.234	1.163	0.64	1.835	0.673	0.815	0.245	0.522	0.0665
Rc3h2	0.095	0.031	0.365	0.087	1.358	0.924	0.975	0.715	0.931	0.175
Taf2	0.645	0.071	0.155	0.094	0.247	0.519	0.943	0.877	0.925	0.805
Zdhhc17	1.284	1.715	1.613	1.539	0.713	0.199	0.0864	0.107	0.124	0.476
Zmat4	0.556	1.634	0.45	1.426	0.414	0.578	0.102	0.653	0.154	0.679
Fubp3	0.048	0.447	0.261	0.564	0.599	0.962	0.655	0.794	0.573	0.549
Zbtb26	0.26	0.071	0.004	0.642	1.378	0.795	0.943	0.997	0.521	0.168
Zhx3	0.455	0.199	0.118	0.432	0.372	0.649	0.842	0.906	0.666	0.71
L3mbtl4	0.697	0.345	0.759	0.259	0.803	0.485	0.73	0.448	0.796	0.422
Rfx6	0.342	0.244	0.572	0.443	0.111	0.732	0.807	0.567	0.658	0.912
Zmiz1	0.748	0.65	0.171	0.795	0.251	0.454	0.516	0.864	0.427	0.802
Ep300	1.191	0.006	1.775	0.013	1.198	0.234	0.995	0.0759	0.99	0.231
Zfp414	2.078	0.602	1.852	0.253	1.331	0.0377	0.547	0.064	0.8	0.183
Zfp236	0.403	0.47	1.099	0.552	0.142	0.687	0.638	0.272	0.581	0.887
Zfp516	0.464	0.9	0.809	0.912	0.464	0.643	0.368	0.418	0.362	0.643
Zfp335	0.308	0.011	0.346	0.004	0.728	0.758	0.991	0.729	0.997	0.466
Zfp786	0.34	0.613	1.4	0.723	0.584	0.734	0.54	0.162	0.469	0.559
AW146020	1.552	0.109	1.291	0.614	0.633	0.121	0.913	0.197	0.539	0.527
Zfp78	0.479	0.26	0.145	0.388	0.138	0.632	0.795	0.885	0.698	0.89
Zfp82	0.173	0.013	0.59	0.001	0.02	0.863	0.99	0.555	0.999	0.984
Snapc5	0.628	0.425	0.79	0.151	0.768	0.53	0.671	0.429	0.88	0.443
Zmynd12	0.759	0.117	1.041	0.947	0.519	0.448	0.907	0.298	0.344	0.604
Zfp780b	0.682	0.507	1.036	0.996	2.305	0.495	0.612	0.3	0.319	0.0212
Morc3	0.365	0.842	1.81	0.623	0.165	0.715	0.4	0.0703	0.533	0.869
Nr1d2	0.344	0.302	0.957	0.552	1.761	0.731	0.763	0.339	0.581	0.0783
Zranb1	0.559	0.851	1.242	0.975	0.604	0.576	0.395	0.214	0.329	0.546
Batf3	1.798	0.262	0.204	0.265	1.508	0.0721	0.793	0.838	0.791	0.132
Zcwpw1	0.789	0.155	0.136	0.384	0.605	0.43	0.877	0.892	0.701	0.545

Zhx2	1.238	1.766	1.419	1.914	1.32	0.216	0.0774	0.156	0.0556	0.187
Baz2b	0.319	0.152	2.127	0.159	2.103	0.75	0.879	0.0334	0.874	0.0354
Hdac1	0.878	1.798	2.977	1.403	1.055	0.38	0.0722	0.00291	0.161	0.292
Hmg1l1	0.112	1.252	1.087	0.286	0.294	0.911	0.211	0.277	0.775	0.769
Zfp560	0.114	0.204	1.71	0.503	1.301	0.909	0.838	0.0872	0.615	0.193
Znhit3	0.659	0.332	0.344	0.602	0.464	0.51	0.74	0.731	0.547	0.643
Zfp960	0.625	0.018	1.76	0.011	1.926	0.532	0.986	0.0783	0.991	0.0541
Zbtb9	1.008	0.738	0.51	0.982	0.482	0.314	0.461	0.61	0.326	0.63
E2f6	1.078	1.342	1.419	1.198	1.349	0.281	0.179	0.156	0.231	0.177
Sall2	0.984	2.372	1.175	2.219	0.716	0.325	0.0177	0.24	0.0265	0.474
Fbxw7	0.707	2.93	1.579	2.373	0.908	0.479	0.00339	0.114	0.0176	0.364
Klf13	0.626	0.077	0.93	0.259	1.26	0.531	0.939	0.352	0.796	0.208
Dmrt1	1.342	0.503	0.154	0.742	0.331	0.18	0.615	0.878	0.458	0.741
Solh	0.473	0.152	1.079	0.028	1.248	0.636	0.879	0.281	0.978	0.212
Hmgn5	0.353	2.234	1.743	1.899	1.099	0.724	0.0255	0.0813	0.0576	0.272
Preb	0.74	0.473	0.379	0.379	1.118	0.459	0.636	0.705	0.705	0.263
Olig2	0.127	0.026	0.094	0.024	0.107	0.899	0.979	0.925	0.981	0.915
Olig1	0.559	1.16	1.495	0.503	0.861	0.576	0.246	0.135	0.615	0.389
Irx4	1.371	0.063	0.097	0.121	0.494	0.17	0.95	0.923	0.904	0.621
Fubp1	0.799	1.737	1.121	1.398	0.575	0.424	0.0824	0.262	0.162	0.565
Ankzf1	0.695	1.28	1.222	0.928	0.499	0.487	0.2	0.222	0.354	0.618
Zfp644	0.173	0.1	0.951	0.234	1.407	0.863	0.92	0.342	0.815	0.159
Carhsp1	0.522	1.829	1.025	1.497	1.957	0.602	0.0674	0.305	0.135	0.0504
Zfp622	0.802	0.926	0.607	0.256	0.247	0.423	0.354	0.544	0.798	0.805
Zfp410	1.2	0.604	0.86	0.812	0.512	0.23	0.546	0.39	0.417	0.609
Zkscan6	1.486	0.274	1.219	0.654	1.397	0.137	0.784	0.223	0.513	0.162
Dnlz	2.223	0.225	0.009	0.533	1.308	0.0262	0.822	0.993	0.594	0.191
Zmiz2	0.762	0.114	0.255	0.028	0.083	0.446	0.909	0.799	0.978	0.934
Batf	0.444	0.131	0.519	0.234	0.034	0.657	0.896	0.604	0.815	0.973
Atoh7	0.414	1.928	1.176	0.564	1.081	0.679	0.0538	0.24	0.573	0.28
Hif3a	0.192	0.296	0.135	0.362	0.993	0.848	0.767	0.893	0.717	0.321
Ybx2	0.338	0.213	0	0.159	0.011	0.735	0.831	1	0.874	0.991
Insm1	0.654	0.921	2.551	0.819	1.2	0.513	0.357	0.0107	0.413	0.23
Zranb2	1.591	0.327	0.784	0.861	0.837	0.112	0.744	0.433	0.389	0.403
Rfx5	0.189	1.395	3.117	0.68	0.667	0.85	0.163	0.00183	0.497	0.505
Irf7	0.085	0.008	0.001	0.092	0.194	0.932	0.994	0.999	0.927	0.846
Irf3	1.338	1.678	0.99	2.087	0.473	0.181	0.0934	0.322	0.0369	0.636
Irf6	0.443	0.723	0.051	0.183	0.47	0.658	0.47	0.959	0.855	0.638

Irx5	1.269	3.661	1.667	2.235	1.183	0.204	0.000251	0.0955	0.0254	0.237
Zfp326	0.095	0.243	1.318	0.028	0.425	0.924	0.808	0.187	0.978	0.671
Barhl1	0.861	0.248	0.309	0.613	1.187	0.389	0.804	0.757	0.54	0.235
Nfat5	1.324	0.066	0.004	0.637	0.157	0.185	0.947	0.997	0.524	0.875
Zkscan4	0.3	0.216	0.048	0.253	0.105	0.764	0.829	0.962	0.8	0.916
Scrt2	0.469	0.67	0.36	0.509	1.324	0.639	0.503	0.719	0.611	0.186
Foxo4	0.469	0.278	0.165	0.487	0.255	0.639	0.781	0.869	0.626	0.799
Plagl2	1.049	0.22	0.272	0.255	0.255	0.294	0.826	0.786	0.799	0.799
Fezf2	0.722	1.674	1.255	1.449	1.097	0.47	0.0941	0.209	0.147	0.273
Rcan1	0.407	2.116	2.245	1.443	0.763	0.684	0.0344	0.0248	0.149	0.446
Tfip11	0.625	0.404	0.559	0.553	0.275	0.532	0.686	0.576	0.58	0.783
Hes6	0.73	0.923	0.871	1.361	1.446	0.465	0.356	0.384	0.174	0.148
Smad9	0.303	0.099	0.128	0.01	0.041	0.762	0.921	0.898	0.992	0.967
Tcerg1	0.628	0.234	1.284	0.085	0.157	0.53	0.815	0.199	0.932	0.875
Msgn1	1.22	0.429	0.121	0.825	0.009	0.222	0.668	0.904	0.409	0.993
Heyl	0.249	1.641	2.42	0.465	1.188	0.803	0.101	0.0155	0.642	0.235
Patz1	1.118	0.898	2.541	0.847	1.364	0.264	0.369	0.0111	0.397	0.173
Dmrtb1	0.104	0.368	1.642	0.09	0.102	0.917	0.713	0.101	0.928	0.919
Zfp113	0.246	0.565	0.371	0.53	0.269	0.806	0.572	0.711	0.596	0.788
Aatf	1.24	3.279	0.961	3.04	1.899	0.215	0.00104	0.336	0.00237	0.0575
Zmym3	0.219	1.182	1.377	0.145	2.041	0.827	0.237	0.169	0.885	0.0413
Spen	0.489	1.718	0.202	1.255	2.184	0.625	0.0857	0.84	0.21	0.0289
Csda	0.553	2.142	0.918	2.499	2.058	0.58	0.0322	0.359	0.0125	0.0396
Foxo1	0.872	0.759	1.69	1.209	1.297	0.383	0.448	0.0911	0.227	0.195
Foxo3	0.136	0.129	0.025	0.102	0.097	0.892	0.897	0.98	0.919	0.923
Zbtb20	0.112	1.287	3.567	1.219	2.01	0.911	0.198	0.000362	0.223	0.0444
Elf4	0.475	0.348	0.361	0.577	0.665	0.635	0.728	0.718	0.564	0.506
Zfp235	0.256	3.862	1.5	2.492	1.794	0.798	0.000112	0.133	0.0127	0.0728
Zfp111	0.995	0.082	2.097	0.122	0.59	0.32	0.935	0.036	0.903	0.555
Plag1	0.161	0.031	0.187	0.073	0.001	0.872	0.975	0.852	0.942	0.999
Litaf	0.384	2.893	1.098	1.67	1.174	0.701	0.00382	0.272	0.0948	0.24
Ascl3	1.603	0.832	0.422	1.742	1.018	0.109	0.406	0.673	0.0814	0.309
Zbtb33	0.952	1.38	0.52	1.791	0.81	0.341	0.168	0.603	0.0733	0.418
Gmeb1	0.469	0.626	0.075	0.598	0.469	0.639	0.531	0.94	0.55	0.639
Insm2	1.059	0.011	0.033	0.333	0.18	0.29	0.991	0.974	0.739	0.857
Gtf2ird1	0.984	1.641	1.185	1.258	1.041	0.325	0.101	0.236	0.209	0.298
Tbx20	0.824	0.365	0.126	0.38	0.321	0.41	0.715	0.9	0.704	0.748
Zfp276	0.222	0.003	0.3	0.077	0.543	0.824	0.998	0.764	0.939	0.587

Zc3h8	0.487	0.822	0.963	0.75	0.862	0.626	0.411	0.336	0.453	0.388
Zmynd15	0.61	0.024	0.015	0.114	0.1	0.542	0.981	0.988	0.909	0.92
Zfp112	0.296	0.68	1.229	0.631	1.368	0.767	0.497	0.219	0.528	0.171
Tbx21	0.161	1.262	1.565	1.056	2.299	0.872	0.207	0.118	0.291	0.0215
Rbak	0.155	0.198	1.282	0.447	1.358	0.877	0.843	0.2	0.655	0.174
Zfp318	0.292	1.3	1.642	0.063	1.013	0.77	0.194	0.101	0.95	0.311
Hic2	0.85	1.53	0.01	1.9	1.194	0.395	0.126	0.992	0.0574	0.232
Sall1	0.122	1.386	0.437	0.906	1.984	0.903	0.166	0.662	0.365	0.0473
Zbtb32	0.432	1.896	1.055	0.432	0.866	0.666	0.0579	0.291	0.666	0.387
Bcl11b	0.762	1.518	1.91	1.174	1.158	0.446	0.129	0.0561	0.241	0.247
Mlxipl	0.894	0.008	0.025	0.345	0.001	0.371	0.994	0.98	0.73	0.999
Thap11	0.003	1.638	2.594	1.349	2.307	0.998	0.101	0.00949	0.177	0.021
Edf1	0.233	0	0.107	0.005	0.156	0.816	1	0.915	0.996	0.876
Zfp191	0.564	0.901	1.153	0.608	1.141	0.573	0.368	0.249	0.543	0.254
Foxj2	0.668	1.874	0.281	2.024	0.702	0.504	0.061	0.779	0.043	0.483
Zfp872	0.523	0.018	1.345	0.043	2	0.601	0.986	0.179	0.966	0.0455
Zcchc17	0.671	1.723	3.156	1.131	0.752	0.502	0.0849	0.0016	0.258	0.452
Klf14	0.818	0.099	0.691	0.097	0.651	0.413	0.921	0.49	0.923	0.515
Zfp827	0.758	1.899	1.352	2.081	1.227	0.448	0.0576	0.176	0.0374	0.22
Zfp800	0.338	1.196	1.166	0.59	0.114	0.735	0.232	0.244	0.555	0.909
Zfp296	0.642	0.715	0.092	1.519	1.177	0.521	0.475	0.927	0.129	0.239
Yeats4	0.005	1.625	1.802	0.402	1.252	0.996	0.104	0.0715	0.688	0.211
Foxb1	0.262	0.321	1.1	0.196	1.516	0.793	0.748	0.272	0.845	0.13
Irx6	0.094	0.001	0.078	0.001	0.043	0.925	0.999	0.938	0.999	0.966
Sp5	0.43	0.459	0.063	0.482	0.478	0.667	0.646	0.95	0.63	0.633
Zfp280b	0.66	0.48	0.94	0.033	0.534	0.509	0.631	0.347	0.974	0.593
Zfp110	1.479	0.883	2.352	0.835	1.165	0.139	0.377	0.0187	0.404	0.244
Zfand6	0.021	0.469	1.243	0.068	1.503	0.983	0.639	0.214	0.946	0.133
Zfp784	0.613	0.006	0.036	0.108	0.257	0.54	0.995	0.971	0.914	0.797
Zfp524	0.969	1.809	2.029	0.735	0.461	0.333	0.0705	0.0424	0.462	0.645
Sarnp	0.342	0.021	1.271	0.357	1.337	0.732	0.983	0.204	0.721	0.181
Zdhhc12	0.929	0.063	0.058	0.433	0.131	0.353	0.95	0.954	0.665	0.896
Dmap1	0.455	0.85	0.123	0.991	1.28	0.649	0.395	0.902	0.322	0.201
Klf15	0.045	0.013	2.155	0.02	1.706	0.964	0.99	0.0312	0.984	0.0881
Blzf1	1.319	0.243	1.037	0.961	0.29	0.187	0.808	0.3	0.336	0.772
Zfand1	1.038	2.324	1.076	2.556	1.28	0.299	0.0201	0.282	0.0106	0.2
Taf12	1.481	2.899	0.487	1.875	1.61	0.139	0.00375	0.626	0.0608	0.107
Zmat2	0.683	1.339	2.064	0.772	0.701	0.495	0.181	0.039	0.44	0.483

Zmynd11	0	0.534	0.512	0.048	0.648	1	0.593	0.609	0.962	0.517
2210012G02Rik	0.821	0.333	0.931	0.299	1.107	0.412	0.739	0.352	0.765	0.268
Drap1	0.23	0.77	0.472	0.54	0.967	0.818	0.442	0.637	0.589	0.333
Zfp474	1.736	0.102	0.192	0.745	0.482	0.0825	0.919	0.848	0.457	0.63
Zxdb	0.204	1.178	0.178	0.87	1.196	0.838	0.239	0.859	0.384	0.232
Tcf25	1.015	1.343	1.511	1.358	0.946	0.31	0.179	0.131	0.175	0.344
Lztr1	0.82	0.968	1.293	0.54	1.079	0.412	0.333	0.196	0.589	0.281
Hmg20a	0.073	0.485	0.549	0.046	0.199	0.942	0.628	0.583	0.963	0.842
Cir1	0.051	0.174	1.459	0.02	0.611	0.959	0.862	0.145	0.984	0.541
Zdhhc6	0.48	0.242	0.586	0.29	0.869	0.631	0.809	0.558	0.772	0.385
Zfp830	0.888	0.313	0.915	0.273	0.273	0.375	0.754	0.36	0.785	0.785
Zbtb8os	0.373	0.244	0.048	0.159	0.372	0.709	0.807	0.962	0.874	0.71
Zfp787	0.733	0.302	0.87	0.181	1.161	0.463	0.763	0.384	0.856	0.246
Rnf141	1.213	2.395	0.948	2.018	1.168	0.225	0.0166	0.343	0.0435	0.243
Zmat5	0.716	1.393	0.756	1.721	2.654	0.474	0.163	0.449	0.0852	0.00797
Zmynd19	0.385	0.513	0.951	0.808	1.424	0.7	0.608	0.342	0.419	0.154
Zcrb1	0.478	0.497	0.298	0.596	0.483	0.633	0.619	0.766	0.551	0.629
Pfdn1	0.353	0.189	0.005	0.775	0.051	0.724	0.85	0.996	0.438	0.959
Gatad1	1.023	0.837	1.02	0.568	0.302	0.306	0.403	0.308	0.57	0.763
Zfp329	0.654	0.653	0.978	0.204	1.05	0.513	0.514	0.328	0.838	0.294
Zkscan14	1.118	0.711	0.24	0.256	0.444	0.263	0.477	0.81	0.798	0.657
Zfp422	1.396	0.934	0.946	0.55	0.529	0.163	0.35	0.344	0.582	0.597
Lass4	0.82	0.19	0.026	0.308	0.636	0.412	0.849	0.979	0.758	0.525
Zc3h13	1.03	3.182	2.233	2.738	1.588	0.303	0.00146	0.0255	0.00619	0.112
Gcfc1	0.358	1.055	2.371	0.534	1.52	0.72	0.292	0.0177	0.593	0.128
Zfp606	1.834	0.169	0.972	0.642	2.2	0.0667	0.866	0.331	0.521	0.0278
Zfp639	0.303	0.107	1.096	0.16	0.803	0.762	0.915	0.273	0.873	0.422
Ilf2	0.815	0.646	0.695	0.257	0.507	0.415	0.518	0.487	0.797	0.612
Mrrf	0.418	1.393	0.07	1.123	1.224	0.676	0.164	0.944	0.261	0.221
Zfp169	0.08	0.611	0.219	0.192	1.189	0.936	0.541	0.827	0.848	0.234
Zcchc3	1.526	2.069	1.618	1.702	0.754	0.127	0.0386	0.106	0.0887	0.451
Zcchc10	0.487	0.979	2.181	0.206	0.517	0.626	0.328	0.0292	0.837	0.605
Zfp706	0.532	0.809	0.984	0.503	0.429	0.595	0.418	0.325	0.615	0.668
Zfp593	1.05	0.479	0.452	0.604	1.349	0.294	0.632	0.651	0.546	0.177
Rchy1	1.132	1.69	0.183	1.188	0.387	0.258	0.0909	0.855	0.235	0.699
Zdhhc21	0.107	0.221	0.025	0.142	0.082	0.915	0.825	0.98	0.887	0.935
Zmym1	0.561	0.639	0.053	0.268	0.556	0.575	0.523	0.958	0.789	0.578
Ciz1	0.601	0.716	1.188	0.483	0.821	0.548	0.474	0.235	0.629	0.411

Phf5a	0.445	2.776	0.264	2.116	1.369	0.656	0.0055	0.792	0.0343	0.171
Zfp579	0.403	0.911	0.509	0.013	0.36	0.687	0.362	0.611	0.99	0.719
Zfyve21	1.029	1.533	0.119	1.719	0.916	0.304	0.125	0.905	0.0857	0.36
Mrpl28	0.674	1.116	0.184	1.103	1.377	0.5	0.264	0.854	0.27	0.168
Zfp740	1.184	1.246	1.4	2.051	1.801	0.236	0.213	0.161	0.0402	0.0717
Rreb1	0.564	1.097	0.718	0.04	0.923	0.573	0.273	0.473	0.968	0.356
Phtf2	2.279	2.115	2.083	1.814	0.828	0.0227	0.0344	0.0372	0.0696	0.407
Zfand2b	0.215	0.005	1.014	0.055	1.05	0.83	0.996	0.311	0.956	0.294
Foxk2	0.906	0.135	0.57	0.404	0.524	0.365	0.893	0.569	0.686	0.6
Tulp4	0.19	0.36	1.44	0.315	0.568	0.849	0.719	0.15	0.753	0.57
Zfp467	1.236	1.114	1.036	1.211	1.297	0.216	0.265	0.3	0.226	0.195
Zfp580	0.395	0.432	0.36	0.433	0.707	0.693	0.666	0.719	0.665	0.48
Thap7	0.778	0.016	0.542	0.407	1.205	0.437	0.987	0.588	0.684	0.228
Zfp707	0.265	0.432	0.485	0.41	1.25	0.791	0.666	0.628	0.682	0.211
Zdhhc3	0.503	0.783	1.077	0.858	0.981	0.615	0.433	0.282	0.391	0.326
Zc3h15	0.009	0.097	0.648	0	0.441	0.993	0.923	0.517	1	0.659
Zcchc9	0.537	0.083	1.601	0.07	1.172	0.591	0.934	0.109	0.944	0.241
Cnot8	0.833	0.776	0.931	1.083	1.937	0.405	0.438	0.352	0.279	0.0528
Zfp688	0.338	0.445	0.187	0.342	0.812	0.735	0.656	0.852	0.732	0.417
Zfp397	0.436	0.014	1.086	0.237	2.194	0.663	0.989	0.277	0.813	0.0282
Elf2	2.627	1.176	1.525	0.905	0.243	0.00861	0.239	0.127	0.366	0.808
Arap1	0.237	0.135	0.131	0.124	0.872	0.813	0.893	0.896	0.901	0.383
Casz1	0.957	1.394	0.696	1.054	0.332	0.338	0.163	0.486	0.292	0.74
Zswim7	0.114	0.843	1.593	1.472	0.349	0.909	0.399	0.111	0.141	0.727
Zfp511	0.336	0.019	0.09	0.028	0.58	0.737	0.985	0.928	0.978	0.562
Tcf23	0.316	0.008	0.001	0.008	0.023	0.752	0.994	0.999	0.994	0.982
Zfp219	0.031	0.021	0.21	0.018	0.44	0.975	0.983	0.834	0.986	0.66
Znhit1	0.324	0.292	0.403	0.304	0.429	0.746	0.77	0.687	0.761	0.668
Mier2	0.482	0.562	0	0.542	0.852	0.63	0.574	1	0.588	0.394
Atad2	0.793	1.755	1.178	0.884	1.055	0.428	0.0792	0.239	0.377	0.291
Bbx	0.602	0.741	1.788	0.048	0.41	0.547	0.458	0.0738	0.962	0.682
Zdhhc2	0.76	3.354	1.854	3.425	1.522	0.447	0.000797	0.0637	0.000614	0.128
Zc3h11a	0.619	0.82	2.28	0.315	1.278	0.536	0.412	0.0226	0.753	0.201
Zdhhc24	0.179	0.113	0.562	0.064	0.295	0.858	0.91	0.574	0.949	0.768
Zcchc8	0.507	0.734	2.076	0.164	0.875	0.612	0.463	0.0379	0.87	0.382
Prdm16	1.087	0.034	0.303	0.299	0.434	0.277	0.973	0.762	0.765	0.664
Nolc1	0.902	1.074	0.143	0.626	0.911	0.367	0.283	0.886	0.531	0.362
Prdm5	1.248	0.045	0.021	1.18	1.902	0.212	0.964	0.983	0.238	0.0571

Pcgf6	0.292	2.889	0.403	0.571	1.193	0.77	0.00386	0.687	0.568	0.233
Zfp597	1.283	0.082	0.066	0.664	0.29	0.2	0.935	0.947	0.507	0.772
Hsfy2	0.296	0.639	0.055	0.857	0.27	0.767	0.523	0.956	0.392	0.787
Atoh8	0.425	0.147	0.665	0.023	0.262	0.671	0.883	0.506	0.982	0.793
Zfp689	0.464	0.222	0.056	0.373	0.203	0.643	0.824	0.955	0.709	0.839
Rfx4	0.371	2.292	0.744	0.969	0.664	0.711	0.0219	0.457	0.333	0.507
Mier1	0.58	0.154	0.17	0.312	0.161	0.562	0.878	0.865	0.755	0.872
Zdhhc11	0.542	0.147	0.601	0.309	0.006	0.588	0.883	0.548	0.757	0.995
Dmrtc2	0.419	0.084	0.253	0.341	0.215	0.675	0.933	0.8	0.733	0.83
Foxn3	0.622	1.178	1.827	0.873	1.022	0.534	0.239	0.0677	0.383	0.307
Obox1	0.823	0.07	0.611	0.124	0.426	0.41	0.944	0.541	0.901	0.67
Isx	0.49	0.769	0.522	0.434	1.477	0.624	0.442	0.602	0.664	0.14
Cic	0.051	1.213	0.152	0.601	1.468	0.959	0.225	0.879	0.548	0.142
Zbtb43	0.565	0.536	0.23	0.791	1.121	0.572	0.592	0.818	0.429	0.262
Zswim2	1.096	0.213	0.782	0.031	0.065	0.273	0.831	0.434	0.975	0.948
Zcchc24	0.447	0.757	0.62	0.583	0.899	0.655	0.449	0.535	0.56	0.369
Lass5	0.436	0.043	0.358	0.114	0.584	0.663	0.966	0.72	0.909	0.559
Nanog	1.199	0.043	1.006	0.608	0.417	0.231	0.966	0.314	0.543	0.677
Zswim1	0.697	0.005	0.216	0.077	0.346	0.486	0.996	0.829	0.939	0.729
Zfyve19	0.408	0.112	0.466	0.058	0.822	0.683	0.911	0.641	0.954	0.411
Zfp654	0.005	1.012	1.744	0.118	1.557	0.996	0.311	0.0812	0.906	0.119
Tsc22d2	0.411	1.135	0.651	0.246	0.368	0.681	0.256	0.515	0.806	0.713
Zbed3	0.882	1.998	0.587	2.695	1.962	0.378	0.0457	0.557	0.00703	0.0498
Zfp157	0.476	0.039	0.737	0.216	0.707	0.634	0.969	0.461	0.829	0.479
Zfp661	1.022	0.097	0.194	0.845	0.656	0.307	0.923	0.846	0.398	0.512
Zfp558	0.327	0.682	0.483	0.513	1.369	0.744	0.495	0.629	0.608	0.171
Zfp777	0.154	0.013	0.238	0.024	0.336	0.878	0.99	0.812	0.981	0.737
Zfp131	0.124	0.315	0.607	0.211	0.607	0.901	0.753	0.544	0.833	0.544
Zfp566	0.771	0.696	0.423	0.341	1.37	0.441	0.487	0.672	0.733	0.171
Bclaf1	0.187	0.126	1.114	0.095	1.51	0.852	0.9	0.265	0.924	0.131
Zufsp	0.731	0.126	0.23	0.056	0.029	0.465	0.9	0.818	0.955	0.977
Zfp655	0.275	0.132	1.118	0.079	0.188	0.783	0.895	0.264	0.937	0.851
Zfp444	0.323	0.45	1.792	0.143	0.839	0.747	0.653	0.0731	0.886	0.401
Zfp518a	0.794	0.148	0.114	1.09	0.803	0.427	0.882	0.909	0.276	0.422
Zcchc12	1.147	2.9	0.838	2.698	1.299	0.251	0.00373	0.402	0.00697	0.194
Zfp248	1.541	0.317	0.651	0.512	0.919	0.123	0.751	0.515	0.609	0.358
Zfp74	1.042	0.074	1.684	0.211	2.464	0.297	0.941	0.0922	0.833	0.0137
Zkscan3	0.298	1.644	0.118	1.494	2.413	0.766	0.1	0.906	0.135	0.0158

Zfp839	1.08	0.126	0.196	1.028	0.157	0.28	0.9	0.845	0.304	0.875
Prdm4	0.059	0.637	0.026	0.657	0.935	0.953	0.524	0.979	0.511	0.35
Zdhhc4	0.852	0.216	0.085	0.911	0.345	0.394	0.829	0.932	0.362	0.73
Fezf1	1.628	2.205	0.478	1.912	0.478	0.104	0.0275	0.633	0.0558	0.633
Gpbp1	0.206	0.006	1.103	0.079	0.928	0.837	0.995	0.27	0.937	0.353
Hbp1	1.023	0.273	0.219	0.717	0.468	0.306	0.785	0.827	0.473	0.64
Rhox13	0.277	0.231	0.003	0.092	0.043	0.782	0.817	0.998	0.927	0.966
Zbtb8a	1.105	1.477	0.364	0.487	0.562	0.269	0.14	0.716	0.626	0.574
Zdbf2	0.122	0.503	0.173	0.839	1.441	0.903	0.615	0.863	0.401	0.15
Ift57	0.466	1.61	1.628	1.935	2.805	0.641	0.107	0.104	0.053	0.00504
Zfp263	2.077	0.365	1.036	0.651	0.745	0.0378	0.715	0.3	0.515	0.456
Foxp4	0.321	1.49	0.233	1.344	0.719	0.748	0.136	0.816	0.179	0.472
Rnf6	0.097	0.838	0.572	0.3	0.543	0.923	0.402	0.567	0.764	0.587
Nfx1	1.281	1.161	0.636	0.295	0.948	0.2	0.246	0.525	0.768	0.343
Zdhhc16	0.502	0.315	1.656	0.089	0.79	0.616	0.753	0.0976	0.929	0.429
Hopx	0.957	1.165	2.679	1.013	1.39	0.339	0.244	0.00739	0.311	0.164
Cxxc1	1.184	0.408	0.786	0.754	0.934	0.236	0.683	0.432	0.451	0.35
Crtc2	1.204	1.674	1.302	1.213	0.893	0.229	0.0942	0.193	0.225	0.372
Zfp84	0.864	0.038	0.41	0.184	0.86	0.388	0.97	0.682	0.854	0.39
Zfp819	0.353	0.292	0.231	0.203	0.65	0.724	0.77	0.817	0.839	0.516
Sohlh2	1.107	0.206	0.083	0.169	0.564	0.268	0.837	0.934	0.866	0.573
Zswim5	0.875	0.031	0.623	0.49	0.428	0.381	0.975	0.533	0.624	0.669
Batf2	0.261	0.421	0.003	0.103	0.376	0.794	0.674	0.998	0.918	0.707
Morc2a	0.512	0.927	0.852	0.344	0.688	0.609	0.354	0.394	0.731	0.491
Gzf1	0.317	0.103	0.203	0.524	0.128	0.751	0.918	0.839	0.6	0.898
Nkx6-3	1.519	0.155	0.041	0.622	0.844	0.129	0.877	0.967	0.534	0.399
Zkscan1	0.553	0.738	1.826	0.445	1.79	0.58	0.46	0.0679	0.656	0.0734
Zmynd17	1.142	1.037	0.67	0.84	0.345	0.253	0.3	0.503	0.401	0.73
Zcchc13	0.376	0.031	0.016	0.024	0.178	0.707	0.975	0.987	0.981	0.859
Zbtb49	0.578	0.136	0.003	0.21	0.107	0.563	0.892	0.998	0.834	0.915
Zbtb3	0.949	0	0	0.38	0.028	0.342	1	1	0.704	0.978
Taf1d	0.278	2.089	2.454	1.575	0.733	0.781	0.0367	0.0141	0.115	0.464
Wbp7	1.163	0.224	0.222	0.977	1.111	0.245	0.823	0.824	0.328	0.266
Pou5f2	1.106	0.418	1.343	0.841	2.006	0.269	0.676	0.179	0.4	0.0449
Zc3h14	0.014	0.058	0.617	0.066	0.821	0.989	0.954	0.537	0.947	0.412
Zbtb4	0.67	2.209	1.982	1.627	0.71	0.503	0.0272	0.0475	0.104	0.478
Kdm5b	1.096	1.637	0.634	1.454	0.215	0.273	0.102	0.526	0.146	0.83
Morc4	0.712	0.279	0.035	0.354	0.031	0.476	0.78	0.972	0.723	0.975

Klf17	0.305	0.005	0.199	0.118	0.611	0.76	0.996	0.842	0.906	0.541
Zfp821	0.192	0.389	0.004	0.268	0.911	0.848	0.697	0.997	0.789	0.362
Zdhhc20	0.24	0.079	0.294	0.202	0.38	0.81	0.937	0.769	0.84	0.704
Zmym2	0.399	0.68	1.453	0.671	2.004	0.69	0.496	0.146	0.502	0.045
Zc3h18	0.502	1.049	0.686	1.357	1.691	0.616	0.294	0.493	0.175	0.0909
Gon4l	0.851	0.021	0.114	0.296	0.702	0.395	0.983	0.909	0.767	0.483
Tbx18	1.149	2.167	1.832	1.031	0.465	0.251	0.0303	0.0669	0.303	0.642
Msrb2	0.556	0.097	0.167	0.073	0.751	0.578	0.923	0.867	0.942	0.453
Lass2	0.709	1.918	1.844	1.188	1.392	0.478	0.0551	0.0652	0.235	0.164
Gpbp1l1	0.198	0.418	0.705	0.432	0.572	0.843	0.676	0.481	0.666	0.567
A930001N09Rik	0.829	1.215	0.329	1.164	0.745	0.407	0.224	0.742	0.245	0.456
Zfp142	1.085	1.158	0.847	1.017	0.731	0.278	0.247	0.397	0.309	0.465
Nkrf	0.944	1.679	1.185	1.473	0.992	0.345	0.0931	0.236	0.141	0.321
Zfp266	0.985	0.053	1.776	0.171	1.462	0.325	0.958	0.0758	0.864	0.144
Prdm8	0.87	1.736	2.856	1.448	1.001	0.384	0.0825	0.00429	0.148	0.317
Csrnp3	0.91	0.028	0.025	0.148	0.507	0.363	0.978	0.98	0.882	0.612
Zfp712	0.389	0.533	1.753	0.117	0.767	0.697	0.594	0.0797	0.907	0.443
Zfp687	1.219	1.402	1.344	1.951	0.854	0.223	0.161	0.179	0.0511	0.393
Creb3l4	0.14	0.103	0.181	0.008	0.251	0.889	0.918	0.856	0.994	0.802
Zfyve20	0.601	1.985	1.658	2.112	1.526	0.548	0.0471	0.0974	0.0347	0.127
Zfp449	0.335	0.228	0.851	0.128	0.941	0.738	0.82	0.395	0.898	0.347
Brd8	1.526	0.147	0.011	1.418	0.034	0.127	0.883	0.991	0.156	0.973
Zc3h6	0.698	1.335	1.021	1.265	1.018	0.485	0.182	0.307	0.206	0.309
Zc3hav1	0.779	1.173	0.383	0.978	0.805	0.436	0.241	0.702	0.328	0.421
Brpf1	1.481	0.616	0.968	1.857	1.929	0.139	0.538	0.333	0.0634	0.0538
Zcchc4	1.148	0.959	0.727	0.711	0.802	0.251	0.338	0.467	0.477	0.422
Tsc22d4	0.92	0.008	0.671	0.001	0.029	0.358	0.994	0.502	0.999	0.977
Zfp623	0.928	0.341	0.033	0.475	0.065	0.353	0.733	0.974	0.635	0.948
Scyl1	0.437	1.714	0.473	0.851	1.84	0.662	0.0866	0.636	0.395	0.0657
Sp2	0.975	0.025	0.154	0.519	0.464	0.33	0.98	0.878	0.604	0.643
Zfp319	0.105	1.282	1.048	1.293	0.095	0.916	0.2	0.295	0.196	0.924
Bhlhe41	0.108	0.004	0.34	0.046	0.757	0.914	0.997	0.734	0.963	0.449
Spz1	1.089	0.02	0.357	0.265	0.458	0.276	0.984	0.721	0.791	0.647
Zxdc	0.05	0.614	0.246	0.816	0.451	0.96	0.539	0.806	0.415	0.652
Pbx4	0.882	2.156	2.857	1.021	1.189	0.378	0.0311	0.00427	0.307	0.234
Mynn	0.173	0.706	1.498	0.029	2.283	0.863	0.48	0.134	0.977	0.0225
Zfhx4	0.058	1.337	2.091	1.536	2.76	0.954	0.181	0.0365	0.125	0.00578
Zfp202	0.295	0.069	0.088	0.041	0.329	0.768	0.945	0.93	0.967	0.742

Tbl1xr1	0.796	0.598	0.156	0.716	0.389	0.426	0.55	0.876	0.474	0.697
Zbtb22	0.801	1.061	1.605	0.965	0.502	0.423	0.289	0.109	0.335	0.616
Jdp2	0.256	2.9	0.32	1.132	1.711	0.798	0.00373	0.749	0.258	0.087
Tcfcp2l1	0.716	0.344	0.299	0.093	0.423	0.474	0.731	0.765	0.926	0.672
Zfpl1	0.522	0.018	0.726	0.164	1.519	0.602	0.986	0.468	0.87	0.129
Tcfap4	1.302	1.88	0.697	1.795	2.001	0.193	0.0601	0.486	0.0726	0.0454
Glis2	1.075	0.127	0.066	0.248	0.552	0.282	0.899	0.947	0.804	0.581
Trps1	0.485	0	0.001	0	0.003	0.628	1	0.999	1	0.998
Tbx19	0.299	0.108	0.294	0.387	0.203	0.765	0.914	0.769	0.699	0.839
Hes7	0.64	0.113	0.157	0.506	1.041	0.522	0.91	0.875	0.613	0.298
Zfp192	0.86	0.053	0.055	0.117	0.699	0.39	0.958	0.956	0.907	0.484
Klf7	0.189	0.995	1.266	1.258	1.323	0.85	0.32	0.205	0.209	0.186
Aff4	0.183	0.428	0.958	0.235	1.3	0.855	0.669	0.338	0.814	0.194
Strn3	0.396	0.095	2.208	0.252	2.479	0.692	0.924	0.0273	0.801	0.0132
Zfp423	0.381	1.96	1.172	0.545	1.053	0.703	0.05	0.241	0.586	0.293
Olig3	0.662	0.406	0.342	0.237	0.581	0.508	0.685	0.732	0.813	0.561
Hmgb2	1.09	3.459	2.423	2.164	0.725	0.276	0.000541	0.0154	0.0305	0.469
Zfp451	0.953	1.651	0.237	0.445	1.492	0.341	0.0988	0.813	0.656	0.136
Mael	0.462	0.083	0.138	0.016	0.844	0.644	0.934	0.89	0.987	0.399
Znfx1	1.361	0.905	1.16	1.022	1.297	0.174	0.365	0.246	0.307	0.195
Sall4	0.545	0.014	0.114	0.216	0.262	0.586	0.989	0.909	0.829	0.793
Kdm1a	0.388	1.676	0.595	0.365	0.253	0.698	0.0937	0.552	0.715	0.8

8.2. The Reactome pathways for the 24 vs. 0 hour signature

Set	NES	p-value	Ledge
Toll Like Receptor 9 (TLR9) Cascade	3.741	0.000183	Nfkbia, Irf7, Nfkb2, Pik3c3, Mapkapk3, Dusp3, Mef2c, Mapk10, Ager, Myd88, Fos, Ikbkg, Ubc, Mapk3, App, Atf1, Map2k6, Nod1, Map2k1, Irak4, Map2k3, Hmg1l1, Ppp2r5d, Pik3r4, Nfkb1, Rps6ka3, Rps6ka2, Tlr7
Toll Receptor Cascades	3.468	0.000525	Nfkbia, Irf7, Nfkb2, Pik3c3, Mapkapk3, Dusp3, Mef2c, Lgmn, Mapk10, Ager, Ly96, Tlr2, Myd88, Cd180, Fos, Ikbkg, Sigirr, Ubc, Mapk3, Tlr6, App, Atf1, Map2k6, Nod1, Hspd1, Map2k1, Irak4, Map2k3, Hmg1l1, Ppp2r5d, Ctss, Unc93b1, Irf3, Pik3r4, Lbp, Nfkb1, Rps6ka3, Rps6ka2, Tlr7
Toll Like Receptor 4 (TLR4) Cascade	3.434	0.000596	Nfkbia, Irf7, Nfkb2, Mapkapk3, Dusp3, Mef2c, Mapk10, Ager, Ly96, Tlr2, Myd88, Cd180, Fos, Ikbkg, Sigirr, Ubc, Mapk3, Tlr6, App, Atf1, Map2k6, Nod1, Hspd1, Map2k1, Irak4, Map2k3, Hmg1l1, Ppp2r5d, Irf3, Lbp, Nfkb1, Rps6ka3, Rps6ka2
TRAF6 Mediated Induction of proinflammatory cytokines	3.084	0.00204	Nfkbia, Nfkb2, Mapkapk3, Dusp3, Mef2c, Mapk10, Ager, Fos, Ikbkg, Ubc, Mapk3, App, Atf1, Map2k6, Nod1, Map2k1, Map2k3, Hmg1l1, Ppp2r5d, Nfkb1, Rps6ka3, Rps6ka2
TRAF6 mediated NF-kB activation	2.975	0.00293	Nfkbia, Trim25, Ddx58, Ifih1, Nfkb2, Ager
MyD88:Mal cascade initiated on plasma membrane	2.949	0.00319	Nfkbia, Nfkb2, Mapkapk3, Dusp3, Mef2c, Mapk10, Ager, Ly96, Tlr2, Myd88, Fos, Ikbkg, Sigirr, Ubc, Mapk3, Tlr6, App, Atf1, Map2k6, Nod1, Hspd1, Map2k1, Irak4, Map2k3, Hmg1l1, Ppp2r5d, Nfkb1, Rps6ka3, Rps6ka2, Ppp2cb, Mapk14, Tirap, Saa3
Toll Like Receptor 2 (TLR2) Cascade	2.949	0.00319	Nfkbia, Nfkb2, Mapkapk3, Dusp3, Mef2c, Mapk10, Ager, Ly96, Tlr2, Myd88, Fos, Ikbkg, Sigirr, Ubc, Mapk3, Tlr6, App, Atf1, Map2k6, Nod1, Hspd1, Map2k1, Irak4, Map2k3, Hmg1l1, Ppp2r5d, Nfkb1, Rps6ka3, Rps6ka2, Ppp2cb, Mapk14, Tirap, Saa3
Toll Like Receptor TLR1:TLR2 Cascade	2.949	0.00319	Nfkbia, Nfkb2, Mapkapk3, Dusp3, Mef2c, Mapk10, Ager, Ly96, Tlr2, Myd88, Fos, Ikbkg, Sigirr, Ubc, Mapk3, Tlr6, App, Atf1, Map2k6, Nod1, Hspd1, Map2k1, Irak4, Map2k3,

			Hmg1l1, Ppp2r5d, Nfkb1, Rps6ka3, Rps6ka2, Ppp2cb, Mapk14, Tirap, Saa3
Toll Like Receptor TLR6:TLR2 Cascade	2.949	0.00319	Nfkbia, Nfkb2, Mapkapk3, Dusp3, Mef2c, Mapk10, Ager, Ly96, Tlr2, Myd88, Fos, Ikbkg, Sigirr, Ubc, Mapk3, Tlr6, App, Atf1, Map2k6, Nod1, Hspd1, Map2k1, Irak4, Map2k3, Hmg1l1, Ppp2r5d, Nfkb1, Rps6ka3, Rps6ka2, Ppp2cb, Mapk14, Tirap, Saa3
MyD88 dependent cascade initiated on endosome	2.876	0.00403	Nfkbia, Irf7, Nfkb2, Mapkapk3, Dusp3, Mef2c, Mapk10, Ager, Myd88, Fos, Ikbkg, Ubc, Mapk3, App, Atf1, Map2k6, Nod1, Map2k1, Irak4, Map2k3, Hmg1l1, Ppp2r5d, Nfkb1, Rps6ka3, Rps6ka2, Tlr7
Toll Like Receptor 7/8 (TLR7/8) Cascade	2.876	0.00403	Nfkbia, Irf7, Nfkb2, Mapkapk3, Dusp3, Mef2c, Mapk10, Ager, Myd88, Fos, Ikbkg, Ubc, Mapk3, App, Atf1, Map2k6, Nod1, Map2k1, Irak4, Map2k3, Hmg1l1, Ppp2r5d, Nfkb1, Rps6ka3, Rps6ka2, Tlr7
Activated TLR4 signalling	2.867	0.00414	Nfkbia, Irf7, Nfkb2, Mapkapk3, Dusp3, Mef2c, Mapk10, Ager, Ly96, Tlr2, Myd88, Fos, Ikbkg, Sigirr, Ubc, Mapk3, Tlr6, App, Atf1, Map2k6, Nod1, Hspd1, Map2k1, Irak4, Map2k3, Hmg1l1, Ppp2r5d, Irf3, Nfkb1, Rps6ka3, Rps6ka2
MyD88-independent cascade initiated on plasma membrane	2.845	0.00444	Nfkbia, Irf7, Nfkb2, Mapkapk3, Dusp3, Mef2c, Mapk10, Ager, Ly96, Fos, Ikbkg, Ubc, Mapk3, App, Atf1, Map2k6, Nod1, Map2k1, Map2k3, Hmg1l1, Ppp2r5d, Irf3, Nfkb1, Rps6ka3, Rps6ka2
NFkB and MAP kinases activation mediated by TLR4 signaling repertoire	2.804	0.00504	Nfkbia, Nfkb2, Mapkapk3, Dusp3, Mef2c, Mapk10, Ager, Ly96, Fos, Ikbkg, Ubc, Mapk3, App, Atf1, Map2k6, Nod1, Map2k1, Map2k3, Hmg1l1, Ppp2r5d, Nfkb1, Rps6ka3, Rps6ka2
TRAF6 mediated induction of NFkB and MAP kinases upon TLR7/8 or 9 activation	2.737	0.0062	Nfkbia, Nfkb2, Mapkapk3, Dusp3, Mef2c, Mapk10, Ager, Myd88, Fos, Ikbkg, Ubc, Mapk3, App, Atf1, Map2k6, Nod1, Map2k1, Irak4, Map2k3, Hmg1l1, Ppp2r5d, Nfkb1, Rps6ka3, Rps6ka2, Tlr7
Androgen biosynthesis	2.723	0.00648	Srd5a1, Srd5a2, Hsd3b1, Cga, Hsd3b2, Hsd17b3
TAK1 activates NFkB by phosphorylation and activation of IKKs complex	2.644	0.00819	Nfkbia, Nfkb2, Ager, Ikbkg, App, Nod1, Hmg1l1

Interferon alpha/beta signaling	2.583	0.00979	Usp18, Irf9, Irf1, Stat1, Ifitm3, Irf7, Stat2, Ifi27l1, Oas1a, Ifi35, Gm14446, Isg15, Irf4, Oasl1, H2-Q2, H2-Q10
Signal regulatory protein (SIRP) family interactions	2.577	0.00995	Ptk2, Sirpa, Skap2, Cd47, Fyb, Sirpb1a, Tyrobp
Platelet calcium homeostasis	2.575	0.01	Trpc7, Stim1, Atp2b4, Atp2b1, Atp2a3, P2rx1, Trpc6, Slc8a1, Atp2b2
Toll Like Receptor 3 (TLR3) Cascade	2.563	0.0104	Nfkbia, Irf7, Nfkb2, Mapkapk3, Dusp3, Mef2c, Mapk10, Ager, Fos, Ikbkg, Ubc, Mapk3, App, Atf1, Map2k6, Nod1, Map2k1, Map2k3, Hmg1l1, Ppp2r5d, Irf3, Nfkb1, Rps6ka3, Rps6ka2, Zbp1, Ppp2cb, Mapk14, Saa3
TRIF mediated TLR3 signaling	2.563	0.0104	Nfkbia, Irf7, Nfkb2, Mapkapk3, Dusp3, Mef2c, Mapk10, Ager, Fos, Ikbkg, Ubc, Mapk3, App, Atf1, Map2k6, Nod1, Map2k1, Map2k3, Hmg1l1, Ppp2r5d, Irf3, Nfkb1, Rps6ka3, Rps6ka2, Zbp1, Ppp2cb, Mapk14, Saa3
RIG-I/MDA5 mediated induction of IFN-alpha/beta pathways	2.457	0.014	Nfkbia, Trim25, Irf1, Ddx58, Irf7, Tnfaip3, Ifih1, Nfkb2, Isg15
CDO in myogenesis	2.419	0.0156	Mef2c, Cdon, Mef2d, Bnip2, Ctnna1, Map2k6, Myog, Myod1, Tcf12, Mapk14, Ctnna2
Myogenesis	2.419	0.0156	Mef2c, Cdon, Mef2d, Bnip2, Ctnna1, Map2k6, Myog, Myod1, Tcf12, Mapk14, Ctnna2
Innate Immune System	2.331	0.0197	Nfkbia, Trim25, Irf1, Ddx58, Irf7, Tnfaip3, Birc3, Ifih1, Nfkb2, Txnip, Pik3c3, C8b, Isg15, Mapkapk3, Dusp3, Mef2c, Lgmn, C1qc, Mapk10, C8a, Ager, Ly96, Tlr2, Myd88, Bcl2, Cd180, Ube2l6, Fos, Ikbkg, Sigirr, Ubc, Casp4, Mapk3, Tlr6, App, Atf1, Map2k6, Nod1, Dak, Gm15386, Hspd1, Map2k1, Irak4, Map2k3, Hmg1l1, Ppp2r5d, Otud5, Ctss, Unc93b1, Irf3, C6, Pik3r4, Dhx58, Lbp, Nfkb1, Casp9, Rps6ka3, Rps6ka2, Tlr7
Post-translational modification: synthesis of GPI-anchored proteins	2.322	0.0202	Pigl, Pigv, Dpm2, Pigf, Pigw, Pigt, Pign, Pigp, Dpm1, Pigx, Dpm3, Pigq, Piga, Pigc, Plaur, Pgap1, Pigh, Sema6d, Gpaa1, Pigu, Pigk
RIP-mediated NFkB activation via DAI	2.302	0.0213	Nfkbia, Nfkb2, Ager

Viral dsRNA:TLR3:TRIF Complex Activates RIP1	2.302	0.0213	Nfkbia, Nfkb2, Ager
Basigin interactions	2.235	0.0254	Slc7a8, Slc3a2, Ppil2, Slc7a11, Atp1b1, Slc16a3, Slc7a5, Bsg, Cav1
Cytosolic sensors of pathogen-associated DNA	2.208	0.0273	Nfkbia, Nfkb2, Ager, Ikbkg, App, Hmg1l1, Irf3, Nfkb1, Zbp1, Saa3
DAI mediated induction of type I IFNs	2.208	0.0273	Nfkbia, Nfkb2, Ager, Ikbkg, App, Hmg1l1, Irf3, Nfkb1, Zbp1, Saa3
Platelet homeostasis	2.191	0.0284	Pde3a, Kcnmb1, Gng4, Trpc7, Stim1, Atp2b4, Pde2a, Atp2b1, Nos1, Pde5a, Atp2a3, Gng13, Gng8, Gucy1a2, P2rx1, Apob, Pde9a, Trpc6, Ppp2r5d, Pecam1, Gucy1b3, Fgr, Ppp2cb, Mapk14, Slc8a1
Interferon gamma signaling	2.185	0.0289	Irf9, Irf1, Stat1, Vcam1, Irf7, Oas1a, Gbp3, Icam1, Irf4, Pml, Oasl1, Gbp7, H2-Q2, B2m, H2-Q10, Camk2d, Mt2
CDC6 association with the ORC:origin complex	2.142	0.0322	Orc1, Mcm8, Cdc6, E2f1, Orc4, E2f2, Orc3, Orc2, Orc6
MyD88 cascade initiated on plasma membrane	2.089	0.0368	Nfkbia, Nfkb2, Mapkapk3, Dusp3, Mef2c, Mapk10, Ager, Ly96, Myd88, Fos, Ikbkg, Ubc, Mapk3, App, Atf1, Map2k6, Nod1, Map2k1, Irak4, Map2k3, Hmg1l1, Ppp2r5d, Nfkb1, Rps6ka3, Rps6ka2
Toll Like Receptor 10 (TLR10) Cascade	2.089	0.0368	Nfkbia, Nfkb2, Mapkapk3, Dusp3, Mef2c, Mapk10, Ager, Ly96, Myd88, Fos, Ikbkg, Ubc, Mapk3, App, Atf1, Map2k6, Nod1, Map2k1, Irak4, Map2k3, Hmg1l1, Ppp2r5d, Nfkb1, Rps6ka3, Rps6ka2
Toll Like Receptor 5 (TLR5) Cascade	2.089	0.0368	Nfkbia, Nfkb2, Mapkapk3, Dusp3, Mef2c, Mapk10, Ager, Ly96, Myd88, Fos, Ikbkg, Ubc, Mapk3, App, Atf1, Map2k6, Nod1, Map2k1, Irak4, Map2k3, Hmg1l1, Ppp2r5d, Nfkb1, Rps6ka3, Rps6ka2
Synthesis of glycosylphosphatidylinositol (GPI)	2.088	0.0368	Pigl, Pigv, Dpm2, Pigf, Pigw, Pign, Pigp
Signaling by the B Cell Receptor (BCR)	2.079	0.0376	Nfkbia, Cdkn1a, Trpc1, Nfkbie, Plcg2, Rasgrp1, Sykb, Stim1, Lyn, Card11, Btk, Cd79a, Ikbkg, Pik3ap1, Ubc, Psmb8, Psmd9, Hras1, Bcl10, Nr4a1, Akt3, Psmc2, Akt1, Psmd11,

			Kras, Foxo4, Nfkb1, Casp9, Mlst8, Psmd7, Dapp1, Psma2
Antigen Activates B Cell Receptor Leading to Generation of Second Messengers	2.071	0.0383	Trpc1, Plcg2, Sykb, Stim1, Lyn, Btk, Cd79a, Pik3ap1
Effects of PIP2 hydrolysis	2.065	0.0389	Dgka, Trpc7, Dgkb, Dgki, Rasgrp1, Prkcd, Dgkh, Prkcq, Trpc6
Nitric oxide stimulates guanylate cyclase	2.009	0.0446	Pde3a, Kcnmb1, Pde2a, Nos1, Pde5a, Gucy1a2, Pde9a, Gucy1b3
Trafficking and processing of endosomal TLR	1.998	0.0457	Lgmn, Ctss, Unc93b1, Tlr7, Tlr8, Ctsb
Interferon Signaling	1.961	0.0499	Usp18, Irf9, Trim25, Irf1, Stat1, Ddx58, Ifitm3, Vcam1, Irf7, Stat2, Ifi27l1, Eif2ak2, Oas1a, Ifi35, Gm14446, Gbp3, Icam1, Isg15, Irf4, Pml, Oasl1, Gbp7, H2-Q2, B2m, H2-Q10, Camk2d, Mt2, Ifnar1

8.3. The Reactome pathways for the 72 vs. 0 hour signature

Set	NES	p-value	Ledge
Cyclin A/B1 associated events during G2/M transition	3.95	7.82e-05	Cdc25b, Ccna2, Cdk1, Ccnb2, Cdc25c, Mnat1, Plk1, Wee1, Cdc25a
G alpha (z) signalling events	3.601	0.000317	Prkce, Gng2, Gnai1, Rgs17, Rgs4, Adcy5, Gng3, Adcy2, Adra2a, Gnai2, Prkch, Gng12, Rgs20, Gnb4, Gnaz, Prkca, Adcy1, Adcy7, Gng10
Interleukin-6 signaling	3.417	0.000633	Il6st, Stat3, Jak2, Stat1, Ptpn11, Socs3, Il6ra, Tyk2
N-glycan trimming in the ER and Calnexin/Calreticulin cycle	3.396	0.000684	Ganab, Man1b1, Uggt1, Calr, Pdia3, Mlec, Prkcsh, Mogs, Canx, Edem1
Signaling by Robo receptor	3.283	0.00103	Pak7, Robo2, Cap2, Nck2, Pfn2, Pak1, Clasp2, Srgap1, Arhgap39, Sos1, Srgap2, Slit2, Pak3, Evl, Pak4, Robo1, Clasp1, Pfn1
Opioid Signalling	3.276	0.00105	Gnal, Pde4b, Gng2, Gnai1, Ppp3cc, Prkar1b, Ppp3ca, Ppp1r1b, Adcy5, Camk4, Plcb3, Plcb4, Gng3, Adcy2, Ppp3r1, Gnao1, Prkar2a, Prkacb, Gnai2, Gng12, Pde4a, Pde1a, Mapk1, Gnb4, Oprm1, Gnaz, Prkar2b, Prkca, Adcy1, Adcy7, Gng10, Plcb1, Plcb2, Ppp1ca, Itpr2
DARPP-32 events	3.197	0.00139	Pde4b, Ppp3cc, Prkar1b, Ppp3ca, Ppp1r1b, Ppp3r1, Prkar2a, Prkacb, Pde4a
Gap-filling DNA repair synthesis and ligation in GG-NER	3.163	0.00156	Lig1, Pole, Rpa1, Pold3, Pold1, Pcna, Pole2, Rfc1, Rfc4, Rfc3, Rfc5, Pold2, Rfc2
Gap-filling DNA repair synthesis and ligation in TC-NER	3.163	0.00156	Lig1, Pole, Rpa1, Pold3, Pold1, Pcna, Pole2, Rfc1, Rfc4, Rfc3, Rfc5, Pold2, Rfc2
DSCAM interactions	3.025	0.00249	Dcc, Ntn1, Mapk8, Dscam, Mapk12, Pak1, Dscaml1
Calnexin/calreticulin cycle	3.005	0.00266	Ganab, Man1b1, Uggt1, Calr, Pdia3, Prkcsh, Canx, Edem1
Activation of Rac	3.002	0.00268	Pak7, Nck2, Pak1, Sos1, Slit2, Pak3, Pak4, Robo1
Processive synthesis on the C-	2.997	0.00273	Lig1, Rpa1, Pold3, Pold1, Pcna, Fen1, Dna2

strand of the telomere			
N-glycan antennae elongation in the medial/trans-Golgi	2.97	0.00298	St8sia3, Fut8, B4galt5, Mgat3, Mgat4b, B4galt6, Man2a1, St3gal4
Repair synthesis for gap-filling by DNA polymerase in TC-NER	2.961	0.00307	Pole, Rpa1, Pold3, Pold1, Pcna, Pole2, Rfc1, Rfc4, Rfc3, Rfc5, Pold2, Rfc2
Repair synthesis of patch ~27-30 bases long by DNA polymerase	2.961	0.00307	Pole, Rpa1, Pold3, Pold1, Pcna, Pole2, Rfc1, Rfc4, Rfc3, Rfc5, Pold2, Rfc2
Base Excision Repair	2.931	0.00338	Lig1, Pold3, Pold1, Pcna, Fen1, Xrcc1, Mpg, Mutyh, Pold2, Apex1, Lig3, Mbd4, Nthl1, Pold4
Resolution of Abasic Sites (AP sites)	2.931	0.00338	Lig1, Pold3, Pold1, Pcna, Fen1, Xrcc1, Mpg, Mutyh, Pold2, Apex1, Lig3, Mbd4, Nthl1, Pold4
Amino acid synthesis and interconversion (transamination)	2.922	0.00347	Gpt2, Psat1, Psph, Gls, Phgdh, Pycr1, Asns
Transport to the Golgi and subsequent modification	2.904	0.00369	St8sia3, Man1a, Fut8, B4galt5, Mgat3, Mgat4b, B4galt6, Sec31a, Man2a1, St3gal4, Lman1, Man1c1, Man1a2, Sec13, Sec23a, Mgat5, Mcfd2, St6gal1
Botulinum neurotoxicity	2.888	0.00387	Vamp1, Stx7, Stx1a, Stx6, Stx12, Vamp2, Syt2, Syt1, Stx1b, Snap25, Stx11, Stx2
Removal of DNA patch containing abasic residue	2.867	0.00414	Lig1, Pold3, Pold1, Pcna, Fen1, Mpg, Mutyh, Pold2
Resolution of AP sites via the multiple-nucleotide patch replacement pathway	2.867	0.00414	Lig1, Pold3, Pold1, Pcna, Fen1, Mpg, Mutyh, Pold2
DNA Replication	2.86	0.00424	Lig1, Ccna2, Cenpn, Mcm2, Aurkb, Mcm5, Kntc1, Pole, Mcm6, Cdca8, Rpa1, Mcm4, Birc5, Pold3, Incenp, E2f2, Bub1b, Pold1, Pcna, Cenpa, Zw10, Spc25, Nup107, Spc24, Kif23, Fen1, Kif20a, Smc1a, Psmc1, Fbxo5, Cdc7, Psma1, Dbf4, Prim1, Kif2c, Ska1, Dna2, Fam33a, Mcm10, Mcm3, Psmc4, Ccdc99, Bub1, Gmnn, Plk1, Nsl1, Sgol1, Pmf1, Pole2, Zwilch, Cdc45, Rfc1, Pola2, Cenpo, Ercc6l, Cenpf, Cdk2, Nup85, Gins2, Cdc6, Cdc20, Rcc2, Cenpq, Rfc4, Nuf2, Mcm7, Ppp2r5e, Cdt1, Dsn1, Orc2, Sgol2, Rfc3, Mad2l1, Gins4, Cenph, Nup37, Cenpe, Nup133, Cenpk, Psmc2, Rfc5, Kif2a,

			Rad21, Pold2, Cenpm, Gins1, Ppp2r5b, Ndc80, Clasp2, Rfc2, Cdkn1b, Mlf1ip, Pafah1b1, Psmd4, Psmd7, Mcm8, Zwint, Psma4, Psmd5, Psmd12, Psmc3, Sec13, Clasp1, Psmc6, Mapre1, Casc5, Psmb2, Xpo1, Gorasp1
Neuronal System	2.859	0.00425	Gnal, Cacna2d3, Vamp1, Kcnab1, Gng2, Stx7, Hcn1, Hcn4, Grin2a, Gnai1, Gabrg3, Camk2g, Slc38a2, Chrnb2, Gria4, Kcnb2, Dlg4, Kcnj2, Kcnk10, Syn2, Gabbr2, Grip1, Stx1a, Kcnb1, Gabbr1, Gls, Kcnh1, Gjc1, Akap5, Stx6, Grik2, Adcy5, Camk4, Kcnn1, Stx12, Kcnj6, Kcnh8, Gabrb3, Plcb3, Vamp2, Syn1, Syt2, Syt1, Gad1, Panx1, Kcnh7, Cacng4, Gng3, Kcnq2, Stx1b, Dnajc5, Kcnma1, Adcy2, Rasgrf2, Cacna1b, Grin2b, Cacna2d1, Rps6ka3, Grip2, Hspa8, Gabrg2, Slc1a7, Nsf, Snap25, Camkk1, Gria2, Kcng2, Slc1a3, Grin1, Gjd2, Ap2b1, Prkacb, Gabra5, Kcna5, Kcnv1, Gnai2, Gad2, Cplx1, Kcnn2, Cacnb1, Gng12, Camk2b, Gabra3, Hcn3, Stx11, Comt, Stxbp1, Cacna1a, Kcnc1, Chrna4, Arhgef9, Ap2a2, Gria1, Kcnmb2, Cacnb4, Kcnk1, Slc1a1, Mapk1, Gnb4, Kcnh3, Cacng3, Stx2, Rasgrf1, Kcnmb4
Asparagine N-linked glycosylation	2.85	0.00437	St8sia3, Gfpt2, Man1a, Fut8, Alg2, B4galt5, Ganab, Man1b1, Uggt1, Mgat3, Mgat4b, B4galt6, Tusc3, Rpn2, Sec31a, Calr, Dpagt1, Pgm3, Pdia3, Ddost, Man2a1, Alg3, Stt3a, St3gal4, Lman1, Man1c1, Man1a2, Sec13, Mlec, Prkcsh, Sec23a, Alg8, Mogs, Mgat5, Canx, Mcfd2, Edem1
Transport of the SLBP Dependant Mature mRNA	2.833	0.0046	Ncbp1, Nup205, Nup188, Nup107, Nup93, Slbp, Nup50, Nup85, Nup62, Nup37, Nupl1, Nup133, Nup214, Nup155, Rae1, Nxf1, Thoc4, Nup88, Ncbp2, Nup43
Removal of the Flap Intermediate from the C-strand	2.81	0.00495	Rpa1, Pold3, Pold1, Pcna, Fen1, Dna2
S Phase	2.799	0.00513	Lig1, Cdc25b, Ccna2, Mcm2, Mcm5, Pole, Mcm6, Rpa1, Mcm4, Pold3, Pold1, Pcna, Skp2, Fen1, Cdk4, Psmc1, Psma1, Prim1, Dna2, Mcm3, Psmc4, Mnat1, Ccne1, Pole2, Cdc45, Rfc1, Pola2, Cdk2, Gins2, Cdc6, Rfc4, Mcm7, Cdt1, Orc2, Rfc3, Gins4, Psmc2, Rfc5, Myc, Max, Pold2, Wee1, Gins1, Rfc2, Cdkn1b, Cdc25a, Psmd4, Psmd7, Mcm8, Psma4, Psmd5, Psmd12, Psmc3
Transport of the SLBP independent Mature mRNA	2.772	0.00558	Ncbp1, Nup205, Nup188, Nup107, Nup93, Nup50, Nup85, Nup62, Nup37, Nupl1, Nup133, Nup214, Nup155, Rae1, Nxf1, Thoc4, Nup88, Ncbp2, Nup43

Extension of Telomeres	2.765	0.0057	Lig1, Pole, Rpa1, Pold3, Pold1, Pcna, Fen1, Prim1, Dna2, Pole2, Rfc1, Pola2, Rfc4, Rfc3, Ruvbl1, Rfc5, Ruvbl2, Pold2, Rfc2
Transport of Ribonucleoproteins into the Host Nucleus	2.735	0.00624	Nup205, Nup188, Nup107, Kpnb1, Nup93, Nup50, Nup85, Kpna1, Nup62, Nup37, Nupl1, Nup133, Nup214, Nup155, Rae1
Transport of Mature mRNAs Derived from Intronless Transcripts	2.714	0.00665	Ncbp1, Nup205, Nup188, Nup107, Nup93, Slbp, Nup50, Nup85, Nup62, Nup37, Nupl1, Nup133, Nup214, Cpsf1, Nup155, Rae1, Nxf1, Thoc4, Nup88, Ncbp2, Nup43
Neurotransmitter Receptor Binding And Downstream Transmission In The Postsynaptic Cell	2.713	0.00667	Gnal, Gng2, Grin2a, Gnai1, Gabrg3, Camk2g, Chrnb2, Gria4, Dlg4, Kcnj2, Gabbr2, Grip1, Gabbr1, Akap5, Grik2, Adcy5, Camk4, Kcnj6, Gabrb3, Plcb3, Cacng4, Gng3, Adcy2, Rasgrf2, Grin2b, Rps6ka3, Grip2, Gabrg2, Nsf, Camkk1, Gria2, Grin1, Ap2b1, Prkacb, Gabra5, Gnai2, Gng12, Camk2b, Gabra3, Chrna4, Arhgef9, Ap2a2, Gria1, Mapk1, Gnb4, Cacng3, Rasgrf1
Interactions of Vpr with host cellular proteins	2.691	0.00712	Nup205, Nup188, Nup107, Slc25a5, Nup93, Nup50, Nup85, Kpna1, Nup62, Nup37, Nupl1, Nup133, Nup214, Banf1, Nup155, Rae1
Mitotic M-M/G1 phases	2.687	0.00721	Cenpn, Mcm2, Aurkb, Mcm5, Kntc1, Pole, Mcm6, Cdca8, Rpa1, Mcm4, Birc5, Incenp, E2f2, Bub1b, Cenpa, Zw10, Spc25, Nup107, Spc24, Kif23, Kif20a, Smc1a, Psmc1, Fbxo5, Cdc7, Psma1, Dbf4, Prim1, Kif2c, Ska1, Fam33a, Mcm10, Mcm3, Psmc4, Ccdc99, Bub1, Gmnn, Plk1, Nsl1, Sgol1, Pmf1, Pole2, Zwilch, Cdc45, Pola2, Cenpo, Ercc6l, Cenpf, Cdk2, Nup85, Cdc6, Cdc20, Rcc2, Cenpq, Nuf2, Mcm7, Ppp2r5e, Cdt1, Dsn1, Orc2, Sgol2, Mad2l1, Cenph, Nup37, Cenpe, Nup133, Cenpk, Psmc2, Kif2a, Rad21, Cenpm, Ppp2r5b, Ndc80, Clasp2, Mlf1ip, Pafah1b1, Psmd4, Psmd7, Mcm8, Zwint, Psma4, Psmd5, Psmd12, Psmc3, Sec13, Clasp1, Psmc6, Mapre1, Casc5, Psmb2, Xpo1, Gorasp1
Transport of Mature mRNA Derived from an Intronless Transcript	2.651	0.00801	Ncbp1, Nup205, Nup188, Nup107, Nup93, Nup50, Nup85, Nup62, Nup37, Nupl1, Nup133, Nup214, Cpsf1, Nup155, Rae1, Nxf1, Thoc4, Nup88, Ncbp2, Nup43
Telomere C-strand (Lagging Strand) Synthesis	2.6	0.00932	Lig1, Pole, Rpa1, Pold3, Pold1, Pcna, Fen1, Prim1, Dna2, Pole2, Rfc1, Pola2, Rfc4, Rfc3, Rfc5, Pold2, Rfc2

Proteolytic cleavage of SNARE complex proteins	2.599	0.00934	Vamp1, Stx7, Stx1a, Stx6, Stx12, Vamp2, Stx1b, Snap25, Stx11, Stx2
Lagging Strand Synthesis	2.588	0.00964	Lig1, Rpa1, Pold3, Pold1, Pcna, Fen1, Prim1, Dna2, Rfc1, Pola2, Rfc4, Rfc3, Rfc5, Pold2, Rfc2
DNA strand elongation	2.585	0.00975	Lig1, Mcm2, Mcm5, Mcm6, Rpa1, Mcm4, Pold3, Pold1, Pcna, Fen1, Prim1, Dna2, Mcm3, Cdc45, Rfc1, Pola2, Gins2, Rfc4, Mcm7, Rfc3, Gins4, Rfc5, Pold2, Gins1, Rfc2, Mcm8
Cyclin A:Cdk2-associated events at S phase entry	2.577	0.00998	Cdc25b, Ccna2, Skp2, Psmc1, Psma1, Psmc4, Mnat1, Ccne1, Cdk2, Psmc2, Myc, Max, Wee1, Cdkn1b, Cdc25a, Psmd4, Psmd7, Psma4, Psmd5, Psmd12, Psmc3, Psmc6, Psmb2, Cks1b
Synthesis of DNA	2.568	0.0102	Lig1, Ccna2, Mcm2, Mcm5, Pole, Mcm6, Rpa1, Mcm4, Pold3, Pold1, Pcna, Fen1, Psmc1, Psma1, Prim1, Dna2, Mcm3, Psmc4, Pole2, Cdc45, Rfc1, Pola2, Cdk2, Gins2, Cdc6, Rfc4, Mcm7, Cdt1, Orc2, Rfc3, Gins4, Psmc2, Rfc5, Pold2, Gins1, Rfc2, Cdkn1b, Psmd4, Psmd7, Mcm8, Psma4, Psmd5, Psmd12, Psmc3, Psmc6, Psmb2
M Phase	2.558	0.0105	Cenpn, Aurkb, Kntc1, Cdca8, Birc5, Incenp, Bub1b, Cenpa, Zw10, Spc25, Nup107, Spc24, Kif23, Kif20a, Smc1a, Fbxo5, Kif2c, Ska1, Fam33a, Ccdc99, Bub1, Plk1, Nsl1, Sgol1, Pmf1, Zwilch, Cenpo, Ercc6l, Cenpf, Nup85, Cdc20, Rcc2, Cenpq, Nuf2, Ppp2r5e, Dsn1, Sgol2, Mad2l1, Cenph, Nup37, Cenpe, Nup133, Cenpk, Kif2a, Rad21, Cenpm, Ppp2r5b, Ndc80, Clasp2, Mlf1ip, Pafah1b1, Zwint, Sec13, Clasp1, Mapre1, Casc5, Xpo1, Gorasp1
Cell Cycle, Mitotic	2.558	0.0105	Lig1, Cdc25b, Ccna2, Cenpn, Mcm2, Top2a, Aurkb, Mcm5, Kntc1, Pole, Mcm6, Cdca8, Rpa1, Mcm4, Birc5, Cdk1, Ccnb2, Pold3, Incenp, E2f2, Bub1b, Pold1, Dhfr, Ube2d1, Pcna, Cenpa, Tubgcp2, Zw10, Spc25, Nup107, Spc24, Skp2, Kif23, Fen1, Kif20a, Aurka, Cdk4, Cdc25c, Smc1a, Psmc1, Fbxo5, Cdc7, Psma1, Dbf4, Prim1, Kif2c, Ska1, Nek2, Dna2, Cenpj, Fam33a, Mcm10, Mcm3, Psmc4, Ube2c, Ccdc99, Mnat1, Ccne1, Bub1, Gmnn, Plk1, Nsl1, Sgol1, Pmf1, Pole2, Zwilch, Rrm2, Cdc45, Rfc1, Ccnd3, Pola2, Cenpo, Ercc6l, Rbl1, Cenpf, Cdk2, Mybl2, Nup85, Gins2, Cdc6, Cdc20, Rcc2, Cenpq, Rfc4, Nuf2, Mcm7, Cep152, Ppp2r5e, Tyms, Cdt1, Dsn1, Orc2, Sgol2, Rfc3, Mad2l1, Gins4, Csnk1d, Cdc23, Cenph, Nup37, Cenpe, Nup133, Cdc26, Cenpk, Psmc2, Rfc5, Myc, Kif2a, Dync1i2, Max, Rad21, Plk4, Tubg1, Pold2, Cenpm, Wee1, Gins1, Ppp2r5b, Ndc80, Clasp2, Rfc2, Hdac1, Cdkn1b,

			Cdc25a, E2f4, Mlf1ip, Ywhag, Pafah1b1, Psmd4, Cdc16, Psmd7, Nedd1, Pttg1, Cep76, Mcm8, Zwint, Cetn2, Anapc1, Psma4, Psmd5, Psmd12, Psmc3, Cdkn2c, Sec13, Clasp1, Psmc6, Mapre1, Dyrk1a, Cep135, Casc5, Psmb2, Prkar2b, Xpo1, Gorasp1, Cks1b
CRMPs in Sema3A signaling	2.554	0.0106	Nrp1, Plxna2, Plxna4, Crmp1, Dpysl3, Cdk5r1, Sema3a, Dpysl5, Fyn, Gsk3b
Nuclear import of Rev protein	2.532	0.0113	Nup205, Nup188, Nup107, Kpnb1, Ran, Nup93, Nup50, Rcc1, Nup85, Nup62, Nup37, Nupl1, Nup133, Npm1, Nup214, Nup155, Rae1
Transmission across Chemical Synapses	2.518	0.0118	Gnal, Cacna2d3, Gng2, Grin2a, Gnai1, Gabrg3, Camk2g, Slc38a2, Chrnb2, Gria4, Dlg4, Kcnj2, Syn2, Gabbr2, Grip1, Stx1a, Gabbr1, Gls, Akap5, Grik2, Adcy5, Camk4, Kcnj6, Gabrb3, Plcb3, Vamp2, Syn1, Syt1, Gad1, Cacng4, Gng3, Dnajc5, Adcy2, Rasgrf2, Cacna1b, Grin2b, Cacna2d1, Rps6ka3, Grip2, Hspa8, Gabrg2, Slc1a7, Nsf, Snap25, Camkk1, Gria2, Slc1a3, Grin1, Ap2b1, Prkacb, Gabra5, Gnai2, Gad2, Cplx1, Cacnb1, Gng12, Camk2b, Gabra3, Comt, Stxbp1, Cacna1a, Chrna4, Arhgef9, Ap2a2, Gria1, Cacnb4, Slc1a1, Mapk1, Gnb4, Cacng3, Rasgrf1
Unwinding of DNA	2.516	0.0119	Mcm2, Mcm5, Mcm6, Mcm4, Mcm3, Cdc45, Gins2, Mcm7, Gins4, Gins1, Mcm8
Vpr-mediated nuclear import of PICs	2.504	0.0123	Nup205, Nup188, Nup107, Nup93, Nup50, Nup85, Kpna1, Nup62, Nup37, Nupl1, Nup133, Nup214, Banf1, Nup155, Rae1
Mitotic Prometaphase	2.498	0.0125	Cenpn, Aurkb, Kntc1, Cdca8, Birc5, Incenp, Bub1b, Cenpa, Zw10, Spc25, Nup107, Spc24, Smc1a, Kif2c, Ska1, Fam33a, Ccdc99, Bub1, Plk1, Nsl1, Sgol1, Pmf1, Zwilch, Cenpo, Ercc6l, Cenpf, Nup85, Cdc20, Rcc2, Cenpq, Nuf2, Ppp2r5e, Dsn1, Sgol2, Mad2l1, Cenph, Nup37, Cenpe, Nup133, Cenpk, Kif2a, Rad21, Cenpm, Ppp2r5b, Ndc80, Clasp2, Mlf1ip, Pafah1b1, Zwint, Sec13, Clasp1, Mapre1, Casc5, Xpo1
NEP/NS2 Interacts with the Cellular Export Machinery	2.471	0.0135	Nup205, Nup188, Nup107, Ran, Nup93, Nup50, Nup85, Nup62, Nup37, Nupl1, Nup133, Nup214, Nup155, Rae1, Xpo1, Nup88, Nup43
Cell Cycle	2.442	0.0146	Lmnb1, Lig1, Cdc25b, Ccna2, Cenpn, Mcm2, Top2a, Aurkb, Mcm5, Kntc1, Pole, Mcm6, Cdca8, Rpa1, Mcm4, Birc5, Cdk1,

			Ccnb2, Pold3, Incenp, E2f2, Bub1b, Pold1, Dhfr, Ube2d1, Pcna, Cenpa, Tubgcp2, Zw10, Spc25, Nup107, Hjurp, Spc24, Skp2, Kif23, Fen1, Kif20a, Aurka, Cdk4, Cdc25c, Smc1a, Psmc1, Tinf2, Fbxo5, Cdc7, Psma1, Dbf4, Hus1, Prim1, Kif2c, Ska1, Nek2, Dna2, Cenpj, Fam33a, Mcm10, Mcm3, Brca1, Psmc4, Ube2c, Ccdc99, Mnat1, Ccne1, Bub1, Gmnn, Plk1, Nsl1, Sgol1, Pmf1, Pole2, Zwilch, Rrm2, Cdc45, Rfc1, Ccnd3, Pola2, Cenpo, Ercc6l, H2afz, Rbl1, Cenpf, Cdk2, Clspn, Mybl2, Nup85, Gins2, Cdc6, Cdc20, Rcc2, Cenpq, Rfc4, Nuf2, Mcm7, Cep152, Ppp2r5e, Tyms, Cdt1, Dsn1, Orc2, Sgol2, Terf1, Rfc3, Mad2l1, Gins4, Csnk1d, Cdc23, Cenph, Nup37, Cenpe, Syne1, Nup133, Ruvbl1, Cdc26, Npm1, Cenpk, Psmc2, Rec8, Rfc5, Myc, Kif2a, Dync1i2, Max, Rad21, Plk4, Tubg1, Ruvbl2, Pold2, Cenpm, Wee1, Gins1, Ppp2r5b, Ndc80, Clasp2, Mis18bp1, Chek1, Rfc2, Hdac1, Cdkn1b, Cdc25a, E2f4, Mlf1ip, Ywhag, Pafah1b1, Psmd4, Cdc16, Rbbp7, Psmd7, Nedd1, Pttg1, Cep76, Mcm8, Zwint, Chek2, Cetn2, Anapc1, Psma4, Psmd5, Trp53, 2610039C10Rik, Dkc1, Psmd12, Psmc3, Cdkn2c, Sec13, Clasp1, Psmc6, Mapre1, Dyrk1a, Cep135, Casc5, Psmb2, Prkar2b, Xpo1, Gorasp1, Cks1b
G beta:gamma signalling through PLC beta	2.439	0.0147	Gng2, Plcb3, Gng3, Gng12, Gnb4, Gng10, Plcb1, Plcb2, Gng7, Gnb5, Gng4, Gngt2
Cell Cycle Checkpoints	2.43	0.0151	Mcm2, Mcm5, Mcm6, Rpa1, Mcm4, Cdk1, Ccnb2, Bub1b, Ube2d1, Cdc25c, Psmc1, Cdc7, Psma1, Dbf4, Hus1, Mcm10, Mcm3, Psmc4, Ube2c, Ccne1, Cdc45, Cdk2, Clspn, Cdc6, Cdc20, Rfc4, Mcm7, Orc2, Rfc3, Mad2l1, Cdc23, Cdc26, Psmc2, Rfc5, Wee1, Chek1, Rfc2, Cdkn1b, Cdc25a, Psmd4, Cdc16, Psmd7, Mcm8, Chek2, Anapc1, Psma4, Psmd5, Trp53, Psmd12, Psmc3, Psmc6, Psmb2
Leading Strand Synthesis	2.426	0.0153	Pold3, Pold1, Pcna, Prim1, Rfc1, Pola2, Rfc4, Rfc3, Rfc5, Pold2, Rfc2
Polymerase switching	2.426	0.0153	Pold3, Pold1, Pcna, Prim1, Rfc1, Pola2, Rfc4, Rfc3, Rfc5, Pold2, Rfc2
Polymerase switching on the C-strand of the telomere	2.426	0.0153	Pold3, Pold1, Pcna, Prim1, Rfc1, Pola2, Rfc4, Rfc3, Rfc5, Pold2, Rfc2
Rev-mediated nuclear export of HIV-1 RNA	2.416	0.0157	Nup205, Nup188, Nup107, Ran, Nup93, Nup50, Rcc1, Nup85, Nup62, Nup37, Nupl1, Nup133, Nup214, Nup155, Rae1, Ranbp1, Xpo1, Nup88, Nup43

Disease	2.414	0.0158	Pcsk2, Prkce, Lig1, Vamp1, Grb2, Stx7, Stam, App, Srpr, Igfbp4, Pag1, Cdk1, Adam12, Ap1s2, Ncbp1, Atp6v0d1, Nup205, Nup188, Nup107, Cxcr4, Spry2, Fen1, Pdia6, Stx1a, Psmc1, Bche, Psma1, Hspa5, Ap1m1, Hsp90b1, Prkar1b, Mmp2, Dnajb11, Adam17, Stx6, Psmc4, Elmo1, Kpnb1, Adcy5, Slc25a5, Ran, Camk4, Mnat1, Nup93, Stx12, Gtf2e1, Mbtps1, Tpp1, Herpud1, Ssrp1, Vamp2, Syt2, Asns, Syt1, Nup50, Rcc1, H2afz, Tln1, Stx1b, Nup85, Ywhab, Them4, Pik3r1, Kpna1, Casp9, Supt16h, Trib3, Atf4, Sec31a, Adcy2, Hdgf, Myo5a, Ddx11, Mfge8, Calr, Nup62, Rngtt, Snap25, Ptpn11, Exosc8, Akt3, Sh3kbp1, Rps3a, Sh3gl2, Exosc3, Serp1, Igf2, Nup37, Xrcc5, Gtf2e2, Th1l, Dock2, Prkar2a, Nupl1, Igf2bp2, Ap2b1, Nup133, Prkacb, Npm1, Pten, Psmc2, Acadvl, Myc, Nup214, Mapkap1, Rpl6, Banf1, Shc1, Rps23, Mapk3, Nup155, Dnajc3, Ppp2r5b, Taf6, Fyn, Stx11, Igf1, Cdkn1b, Ap2a2, Phlpp1, Pappa2, Pde1a, Sos1, Gsk3b, Psmd4, Rae1, Egfr, Psmd7, Exoc5, Rplp0, Rps5, Mapk1, Rps6, Psma4, Stx2, Psmd5, Igf2bp1, Ranbp1, Hyou1, Psmd12, Apcs, Psmc3, Rpl4, Rpl19, Rpl27a, Igfbp5, Cul7, Exosc2, Rnmt, Taf12, Cd28, Gtf2f2, Ssr1, Srprb, Rps8, Psmc6, Igfbp2, Psmb2, Prkar2b, Hist1h3c, Xpo1, Prkca, Nup88, Adcy1, Rps7, Pacs1, Rps16, Gtf2h4, Actb, Polr2j, Exoc6, Ncbp2, Wipi1, Adcy7, Hist3h2bb-ps, Rps10, Exosc9, Hist2h2be, Gtf2h3, Nup43, Kdelr3, Slc30a5, Snca, Exoc8, Rpl3, Nfyc, Canx, Pcsk1, Rdbp, Edem1, Gtf2f1, Itpr2, Rpl18a, Rpsa, Rps11, Rps4x, Stx5a, Rps9, Arhgef7
Axon guidance	2.373	0.0177	Gfra2, Cntn1, Plxnc1, Grb2, Nrp1, Pak7, Robo2, Scn3b, Dcc, Rgmb, Met, Cdk1, Unc5c, Gfra1, Sema4a, Prnp, Dlg4, Plxna2, Ntn1, Dcx, Plxna4, Cap2, Unc5d, Crmp1, Nfasc, Sema6d, Dnm3, Cacna1i, Nrcam, Myo10, Col1a2, Col5a1, Alcam, 4930506M07Rik, Ank3, Dpysl3, Erbb2, Cdk5r1, Scn3a, Spnb2, Nck2, Sema3a, Tln1, Kcnq2, Col2a1, Ywhab, Hsp90ab1, Scn2a1, Limk2, Rps6ka3, Sema7a, Ptpn11, Ablim1, Kif4, Ablim3, Sh3gl2, L1cam, Pitpna, Dpysl5, Ap2b1, Ncam1, Cacna1d, Scn8a, Neo1, Pfn2, Cacna1h, Rdx, St8sia4, Cacnb1, Chl1, Mapk3, Ezr, Pak1, Lama1, Clasp2, Scn9a, Fyn, Col3a1, Srgap1, Ap2a2, Arhgap39, Cacnb4, Sos1, Gsk3b, Srgap2, Unc5a, Egfr, Slit2, Fgfr1, Cacna1c, Spnb3, Stip1, Mapk1, Pak3, Evl, Sdcbp, Pak4, Cntnap1, Robo1, Ncan, Clasp1
Interactions of Rev with host cellular proteins	2.372	0.0177	Nup205, Nup188, Nup107, Kpnb1, Ran, Nup93, Nup50, Rcc1, Nup85, Nup62, Nup37, Nupl1, Nup133, Npm1, Nup214, Nup155, Rae1, Ranbp1, Xpo1, Nup88, Nup43

Processing of Capped Intron-Containing Pre-mRNA	2.37	0.0178	Hnrnpl, Hnrnpf, Ptbp1, Srsf2, Sf3a3, Ncbp1, Nup205, Nup188, Nup107, Hnrnpm, Eftud2, Smc1a, Sf3b2, Nup93, Slbp, Pcbp2, Nup50, Hnrnpul1, Snrnp200, Nup85, Prpf4, Lsm2, Mettl3, Nup62, Hnrnpa2b1, Sf3b3, Nup37, Hnrnpu, Snrpa, Dhx38, Nupl1, Nup133, Sf3a1, Nup214, Hnrnpa1, Pcbp1, Srsf1, Srsf3, Cpsf1, Nup155, Snrnp70, Prpf8, Rae1, Cstf1, Magoh, Ddx23, Sf3b4, Snrpb, Cd2bp2, U2af1, Gtf2f2, Nxf1, Thoc4, Srsf6, Nup88, Polr2j, Nudt21, Ncbp2, Nup43
G2/M Checkpoints	2.368	0.0179	Mcm2, Mcm5, Mcm6, Rpa1, Mcm4, Cdk1, Ccnb2, Cdc25c, Cdc7, Dbf4, Hus1, Mcm10, Mcm3, Cdc45, Cdk2, Clspn, Cdc6, Rfc4, Mcm7, Orc2, Rfc3, Rfc5, Wee1, Chek1, Rfc2, Cdc25a, Mcm8, Chek2
Resolution of AP sites via the single-nucleotide replacement pathway	2.363	0.0181	Xrcc1, Mpg, Mutyh, Apex1, Lig3, Mbd4, Nthl1
GABA synthesis, release, reuptake and degradation	2.361	0.0182	Stx1a, Vamp2, Syt1, Gad1, Dnajc5, Hspa8, Snap25, Gad2, Cplx1, Stxbp1, Slc6a13, Abat
mRNA Processing	2.36	0.0183	Hnrnpl, Hnrnpf, Ptbp1, Srsf2, Sf3a3, Ncbp1, Nup205, Nup188, Nup107, Hnrnpm, Eftud2, Smc1a, Sf3b2, Mnat1, Nup93, Slbp, Pcbp2, Nup50, Hnrnpul1, Snrnp200, Nup85, Prpf4, Lsm2, Mettl3, Nup62, Rngtt, Hnrnpa2b1, Sf3b3, Nup37, Hnrnpu, Snrpa, Dhx38, Nupl1, Nup133, Sf3a1, Nup214, Hnrnpa1, Pcbp1, Srsf1, Lsm11, Srsf3, Cpsf1, Nup155, Snrnp70, Prpf8, Rae1, Cstf1, Magoh, Ddx23, Sf3b4, Snrpb, Rnmt, Cd2bp2, U2af1, Gtf2f2, Nxf1, Thoc4, Srsf6, Nup88, Gtf2h4, Polr2j, Nudt21, Ncbp2, Gtf2h3, Nup43
Processive synthesis on the lagging strand	2.33	0.0198	Lig1, Rpa1, Pold3, Pold1, Pcna, Fen1, Prim1, Dna2, Pola2
Ion transport by P-type ATPases	2.302	0.0213	Atp8a1, Atp9a, Atp10a, Atp10b, Atp2b2, Atp1a1, Atp4b, Atp11c, Atp1a3, Atp8b1, Atp2a3, Atp8a2, Atp11b, Atp2b1
DNA Replication Pre-Initiation	2.301	0.0214	Mcm2, Mcm5, Pole, Mcm6, Rpa1, Mcm4, E2f2, Psmc1, Cdc7, Psma1, Dbf4, Prim1, Mcm10, Mcm3, Psmc4, Gmnn, Pole2, Cdc45, Pola2, Cdk2, Cdc6, Mcm7, Cdt1, Orc2, Psmc2, Psmd4, Psmd7, Mcm8, Psma4, Psmd5, Psmd12, Psmc3, Psmc6, Psmb2
M/G1 Transition	2.301	0.0214	Mcm2, Mcm5, Pole, Mcm6, Rpa1, Mcm4, E2f2, Psmc1, Cdc7, Psma1, Dbf4, Prim1, Mcm10, Mcm3, Psmc4, Gmnn, Pole2,

			Cdc45, Pola2, Cdk2, Cdc6, Mcm7, Cdt1, Orc2, Psmc2, Psmd4, Psmd7, Mcm8, Psma4, Psmd5, Psmd12, Psmc3, Psmc6, Psmb2
Removal of licensing factors from origins	2.289	0.0221	Ccna2, Mcm2, Mcm5, Mcm6, Mcm4, Psmc1, Psma1, Mcm10, Mcm3, Psmc4, Gmnn, Cdk2, Cdc6, Mcm7, Cdt1, Orc2, Psmc2, Cdkn1b, Psmd4, Psmd7, Mcm8, Psma4, Psmd5, Psmd12, Psmc3, Psmc6, Psmb2
Transport of Mature mRNA derived from an Intron-Containing Transcript	2.288	0.0221	Srsf2, Ncbp1, Nup205, Nup188, Nup107, Nup93, Nup50, Nup85, Nup62, Nup37, Dhx38, Nupl1, Nup133, Nup214, Srsf1, Srsf3, Nup155, Rae1, Magoh, U2af1, Nxf1, Thoc4, Srsf6, Nup88, Ncbp2, Nup43
Ion channel transport	2.265	0.0235	Atp8a1, Atp9a, Gabrg3, Atp10a, Atp10b, Gabrb3, Atp2b2, Gabrg2, Atp1a1, Atp4b, Gabra5, Glra3, Atp11c, Gabra3, Atp1a3, Atp8b1, Arhgef9, Atp2a3, Atp8a2, Atp11b, Glra2, Atp2b1
Activation of ATR in response to replication stress	2.259	0.0239	Mcm2, Mcm5, Mcm6, Rpa1, Mcm4, Cdc25c, Cdc7, Dbf4, Hus1, Mcm10, Mcm3, Cdc45, Cdk2, Clspn, Cdc6, Rfc4, Mcm7, Orc2, Rfc3, Rfc5, Chek1, Rfc2, Cdc25a, Mcm8
Regulation of Glucokinase by Glucokinase Regulatory Protein	2.245	0.0248	Nup205, Nup188, Nup107, Nup93, Nup50, Nup85, Nup62, Nup37, Nupl1, Nup133, Nup214, Nup155, Rae1
G-protein mediated events	2.243	0.0249	Gnal, Gnai1, Prkar1b, Adcy5, Camk4, Plcb3, Plcb4, Adcy2, Gnao1, Prkar2a, Prkacb, Gnai2, Pde1a, Mapk1, Gnaz, Prkar2b, Prkca, Adcy1, Adcy7, Plcb1, Plcb2, Itpr2
Removal of the Flap Intermediate	2.241	0.025	Rpa1, Pold3, Pold1, Pcna, Fen1, Prim1, Dna2, Pola2
Orc1 removal from chromatin	2.239	0.0252	Ccna2, Mcm2, Mcm5, Mcm6, Mcm4, Psmc1, Psma1, Mcm3, Psmc4, Cdk2, Cdc6, Mcm7, Cdt1, Orc2, Psmc2, Cdkn1b, Psmd4, Psmd7, Mcm8, Psma4, Psmd5, Psmd12, Psmc3, Psmc6, Psmb2
Switching of origins to a post-replicative state	2.239	0.0252	Ccna2, Mcm2, Mcm5, Mcm6, Mcm4, Psmc1, Psma1, Mcm3, Psmc4, Cdk2, Cdc6, Mcm7, Cdt1, Orc2, Psmc2, Cdkn1b, Psmd4, Psmd7, Mcm8, Psma4, Psmd5, Psmd12, Psmc3, Psmc6, Psmb2
Regulation of DNA replication	2.234	0.0255	Ccna2, Mcm2, Mcm5, Mcm6, Mcm4, E2f2, Psmc1, Psma1, Mcm10, Mcm3, Psmc4, Gmnn, Cdk2, Cdc6, Mcm7, Cdt1, Orc2, Psmc2, Cdkn1b, Psmd4, Psmd7, Mcm8, Psma4, Psmd5,

			Psmd12, Psmc3, Psmc6, Psmb2
Transport of Mature Transcript to Cytoplasm	2.231	0.0257	Srsf2, Ncbp1, Nup205, Nup188, Nup107, Nup93, Slbp, Nup50, Nup85, Nup62, Nup37, Dhx38, Nupl1, Nup133, Nup214, Srsf1, Srsf3, Cpsf1, Nup155, Rae1, Magoh, U2af1, Nxf1, Thoc4, Srsf6, Nup88, Ncbp2, Nup43
L1CAM interactions	2.222	0.0263	Cntn1, Nrp1, Scn3b, Dlg4, Dcx, Nfasc, Dnm3, Nrcam, Alcam, 4930506M07Rik, Ank3, Scn3a, Spnb2, Kcnq2, Scn2a1, Rps6ka3, Kif4, Sh3gl2, L1cam, Ap2b1, Ncam1, Scn8a, Rdx, Chl1, Mapk3, Ezr, Pak1, Lama1, Scn9a, Ap2a2, Egfr, Fgfr1, Spnb3, Stip1, Mapk1, Sdcbp, Cntnap1, Ncan, Dnm1, Scn1a, Scn2b, Dpysl2, Ank1, Spna2, Scn1b, Kcnq3, Csnk2b, Itga1, Dlg3
Depolarization of the Presynaptic Terminal Triggers the Opening of Calcium Channels	2.21	0.0271	Cacna2d3, Cacng4, Cacna1b, Cacna2d1, Cacnb1, Cacna1a, Cacnb4
Cyclin E associated events during G1/S transition	2.187	0.0287	Ccna2, Skp2, Psmc1, Psma1, Psmc4, Mnat1, Ccne1, Cdk2, Psmc2, Myc, Max, Wee1, Cdkn1b, Cdc25a, Psmd4, Psmd7, Psma4, Psmd5, Psmd12, Psmc3, Psmc6, Psmb2, Cks1b
G1/S Transition	2.177	0.0295	Ccna2, Mcm2, Mcm5, Pole, Mcm6, Rpa1, Mcm4, Cdk1, Dhfr, Pcna, Skp2, Psmc1, Fbxo5, Cdc7, Psma1, Dbf4, Prim1, Mcm10, Mcm3, Psmc4, Mnat1, Ccne1, Pole2, Rrm2, Cdc45, Pola2, Cdk2, Cdc6, Mcm7, Tyms, Cdt1, Orc2, Psmc2, Myc, Max, Wee1, Cdkn1b, Cdc25a, Psmd4, Psmd7, Mcm8, Psma4, Psmd5, Psmd12, Psmc3, Psmc6, Psmb2, Cks1b
Netrin-1 signaling	2.172	0.0298	Dcc, Rgmb, Unc5c, Ntn1, Unc5d, Myo10, Ptpn11, Ablim1, Ablim3, Pitpna, Neo1, Ezr, Fyn, Unc5a, Slit2, Robo1
Netrin mediated repulsion signals	2.148	0.0317	Dcc, Unc5c, Ntn1, Unc5d, Ptpn11, Fyn, Unc5a
Regulation of Insulin Secretion	2.147	0.0318	Gng2, Gnai1, Chrm3, Stx1a, Kcnb1, Prkar1b, Akap5, Adcy5, Slc25a5, Rapgef4, Plcb3, Vamp2, Gng3, Ctnnb1, Gna14, Adra2a, Snap25, Gnao1, Kcng2, Prkar2a, Cacna1d, Prkacb, Gnai2, Gng12, Stxbp1, Cacna1a, Cacna1c, Gnb4, Gnaq, Gpr119, Prkar2b, Dpp4, Prkca, Kcnc2, Abcc8, Cacnb3, Gng10, Plcb1, Plcb2, Gna15, Pcsk1, Itpr2
Regulation of Insulin Secretion by Glucagon-like Peptide-1	2.122	0.0338	Gng2, Kcnb1, Prkar1b, Akap5, Adcy5, Rapgef4, Gng3, Kcng2, Prkar2a, Prkacb, Gng12, Gnb4, Prkar2b, Kcnc2, Gng10, Itpr2,

			Gng7, Gnb5, Rapgef3, Gng4, Gngt2
SHC1 events in EGFR signaling	2.12	0.034	Grb2, Cdk1, Ywhab, Shc1, Mapk3, Sos1, Egfr, Mapk1
mRNA Splicing	2.117	0.0342	Hnrnpl, Hnrnpf, Ptbp1, Srsf2, Sf3a3, Ncbp1, Hnrnpm, Eftud2, Smc1a, Sf3b2, Pcbp2, Hnrnpul1, Snrnp200, Prpf4, Lsm2, Hnrnpa2b1, Sf3b3, Hnrnpu, Snrpa, Dhx38, Sf3a1, Hnrnpa1, Pcbp1, Srsf1, Srsf3, Cpsf1, Snrnp70, Prpf8, Cstf1, Magoh, Ddx23, Sf3b4, Snrpb, Cd2bp2, U2af1, Gtf2f2, Thoc4, Srsf6, Polr2j, Nudt21, Ncbp2
mRNA Splicing - Major Pathway	2.117	0.0342	Hnrnpl, Hnrnpf, Ptbp1, Srsf2, Sf3a3, Ncbp1, Hnrnpm, Eftud2, Smc1a, Sf3b2, Pcbp2, Hnrnpul1, Snrnp200, Prpf4, Lsm2, Hnrnpa2b1, Sf3b3, Hnrnpu, Snrpa, Dhx38, Sf3a1, Hnrnpa1, Pcbp1, Srsf1, Srsf3, Cpsf1, Snrnp70, Prpf8, Cstf1, Magoh, Ddx23, Sf3b4, Snrpb, Cd2bp2, U2af1, Gtf2f2, Thoc4, Srsf6, Polr2j, Nudt21, Ncbp2
Activation of Kainate Receptors upon glutamate binding	2.116	0.0344	Gng2, Dlg4, Grik2, Plcb3, Gng3, Gng12, Gnb4, Gng10, Plcb1, Plcb2, Dlg3, Gng7, Grik1, Gnb5, Gng4, Gngt2
CDO in myogenesis	2.112	0.0347	Ctnna2, Ctnna1, Bnip2, Mef2b, Ctnnb1, Cdh4, Boc, Neo1, Tcf3, Mapk12, Cdon, Map2k6, Ntn3
Myogenesis	2.112	0.0347	Ctnna2, Ctnna1, Bnip2, Mef2b, Ctnnb1, Cdh4, Boc, Neo1, Tcf3, Mapk12, Cdon, Map2k6, Ntn3
Homologous Recombination Repair	2.108	0.0351	Lig1, Rpa1, Rad51, Brca1, Brip1, Mre11a, Mdc1, Nbn, Brca2
Homologous recombination repair of replication-independent double-strand breaks	2.108	0.0351	Lig1, Rpa1, Rad51, Brca1, Brip1, Mre11a, Mdc1, Nbn, Brca2
Glutamate Neurotransmitter Release Cycle	2.099	0.0358	Slc38a2, Stx1a, Gls, Vamp2, Syt1, Slc1a7, Snap25, Cplx1, Stxbp1, Slc1a1
GRB2 events in ERBB2 signaling	2.095	0.0361	Nrg1, Grb2, Cdk1, Nrg3, Erbb2, Ywhab, Mapk3, Nrg2, Sos1, Egfr, Mapk1
Activation of the pre-replicative complex	2.079	0.0376	Mcm2, Mcm5, Pole, Mcm6, Rpa1, Mcm4, Cdc7, Dbf4, Prim1, Mcm10, Mcm3, Pole2, Cdc45, Pola2, Cdk2, Cdc6, Mcm7, Cdt1, Orc2

Unfolded Protein Response	2.066	0.0388	Srpr, Atp6v0d1, Pdia6, Hspa5, Hsp90b1, Dnajb11, Mbtps1, Tpp1, Herpud1, Asns, Tln1, Atf4, Sec31a, Hdgf, Ddx11, Calr, Exosc8, Exosc3, Serp1, Acadvl, Shc1, Dnajc3, Ppp2r5b, Hyou1, Cul7, Exosc2, Ssr1, Srprb, Wipi1, Exosc9, Kdelr3, Nfyc, Edem1
ADP signalling through P2Y purinoceptor 12	2.061	0.0393	Gng2, Gnai1, Gng3, Gnai2, Gng12, Gnb4, Gng10, Gng7, Gnb5, Gng4, Gngt2
Kinesins	2.048	0.0406	Kif5c, Racgap1, Kif22, Kifap3, Kif11, Kif23, Kif20a, Kif15, Kif2c, Kif3c, Kifc1, Kif5a, Kif4, Cenpe, Kif2a, Kif3a, Klc3, Kif3b, Klc1
Export of Viral Ribonucleoproteins from Nucleus	2.046	0.0407	Nup205, Nup188, Nup107, Ran, Nup93, Nup50, Nup85, Nup62, Nup37, Nupl1, Nup133, Nup214, Nup155, Rae1, Xpo1, Nup88, Nup43
GABA receptor activation	2.032	0.0421	Gnal, Gng2, Gnai1, Gabrg3, Kcnj2, Gabbr2, Gabbr1, Adcy5, Kcnj6, Gabrb3, Gng3, Adcy2, Gabrg2, Gabra5, Gnai2, Gng12, Gabra3, Arhgef9
Diabetes pathways	2.021	0.0433	Pcsk2, Srpr, Igfbp4, Atp6v0d1, Pdia6, Stx1a, Bche, Hspa5, Hsp90b1, Mmp2, Dnajb11, Mbtps1, Tpp1, Herpud1, Vamp2, Asns, Tln1, Atf4, Sec31a, Hdgf, Myo5a, Ddx11, Calr, Snap25, Exosc8, Exosc3, Serp1, Igf2, Igf2bp2, Acadvl, Myc, Shc1, Dnajc3, Ppp2r5b, Igf1, Pappa2, Exoc5, Igf2bp1, Hyou1, Igfbp5, Cul7, Exosc2, Ssr1, Srprb, Igfbp2, Actb, Exoc6, Wipi1, Exosc9, Kdelr3, Slc30a5, Exoc8, Nfyc, Pcsk1, Edem1, Exoc4, Slc30a6, Slc30a7, Exosc7, Nfya, Cpe, Exoc2, Dis3, Mboat4, Sec11c, Exosc5, Parn, Mbtps2
Mitotic G1-G1/S phases	2.02	0.0434	Ccna2, Mcm2, Top2a, Mcm5, Pole, Mcm6, Rpa1, Mcm4, Cdk1, E2f2, Dhfr, Pcna, Skp2, Cdk4, Psmc1, Fbxo5, Cdc7, Psma1, Dbf4, Prim1, Mcm10, Mcm3, Psmc4, Mnat1, Ccne1, Pole2, Rrm2, Cdc45, Ccnd3, Pola2, Rbl1, Cdk2, Mybl2, Cdc6, Mcm7, Tyms, Cdt1, Orc2, Psmc2, Myc, Max, Wee1, Hdac1, Cdkn1b, Cdc25a, E2f4, Psmd4, Psmd7, Mcm8, Psma4, Psmd5, Psmd12, Psmc3, Cdkn2c, Psmc6, Dyrk1a, Psmb2, Cks1b
Inhibition of Insulin Secretion by Adrenaline/Noradrenaline	2.013	0.0441	Gng2, Gnai1, Adcy5, Gng3, Adra2a, Gnao1, Cacna1d, Gnai2, Gng12, Cacna1c, Gnb4, Cacnb3, Gng10, Gng7, Gnb5, Gng4, Gngt2
Adenylate cyclase inhibitory	2.007	0.0448	Gnal, Gnai1, Adcy5, Adcy2, Gnai2, Adcy1, Adcy7

pathway			
Inhibition of adenylate cyclase pathway	2.007	0.0448	Gnal, Gnai1, Adcy5, Adcy2, Gnai2, Adcy1, Adcy7
Sema3A PAK dependent Axon repulsion	2.006	0.0449	Nrp1, Plxna2, Plxna4, Sema3a, Hsp90ab1, Pak1, Fyn
Chromosome Maintenance	1.998	0.0457	Lmnb1, Lig1, Cenpn, Pole, Rpa1, Pold3, Pold1, Pcna, Cenpa, Hjurp, Fen1, Smc1a, Tinf2, Prim1, Dna2, Brca1, Pole2, Rfc1, Pola2, Cenpo, H2afz, Cenpq, Rfc4, Terf1, Rfc3, Cenph, Syne1, Ruvbl1, Npm1, Cenpk, Rec8, Rfc5, Rad21, Ruvbl2, Pold2, Mis18bp1, Rfc2, Mlf1ip, Rbbp7, 2610039C10Rik, Dkc1
Presynaptic function of Kainate receptors	1.995	0.046	Gng2, Plcb3, Gng3, Gng12, Gnb4, Gng10, Plcb1, Plcb2, Gng7, Gnb5, Gng4, Gngt2
APC/C-mediated degradation of cell cycle proteins	1.986	0.0471	Ccna2, Aurkb, Cdk1, Bub1b, Ube2d1, Skp2, Aurka, Psmc1, Fbxo5, Psma1, Psmc4, Ube2c, Plk1, Cdk2, Cdc20, Mad2l1, Cdc23, Cdc26, Psmc2, Psmd4, Cdc16, Psmd7, Pttg1, Anapc1, Psma4, Psmd5, Psmd12, Psmc3, Psmc6, Psmb2
Regulation of mitotic cell cycle	1.986	0.0471	Ccna2, Aurkb, Cdk1, Bub1b, Ube2d1, Skp2, Aurka, Psmc1, Fbxo5, Psma1, Psmc4, Ube2c, Plk1, Cdk2, Cdc20, Mad2l1, Cdc23, Cdc26, Psmc2, Psmd4, Cdc16, Psmd7, Pttg1, Anapc1, Psma4, Psmd5, Psmd12, Psmc3, Psmc6, Psmb2
Assembly of the pre-replicative complex	1.976	0.0482	Mcm2, Mcm5, Mcm6, Mcm4, E2f2, Psmc1, Psma1, Mcm3, Psmc4, Gmnn, Cdc6, Mcm7, Cdt1, Orc2, Psmc2, Psmd4, Psmd7, Mcm8, Psma4, Psmd5, Psmd12, Psmc3, Psmc6, Psmb2
Metal ion SLC transporters	1.973	0.0485	Slc41a2, Slc11a2, Slc39a10, Slc31a1, Slc39a7, Slc39a1, Slc39a6, Slc40a1, Heph, Slc30a5, Slc41a1, Slc30a6, Slc39a5, Slc30a3, Slc30a7, Slc30a8, Slc30a1
Activation of NMDA receptor upon glutamate binding and postsynaptic events	1.968	0.0491	Grin2a, Camk2g, Gria4, Dlg4, Camk4, Rasgrf2, Grin2b, Rps6ka3, Camkk1, Gria2, Grin1, Prkacb, Camk2b, Gria1, Mapk1, Rasgrf1
Reduction of cytosolic Ca++ levels	1.968	0.0491	Slc8a3, Slc8a1, Atp2b2, Slc8a2, Atp2a3, Atp2b1, Atp2b3
G-protein beta:gamma signalling	1.963	0.0497	Gng2, Plcb3, Gng3, Akt3, Gng12, Gnb4, Gng10, Plcb1, Plcb2,

			Gng7, Pik3r5, Rhoa, Gnb5, Gng4, Gngt2

8.4. The Reactome pathways for the 168 vs. 0 hour signature

Set	NES	p-value	Ledge
G alpha (z) signalling events	3.449	0.000562	Rgs4, Prkch, Adcy2, Rgs19, Gng4, Prkcd, Gng3, Gnb1, Gnb5, Rgs20, Gng12, Adcy5, Adcy9, Rgs17, Gng2, Gng7, Gnb4, Prkca, Gnb3, Adra2c, Gnai1
Activation of Rac	2.867	0.00414	Slit2, Pak1, Nck2, Pak6, Gpc1, Rac1, Pak3, Pak7
NOD1/2 Signaling Pathway	2.77	0.00561	Casp2, Tnfaip3, Map2k6, Mapk11, Tab2, Casp4, Casp8, Map3k7, Nod2, Birc2, Cyld, Casp9
Nucleotide-binding domain, leucine rich repeat containing receptor (NLR) signaling pathways	2.755	0.00587	Casp2, Bcl2l1, Txnip, Tnfaip3, Map2k6, Mapk11, P2rx7, Tab2, Casp4, Casp8, Map3k7, Nod2, Birc2, Panx1, Cyld, Casp9
Inactivation of APC/C via direct inhibition of the APC/C complex	2.755	0.00587	Cdc23, Bub1b, Anapc4, Mad2l1, Ube2d1, Cdc26, Cdc20, Bub3, Anapc1, Anapc2, Cdc27, Cdc16
Inhibition of the proteolytic activity of APC/C required for the onset of anaphase by mitotic spindle checkpoint components	2.755	0.00587	Cdc23, Bub1b, Anapc4, Mad2l1, Ube2d1, Cdc26, Cdc20, Bub3, Anapc1, Anapc2, Cdc27, Cdc16
Other semaphorin interactions	2.717	0.00659	Sema4a, Sema5a, Sema7a, Sema6a, Plxnc1, Plxna4, Plxnd1
Rho GTPase cycle	2.71	0.00674	Rhou, Rasgrf2, Arhgap26, Rhoq, Rhob, Syde2, Ralbp1, Arhgap28, Trip10, Racgap1, Arhgap5, Arhgap31, Ngef, Rac3, Rhoc, Ect2, Mcf2, Arap3, Arhgef4, Mcf2l, Rhoj, Arhgap15, Gdi1, Arhgap11a, Bcr, Gmip, Abr, A2m, Arhgef2, Rasgrf1, Stard13, Arhgap19, Srgap2, Rhov, Ocrl, Itsn1, Akap13, Plekhg5, Arhgdia, Depdc1b, Rac1, Arhgap44, Arhgef18, Rhobtb1, Arhgef11
Signaling by Rho GTPases	2.71	0.00674	Rhou, Rasgrf2, Arhgap26, Rhoq, Rhob, Syde2, Ralbp1, Arhgap28, Trip10, Racgap1, Arhgap5, Arhgap31, Ngef, Rac3, Rhoc, Ect2, Mcf2, Arap3, Arhgef4, Mcf2l, Rhoj, Arhgap15, Gdi1, Arhgap11a, Bcr, Gmip, Abr, A2m, Arhgef2, Rasgrf1, Stard13, Arhgap19, Srgap2, Rhov, Ocrl, Itsn1, Akap13, Plekhg5, Arhgdia, Depdc1b,

			Rac1, Arhgap44, Arhgef18, Rhobtb1, Arhgef11
APC-Cdc20 mediated degradation of Nek2A	2.61	0.00906	Nek2, Cdc23, Bub1b, Anapc4, Mad2l1, Ube2d1, Cdc26, Cdc20, Bub3, Anapc1, Anapc2, Cdc27
GABA synthesis, release, reuptake and degradation	2.537	0.0112	Gad1, Aldh5a1, Syt1, Slc6a13, Slc6a11, Stxbp1, Slc6a1, Cplx1, Stx1a, Slc32a1, Snap25, Abat, Vamp2, Rab3a
Recycling pathway of L1	2.522	0.0117	Kif4, Msn, Src, Rps6ka1, Ap2a2, L1cam, Rdx, Dpysl2, 4930506M07Rik, Dnm1, Ezr, Dnm3, Cltc, Ap2a1, Rps6ka4, Rps6ka6, Ap2m1, Ap2b1
Phosphorylation of the APC/C	2.51	0.0121	Cdk1, Cdc23, Anapc4, Ube2d1, Cdc26, Anapc1, Anapc2, Plk1, Cdc27, Cdc16
Nuclear signaling by ERBB4	2.407	0.0161	Stat5a, Stat5b, Hbegf, Cul1, Cxcl12, Tab2, Nrg1, Aph1b, Psenen, Pgr, Nrg3, Adam17, Psen1, Gfap, Wwox
Interleukin-6 signaling	2.376	0.0175	Stat3, Socs3, Jak1, Il6ra
p38MAPK events	2.323	0.0202	Src, Ralgds, Mapk11, Ralb, Rala, Hras1, Mapkapk3, Nras, Mapkapk2
activated TAK1 mediates p38 MAPK activation	2.291	0.0219	Map2k6, Mapk11, Tab2, Map3k7, Nod2, Mapkapk3, Mapkapk2, Ripk2, Tab1, Tab3
Cyclin A/B1 associated events during G2/M transition	2.286	0.0222	Xpo1, Ccna2, Ccnb2, Cdc25b, Cdk1
Interleukin-2 signaling	2.271	0.0231	Grb2, Stat5a, Stat5b, Pik3r3, Pik3cd, Jak1, Pik3cb, Mapk3, Gab2, Cdk1, Jak3, Il2rb, Pik3r1, Hras1, Ptk2b, Ywhab
Growth hormone receptor signaling	2.237	0.0253	Stat3, Socs3, Cish, Stat5a, Stat5b, Mapk3, Ptpn1
TAK1 activates NFkB by phosphorylation and activation of IKKs complex	2.202	0.0277	Rela, Nfkb2, Nfkbia, Tab2, Nfkbib, Hmg1l1, Map3k7, Nod2
Mitotic Prometaphase	2.196	0.0281	Cenpf, Xpo1, Zwilch, Ndel1, Kntc1, Casc5, Cenpp, Sgol1, Fam33a, Bub1, Nuf2, Smc1a, Birc5, Cenpa, Cenpi, Cenpe, Incenp, Aurkb, Rad21, Spc25, Ppp2r5b, Nsl1, Ckap5, Cenpq, Ndc80, Cenpk, Bub1b, Kif18a, Sgol2, Nup160, Mad2l1, Cenpn, Ranbp2, Ccdc99, Nup107, Mlf1ip, Cdc20, Bub3, Itgb3bp, Ska1, Cenpm,

			Ercc6l, Plk1, Nup85, Ppp2r5e, Pmf1, Smc3, Kif2c, Stag2, Cenpl, Seh1l, Ppp2r5d, Ahctf1, Stag1, Zwint, Cenpt, Cdca8, Spc24, Taok1
Signaling by Robo receptor	2.193	0.0283	Slit2, Pak1, Nck2, Vasp, Pak6, Cap1, Srgap2, Evl, Gpc1, Robo2, Rac1, Pak3, Pak7
Circadian Clock	2.193	0.0283	Srebf1, Ccrn4l, Arntl2, Csnk1e, Cul1, Fbxl3, Bhlhe41, Serpine1, Med1, Cpt1a, Nr3c1, Hif1a, Atf2, Per2, Bhlhe40, Ncoa6, Nr1d1, Carm1
M Phase	2.149	0.0317	Cenpf, Xpo1, Kif23, Zwilch, Ndel1, Kntc1, Casc5, Cenpp, Sgol1, Fam33a, Bub1, Nuf2, Smc1a, Birc5, Cenpa, Kif20a, Cenpi, Cenpe, Incenp, Aurkb, Rad21, Spc25, Ppp2r5b, Nsl1, Ckap5, Cenpq, Ndc80, Cenpk, Bub1b, Kif18a, Sgol2, Nup160, Mad2l1, Cenpn, Ranbp2, Ccdc99, Nup107, Fbxo5, Mlf1ip, Cdc20, Bub3, Itgb3bp, Ska1, Cenpm, Ercc6l, Plk1, Nup85, Ppp2r5e, Pmf1, Smc3, Kif2c, Stag2
Mitotic Spindle Checkpoint	2.126	0.0335	Cdc23, Bub1b, Anapc4, Mad2l1, Ube2d1, Cdc26, Cdc20, Bub3, Anapc1, Anapc2, Cdc27, Cdc16
TRAF6 Mediated Induction of proinflammatory cytokines	2.086	0.0369	Rela, Nfkb2, Map2k6, Nfkbia, Mapk3, Mapk11, Rps6ka1, Cdk1, Tab2, Nfkbib, Hmg1l1, Map3k7, Jun, Nod2, Mapk9, Map2k4, Dusp3, Mapk7, Dusp6, Mapkapk3, Mapk10, Atf2
Regulated proteolysis of p75NTR	2.084	0.0372	Rela, Aph1b, Psenen, Adam17, Psen1
APC/C:Cdc20 mediated degradation of Cyclin B	2.05	0.0403	Cdk1, Cdc23, Anapc4, Ube2d1, Cdc26, Cdc20, Anapc1, Anapc2, Cdc27, Cdc16
Dopamine Neurotransmitter Release Cycle	2.05	0.0403	Syn3, Syn1, Syt1, Stxbp1, Cplx1, Stx1a
Serotonin Neurotransmitter Release Cycle	2.05	0.0403	Syn3, Syn1, Syt1, Stxbp1, Cplx1, Stx1a
Double-Strand Break Repair	2.05	0.0404	Brca1, Brca2, Mdc1, Brip1, Xrcc5, Atm, Prkdc, Rad51, Lig1, Rpa1, Nbn
Metal ion SLC transporters	2.044	0.041	Slc11a2, Slc39a6, Slc41a2, Slc30a3, Cp, Slc31a1, Slc30a1, Slc39a8, Slc30a2, Slc39a3

Signalling to RAS	2.018	0.0436	Grb2, Src, Ralgds, Mapk3, Mapk11, Shc2, Cdk1, Ralb, Rala, Ngf, Hras1, Ywhab, Mapkapk3, Nras, Mapkapk2, Sos1, Map2k1
MAP kinase activation in TLR cascade	1.996	0.046	Map2k6, Mapk3, Mapk11, Rps6ka1, Cdk1, Tab2, Map3k7, Jun, Nod2, Mapk9, Map2k4, Dusp3, Mapk7, Dusp6, Mapkapk3, Mapk10, Atf2, Mapkapk2, Ppp2r5d, Map2k1, Ripk2, Tab1, Mapk1, Tab3, Ppp2r1a
Activation of the AP-1 family of transcription factors	1.992	0.0464	Mapk3, Mapk11, Jun, Mapk9, Mapk10, Atf2
Interleukin-7 signaling	1.984	0.0472	Stat5a, Stat5b, Pik3r3, Jak1, Jak3, Pik3r1, Il7
Inhibition of replication initiation of damaged DNA by RB1/E2F1	1.967	0.0492	Pola1, Prim1, Prim2, Pola2, Rb1, E2f1, Tfdp1, Ppp2r1a

8.5. The Reactome pathways for the 72 vs. 24 hour signature

Set	NES	p-value	Ledge
Neurotransmitter Receptor Binding And Downstream Transmission In The Postsynaptic Cell	4.022	5.76e-05	Gnal, Kcnj6, Gabrg3, Gng4, Gria4, Gabrb3, Grin2a, Camk4, Grik2, Grip1, Gabbr2, Adcy5, Plcb3, Gng2, Rasgrf1, Rps6ka3, Gnai2, Adcy8, Grin2b, Chrna7, Rasgrf2, Grik1, Gabra5, Grip2, Adcy2, Camk2d, Kcnj2, Dlg4, Gabrb2, Camk2g, Akap5, Chrnb2, Cacng4, Grin1, Gabbr1, Prkca, Gnai1, Cacng2, Plcb1, Adcy1, Chrne, Myo6, Gabrg2, Gabra3, Camk2b, Gria3, Gabra2, Ap2b1, Grik4, Braf, Cacng3, Kcnj3, Nsf, Gng13, Gria2
G alpha (z) signalling events	3.956	7.64e-05	Prkce, Gng4, Rgs4, Adcy5, Gng2, Gnai2, Adcy8, Rgs17, Rgs20, Adcy2, Prkca, Gnai1, Adcy1
Interleukin-6 signaling	3.684	0.000229	Stat1, Stat3, Jak2, Il6st, Il6, Tyk2, Socs3
GABA A receptor activation	3.661	0.000252	Gabrg3, Gabrb3, Gabra5, Gabrb2, Gabrg2, Gabra3, Gabra2
DSCAM interactions	3.487	0.000488	Dscam, Dcc, Ntn1, Mapk8, Pak1, Dscaml1
Transmission across Chemical Synapses	3.444	0.000573	Gnal, Cacna2d3, Kcnj6, Gabrg3, Gad2, Gng4, Syt1, Gria4, Slc6a13, Gls, Gabrb3, Grin2a, Camk4, Grik2, Grip1, Gabbr2, Adcy5, Plcb3, Gng2, Rasgrf1, Snap25, Rps6ka3, Gnai2, Adcy8, Grin2b, Chrna7, Rasgrf2, Gad1, Syn1, Grik1, Gabra5, Stxbp1, Vamp2, Grip2, Adcy2, Camk2d, Cacna1a, Cacna1b, Kcnj2, Dlg4, Gabrb2, Camk2g, Akap5, Chrnb2, Cacng4, Grin1, Gabbr1, Prkca, Dnajc5, Abat, Gnai1, Cacng2, Plcb1, Adcy1, Syn2, Slc38a2, Cplx1, Slc1a1, Cacna2d1, Slc38a1, Chrne, Myo6, Gabrg2, Comt, Gabra3, Camk2b, Gria3, Gabra2, Ap2b1, Grik4, Braf, Cacng3, Kcnj3, Stx1a, Slc1a7, Nsf, Gng13, Gria2, Cacnb1, Slc1a3, Rps6ka2, Kcnj9
Neuronal System	3.255	0.00113	Gnal, Kcnh8, Cacna2d3, Vamp1, Kcnj6, Gabrg3, Gad2, Hcn4, Kcnk10, Kcnq3, Kcnmb1, Gng4, Syt1, Gria4, Slc6a13, Kcnab1, Gls, Kcnn2, Gabrb3, Grin2a, Camk4, Grik2, Grip1, Kcnh1, Gabbr2, Adcy5, Plcb3, Gng2, Rasgrf1, Snap25, Rps6ka3, Gnai2, Stx1b, Kcnh7, Adcy8, Grin2b, Kcnma1, Hcn1, Kcng2, Chrna7, Kcnq1, Rasgrf2, Kcnc2, Gad1, Syn1, Stx7, Grik1, Gabra5, Stxbp1, Vamp2, Grip2, Adcy2, Camk2d, Cacna1a, Cacna1b, Kcnj2, Kcnq2, Dlg4, Kcnv1, Gabrb2, Camk2g, Kcnb2, Akap5, Chrnb2, Cacng4, Grin1, Gabbr1, Prkca, Dnajc5,

			Abat, Gnai1, Cacng2, Plcb1, Adcy1, Syn2, Slc38a2, Gjd2, Cplx1, Slc1a1, Cacna2d1, Kcna1, Kcnc1, Slc38a1, Chrne, Myo6, Gabrg2, Comt, Stx12, Kcnn1, Gabra3, Stx6, Stx2, Camk2b, Gria3, Kcnd2, Gabra2, Ap2b1, Syt2, Panx1, Grik4, Braf, Cacng3, Kcna5, Kcnj3, Stx1a, Slc1a7, Nsf, Gng13, Gria2, Kcnmb2, Cacnb1, Slc1a3, Rps6ka2, Kcnk6, Kcnj9
Signaling by Robo receptor	3.25	0.00115	Nck2, Srgap1, Robo2, Pak6, Pak7, Pak1, Clasp2, Pak3, Srgap2, Cap1, Clasp1, Evl, Arhgap39, Pfn1, Srgap3, Pak4
Removal of DNA patch containing abasic residue	3.145	0.00166	Mutyh, Mpg, Pold4, Pold3, Apex1, Pold2, Pcna, Pold1, Nthl1, Lig1, Mbd4, Smug1, Fen1, Polb
Resolution of AP sites via the multiple-nucleotide patch replacement pathway	3.145	0.00166	Mutyh, Mpg, Pold4, Pold3, Apex1, Pold2, Pcna, Pold1, Nthl1, Lig1, Mbd4, Smug1, Fen1, Polb
GABA receptor activation	3.015	0.00257	Gnal, Kcnj6, Gabrg3, Gng4, Gabrb3, Gabbr2, Adcy5, Gng2, Gnai2, Adcy8, Gabra5, Adcy2, Kcnj2, Gabrb2, Gabbr1, Gnai1, Adcy1, Gabrg2, Gabra3, Gabra2
DCC mediated attractive signaling	2.975	0.00293	Dcc, Ntn1, Fyn, Ablim3, Trio, Ptk2, Ablim2, Wasl, Ablim1
Regulation of IFNA signaling	2.926	0.00344	Usp18, Stat1, Stat2, Ptpn6, Tyk2, Ifnar1, Socs3
Opioid Signalling	2.885	0.00391	Gnal, Pde4b, Gng4, Ppp3cc, Camk4, Adcy5, Plcb3, Gng2, Gnai2, Adcy8, Oprm1, Gnao1, Adcy2, Ppp1r1b, Pde1c, Ppp3ca, Prkca, Ppp1ca, Gnai1, Plcb1, Adcy1
Nephrin interactions	2.872	0.00407	Magi2, Nck2, Pik3r1, Spnb2, Nphs1, Fyn, Cask, Actn3, Actn4, Wasl, Spna2, Kirrel2
Platelet homeostasis	2.782	0.0054	Slc8a3, Kcnmb1, Gng4, Slc8a1, Pde10a, Gng2, Gucy1a2, Atp2b2, Atp2b1, Kcnma1, Trpc7, Stim1, Pde3a, Ptpn6, Pde11a, Ppp2r5e, Gucy1b3, Fgr, Prkg1, Pde1a, Atp2b3, Gng13, Atp2b4, Kcnmb2, Ppp2r5d, Ppp2r5b, P2rx1, Mapk14, Ptpn11, Gng8, Itpr2, Kcnmb4, Gnb5, Pde3b, Nos1
GABA synthesis, release, reuptake and degradation	2.706	0.00682	Gad2, Syt1, Slc6a13, Snap25, Gad1, Stxbp1, Vamp2, Dnajc5, Abat, Cplx1
G beta:gamma signalling through	2.702	0.00689	Gng4, Plcb3, Gng2, Plcb1, Gng13, Gng8, Plcb2, Gnb5, Gnb2,

PLC beta			Gng3, Gnb4, Gng7, Gngt2, Gnb3, Gng10, Gnb1, Gng12
Interaction between L1 and Ankyrins	2.643	0.00822	Kcnq3, Scn8a, Nfasc, Nrcam, Ank3, Spnb2, Scn3a, Kcnq2, Scn1a, Scn3b, Scn2a1, Ank1, Spnb3, Spna2, Scn7a, L1cam, Scn1b
Activation of NMDA receptor upon glutamate binding and postsynaptic events	2.637	0.00837	Gria4, Grin2a, Camk4, Rasgrf1, Rps6ka3, Adcy8, Grin2b, Rasgrf2, Camk2d, Dlg4, Camk2g, Grin1, Adcy1, Camk2b, Gria3, Braf, Gria2, Rps6ka2
Base Excision Repair	2.593	0.0095	Mutyh, Mpg, Pold4, Pold3, Xrcc1, Apex1, Pold2, Pcna, Pold1, Nthl1
Resolution of Abasic Sites (AP sites)	2.593	0.0095	Mutyh, Mpg, Pold4, Pold3, Xrcc1, Apex1, Pold2, Pcna, Pold1, Nthl1
Adenylate cyclase inhibitory pathway	2.52	0.0117	Gnal, Adcy5, Gnai2, Adcy8, Adcy2, Gnai1, Adcy1
Inhibition of adenylate cyclase pathway	2.52	0.0117	Gnal, Adcy5, Gnai2, Adcy8, Adcy2, Gnai1, Adcy1
Activation of GABAB receptors	2.487	0.0129	Gnal, Kcnj6, Gng4, Gabbr2, Adcy5, Gng2, Gnai2, Adcy8, Adcy2, Kcnj2, Gabbr1, Gnai1, Adcy1
GABA B receptor activation	2.487	0.0129	Gnal, Kcnj6, Gng4, Gabbr2, Adcy5, Gng2, Gnai2, Adcy8, Adcy2, Kcnj2, Gabbr1, Gnai1, Adcy1
Processive synthesis on the C-strand of the telomere	2.459	0.0139	Rpa1, Pold4, Pold3, Pold2, Pcna, Pold1, Rpa2, Lig1, Dna2, Fen1
L1CAM interactions	2.456	0.014	Sh3gl2, Kcnq3, Dcx, Cntn1, Dnm3, Scn8a, 4930506M07Rik, Nfasc, Rps6ka3, Nrcam, Ank3, Spnb2, Pak1, Scn3a, Csnk2b, Kcnq2, Dlg4, Chl1, Scn1a, Kif4, Alcam, Scn3b, Dnm1, Stip1, Scn2a1, Cntnap1, Ank1, Ap2b1, Spnb3, Fgfr1, Spna2, Rps6ka2, Ncam1, Scn7a, Egfr, Clta, L1cam, Scn1b, Nrp1, Csnk2a2, Mapk1, Itga5, Scn9a
Removal of the Flap Intermediate from the C-strand	2.438	0.0147	Rpa1, Pold4, Pold3, Pold2, Pcna, Pold1
Disease	2.432	0.015	Pcsk2, App, Prkce, Vamp1, Eif2ak2, Sh3gl2, Acadvl, Pag1, Gtf2e1, Syt1, Cdk1, Grb2, Camk4, Mmp2, Hspa5, Adcy5, Dock2, Casp9, Cul7, Myo5a, Stam, Snap25, Bche, Slc30a6,

			Adam17, Taf6, Stx1b, Nup205, Actb, Adcy8, Psmc2, Pik3r1, Tbp, Pdia6, Cpe, Adam12, Mnat1, Nup50, Stx7, Rps23, Hdgf, Vamp2, Srpr, Polr2g, Tpp1, Adcy2, Mbtps1, Rps16, Psmd7, Psma1, Ran, Ap1s2, Calr, Elmo1, Cdkn1b, Th1l, Aaas, Ncbp1, Srprb, Nup188, Ddx11, Ubc, Ncbp2, Pde1c, Fyn, Prkca, Gtf2h4, Psmc4, Rps10, Rps5, Adcy1, Nup107, Nup93, Nup88, Mfge8, Sh3kbp1, Gsk3b, Nup37, Wipi1, Cdkn1a, Rnmt, Ap1m1, Spry2, Rpl3, Rpsa, Psmd5, Tceb3, Rps3a, Stx12, Ssrp1, Rps3, Dnajb11, Rpl19, Rplp0, Kras, Psmd4, Mbtps2, Stx6, Psma4, Taf5, Rpl17, Stx2, Psma7, Rps11, Igfbp4, Spcs1, Npm1, Gtf2h3, Exosc8, Xrcc5, Eps15, Ap2b1, Rcc1, Nup62, Taf9, Rps29, Gtf2f2, Syt2, Igfbp2, Slc25a5, Apcs, Hist1h3c, Sec31a, Psmc1, Rps8, Psmb11, Rpl27a, Pde1a, Herpud1, Rps7, Igf2, Stx1a, Rps25, H2afz, Gfpt1, Prkar1b, Rpl18a, Trib3, Rpl4, Tln1, Rps9, Rpl6, Atp6v0d1, Tatdn2, Hsp90b1, Spcs2, Lig1, Eif2s1, Gosr2, Pten, Rpl27, Rpl35, Rpl11, Serp1, Rpl23a, Exosc3, Exosc1, Rps4x, Supt16h, Mboat4, Ppp2r5b, Cd28, Polr2j, Ywhab, Egfr, Ssr1, Rngtt, Rpl37, Them4, Prkar2a, Nup155, Pappa2, Cpsf4, Hmga1, Fkbp14, Hyou1, Psmc3, Psmd9, Igf2bp3, Egf, Clta, Akt1, Psme3, Ptpn11, Adcy4, Hist1h2bm, Pacs1, Itpr2, Psmc5, Hist1h2bp, Polr2c, Nup43, Exosc9, D17Wsu104e, Rpl34, Rplp1, Zbtb17, Cdc37, Rpl7, Cd4, Canx, Rpl24, Cxxc1, Psmb2, Rps6, Banf1, Exoc2, Mapk1, Psma2, Kdelr3, Fen1, Lmna, Tgfbi, Tspyl2, Phlpp1, Rpl14, Rps15a, H2-Q10, Slc30a5, Arhgef7
Botulinum neurotoxicity	2.425	0.0153	Vamp1, Syt1, Snap25, Stx1b, Stx7, Vamp2, Stx12, Stx6, Stx2, Syt2, Stx1a
Transport of the SLBP independent Mature mRNA	2.409	0.016	Nup205, Nup50, Aaas, Nxf1, Ncbp1, Nup188, Ncbp2, Nup107, Nup93, Nup88, Nup37
Netrin mediated repulsion signals	2.406	0.0161	Dcc, Unc5d, Unc5c, Ntn1, Fyn, Ptk2, Ptpn11, Unc5a
G-protein beta:gamma signalling	2.387	0.017	Gng4, Plcb3, Gng2, Pik3r5, Plcb1, Pik3cg, Gng13, Akt1, Gng8, Plcb2, Gnb5, Gnb2, Pdpk1, Gng3, Gnb4, Gng7, Gngt2, Rhoa, Gnb3, Gng10, Gnb1, Gng12
Activation of Kainate Receptors upon glutamate binding	2.38	0.0173	Gng4, Grik2, Plcb3, Gng2, Grik1, Dlg4, Plcb1
Signaling by the B Cell Receptor (BCR)	2.348	0.0189	Nfkbia, Trpc1, Grb2, Casp9, Psmc2, Pik3r1, Stim1, Plcg2, Card11, Psmd7, Psma1, Rasgrp1, Cdkn1b, Ikbkg, Ubc, Fyn, Psmc4, Bcl10, Btk, Sh3kbp1, Gsk3b, Cdkn1a, Cblb, Rel, Psmd5, Kras, Psmd4, Psma4, Psma7, Sykb, Fbxw11, Psmc1,

			Psmb11, Trib3, Pten, Them4, Psmc3, Psmd9, Akt1, Psme3, Itpr2, Nfkbie, Psmc5, Psmb2, Psma2, Phlpp1, Rela, Nfkb1, Cd79a, Dapp1, Shc1, Sos1, Rictor, Prkcb, Pik3cd, Psmd1, Psmd12, Psmb1
Post NMDA receptor activation events	2.343	0.0192	Grin2a, Camk4, Rasgrf1, Rps6ka3, Adcy8, Grin2b, Rasgrf2, Camk2d, Dlg4, Camk2g, Grin1, Adcy1
Activation of the AP-1 family of transcription factors	2.287	0.0222	Mapk8, Mapk10, Mapk9, Fos, Mapk14, Jun, Mapk1
Transport of the SLBP Dependant Mature mRNA	2.282	0.0225	Nup205, Nup50, Aaas, Nxf1, Ncbp1, Nup188, Ncbp2, Nup107, Nup93, Nup88, Nup37
N-glycan trimming in the ER and Calnexin/Calreticulin cycle	2.261	0.0238	Man1b1, Ganab, Calr, Uggt1, Pdia3, Mogs
Glutamate Neurotransmitter Release Cycle	2.23	0.0257	Syt1, Gls, Snap25, Stxbp1, Vamp2, Slc38a2, Cplx1, Slc1a1, Stx1a, Slc1a7
ADP signalling through P2Y purinoceptor 12	2.229	0.0258	Gng4, Gng2, Gnai2, Gnai1, Gng13, Gng8, Gnb5, Gnb2, Gng3, Gnb4, Gng7, Gngt2, Gnb3, P2ry12, Gnai3, Gng10, Gnb1, Gng12
Unfolded Protein Response	2.222	0.0263	Acadvl, Hspa5, Cul7, Pdia6, Hdgf, Srpr, Tpp1, Mbtps1, Calr, Srprb, Ddx11, Wipi1, Dnajb11, Mbtps2, Exosc8, Sec31a, Herpud1, Gfpt1, Tln1, Atp6v0d1, Tatdn2, Hsp90b1, Eif2s1, Gosr2, Serp1, Exosc3, Exosc1, Ppp2r5b, Ssr1, Fkbp14, Hyou1, Exosc9, D17Wsu104e, Zbtb17, Cxxc1, Kdelr3, Lmna, Tspyl2, Klhdc3, Shc1, Exosc7, Ern1, Atf3
Ion channel transport	2.214	0.0269	Atp8a1, Gabrg3, Gabrb3, Atp10b, Atp8a2, Atp2b2, Atp2b1, Atp11b, Atp1b1, Gabra5, Gabrb2, Atp9a, Atp11c, Gabrg2, Glra3, Gabra3, Atp8b1, Gabra2, Glra4, Atp2b3, Atp2b4, Atp8b2, Htr3a, Atp9b, Gabra1, Arhgef9, Atp1a3, Glra2
Activation of Rac	2.2	0.0278	Nck2, Pak6, Pak7, Pak1, Pak3
Repair synthesis for gap-filling by DNA polymerase in TC-NER	2.199	0.0278	Rpa1, Pold4, Pold3, Pold2, Pcna, Pold1, Rfc4, Pole2, Rfc3, Pole, Rpa2
Repair synthesis of patch ~27-30 bases long by DNA polymerase	2.199	0.0278	Rpa1, Pold4, Pold3, Pold2, Pcna, Pold1, Rfc4, Pole2, Rfc3, Pole, Rpa2

MAP kinase activation in TLR cascade	2.197	0.028	Cdk1, Rps6ka3, Map2k4, Mapk8, Mapk10, Ikbkg, Mapkapk3, Irak1, Mef2c, Mapk9, Nod2, Rps6ka2, Ppp2r5d, Fos, Map2k3, Mapk14, Tab3, Nod1, Mef2a, Atf1, Jun, Mapk1, Dusp6, Tab2, Mapkapk2, Dusp3, Dusp4
Inhibition of Insulin Secretion by Adrenaline/Noradrenaline	2.19	0.0285	Gng4, Adcy5, Gng2, Gnai2, Gnao1, Cacna1c, Gnai1, Cacna1d
Gap-filling DNA repair synthesis and ligation in GG-NER	2.177	0.0294	Rpa1, Pold4, Pold3, Pold2, Pcna, Pold1, Rfc4, Pole2, Rfc3, Pole, Rpa2, Lig1
Gap-filling DNA repair synthesis and ligation in TC-NER	2.177	0.0294	Rpa1, Pold4, Pold3, Pold2, Pcna, Pold1, Rfc4, Pole2, Rfc3, Pole, Rpa2, Lig1
Class C/3 (Metabotropic glutamate/pheromone receptors)	2.175	0.0296	Grm7, Gabbr2, Grm4, Gprc6a, Gabbr1, Grm5, Casr, Tas1r3
Platelet calcium homeostasis	2.174	0.0297	Slc8a3, Slc8a1, Atp2b2, Atp2b1, Trpc7, Stim1
Proteolytic cleavage of SNARE complex proteins	2.146	0.0319	Vamp1, Snap25, Stx1b, Stx7, Vamp2, Stx12, Stx6, Stx2, Stx1a
MAPK targets/ Nuclear events mediated by MAP kinases	2.134	0.0328	Rps6ka3, Mapk8, Mapk10, Mef2c, Mapk9, Rps6ka2, Ppp2r5d, Fos, Mapk14, Mef2a, Atf1, Jun, Mapk1, Dusp6, Mapkapk2, Dusp3, Dusp4
Activation of Chaperones by IRE1alpha	2.133	0.0329	Acadvl, Hspa5, Cul7, Pdia6, Hdgf, Srpr, Tpp1, Srprb, Ddx11, Wipi1, Dnajb11, Sec31a, Gfpt1, Tln1, Atp6v0d1, Tatdn2, Gosr2, Serp1, Ppp2r5b, Ssr1, Fkbp14, Hyou1, D17Wsu104e, Zbtb17, Cxxc1, Kdelr3, Lmna, Tspyl2, Klhdc3, Shc1
Interferon alpha/beta signaling	2.1	0.0357	Usp18, Irf1, Ifitm3, Irf9, Irf7, Stat1, Gm14446, Irf4, Ifi35, Stat2, Irf3, Ptpn6, Ifi27l1, Isg15, Oas1a, Tyk2, Ifnar1, Oasl1
Other semaphorin interactions	2.089	0.0367	Plxnc1, Sema6d, Sema6a, Sema7a, Sema4a, Plxna4
Activation of Chaperone Genes by XBP1(S)	2.086	0.037	Acadvl, Cul7, Pdia6, Hdgf, Srpr, Tpp1, Srprb, Ddx11, Wipi1, Dnajb11, Sec31a, Gfpt1, Tln1, Atp6v0d1, Tatdn2, Gosr2, Serp1, Ppp2r5b, Ssr1, Fkbp14, Hyou1, D17Wsu104e, Zbtb17, Cxxc1, Kdelr3, Lmna, Tspyl2, Klhdc3, Shc1
DARPP-32 events	2.082	0.0374	Pde4b, Ppp3cc, Ppp1r1b, Ppp3ca, Ppp1ca, Prkar1b, Ppp2r5d, Prkar2a, Ppp3r1

Calnexin/calreticulin cycle	2.076	0.0379	Man1b1, Ganab, Calr, Uggt1, Pdia3
Removal of the Flap Intermediate	2.065	0.0389	Rpa1, Pold4, Pold3, Pola2, Pold2, Pcna, Pold1, Rpa2, Prim1, Prim2, Dna2, Fen1
Resolution of AP sites via the single-nucleotide replacement pathway	2.059	0.0395	Mutyh, Mpg, Xrcc1, Apex1, Nthl1, Mbd4, Smug1, Polb
Glucose transport	2.058	0.0396	Slc2a4, Nup205, Nup50, Aaas, Nup188, Nup107, Nup93, Nup88, Nup37, Slc2a3, Nup62, Hk3, Slc2a2, Gck, Nup155
Depolarization of the Presynaptic Terminal Triggers the Opening of Calcium Channels	2.058	0.0396	Cacna2d3, Cacna1a, Cacna1b, Cacng4, Cacng2, Cacna2d1
Antigen Activates B Cell Receptor Leading to Generation of Second Messengers	2.053	0.0401	Trpc1, Grb2, Pik3r1, Stim1, Plcg2, Fyn, Btk, Sh3kbp1, Cblb, Sykb
TRAF6 Mediated Induction of proinflammatory cytokines	2.051	0.0403	Nfkbia, Nfkb2, App, Cdk1, Rps6ka3, Map2k4, Mapk8, Mapk10, Ikbkg, Mapkapk3, Ubc, Irak1, Mef2c, Mapk9, Nod2, Rps6ka2, Ppp2r5d, Fos, Map2k3, Mapk14, Tab3, Nod1, Mef2a, Atf1, Jun, Mapk1, Dusp6, Rela, Nfkb1, Tab2, Mapkapk2, Dusp3, Dusp4
Processive synthesis on the lagging strand	2.04	0.0413	Rpa1, Pold4, Pold3, Pola2, Pold2, Pcna, Pold1, Rpa2, Prim1, Lig1, Prim2, Dna2, Fen1
Regulation of Insulin Secretion by Acetylcholine	2.038	0.0416	Chrm3, Gna14, Plcb3, Gna15, Prkca, Plcb1
Cell Cycle Checkpoints	2.028	0.0426	Cdc7, Cdk1, Bub1b, Rpa1, Mcm5, Wee1, Mcm2, Cdc23, Psmc2, Ccnb2, Trp53, Bub3, Psmd7, Psma1, Cdkn1b, Cdc20, Ubc, Cdk2, Psmc4, Ube2c, Cdkn1a, Cdc45, Psmd5, Rfc4, Ccne1, Ube2d1, Psmd4, Psma4, Orc6, Psma7, Mcm10, Mcm7, Rfc3, Psmc1, Psmb11, Rpa2, Dbf4, Rad9, Psmc3, Psmd9, Cdc25c, Mcm3, Psme3, Rad1, Cdc26, Psmc5, Mad2l1, Atrip, Psmb2, Psma2, Rfc2, Rad9b, Mcm4, Anapc11, Hus1, Psmd1, Psmd12, Orc4, Psmb1, Mcm6, Rpa3
Nitric oxide stimulates guanylate cyclase	2.026	0.0427	Kcnmb1, Pde10a, Gucy1a2, Kcnma1, Pde3a, Pde11a, Gucy1b3, Prkg1, Pde1a, Kcnmb2

Asparagine N-linked glycosylation	2.026	0.0428	Man1b1, Man1a, Fut8, Gfpt2, St8sia3, Mcfd2, B4galt5, Ganab, B4galt6, Man1c1, Alg3, Calr, Rpn2, Alg8, Mgat4b, Uggt1, Mgat3, Pdia3, Man1a2, Sec13, Mogs, Sec31a, Mgat4c, Dpagt1, Rpn1, Gfpt1, Ddost, Alg2, Pgm3, Mgat2, Gmppa, Mgat5, Dolpp1
N-glycan antennae elongation in the medial/trans-Golgi	2.018	0.0436	Fut8, St8sia3, B4galt5, B4galt6, Mgat4b, Mgat3, Mgat4c, Mgat2, Mgat5
Glutamate Binding, Activation of AMPA Receptors and Synaptic Plasticity	2.017	0.0437	Gria4, Grip1, Grip2, Camk2d, Dlg4, Camk2g, Akap5, Cacng4, Prkca, Cacng2, Myo6, Camk2b, Gria3, Ap2b1, Cacng3, Nsf, Gria2
Trafficking of AMPA receptors	2.017	0.0437	Gria4, Grip1, Grip2, Camk2d, Dlg4, Camk2g, Akap5, Cacng4, Prkca, Cacng2, Myo6, Camk2b, Gria3, Ap2b1, Cacng3, Nsf, Gria2
JNK (c-Jun kinases) phosphorylation and activation mediated by activated human TAK1	2.012	0.0443	Map2k4, Mapk8, Mapk10, Ikbkg, Irak1, Mapk9, Nod2, Tab3, Nod1
Presynaptic function of Kainate receptors	2.005	0.045	Gng4, Plcb3, Gng2, Plcb1, Gng13, Gng8, Plcb2, Gnb5, Gnb2, Gng3, Gnb4, Gng7, Gngt2, Gnb3, Gng10, Gnb1, Gng12
MyD88-independent cascade initiated on plasma membrane	2.003	0.0452	Nfkbia, Irf7, Nfkb2, App, Cdk1, Rps6ka3, Map2k4, Mapk8, Mapk10, Irf3, Ikbkg, Mapkapk3, Ubc, Irak1, Mef2c, Mapk9, Ly96, Nod2, Rps6ka2, Ppp2r5d, Fos, Map2k3, Mapk14, Tab3, Nod1, Mef2a, Atf1, Jun, Mapk1, Dusp6, Rela, Nfkb1, Tab2, Mapkapk2, Dusp3, Dusp4, Ager, Ticam2
Adenylate cyclase activating pathway	1.988	0.0468	Gnal, Adcy5, Adcy8, Adcy2, Adcy1
Facilitative Na+-independent glucose transporters	1.978	0.048	Slc2a4, Slc2a7, Slc2a3, Slc2a12, Slc2a2, Slc2a10, Slc2a5
Transport of Mature mRNA Derived from an Intronless Transcript	1.967	0.0492	Nup205, Nup50, Aaas, Nxf1, Ncbp1, Nup188, Ncbp2, Nup107, Nup93, Nup88, Nup37
Axon guidance	1.967	0.0492	Rnd1, Gfra2, Met, Plxnc1, Dcc, Nck2, Trpc1, Sh3gl2, Kcnq3, Unc5d, Srgap1, Dcx, Robo2, Cdk1, Grb2, Cntn1, Rhog, Dnm3, Scn8a, Pak6, Pak7, 4930506M07Rik, Unc5c, Nfasc, Sema6d,

			Sema6a, Rps6ka3, Cacna1i, Ntn1, Nrcam, St8sia4, Trpc7, Ank3, Spnb2, Pak1, Siah2, Rgmb, Dpysl3, Scn3a, Csnk2b, Kcnq2, Dlg4, Chl1, Gfra1, Scn1a, Crmp1, Clasp2, Fyn, Artn, Sema7a, Kif4, Cacna1c, Col2a1, Alcam, Dpysl5, Col1a2, Gsk3b, Sema4a, Ablim3, Scn3b, Dnm1, Pak3, Stip1, Scn2a1, Srgap2, Cntnap1, Kras, Ank1, Cdk5r1, Cacna1d, Cap1, Clasp1, Ap2b1, Plxna4, Spnb3, Col4a5, Fgfr1, Trio, Tln1, Ptk2, Cacna1h, Neo1, Ablim2, Cfl1, Wasl, Rhob, Cacnb1, Spna2, Rps6ka2, Ablim1, Ncam1, Sema3a, Evl, Scn7a, Ywhab, Egfr, Erbb2, Hfe2, Arhgap39, Pitpna, Fes, Plxna2, Pfn1, Srgap3, Pak4, Cacna1s, Hsp90ab1, Pip5k1c, Clta, Ptpn11, 2900073G15Rik, L1cam, Unc5a, Myl6

8.6. The Reactome pathways for the 168 vs. 72 hour signature

Set	NES	p-value	Ledge
Amino acid synthesis and interconversion (transamination)	4.147	3.37e-05	Psat1, Asns, Psph, Glul, Aldh18a1, Gpt2, Gls, Got2, Got1, Gpt, Phgdh
Activation of Rac	3.573	0.000352	Nck2, Pak3, Sos1, Slit2, Pak4, Pak7, Pak1, Pak6
Signaling by Robo receptor	3.278	0.00105	Nck2, Vasp, Pak3, Cap1, Sos1, Arhgap39, Clasp2, Pfn1, Slit2, Pfn2, Pak4, Pak7, Pak1
Regulation of IFNA signaling	3.207	0.00134	Ifnar2, Stat2, Socs3, Tyk2, Ptpn6, Jak1, Usp18, Stat1
GABA A receptor activation	2.862	0.00421	Gabra1, Gabra3, Gabra5, Gabrb2, Gabra2, Arhgef9, Gabrg3, Gabra4, Gabrg2
Cytosolic tRNA aminoacylation	2.702	0.00689	Mars, Cars, Gars, Aars, Nars, Tars, Iars, Farsa, Kars, Yars, Aimp2, Lars, Sars, Wars, Vars
Zinc influx into cells by the SLC39 gene family	2.697	0.007	Slc39a10, Slc39a1, Slc39a6, Slc39a8, Slc39a7
PPARA Activates Gene Expression	2.608	0.0091	Srebf1, Havcr2, Hmgcr, Me1, Grhl1, Chd9, Txnrd1, Trib3, Smarcd3, Plin2, Tead2, Ncoa1, Ncoa2, Ankrd1, Ncoa6, Nfya, Med31, Esrra, Med4, Tead3, Cdk19, Cyp1a1, Fdft1, Cpt1a, Ugt1a10, Angptl4, Ppargc1a, Rgl1, Acadm, Med13, Ncor1, Tbl1x, Acsl1, Ccnc, Pparg, Abcb4, Arntl, Med21, Abca1, G0s2, Hmgcs2, Yap1, Srebf2, Tnfrsf21, Agt, Med11, Apoa2, Med15, Slc27a1, BC006779, Fhl2, Wwtr1, Ep300, Med25, Med1, Cpt2, Med30, Med29
Zinc transporters	2.607	0.00914	Slc39a10, Slc39a1, Slc30a7, Slc39a6, Slc39a8, Slc39a7, Slc30a2
tRNA Aminoacylation	2.593	0.00951	Mars, Cars, Gars, Aars, Nars, Tars, Iars, Farsa, Kars, Yars, Yars2, Sars2, Tars2, Aimp2, Lars, Sars, Wars, Iars2, Vars, Nars2, Aimp1, Hars, Dars, Vars2, Qars
Interleukin-6 signaling	2.438	0.0148	Il6st, Jak2, Socs3, Stat3, Tyk2, Cbl, Jak1
Disease	2.407	0.0161	Adcy2, Tgfbi, Atf3, Cdkn1a, Casp9, Hmga1, Pik3r1, Igfbp5, Xpo1, Hdgf, Atf4, Sh3kbp1, Prkce, Preb, Src, Herpud1, Eps15, Ncbp1,

			Rcc1, Stx6, Lmna, Igf2bp1, Asns, Actb, Sos1, Stam, Trib3, Pcsk2, Pappa2, Tcea1, Cul7, Psmf1, Mapk1, Adrbk1, Pag1, Slc30a7, Dock2, Vamp1, Srprb, Exoc3, Sec31a, Rnmt, Ap1s2, Igfbp4, Edem1, Acadvl, Ccnt1, Psip1, Th1l, Wipi1, Pdia5, Aaas, Nmt1, Snca, Rps29, Tln1, Lig1, Exoc6, Syt2, Igf2bp2, Gsn, Ran, Klhdc3, Adcy8, Akt3, Igf1, Exoc7, Psme3, Nup62, Psmc4, Mfge8, Cpsf4, App, Exoc2, Hgs, Adcy1, Mmp2, Ap1m1, Supt5h, Rdbp, Akt1s1, Rpl36a, Nup188, Ranbp2, Akt1, Gm10136, Shc1, Rps18, Gsk3a, Nup93, Nfya, Hist3h2bb-ps, Exosc6, Nupl1, Dnajc3, Rps8, Banf1, Kpnb1, Rps11, Ssrp1, Grb2, Cltc, Nup50, Dcp2, Tceb3, Kpna1, Rpl18a, Prkcd, Exoc5, Psmc1, Psmd4, Stx3, Rps15a, Psmc3, Calr, Sh3gl2, Exosc3, Cbl, Rpl27a, Cdc37, Csk, Gsk3b, Nup133, Nup210, Atf6, Rplp1, Pten, Dnajb11, Rps2, Ap1s1, Ap2a1, Rictor, Ipo5, Exosc5, Rpl26, Mnat1, Vps37c, Grsf1, Rplp0, Rps5, Gtf2h4, Psma1, Arfgap1, Egfr, Rps6, Prkaca, Rps3a, Exosc4, Pde1c, Ccnt2, Igfbp2, Taf12, Taf6, Psmb1, Stx5a, Rpl28, Exosc2, Mdm2, Taf10, Extl3, Hyou1, Ctsg, Zbtb17, Rps4x, Hist3h2ba, Kras, Rpl39, Rplp2, Ercc3, Kdelr3, Eif2ak2, Skp1a, Tgfb1, Gtf2e1, Cd4, Cdk9, Elmo1, Polr2b, Rpl14, Rbx1, Rps26, Ap1m2, Psmc5, Rpl23, Ctdp1, Rpl34, Hras1, Polr2c, Rpl37, Ell, Rpl6, Rps25, Epn1, Foxo4, Camk4, Creb1, Egf, Phlpp1, Hsp90b1, Hist1h2ah, Fen1, Nppa, Cd28, Bche, Nr4a1, Adcy9, Rac1, Rps23, Taf13, Psmc2, Ercc2, Ssr1, Itpr3, Taf4a, Dctn1, Wfs1, H2afz, Rpl35, Taf11, Cxxc1, Ranbp1, Stx4a, Pak2, Pcsk1, Tpr, Psmd3, Tatdn2, Vps28, Psme1, Rpl37a, Gfpt1, Ttr, Clta, Ubc
Sulfur amino acid metabolism	2.394	0.0167	Gclc, Cdo1, Ahcy, Mtap, Cth, Csad, Got1, Suox, Tst, Gclm, Ethe1
Growth hormone receptor signaling	2.351	0.0187	Stat5a, Jak2, Mapk1, Socs3, Stat3, Cish, Lyn, Stat5b
Signaling by ERBB4	2.321	0.0203	Cdkn1a, Casp9, Pik3r1, Stat5a, Sos1, Trib3, Jak2, Mapk1, Erbb3, Cul1, Stat5b, Nrg2, Akt3, Hbegf, Akt1s1, Akt1, Shc1, Gsk3a, Cxcl12, Grb2, Gfap, Gsk3b, Wwp1, Pten, Erbb4, Rictor, Ncor1, Egfr, Aph1b, Nrg1, Tab2, Mdm2, Prlr, Kras, Skp1a, Psenen, Rbx1, Hras1, Nrg3, Foxo4, Creb1, Yap1, Pgr, Egf, Phlpp1
Regulation of Lipid Metabolism by Peroxisome proliferator-activated receptor alpha (PPARalpha)	2.321	0.0203	Srebf1, Havcr2, Hmgcr, Me1, Grhl1, Chd9, Txnrd1, Trib3, Smarcd3, Plin2, Tead2, Ncoa1, Ncoa2, Ankrd1, Ncoa6, Nfya, Med31, Esrra, Med4, Tead3, Cdk19, Cyp1a1, Fdft1, Cpt1a, Ugt1a10, Angptl4, Ppargc1a, Rgl1, Acadm, Med13, Ncor1, Tbl1x, Acsl1, Ccnc, Pparg, Abcb4, Arntl, Med21, Abca1, G0s2, Hmgcs2, Yap1, Srebf2, Tnfrsf21, Agt, Med11, Apoa2, Med15, Slc27a1, BC006779, Fhl2,

			Wwtr1, Sin3b, Ep300, Med25, Med1, Cpt2, Med30, Med29
G alpha (z) signalling events	2.32	0.0204	Adcy2, Prkce, Gnb4, Adcy8, Adcy1, Gng2, Rgs4, Gng4, Adra2b, Gnai2, Rgs19, Gnb1, Prkcd, Gnai1, Prkch, Gnb2, Rgs17, Adra2a, Gnb5, Adcy9, Gng10, Gnai3
Intrinsic Pathway for Apoptosis	2.317	0.0205	Trp53, Casp9, Bak1, Ppp3cc, Casp8, Mapk8, Xiap, Nmt1, Bcl2l1, Akt1, Dynll2, Bax, Bcl2, Ppp3r1, Bmf, E2f1
CDO in myogenesis	2.253	0.0243	Neo1, Cdh4, Ctnna2, Ctnna1, Boc, Mapk12, Tcf3, Spag9, Mapk11, Tcf4, Cdh2, Map2k6
Myogenesis	2.253	0.0243	Neo1, Cdh4, Ctnna2, Ctnna1, Boc, Mapk12, Tcf3, Spag9, Mapk11, Tcf4, Cdh2, Map2k6
N-glycan antennae elongation in the medial/trans-Golgi	2.21	0.0271	Fut8, B4galt3, St8sia2, Mgat3, B4galt2, St6gal1, St8sia6, St8sia3
Unfolded Protein Response	2.185	0.0289	Atf3, Hdgf, Atf4, Preb, Herpud1, Lmna, Asns, Cul7, Srprb, Sec31a, Edem1, Acadvl, Wipi1, Pdia5, Tln1, Klhdc3, Shc1, Gsk3a, Nfya, Exosc6, Dnajc3, Dcp2, Calr, Exosc3, Atf6, Dnajb11, Exosc5, Arfgap1, Exosc4, Exosc2, Extl3, Hyou1, Zbtb17, Kdelr3
Other semaphorin interactions	2.183	0.029	Plxna4, Plxna2, Sema5a
Iron uptake and transport	2.176	0.0295	Tfrc, Fth1, Hmox1, Cybrd1, Atp6v0a2, Cp, Abcg2, Trf, Atp6v1d, Slc11a2, Steap3, Mcoln1, Atp6v0c, Atp6v1e2, Atp6v1g3, Slc46a1, Tcirg1, Atp6v0e, Atp6v0e2, Atp6v1a, Atp6v1c2, Atp6v0b, Heph, Atp6v1c1
Metal ion SLC transporters	2.176	0.0296	Slc39a10, Slc39a1, Slc41a1, Slc30a7, Slc39a6, Slc39a8, Slc39a7, Slc30a2, Cp, Slc11a2, Slc39a5, Slc11a1
Glycogen breakdown (glycogenolysis)	2.137	0.0326	Pgm1, Pygb, Phkb, Phkg1, Pygm
GPVI-mediated activation cascade	2.131	0.0331	Pik3r1, Rhob, Pik3r5, Plcg2, Pik3r3, Lyn, Akt3, Akt1, Rhog, Pik3r2, Vav3, Vav2, Rhoa, Pik3cb, Pik3cg, Gp6, Rac1, Col1a1, Col1a2, Prkcz
DARPP-32 events	2.088	0.0368	Ppp1r1b, Ppp3cc, Pde4b, Ppp2r5d, Ppp3r1, Prkaca, Ppp3ca, Pde4a, Ppp3cb, Ppp1ca, Prkacb, Ppp2cb, Pde4c, Pde4d, Ppp2r1b, Ppp2r1a,

			Ppp2ca
Metabolism of carbohydrates	2.045	0.0409	Pgm1, Pfkfb3, Pygb, Pck2, Pgd, Eno3, Hk2, Galt, G6pdx, G6pc2, Phkb, Aaas, Fbp1, Nup62, Pgam2, Aldoa, Got2, Phkg1, Slc2a1, Got1, Prps1, Nup188, Ranbp2, Mgam, Slc2a4, Nup93, Tkt, Galk1, Nupl1, Ppp2r5d, Nup50, Pkm2, Pfkfb2, Gpi1, Gapdhs, Pygm, Nup133, Nup210, Slc2a5, Ugp2, Mdh2, Khk, Prkaca, Pgam1, Pcx, Slc25a12, Gys2, Amy1, Gys1, Pklr, Pygl
PI3K events in ERBB2 signaling	2.013	0.0442	Cdkn1a, Casp9, Pik3r1, Trib3, Erbb3, Nrg2, Akt3, Hbegf, Akt1s1, Akt1, Gsk3a, Grb2, Gsk3b, Pten, Erbb4, Rictor, Egfr, Nrg1, Erbb2, Mdm2, Nrg3, Foxo4, Creb1, Egf, Phlpp1, Nr4a1
AKT phosphorylates targets in the cytosol	2.004	0.045	Cdkn1a, Casp9, Akt3, Akt1s1, Akt1, Gsk3a, Gsk3b
Transport to the Golgi and subsequent modification	1.996	0.0459	Preb, Fut8, B4galt3, Lman1, St8sia2, Sec31a, Mgat3, Mgat1, Man1a2, B4galt2, Sec23a, St6gal1, St8sia6
TRAF6 Mediated Induction of proinflammatory cytokines	1.989	0.0467	Rela, Nfkb2, Tab3, Dusp3, Mapk1, Nfkbib, Mapk8, Mapkapk2, Mapk10, Rps6ka3, Map2k4, App, Nfkbia, Ticam1, Ripk2, Mapk11, Ppp2r5d, Ikbkg, Rps6ka1, Map2k6, Tab2, Map3k7, Mapkapk3, Rps6ka5
SHC1 events in ERBB2 signaling	1.988	0.0468	Sos1, Mapk1, Erbb3, Nrg2, Hbegf, Shc1, Grb2, Erbb4, Egfr, Nrg1, Erbb2, Kras, Hras1, Nrg3, Egf
TAK1 activates NFkB by phosphorylation and activation of IKKs complex	1.988	0.0468	Rela, Nfkb2, Tab3, Nfkbib, App, Nfkbia, Ripk2, Ikbkg